The Origin of Ejecta Nebulae Surrounding Massive Stars

Matthew Paul Stroud

Thesis submitted for the Degree of Doctor of Philosophy, in the Faculty of Science of the University of London.

UNIVERSITY

COLLEGE LONDON

December 1997

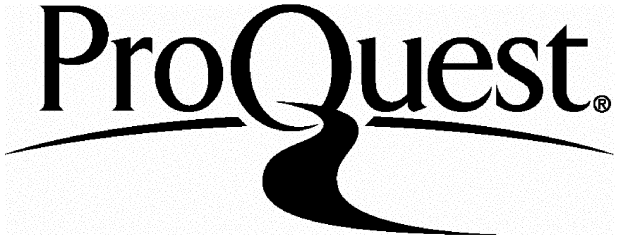

Dedication

To family and friends who made it worthwhile.

Acknowledgements

I would like to thank Linda Smith for guidance during my PhD and for her help in preparing this thesis, which was very much appreciated. I would also like to thank Paul Crowther whose depth of knowledge of WR stars made for many useful and enlightening conversations. During this PhD I have been financially supported by PPARC. Most of all I would like to acknowledge Matt, Kaj, Serena, Orsola, Chris, Richard, Barbara and Phil, who amongst others have made the past three years enjoyable.

Abstract.

Luminous Blue Variables (LBVs) are a rare class of stars which represent a phase in the transition of Of stars into Wolf-Rayet stars. A ubiquitous feature of LBVs is the presence of a circumstellar nebula. These nebulae bare witness to a phase of enhanced mass loss, *the gross characteristics and causes of which are basically unknown.* In this thesis we analyse the chemical and dynamical properties of these nebulae to infer the physical conditions present on the surface of the star at the epoch of ejection.

We have undertaken abundance studies of three LBV nebulae (AG Car, HR Car and He3-519) and found them to consist of partially CNO processed material. Since the application of atmospheric models to LBV stars has shown them to have a CNO equilibrium abundance pattern, this suggests that the epoch of nebular formation occurred before the present LBV phase. From the low expansion velocities of LBV nebulae we infer that the nebulae were ejected from stars with a low surface gravity. We note that this could arise either when a star approaches its Ω limit or during a RSG phase. Since mass loss near the Ω limit is inherently asymmetric and LBV nebulae are in general bipolar, we favour the former possibility. In a dynamical study of the nebula surrounding AG Car we find that it has a prolate geometry, with a disk-like outflow external to the nebula. Since these are hallmarks of mass loss from stars nearing the Ω limit, this reinforces our belief that the mass loss occurred toward the blue.

In addition we have performed abundance studies on the nebula RCW 58 which surrounds the WR star WR 40 and NGC 6164/5 surrounding the Of star HD 148937. We find that both these nebulae have very similar abundance patterns to those nebulae surrounding LBV stars. This suggests that the surface abundance pattern plays an important role in the operation of the ejection mechanism. In this context we note the significance of the surface abundance pattern for the opacity of the outer layers which govern the star's interaction with its modified Eddington limit.

Contents

List of Tables

List of Figures

Chapter 1

Introduction.

1.1 Aims.

In recent years, largely due to increasing computational power, stellar models have become very much more sophisticated. They are now able to broadly reproduce the observational characteristics and population statistics of a wide range of stars. One of the most challenging evolutionary phases to model is the post-main sequence evolution of the most massive stars. This is sensitively dependent on the star's mass loss history which requires a combined core/wind code to be modelled self-consistently. Furthermore any rotation the star has will induce internal mixing, causing it to evolve at a higher luminosity. Such effects can significantly modify the evolutionary tracks, and so need to be incorporated into the models. Through the work of Maeder (1987), Meynet et al. (1994), Langer et al. (1994), Schaerer et al. (1996) and others, progress in these areas has been rapid. However at the present time the evolutionary scenarios predicted by the various models disagree with one another and all have some disagreement with observations.

The highest luminosity region of the HR diagram contains a large number of different classes of star, Of, Wolf-Rayet (WR), Luminous Blue Variable (LBV), Red supergiant (RSG), and Ofpe/WN9 stars to name but a few. Many of these are prob-

ably, in evolutionary terms, interconnected, but what are these connections? Given the complexities of modelling their evolution, we must observationally establish their inter-relations, in order to define the the evolutionary sequences that the computational models must reproduce. Associated with these different evolutionary phases are distinct mass loss characteristics, which become imprinted on the surrounding circumstellar media. This relic mass loss manifests itself as two types of nebulae, Wind Blown Bubbles (WBB) and Ejecta Nebulae. The former arises when a stars powerful main sequence or WR wind sweeps up the surrounding ambient material, into a shell centred on the star. An ejecta nebula is formed primarily from processed stellar material. This thesis is concerned only with ejecta nebulae.

In this thesis we will investigate the abundance pattern and the dynamics of ejecta nebulae surrounding massive stars. These nebulae represent relics from a earlier phase of mass loss. By deriving the nebular parameters we aim to infer the physical conditions present on the surface of the star when the mass was lost. In addition to this we will compare and contrast the nebular abundance pattern of ejecta nebulae surrounding WR stars, LBV stars and an Of star. This will allow us to determine if the nebulae were formed during a common evolutionary phase and may give an indication as to whether the nebulae were formed by a common physical mechanism.

This introduction is comprised of four sections. We will begin by outlining the different evolutionary scenarios that have been developed on the basis of the evolutionary models and observations. We will then review the main observational characteristics of the different classes of star found in the highest luminosity region of the HRD (see Figure 1.1). These represent the basic building blocks of the evolutionary sequences. Next we will evaluate the importance of the physical mechanisms which impact upon the evolution of stars through the different regions of the HRD. Since we are primarily concerned with the formation of LBV nebulae, we will look critically at the mechanisms that have been proposed to produce extreme mass loss.

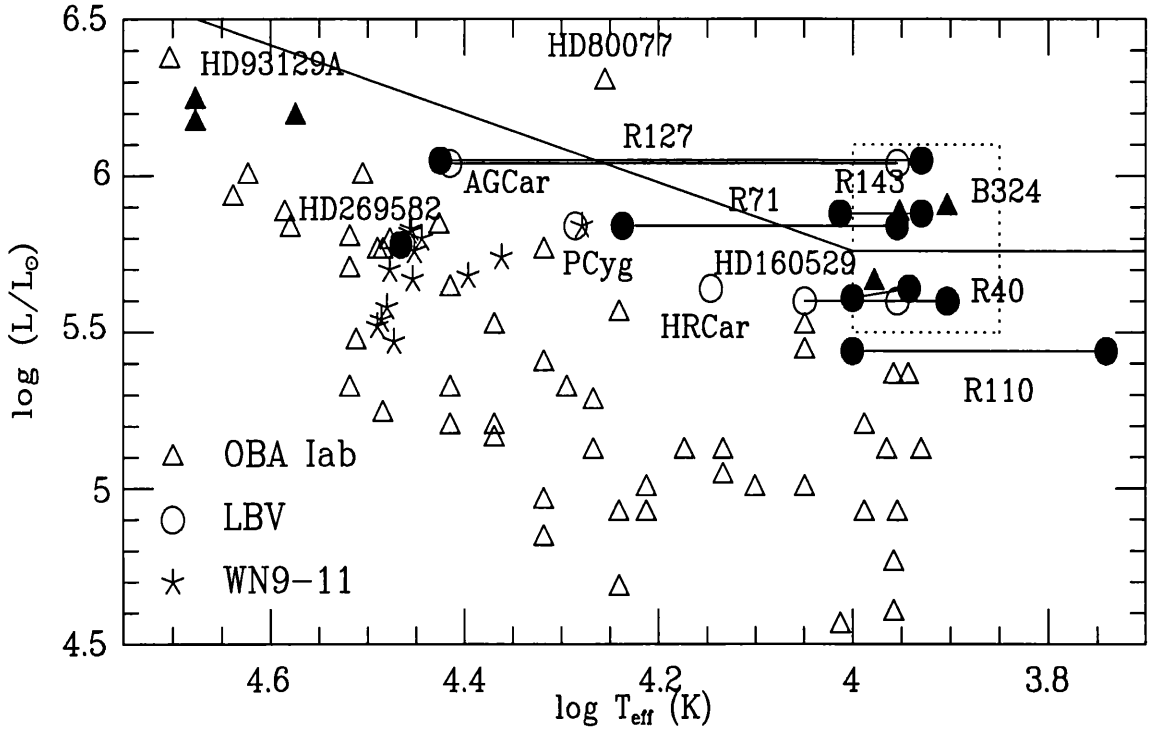

Figure 1.1: An HRD showing the positions of different high luminosity classes of star - filled in symbols represent stars in the LMC, open symbols represent Galactic stars (courtesy of P.A. Crowther).

Finally, we will review the physical and chemical properties of the nebulae which surround the most massive stars.

1.2 The Play - evolutionary scenarios.

In this section we will outline the main evolutionary scenarios which have been proposed for the post-main sequence evolution of the most massive stars. These scenarios connect the four main phases of stellar evolution seen in the most luminous region of the HRD, Of, LBV, RSG and WNL stars. Essentially the LBV and RSG phases are intermediate stages in the evolution of some Of stars into WR stars.

For the highest mass stars the LBV and RSG phases may be avoided by an extremely high rate of mass loss preventing evolution to the blue. This allows the evolution of Of stars directly into WNL stars. Crowther et al. (1995) note that the helium abundance of WN7 stars forms a continuum with that seen in Of stars. This is in contrast with the WN8 class which are not as hydrogen rich as some WN7 stars. Furthermore, WN7 stars tend to be more luminous than WN8 stars. The former typically having a luminosity of $\log(L/L_{\odot})=5.9$ while the latter typically has a luminosity of $\log(L/L_{\odot})=5.5$. Furthermore, WN7 stars have a high frequency of binerity, no ejecta nebulae and tend to be found in clusters (Moffat et al. 1989), all of which is in sharp contrast to WN8 stars. Consequently Crowther et al. (1995) interpret WN7 stars as representing the most massive stars which have evolved directly from Of stars into WR stars.

Within this framework WN8 stars are believed to have passed through either a RSG or LBV phase before becoming a WR star. In this context we note LBVs are highly variable and are believed to have a very low frequency of binarity. The interpretation that they evolve into WN8 stars is then supported by the fact that

WN8 stars show a much greater degree of variability than WN7 stars.

This leads us to ask which Of stars evolve into WN8 stars via a RSG phase and which via an LBV phase. Alternatively, is the LBV phase encountered during the post-RSG evolution of stars in a particular mass range? If so do all stars within this mass range pass through an LBV phase?

One constraint on which massive stars evolve through an LBV phase comes the interpretation of WN7 stars as representing the descendants of the most massive stars, while WN8 stars represent the descendants of RSG or LBV stars. This implies there is a maximum initial mass for stars which can become LBVs. Since the most luminous LBV AG Car has log $L_*/L_\odot = 6.0$ (Smith et al. 1994), we can used the evolutionary models of Meynet et al. (1994) to infer an initial mass of about $60M_\odot$. Because of the uncertainties in the evolutionary models, this value is very approximate. Correspondingly the least luminous LBV HD 168625 has a luminosity of $L_*/L_\odot = 5.3$ this implies an initial mass of $40M_\odot$. Stars less massive than this must evolve into WR stars through a RSG phase.

To conclude our discussion of the evolutionary sequences, we will address the question of whether LBVs are post-RSG objects. Central to this question is the observation that the terminal wind velocities of LBV and slash stars are considerably lower than other BSG of the same spectral type. For instance a B1 supergiant typically has a terminal velocity of about 1000 km s^{-1} while the LBV P Cygni which is a B1Ia+ star has a terminal wind velocity of 185 km s^{-1}. In radiatively wind theory, the terminal velocity is dependent on both the effective temperature and effective gravity. This implies that LBVs have a lower surface gravity than normal BSGs of the same spectral type, implying that they have a high L/M ratio. This strongly suggests that LBVs have recently under gone a phase of heavy mass loss. This would be naturally explained by an earlier RSG phase.

Here we need to make a distinction between stars above and below the Humphreys-Davidson limit (Humphery & Davidson 1979). This is a limiting luminosity above which no RSG are observed (see Section 1.4.1). We will refer to LBVs evolving above the H-D limit as high mass LBVs and those evolving below it as low mass LBVs. The low mass LBV instability strip, which extends below the left-hand edge of the H-D limit, contains BSGs with both high and low terminal wind velocities. This may corresponds to pre- and post-RSG stars. Above the HD limit the HRD takes on a very different appearance, showing an absence of RSG stars. However this does not exclude the possibility that these highest mass stars experience a brief period in the red, which would be observationally hard to detect. The viability of such a scenario depends on the mass loss rates which arise when the star exceeds it's modified Eddington limit. We will pursue these points further in chapters two and seven.

1.3 The Actors - Phases of stellar evolution.

1.3.1 O stars

Our discussion of Of stars will focus on four central topics, the spectral morphology, mass loss, physical conditions and abundances. The Of classification was introduced to indicate the presence of emission features from NIII and HeII in the spectra of some O-stars. These features are thought to arise in the stellar wind and are probably a manifestation of a high mass loss rate. This classification was extended to incorporate O-stars which show evidence of "shell activity", these are termed Of?p stars. This classification is defined by the P-Cygni profiles of the hydrogen Balmer lines and emission from CIII. One of the prototypical objects for this group is HD 148937, which is the subject of chapter five of this thesis.

Only with the advent of Ultra-violet spectroscopy was it realised that virtually

all O and Of stars have some lines with P-Cygni profiles. Such profiles indicate a high mass loss rate and contain information about the characteristics of that mass loss. From the blue edge of the P-Cygni profile we can determine the wind's terminal velocity, which is typically found to be about 2000 km s^{-1}. While the ratio of the emission and absorption components of the profile indicates the steepness of the winds acceleration. Taken together these properties allow us to deduce a β velocity law. With this determined the mass loss rate can be estimated from the shape and depth of the P-Cygni profile. Howarth and Prinja (1989) have applied this method to 203 galactic OB stars finding the mass loss rate to be primally dependent on the stellar luminosity. In general they find mass loss rates of $\log(M/M_{\odot}\ yr^{-1})$ =1.69 and luminosities in the range $\log(L/L_{\odot})$ – 15.4

The effective temperature of O stars ranges from about 30kK up to about 50kK for the O3 spectral type. The stellar intrinsic parameters can be determined through the application of atmospheric models (e.g. Herrero et al. 1992). While their effective gravities typically range from log g=3.5 to 4.5, their radii are in the order of 10-20$R_{\odot}$ and their luminosities encompass $\log L/L_{\odot}$= 4.5–6.0 (Herrero et al. 1992). Consequently, the stellar spectroscopic masses found in Herrero's sample are between 15$M_{\odot}$ and 50$_{\odot}$. Herrero et al (1992) note that these spectroscopic masses are systematically lower than the inferred evolutionary masses and that this discrepancy is particularly acute for the Of-stars. More generally Herrero et al. found a correlation between the degree of mass discrepancy and how close the star was to its Eddington limit. This suggests two possibilities, either the atmospheric models break down when applied to the more extended atmospheres or the evolutionary models underestimate the mass loss.

On the basis of the evolutionary models we would not expect the surface composition of O and Of-stars to show significant signs of CNO processing. However through the application of the atmospheric models to the stellar winds, it has been found that the helium abundance is often considerably enriched (Herrero et al. 1992). For

instance Voels et al. (1989) found α Cam to have a helium abundance (He/[H+He] by mass) of Y=0.46, while Bohannan et al. (1990) found Y=0.50 for a sample of three O4 stars. Herrero et al. note that the most evolved helium abundance is found in the most luminous stars and those with the greatest rotation rates. This suggests that rotational mixing may play a role in producing these enrichments.

1.3.2 Luminous Blue Variables.

The term "Luminous Blue Variable" or LBV was coined by Peter Conti in a review paper for "Observational tests of stellar evolutionary theory (1983)." This term was used to describe stars such as η Car, P-Cygni, R71, R122, the S Dor stars and the Hubble-Sandage Variables. Three types of variability has been identified in LBVs, giant eruptions, normal eruptions, and micro-variations.

Giant eruptions are characterised by the star increasing its visual brightness by at least two orders of magnitude. It is not clear whether this occurs at a constant bolometric luminosity. Associated with these giant eruptions is believed to be a very large increase in the mass loss rate, possibly causing the formation of the surrounding nebula. However the evidence for this is extremely tenuous. The frequency of these giant outbursts is thought to be very low, perhaps only a couple times during the LBV phase, although this is subject to very large uncertainties (Humphreys & Davidson 1994). Based on the population statistics from the LMC, the LBV phase is thought to last 25,000 yrs (Humphreys & Davidson 1994).

Normal eruptions are more frequently observed and so have been more throughly investigated. These occur with a frequency of 10-40 yrs and cause the star to brighten by 1-2 visual magnitudes over a period of a couple of months. These variations occur at a constant bolometric luminosity, with the star's radius increasing by a factor of eight to exchange energy between the UV and visual wavelengths (Appenzeller

and Wolf 1981). The star is coolest (7000-8000K) and therefore visually brightest when its atmosphere is most extended. While at minimum in the quiescent state, it has a smaller radius and is much hotter (12000-30,000K). Superimposed upon these normal eruptions are smaller oscillations of about half a magnitude. These evolve on a time scale of a few months up to a few years.

The origin of these variations is not clear, but essentially two theories have been put forward. The first is that, a large increase in the mass loss rate leads to the creation of a false photosphere in the stellar wind and so a reduction in the effective temperature (Lamers & Fitzpatrick 1987). The second is that some unknown sub-photospheric mechanism causes the stellar radius to increase (Leitherer et al. 1989). An attempt to distinguish these two possibilities has been made by de Koter et al. (1996). They use an atmospheric model to probe the effect of altering the mass loss rate, terminal velocity, rate of acceleration and initial temperature of the wind. They found that the effective radius could not by increased by more than 40%. Consequently they concluded that the reduction in effective temperature results from a genuine increase in the stellar radii, which is probably connected to a reduction in the effective gravity.

Finally the smallest variation are the micro-variations. These consist of fluctuations of less than 0.1 visual magnitudes with a period of between a week and a month (Van Genderen et al. 1990). These variations may not be intrinsically related to the other LBV instabilities since they are also observed in normal supergiants.

The variations in temperature between the minimum and maximum states naturally leads to LBVs having a variable spectral type. Generally, at their hottest LBVs resemble B-supergiants or Ofpe/WN stars showing prominent hydrogen Balmer, HeI and FeII lines. In many lines P-Cygni profiles are clearly observed. At visual maximum the star manifests itself as a A or F supergiant.

A ubiquitous feature of LBVs are their high mass loss rates, which are in the order of $5\times10^{-5}M_{\odot}yr^{-1}$ (Leitherer 1997). Generally the mass loss rate does not vary as the star evolves between maximum and minimum states, although R71 and possibly S Dor, may be exceptions. Leitherer et al. (1987) found that R71 had a mass loss rate 30 times greater at visual minimum compared to visual maximum. The general consistency of the mass loss rate between the maximum and minimum state further argues against the normal outbursts being due to enhanced mass loss creating an extended false photosphere. In addition to the high mass loss rates, LBV winds have low terminal velocities ranging from 100-300 km s^{-1} (Leitherer 1996). For instance a normal B1 supergiant has a terminal wind velocity of 1060 km s^{-1}, compared to 185 km s^{-1} for the LBV P Cygni. Despite the mass loss rates of LBVs being 3-5 times higher than those of normal BSGs (Crowther et al. 1996), their low terminal velocities conspire to make their wind momentum comparable to that of other BSGs.

The most dramatic phase of mass loss is that which forms the circumstellar nebulae so often associated with LBVs. Shedding light on this phase of mass loss will be one of the central themes of this thesis. At the present time *even the gross picture is basically unknown.* Theories for the nebula formation can be broadly divided into two groups, ejection events and interacting wind models. The latter group has been most thoroughly investigated, largely through the work of Garcia-Segura(1996) and Frank (1997). Essentially they have adapted the interacting wind model, developed for planetary nebulae, where the slow asymtopic giant branch wind is swept up into the nebula by the faster wind from the subsequent hotter stellar phases. In the case of LBVs, this corresponds to the LBV wind sweeping up the slow wind lost during the RSG phase. Alternatively the nebula could have been ejected in some discrete event. Since the mechanism lying behind such an ejection is unknown, this has not received much theoretical attention, although it gains strength from observational arguments. Any discrete ejection event would most probably take the form of a very enhanced phase of mass loss, rather than an explosive event which is likely to

disrupt the star.

Excluding η Car the luminosity of LBVs range between log $L/L_{\odot}$=5.4 to 6.1 (Nota et al. 1995). Crowther et al. (1992) have used the mass luminosity relation of Schaerer and Meader (1992) to estimate the present stellar masses of LBVs, yielding a range of $20^{+20}_{-8}M_{\odot}$. Atmospheric codes have been applied to few LBVs. Smith et al (1994) applied a code to AG Car to determine H/He=2.4, while Lennon et al. (1994) analysed R71 finding H/He=2.3, N/Ne=0.003 and N/C=35, by number. This supports the conclusion based on evolutionary models, that LBVs are composed of CNO equilibrium material.

Unlike other stellar classes, the spectral type is not the defining characteristic of an LBV, but rather it is a description which varies through the LBV phase. The label LBV is used in much the same way as the Of star label or WN9 label, yet the LBV grouping is formed in a different way. The common characteristic is the presence of a certain type of variability or some evidence of variability in the recent past. The spectra can be used to guide us as to what type of stars are likely to experience this instability, but no more than this. In the final analysis we wish LBVs to be a physically significant group, containing the stars in which a particular type of variability can operate. This is likely to require a more sophisticated observational definition than we are currently able to prescribe.

No formal definition for LBVs has ever been made, as its hard to say what properties a star must have for the LBV instability to operate. In practice a star will acquire an LBV classification if it satisfies one of two criteria;

- That its luminous and irregularly variable over long periods of time.
- We reasonably believe that the above criteria would be met, if only we had more data.

If a star is only able to meet the second of the criteria then it is usually termed an LBV candidate. An example of this latter category is He3-519, which was proposed as an LBV candidate by Smith et al (1994). This inference was made on the basis that it was spectrally similar to AG Car at minimum and had ejected an LBV type nebula. Had the giant eruption been witnessed then we would regard it as a confirmed LBV. A similar situation exists with P Cygni, which does not display the usual LBV variations at present, but has been witnessed to have under gone a giant eruption in the past. This is regarded as a confirmed LBV.

1.3.3 Ofpe/WN stars

Spectrally Ofpe/WN9 stars (a.k.a slash stars) are similar to Of stars, showing both NIII and HeII emission features. However they also display evidence of lower ionization stages like NII and HeI, which are characteristic of the WN9 spectral class. Ofpe/WN9 stars were first established as a class by Bohannan and Walborn (1989), based on observations of 10 stars in the LMC. Recently Crowther et al. (1995) have reclassified the Ofpe/WN9 stars within an extended WR classification sequence. Using this classification scheme we find that Ofpe/WN9 stars fall into the WN9 and WN10 classes, while the WN11 classification is applicable to LBV stars like AG Car and He3-519 at minimum.

While Ofpe/WN9 stars spectrally bear many similarities to Of and WR stars, their mass loss properties are very different. They are characterised by slow winds and high mass loss rates. Typically terminal wind velocities of about 400 km s^{-1} are found with a mass loss rate of the order of $3\times10^{-5}M_{\odot}yr^{-1}$ (Pasquali et al. 1997). From radiatively driven wind theory it is found that the winds terminal velocity is dependent primarily on the stellar temperature and effective surface gravity. Since Ofpe/WN stars have an effective temperature comparable to that of many Of stars, then the low terminal velocity many be symptomatic of a low effective surface grav-

ity. We will discuss this in more detail later.

An intriguing feature of Ofpe/WN stars is their association with ring nebulae. Walborn (1982) noted the presence of forbidden nitrogen lines in the spectra of four LMC Ofpe/WN stars, this is indicative of the presence of nebulae. In addition to this Nota et al (1996) spectroscopically investigated seven LMC Ofpe/WN stars and detected circumstellar nebulae surrounding five of them.

Using atmospheric models estimates have been made of the intrinsic parameters of Ofpe/WN stars (Pasquali et al. 1997). Typically, they found that the stars had T_*=30-40KK, R_*=20-35$R_\odot$, log$L/L_\odot$=5.4-6.3 and a helium abundance of typically Y=0.6 (by mass).

Many characteristics associated with Ofpe/WN stars are reminiscent of LBVs. We note that Smith et al. (1994) classify both He3-519 and AG Car as WN11 stars. This classification differs from the WN10 status attributed to some Ofpe/WN stars only in that it implies a cooler temperature with emission from NIII being absent. Furthermore LBVs like Ofpe/WN stars tend to be surrounded by ejecta nebulae (Nota et al. 1995). Such similarities have long caused speculation as to whether Ofpe/WN stars represent dormant LBVs. This suspicion was dramatically confirmed in 1983 when the Ofpe/WN star R127 evolved into an A-supergiant over the period of a decade (Stahl et al. 1983; Wolf et al. 1988).

1.3.4 WNL stars.

About one quarter of all WR stars are WNL stars (WN6-9), of these one quarter are WN8,9 (Moffat 1989). Like all Wolf-Rayet stars the spectra of WNL stars are dominated by emission lines formed in their dense winds. WNL stars have prodi-

gious mass loss rates of between 1-10$\times 10^{-5}$, with no systematic variation between spectral types (Prinja et al. 1990). However, the terminal wind velocity does correlate well with spectral type, ranging from 500 km s^{-1} for WN9s up to 3000 km s^{-1} for WN2s. Most stellar winds have a performance number less than unity, that is, the increase of wind momentum is less than the momentum carried by the radiation field. This is not the case for WR stars, where the performance number is significantly greater than unity (Hamann et al 1993). This can be explained by multiple scattering of the photons in an ionically highly stratified wind (Lucy & Abbott 1993).

WNL stars typically have temperatures of 35kK and luminosities in the range log $L/L_{\odot}$=5.5-6.0. Consequently they have radii between $R_{*}=14R_{\odot}$ and $35R_{\odot}$ (Crowther et al. 1995). We note that because of the extreme mass loss rates and so false photospheres, $R_{2/3}$ (the radius at which the optical depth equals 2/3) and R_{*} (the radius implied by the stars effective temperature) can differ substantially. Two distinct groups have been identified within the WNL class (Moffat 1989), one group containing the WN6,7 stars the other, the cooler WN8,9 stars. Moffat (1989) note that the WN6,7s have a high frequency of binarity in contrast to WN8,9. Furthermore WN8,9s tend not to be distributed in clusters and associations. Most revealingly, WN8,9s are by far the most variable of the WR stars. We note that LBVs show no evidence for binarity and have the same spatial distribution as the WN8,9 group. No WN7 stars have ejecta nebulae (Chu 1991).

In general WNL stars show an enrichment in their helium abundance, ranging from about Y=He/(He+H)=0.50 up to nearly Y=1 (Crowther et al 1995). The WN7+abs (WN7 with some absorption features) show a degree of processing comparable to that seen in some O supergiants, while the WN8-11s tend to be composed of slightly more processed material.

1.3.5 Red Supergiants.

Red-supergiants represent one of the most enigmatic phases of stellar evolution. During this phase a great deal of mass is lost through a dusty, high density wind with a low terminal velocity. The radiation pressure on the dust grains plays an important part in driving this wind. However at the present time we are unable to realistically model the formation of dust. Consequently we cannot theoretically predict the mass loss characteristics from RSGs, but must instead rely heavy on observations.

Since we are looking at the RSG phase with regard to possible relations with the LBV phase, we are primally interested in RSGs with luminosities comparable to that of LBVs. These however are extremely rare, numbering only a few. Clearly we must be careful when drawing any conclusions from such a small sample. During the main sequence the powerful stellar wind evacuates the surrounding ISM, leaving the subsequent RSG wind to expand into a very low density medium. This manifests itself as an envelope slowly expanding inside the wind blown bubble (WBB).

Two of the best studied massive post-RSGs are IRC+10420 and HD 179821. These have luminosities of $2\times10^5 L_\odot$ (Nedoluha & Bowers 1992) and $5\times10^5 L_\odot$ (van der Veen et al. 1993) respectively. Both of these yellow supergiants are believed to be in the process of transition between the RSG phase and the LBV or WR phase (Kastner & Weintraub 1995). IRC+10420 is surrounded by a circular envelope with an expansion velocity of 47 km s^{-1}. The envelope surrounding HD 179821 is also circular, but has a lower expansion velocity of 33 km s^{-1}. Both envelopes are estimated to contain $5M_\odot$ and have a dynamical age of 5000 yrs (Kastner & Weintraub 1995). Another well studied circumstellar envelope surrounds the massive RSG μ Cep, which has a luminosity of $4\times10^5 L_\odot$ (Humphreys & Davidson 1979). Interestingly the envelope is bipolar, with an expansion velocity of 47 km s^{-1} (Bernat 1981). More recently the Infra-red Space Observatory has been used to obtain spectra of

the RSG NML Cyg (Justtanont et al 1996). Their analysis concurs well with an earlier analysis by Bowers et al (1993), which found NML Cyg to have a luminosity of $5\times10^5 L_\odot$. The central star is surrounded by a massive envelope formed by the extreme mass loss, which is occurring at a rate of $2\times10^{-4} M_\odot yr^{-1}$ with a terminal velocity of 28 km s^{-1}. Jones et al. (1993) suggest that these stars (with an initial mass of about $40M_\odot$) will have lost about $15M_\odot$ between entering the RSG phase and returning back to the blue. This implies that a post-RSG will return to the blue with about one half its initial mass.

1.4 The Stage - Mass Loss and the HRD.

In this section we will look at the physical processes and phenomena which influence the post-main sequence evolution of these massive stars. We will focus on the physical mechanisms underlying the process of mass loss and consider their manifestations in different evolutionary phases.

1.4.1 The H-D limit.

During 1978 and 1979 Humphreys & Davidson surveyed the temperature and luminosity of very massive stars in the Galaxy and LMC. They used the resulting population distributions to contrast the HR diagrams obtained for the two galaxies. They found little difference, implying that the physical processes governing stellar evolution are basically the same in both regions. This inference gains further support from the observation that both galaxies contain a similar ratio of red to blue supergiants.

By plotting these HR diagrams they found that there is an absence of RSGs of a comparable luminosity to the most luminous BSGs. They describe the zone of the

HRD where no RSGs were found as follows:

"The upper luminosity boundary for both Galactic and LMC supergiants is characterised by (1) decreasing luminosity with decreasing temperature for the hottest stars and (2) an upper limit to the luminosity near M_{bol}= -9.5 to 10mag for stars cooler than 15,000K (Humphreys&Davidson 1979)."

They suggest that this may be accounted for by the high mass loss rates of the most massive stars, preventing their evolution to the red. This zone in which no RSGs are found, is bounded by what has become known as the Humphreys-Davidson limit (H-D limit).

Naturally, this empirical limit has provoked theoretical investigation in search of a physical cause. While it is widely believed that it is an artifact of heavy mass loss, there is no such consensus as to the underlying mechanism by which this occurs. One school of thought suggests that the root of the phenomena lies in the star's encounter with the Eddington limit. However this may trigger a wide range of mass loss mechanisms and which dominates is not clear. Alternatively Stothers and Chin (1993) suggest that an instability arising from the partial ionization of hydrogen and helium in a detached outer layer, causes sporadic bulk ejections of mass from the star. A third possibility is presented by Nieuwenhuijzen et al. (1994), who find that the micro-turbulence increases as a very steep function of the luminosity. It is suggested that this will cause large mass loss rates for the highest luminosity stars. The final mechanism that we will discuss, is the loss of mass through strange mode pulsations. These occur in adiabatic and so tenuous stellar atmospheres (Cox et al. 1997; Glatzel et al. 1994). Consequently this mechanism can be intimately connected to the Eddington limit, since a star will tend to "fluff up" as its effective surface gravity reduces.

In this section we will look at the mass loss characteristics associated with these

mechanisms some detail, as they play a critical role in two of the chapters of this thesis. The rate of mass loss which occurs when a star approaches the modified Eddington limit, is central in chapter 2 to deducing the physical conditions present on the stellar surface when the nebula was ejected. In chapter 6 our dynamical study of the AG Car nebula will aim to shed light on the geometry of the nebula forming mass loss. If, as we will argue the nebula formed while the star is close to the Eddington limit, then the nebula geometry allows an assessment of the role of photon tiring (see below). Consequently, in this section we will introduce these theoretical mechanisms and review their main properties.

1.4.2 The Modified Eddington Limit.

The classical Eddington limit refers to the luminosity at which the radiation field scattering off electrons imparts a force equal and opposite to gravity. At the Eddington limit the star has an effective gravity of zero. However, an effective gravity of zero and no gravity are not the same thing. The absence of any inward radial acceleration is an artifact of the balance of forces at the stellar surface, but the material is still in a gravitational well. Since the luminosity and gravity both have an inverse square dependence, this balance will be maintained even if the surface material is displaced. However, should the mass loss rate become too great the radiation field will not have enough energy to lift the material from the gravitational well and the balance of forces will break down.

In real stars the opacity is not solely due to electron scattering, but also line blocking. Since the ionised species present in a stellar atmosphere are dependent on the temperature, this introduces a dependence of the Eddington limit on the temperature. This version of the limit is known as the modified Eddington limit. Since the number of possible atomic transitions scales roughly as Z^4, heavy elements play an immensely important role. Now we can crudely investigate the response on

the stellar atmosphere to a reduction in the surface gravity using a simple analytical model. The equation of motion for a simple atmosphere can be written;

$$dv/dt + dv/dr + (1/\rho)\mathrm{dP}_g/\mathrm{dr} = -\mathrm{g}_{eff} = -g(1 - (g_r/g))$$

where g_r is the acceleration due to gravity and P_g is the gas pressure.

$$g_r = 4\pi\kappa_\mu H_\mu d\mu$$

Where H_μ is the Eddington flux and κ_μ is the mass absorption coefficient. If we now take the case of a grey atmosphere (κ_μ=const);

$$g_r = (4\pi\kappa_\mu\ /\mathrm{c})\int \mathrm{H}_\mu d\mu = \kappa_\mu \mathrm{L}/4\pi cR^2$$

$$g_r/\mathrm{g} = (\kappa_\mu\ \mathrm{L}\ \mathrm{R}^2)/(4\pi cR^2GM) = L/L_{edd}$$

$$\mathrm{L}_{edd} = (4\pi cGM)/\kappa_\mu$$

And so we obtain an expression for the modified Eddington limit of a simple grey atmosphere. In more realistic models κ_μ is not constant, but is instead largely a function of temperature. By looking at an expression for the scale height (h) of an atmosphere with the mean molecular weight of μ, we can see how the atmosphere responds when the Eddington limit is reached. This shows that at the Eddington limit the atmosphere will expand thermally.

$$\mathrm{h} = \mathrm{RT}/\mathrm{g}_{eff}$$

$$\text{as} \quad \mathrm{g}_{eff} \rightarrow 0$$

$$\mathrm{h} \rightarrow \infty$$

The position of these modified Eddington limits have been calculated by Lamers & Fitzpatrick (1987) using low gravity, plane parallel, LTE model atmospheres. They find that the position of the locus of modified Eddington limits is consistent with the empirical H-D limit. They conclude that the absence of RSGs inside the forbidden zone is attributable to the enhanced mass loss as the effective gravity tends to zero. Appenzeller (1989) notes that a star impinging on its modified Eddington limit will be unstable to subsequent mass loss. Massive stars evolve at a constant

luminosity and so any reduction in mass will increase the L/M ratio, reducing the the modified Eddington limit, leading to an increase in the mass loss rate and so a runnaway effect. This mass loss will eventually reveal hotter layers which have a lower opacity, increasing the modified Eddington limit and causing the mass loss to abate. Appenzeller estimates that each out burst will last a few decades and eject $10^{-2}M_{\odot}$.

The concept of a modified Eddington limit is more subtle than it may at first appear. As $\Gamma \rightarrow 1$ the thermal pressure of the star will cause it to expand until Γ=1, when the material will float off into space. However, as the envelope expands its density will drop reducing the rate of recombination and so increase the degree of ionisation. This leads to a reduction in the opacity and therefore an increase in the modified Eddington limit. So can the modified Eddington limit ever be reached, or in practice will it always reduce to the classical Eddington limit (Humphreys & Davidson 1994). The outer boundary of the star will settle at the radius where there is a balance of forces. If a star of a given radius expands, it does so because there is not a balance of forces at the surface. The subsequent drop in envelope density will oppose the expansion, but it must expand none-the-less, to regain an equlibrium of forces.

These arguments in conjunction with the low surface gravities determined for Ofpe/WN9 stars, which are believed to be dormant LBVs, suggest an intimate connection between the LBV phase and the Eddington limit. Could outbursts of the type described above, account for the ring nebulae so often associated with LBVs? To answer this question we need to know the mass loss characteristics of a star approaching and then exceeding its Eddington limit. As a first step, we will turn to radiatively driven wind theory, which predicts;

$$V^2 = a/(1-a) \times (2GM/R) \times (1-\Gamma)$$

where a is a force multiplier and;

$$\Gamma = L/L_{edd}=(\kappa_\mu \text{ LR}^2)/(4\ \pi cR^2\text{GM})$$

Consequently as the luminosity approachs the Eddington luminosity, Γ tends to unity and so the terminal wind velocity (V) will fall to zero. Associated with this drop in terminal velocity is an increase in the mass loss rate, which reaches a singularity at Γ=1. Clearly in the limit of Γ=1, radiatively driven wind theory breaks down. However, in the light of this theory's sucess in modeling all other stellar winds we will use it as a qualitive guide, before the Eddington limit is reached. Consequently the following picture emerges. As the star evolves toward its modified Eddington limit, its mass loss rate increases and its terminal velocity falls, producing wind properties like those of Ofpe/WN9 stars. As the star continues to evolve closer to the modified Eddington limit other factors, not emboddied in the radiatively driven wind theory, must come into play to stablise this mass loss.

A key factor in regulating this supra-Eddington limit mass loss, may be the process of photon tiring (Owocki & Gayley 1997). By removing mass from the star's gravitational well the radiation field does work. Clearly the amount of work done cannot be greater than the stellar luminosity and so the mass loss rate is aways finite. In particular Owocki & Gayley (1997) raise the possiblity that photon tiring may cause the flow to completely stagnate and fall back toward the star, resulting in some form of mass circulation. Whether this would take the form of something analagous to convection cells or a form of pulsation is not clear. Owocki & Gayley conclude that it may be possible for a supra-Eddington star to not have a sustained mass loss.

Fundamentally the star is producing energy, which to remain in any long term equlibrium, it must lose. A mass circulation will tire the photons, but an exactly equal quantity of energy will be returned to the star when the material drops back down to the base of the circulation. This must either increase the luminosity or temperature. The former would then require an even larger quantity of mass to

be circulated, or the same mass to be moved further out of the gravitational well, in order to retain a surface of Γ=1 (were the material is neutrally buoyant). The former possibility would lead to a runaway effect. While the latter possiblity implies an increasing temperature, this would lead to a reduction in the effective opacity and so a retreat from the modified Eddington limit until Γ=1. Contary to Owocki & Gayley (1997) this suggests that it maybe impossible for a star to exceed its modified Eddington limit for any extended period.

Another form of modified Eddington limit has been identified by Langer (1996), who looks at the interaction between the Eddington limit and rotation. In a non-rotating star there must exist a balance between gravity and radiation pressure at the stellar surface. However, if the star is rotating then the balance is between cetrifugal forces, radiation pressure and gravity. The point were the former overwhelm the latter is termed the "Omega limit". Since no star is devoid of angular momentum, the Omega limit will always be encountered before the modified Eddington limit. As the star approaches the Eddington limit its mass loss will be enhanced. Assuming a radiatively driven wind, Friend & Abbott (1986) find an enhancment by a factor of;

$$\dot{M}/\dot{M}(\mathrm{V}_{rot}=0) = (1/(\Omega)^{0.43}$$
$$\text{where } \Omega=\mathrm{V}_{rot}/\mathrm{V}_{crit}$$

Now as $\Omega \rightarrow 0$ the mass loss tends to ∞. However in practice the mass loss, which is mainly from the equator, involves a loss of angular momentum. This slows the rotation rate, reducing the mass loss. Consequently the faster the star's rate of evolution, the higher the resulting mass loss rate. Langer (1997) has computed models for a $60\mathrm{M}_{\odot}$ core-hydrogen burning star. During this phase Γ varies and this variation is mirrored by the evolution of V_{crit}. A minimum value of V_{crit}=100 km s^{-1} is achieved at the helium opacity peak around 40,000K. Since angular momentum is largely conserved during the main-sequence phase, any star with an initial rotation velocity greater than this will encounter the Ω limit. Through this phase

of stellar evolution Γ drops smoothly and so the critical velocity declines at a uniform rate. Consequently the same mass loss rate results regardless of when, during the H-core burning phase, the Ω limit is reached. The subsequent mass loss rate is therefore determined by the need to lose enough angular momentum to keep Ω less than unity. During the core hydrogen burning phase Langer finds a mass loss rate of the order of $10^{-5}M_{\odot}$ yr^{-1}. After core-hydrogen exhaustion the star will evolve to lower temperatures, encountering the iron opacity peak (12,000K). This evolution is rapid and so angular momentum needs to be lost on a shorter time scale implying a high mass loss rate. If the Ω limit is exceeded the star must respond by losing enough angular momentum and so mass, to reduce Ω to less than unity. This implies a mass loss rate of between 10^{-3} to $10^{-2}M_{\odot}yr^{-1}$ for a $60M_{\odot}$ star (Langer 1997).

However, the radiation field at the equator does not have sufficent energy to lift these mass loss rates out of the stars gravitational well. The flow must stagnate (Owocki privt comm. 1997). Equally the the star must lose angular momentum, which in the absence of magnetic fields requires these high mass loss rates (Langer. 1997). This apparent contradiction may be resolved by the formation of a circumstellar disk. This would allow the necessary mass to be lost from the star without the need to lift the material out of the gravitational well, for which there is not sufficient energy.

To understand the resulting mass loss at least two further effects need to be taken into account. Firstly, how is the star's radiation field modified by the stellar rotation? Secondly, how does the radiation field react to the accumulation of "lost" mass in the equatorial region? To address the first question; essentially the gas pressure is proportional to the square root of the effective gravity;

$$P_g \propto g_{eff}$$

but, the gas pressure is proportional to the temperature. Consequently, a reduction in the effective gravity at the equator reduces its temperature. This in turn reduces the emergent flux, since;

$$F \propto T^4$$

However, the star must still radiate away the same amount of energy, which then implies an anisotropic radiation field. This leads to a greater flux from the polar regions. Furthermore, this affect is reinforced by the stagnation of the equatorial mass flow. The mass deposited in the equatorial region (see above) makes it hard for the radiation to escape at these latitudes. Conseqently the photons are scattered toward the polar regions. This high radiation flux through the polar regions, which paradoxically, leads to the highest mass loss rates occuring from the poles (Owocki 1997).

At the present time supra-Eddington mass loss is not well understood, but qualitively we see the following picture emerge. As the star approches the Omega limit, the mass loss rate increases preferentially at the equator. In this region the mass loss exceeds that which can be lifted from the gravitational well by the radiation field and the flow stagnates. This results in the formation of an active disk. The distortion of the stellar envelope then serves to enhance the radiation flux through the polar regions. This may lead to the highest mass loss rates being achieved at the poles. At this point we will briefly jump considerably ahead of ourselves by noting that at least two of the LBV nebulae studied in this thesis are prolate ellipsoids with evidence of equatorial disks.

1.4.3 The Stothers and Chin instability.

Stothers and Chin (1994) describe the instability mechanism that bears their name, as follows;

"...this dynamical instability arises from a complex interplay between the effects of prior stellar wind mass loss, high radiation pressure, partial ionisation of hydrogen and helium, and large iron opacities, which cause the outer envelope layers cooler than 5×10^5K effectively to float on a powerful radiation field, virtually isolated from the rest of the star. When these layers become dynamically unstable, they detach from the underlying star in a series of violent relaxation oscillations."

For a star to suffer this instability, three criteria must be met. Firstly the initial stellar mass must be high and so supported by a large luminosity. Secondly the L/M ratio must be high. Thirdly, the partial ionisation of hydrogen and helium in some layers, must reduce the mean first generalised adiabatic exponent to below some critical value ($< \Gamma_1 > = 4/3$) triggering the instability. Γ_1 characterises the internal energy of the plasma at a given point in the star. A polytropic model with a polytropic index of n will be dynamically unstable if;

$$n < \Gamma_1/(\Gamma_1 - 1)$$

A polytropic index of about 4 is appropriate for the stars we are considering here, implying a critical value of Γ_1=4/3. More generally Γ_1 is a parameter in the Eddington discriminator A^*, which tests for dynamical stability.

$$A^* = (1/\Gamma_1 \times dlnP/dlnr) - (dln\rho/dlnr)$$

If A* is positive then the star is dynamically stable, if A* is negative then the star is unstable. Γ_1 describes the plasma, the differential terms the stellar structure.

If Γ_1 falls below 4/3 in a given layer then the weighted average of Γ_1 between the surface (R) and some level (r) can also be less than 4/3. While such a region is connected to the star, the star can react by stabilising the region. If however this region were to be come isolated, then the instability can develop. In the Stothers and Chin instability, the powerful radiation field interacts with the iron opacity bump, which peaks in a layer of the star with a given temperature, to isolate the layers above. The effect of the high luminosity through these layers reduces Γ_1 close to 4/3. This is then further reduced below 4/3, by the partial ionization of the hydrogen and helium increasing the opacity, triggering the instability.

They emphasise that the instability is *not triggered by* a density inversion, atmospheric turbulence or the stellar luminosity exceeding the Eddington luminosity. This instability manifests itself at two points in the evolution of very massive stars, once at the termination of core hydrogen burning, then again at the termination of core helium burning.

The first phase, at the end of core hydrogen burning, occurs when the star contracts, evolving from a RSG toward a BSG phase. However the envelope may take several decades to readjust, during which time it is not in a state of equilibrium. It is at this point that the instability sets in ejecting the unstable part of the envelope, in cyclic outbursts until the equilibrium is regained. The instability is always found to occur when the stars effective temperature is less than 12,000K and then only occurs in stars more luminous than $10^6 L_\odot$. The surface hydrogen abundance during this instability is predicted to be X_{surf}=0.2-0.4. It is found that the mass ejected in each outburst is sensitively dependent on the star's temperature, ranging from $10^{-2} M_\odot$ for a F-type supergiant to $1 M_\odot$ for an M-type supergiant. However the reoccurrence time scale is such that no more than a couple of erruptions are expected. In this interpretation the H-D limit is not a true zone of avoidance, but rather marks the end of core hydrogen burning, after which the star will continue its redward excursion, but on a time scale so rapid that we would not expect to see

any stars at this point in their evolution.

The second phase of instability comes 3×10^5yrs later when helium becomes depleted in the core and the envelope attempts a new phase of re-expansion. On this occasion the instability occurs at a hotter temperature of log $T_* = 4.3$. This is because the previous mass loss increases the L/M ratio and so reduces the amount of hydrogen and helium partial ionisation needed to bring $< \Gamma_1 >$ below 4/3. During this phase of instability surface hydrogen abundance is X_{surf}=0.2. Because of the much higher temperature during this second phase of instability, the unstable part of the envelope is much smaller 10^{-6}–10^{-4}M$\odot$ and consequently less mass is lost in each ejection. The re-ocurence time for these outbursts is quite uncertain lying between 1-100yrs, but overall the phase is expected to last about 10^4yrs. Finally, it is found that stars with an initial mass less than 30M$_\odot$ will not lose sufficent mass to suffer this instability. This implies that stars with an initial mass in the range 30-60M$_\odot$ or with a low metalicity, will only undergo this second phase.

Stothers and Chin (1995) investigated the periodicity of the outbursts during this second phase of instability. After the first phase of instability the star becomes a helium burning BSG, until the helium in the core is depleted, where upon the envelope cools and expands. The instability is then encountered causing a sudden loss of mass and so a rapid blueward shift of the stars position in the HRD. The increase in temperature restabilises the envelope structure, but does not halt the envelopes natural tendency to expand, making a further encounter with the instability inevitable. This makes the star hover blueward of the instability limit with a highly constrained mass loss rate. If the mass loss rate is too great the star will evolve blueward, too low and it will re-encouter the instability. Detailed hydrodynamical models (Stothers & Chin 1995) find this mass loss rate at 4-8$\times10^{-5}$M$_\odot$ yr^{-1}. Using the hydrodynamical models they find a relation between the mean period of these oscillations and the stars luminosity.

$$M_{bol} = (-12.9 \pm 0.5) + (2.4 \pm 0.5) log P$$

They suggest a good agreement between this period and the observed mean periods of normal outbursts of LBVs. They also note that the occurrence of shorter periods at higher luminosities is probably incompatible with the star suffering some kind of pulsational variability, like strange mode pulsations.

In summary this model may reproduce a number of features associated with LBVs, as it broadly predicts, their temperature at quiescence, their mass loss rates, the periodicity of the normal outbursts, the masses and the chemical composition of the nebulae. However, in the light of observational and recent theoretical work, this well developed model appears untenable as an explanation of the LBV phenomena.

Typically LBV nebulae have dynamical ages of 10^4yrs. In the models of Stothers and Chin there is a period of 3×10^5yrs between the initial ejection of the nebula (the first phase of instability) and the normal LBV-like outbursts (the second phase of instability). The LBV HD 168625 has a nebula with a dynamical age of 3000yrs (Hutsemekers et al. 1994), while the nebula surrounding HR Car has a dynamical age of 5000yrs (Nota et al. 1996). Fundamentally, the Stothers and Chin instability is associated with the envelope trying to expand toward the end of hydrogen and helium burning. The period between these phases is two orders of magnitudes greater than some nebular dynamical ages. Smith et al (1997) argue that the nebular dynamical ages do not properly reflect the true ages of the nebulae, suggesting that the dynamical ages should be based on the lowest velocity observed, rather than the velocity implied by the dominant peak in the split line-profile. However the lowest velocity components in the nebula line profiles are often very weak and could be material lost during a previous evolutionary phase when the terminal velocity was lower or slow clump material embedded in a fast wind. Even if the lowest possible expansion velocities are used, the implied upward revision to the nebular dynamical ages is only a factor of four, far short of the factor of one hundred needed in the

case of some nebulae.

In the Stothers and Chin model the second phase of instability, evoked to explain the normal LBV outbursts, does so by attributing the variation to"...changes in the size of the optically thick ejected cloud" (Stothers & Chin 1995). However, atmospheric modelling has shown that enhanced mass loss is unable to reproduce the required variation in radii between the maximum and minimum states (Leitherer et al 1989; de Koter et al. 1996). Consequently the assumption made by Stothers and Chin that the ejected mass will cause the effective temperature to vary in the way observed, does not seem justified.

In this framework the LBV nebulae are formed in the first phase of instability. This only occurs for stars with an initial mass greater than $60M_{\odot}$ (Stothers & Chin 1996). Consequently the model predicts that only the LBVs with initial masses greater than this should have nebulae. Contrary to this most LBVs have nebulae (Nota et al. 1995), the vast majority of which are believed to be have had initial masses substantially less than $60M\odot$. This problem is extenuated by the work of Langer (1997) which suggests that the most massive stars will encounter their Ω limit and incur heavy mass loss rates preventing their evolution to the cool temperatures where the nebula forming instability is encountered. This implies that not even the few very massive LBVs should have nebulae.

Stothers and Chin (1996) address some of these difficulties relating to the LBV nebulae, by revising the prediction that they are formed by the first phase of instability. Instead they suggest that the nebulae could "...constitute material ejected more or less continuously during the blue LBV phase its self". This is incompatible with the nebula abundances (Mitra&Dufour 1990; this thesis). With this modification, the model loses much of its rason d'etre, the nebulae remain unexplained, as do the normal LBV variations if they cannot be attributed to enhanced mass loss

(Leitherer et al. 1989; de Koter et al. 1996).

1.4.4 The Effects of Shocks.

We will very briefly draw attention to the possible connection between the H-D limit and micro-turbulence. Nieuwenhuijzen et al. (1994) have proposed that the micro-turbulent line broadening seen in the atmospheres of super- and Hyper-giants, may originate from fields of shocks moving out through the stellar atmosphere. They find that the strength of these shocks increases with increasing stellar luminosity. Consequently they suggest that these shocks could be the origin of the mass loss which manifests itself as the forbidden zone inside the HD-limit.

While these results show that shock wave pressure is undoubtedly of importance in modeling the atmospheres of luminous stars, the work does not demonstrate that this phenomena is intimately connected with the H-D limit. Nieuwenhuijzen et al. (1995), estimate the relative importance of the accelerations due to Newtonian gravity, radiation pressure, wind pressure and shock pressure at various luminosities and temperatures. They conclude that above 10,000K in stars more luminous than log $L/L_{\odot}$=5.4 on a blue-ward evolving track, the shock pressure is the least important of these accelerations. Consequently shock pressure cannot be the dominant factor in explaining the H-D limit.

1.4.5 Strange Mode Pulsations.

We will conclude our discussion of the H-D limit by reviewing recent investigations into strange mode pulsations, which appear to be able to reproduce many of the characteristics associated with LBVs (Glatzel&Kiriakidis 1993; Glatzel 1994; Cox 1996). The possible connection between strange mode instabilities and the H-D limit

were first suggested by Glatzel&Kiriakidis (1993):

"Violent mode-coupling instabilities are identified which could account for the LBV phenomenon. The stability boundary seems to be related to the Humphreys-Davidson limit."

Any adequate explanation of strange-mode instabilities must address two issues, how the strange modes arise and why they become unstable. Strange modes were found to occur in stellar models with a pronounced core-halo structure and a high luminosity to mass ratio. The outer envelope of such a star is comprised of tenuous plasma, which has a low heat capacity, implying that heat cannot be stored. Consequently Glatzel (1994) argues that strange modes cannot have a thermal origin. This means that they cannot be driven by either the κ or η mechanisms, both of which require a store of thermal energy. This is supported by the occurrence of strange modes in numerical models which assume a heat capacity of zero. This implies that strange modes may have an acoustic origin. Further evidence of the acoustic nature of strange modes comes from the fact that their frequencies are related to the sound travel time between the stellar surface and and the outermost opacity maxima.

A physical explanation of the strange-mode phenomena is given in an insightful paper by Glatzel (1994). The key to this interpretation is a demonstration, that in a star where the gas pressure is much less than the radiation pressure, the sound speed is the rate of change of pressure with density at a constant absorption coefficient, rather than the rate of change of pressure with density at a constant temperature. The reason for this is that to evaluate the sound speed a constant temperature, implicitly carries the assumption that it is the thermal motion of the gas which is causing the pressure, but if it is the radiation pressure that is dominant, then this is inappropriate. Consequently the definition must be modified.

$$\beta = P_{gas}/P_{total}$$

$$C^2 = dP_{gas}/d\rho \text{ with temp=const}$$

$$\text{but as } \beta \rightarrow 0$$

$$C_\kappa^2 = dP_{total}/d\rho \text{ with } \kappa = const$$

Where C is the sound speed, P is the pressure and ρ is the density. This allows opacity maxima dua to create acoustic barriers within the structure of the stellar envelope. Each acoustic box/region then has its own spectrum of acoustic modes. However which sound speed is appropriate depends not only on β, but also the frequency of the mode that we are considering. The effect of reducing β is to increase the range of frequencies for which the absorption dependent sound speed becomes applicable.

The instability of the strange modes then arises as a consequence of this redefinition of the sound speed. In the original definition the relation between a change in the pressure and density is a linear one. Consequently the density and pressure pertibations are always in phase and so these modes are stable. In the new definition, the sound speed is given by a differential equation, applicable to the altered physical conditions (i.e insignificant gas pressure compared to the total pressure). This allows a time lag between the pressure and density pertibations, resulting in a growth or decay of the oscilations. That is, these modes are unstable. The differential character of the new expression for the sound speed is caused by the incorporation of the diffusion equation for radiation transport.

While both radial and non-radial strange modes have been found to occur in pulsation models (Cox 1997), it is the former that have aroused most interest with regard to LBVs. This is because radial strange-mode instabilities have fast growth times and acheive large radial amplitudes, of the order of 200 km s^{-1} (Cox 1997). That rate of mass loss associated with these instabilities is unclear since detailed non-linear numerical modelling has yet to be performed. However Glatzel et al (1994) suggest that a mass loss rate of the order of $10^{-3}M_\odot$ yr^{-1} could result from

a pulsationally driven wind.

In the models of Cox (1997) strange mode-instabilities produce explosive motions deep within the star in layers with a temperature of 200,000K. This is consistent with the finding by de Koter et al. (1995) and Lietherer et al. (1989) that LBV outbursts are caused by a deep seated subphotospheric mechanism. The instability strip were these outbursts occur is found to lie between 10,000 and 30,000K, which incorporates both the observed position of the LBVs and the H-D limit. If the star is impinging on its modified Eddington limit, each pulsational cycle will expell mass revealing deeper layers, more enriched in helium and consequently of a lower opacity. The reduced opacity will increase the modified Eddington limit and so eventually terminate the mass loss. Cox et al. (1997) finds that the pulsations through which the mass is lost terminates when the helium reaches a surface abundance of Y=0.4. This has implications for the nebular abundance patterns, in that it suggests that the nebula will be comprised of material slightly less processed than Y=0.4. After this the star will settle and pulsate while it remains in the instability strip. This latter phase may be what we observe as normal LBV outbursts.

1.5 Nebulae Surrounding Massive Stars.

Nebulae are found surrounding many massive post-main sequence stars . From the suveys of Marston et al. (1994, 1997) and Chu et al. (1982, 1988) it has been found that about one third of WR stars are surounded by nebulae. Ring nebulae are most frequently found surrounding the WN sub-type, which accounts for about half of all the nebulae.

These figures include both WBB and ejecta nebulae. The ejecta nebulae that we are concerned with, tend to be associated with WN8 stars, although they are

sometimes found surrounding WN6 and WN5 stars. No ejecta nebulae have been found surrounding any WN7 stars. These findings are consistent with the evolutionary sequence outlined in section 1.2 where we reviewed evidence that WN7 stars represent the product of evolution directly from Of stars into WR stars, without any intermediate LBV or RSG phase. In section 1.3.2 we noted that WN6,7 and WN8,9 stars appear to form two distinct groups, with the former representing the desendents of the most massive stars. The presence of ring nebulae surrounding some WN6 stars suggests that some have evolved through a RSG or LBV phase. This casts doubt on whether WN6 and WN7 stars are evolutionarily connected.

The other type of massive post-main sequence stars with which ejecta nebulae are frequently associated are the LBV stars. Indeed ejecta nebulae are a ubiquitous feature of both LBVs stars and their dormant phase the Of/WN9 stars (Nota et al. 1995). At the present time it is not clear whether the LBV phase follows a RSG phase or whether the LBV phase occurs during the stars redward evolution, preventing any subsequent RSG phase. However, the weight of opinion is that LBVs evolving below the HD limit are post RSG objects. This leads to the question of how and when do they eject their nebulae? This question is the central theme of this thesis. Essentially two possibilities seem viable: that the LBV wind sweeps up the previous RSG wind into a shell (Garcia-Segura et al. 1996) or that the LBV suffers some type of instability leading to a very enhanced mass loss rate (which we will refer to as ejecting a nebula).

How then do we distinguish ejecta nebulae formed by the sweeping up of RSG material from those formed by an ejection event? This issue has been tackled by Garcia-Segura et al. (1996) who has used a hydrodynamic code coupled to the evolutionary code of Langer et al. (1994). In this work the evolution of circumstellar matter surrounding a $60M_{\odot}$ and a $35M_{\odot}$ star has been modelled. The former case includes a period of high mass loss representing the LBV phase, while the latter includes a RSG phase evolving directly into a WR star. The modelling of the LBV

nebula must be teated with caution since the nature of the nebula forming mass loss is not known and so the choice of enhanced mass rate is somewhat arbitary,. This is a critical assumption in the model and at present is not observationally constrained. Indeed if strange mode pulsations or interactions with the Ω limit plays an important role, then this will alter the models predictions. In contrast the modelling of the circumstellar medium surrounding the $35M_{\odot}$ star appears more reliable, with the main uncertainty being the terminal velocity of the RSG wind. This has been addressed by computing two models, one with a terminal velocity of 15 km s^{-1} and the other with a terminal velocity of 75 km s^{-1}. These should be treated as two limiting cases and so give a good indication of what nebulae formed from swept up RSG material could look like.

This work reveals two excellent discriminators between nebulae formed by swepted up RSG material and nebulae of the type seen around LBV stars. These discriminator are the radius and mass of the nebulae. The modelling predicts that nebulae formed from RSG material should not become visible until they have attained a radius of between 3pc and 10pc (depending on the choice of RSG terminal wind velocity). Furthermore virtually all the mass lost in the RSG phase will be visible leading to a nebula mass of between $10M_{\odot}$ and $20M_{\odot}$. In Table 1.1 we give the dynamical properties of a number of ejecta nebulae surrounding WR and LBV stars. From this Table we see several nebulae surrounding WR stars have just the properties predicted for nebulae comprised of swept up RSG material. These objects contrast sharply with those nebulae seen around LBV and some other WR stars, which are characterised by masses of a few $M_{\odot}$ and radii of less than a parsec. All the nebulae studied in this thesis are incompatable with the predicted proporties of nebulae formed from swepted up RSG material and so we favor their formation being caused by a period of enhanced mass loss.

In addition to the dynamical properties of the nebulae, their chemical composition can also shed light on the origin of the nebulae. To date the only abundance

Nebula parameters					
Nebula	Radius (pc)	Expansion velocity (Km sec^{-1})	Dynamical timescale (x10^3yrs)	Nebular mass ($M_\odot$)	Spectral Type
R127	2.2[3]	53[3]	40[3]	3.1	LBV
RCW 58	2.6/3	87/100[1]	30[1]	1.5	WN8
He3-519	1.4[2]	61[2]	20[2]	2	LBV(?)
WRA 751	0.4[5]	26[5]	15[5]	–	LBV(?)
M1-67	0.5[1b]	42[1b]	13[1b]	0.8	WN8
AG Car	0.6[2b]	70[2b]	8.4[2b]	4.2	LBV
NGC 6164/5	1.0[4]	350[4]	3.5[4]	2	Of6.5p
HD 168625	0.15	40[3b]	1[3b]	0.03	LBV(?)
HR Car	0.06[3c]	110[3c]	0.8[3c]	2.1	LBV
P Cygni	0.2[3]	140[3]	0.4-0.8	0.01	LBV
NGC6888	3[6]	85[9]	35[6]	>9	WN
S308	9[7]	60[10]	146	26	WN5

Table 1.1: A review of the dynamical properties of LBV and WR nebulae.

references: (1)Esteban et al. 1991 (b=1990 c=1992), (2)Smith et al. 1994 (b=1996), (3)Nota et al. 1995 (b=1996, c=1996), (4) Leitherer et al. 1996, (5) Hutsemekers et al. 1991, (6) Esteban et al. (1993), (7) Marston et al. (1996), (9) Martson & Meaburn (1988), (10) Chu et al. (1993).

studies which have been attempted for nebulae surrounding LBV stars, are two abundance studies of the nebula surrounding AG Car (Mitra & Dufour 1990; de Freitas Pachaco et al. 1992). The first of these did not accurately detect any temperature diagnostic lines and so were forced to assume an electron temperature, while the second detected the temperature diagnostic lines, but deduced a temperature of 12,400K which is unrealistically high considering the low extcitation of the ionic spiecies observed.

Consequently no reliable abundance studies have been made of nebulae surrounding LBV stars. However, several abundance patterns have been derived for nebulae suounding WR stars (Esteban et al. 1991, 1992; Kwitter et al. 1984). The results of these abundance studies are presented in Table 1.2. These studies find an agreement between the derived abundance patterns and that expected to arise during the RSG phase in the evolutionary models of Meynet et al. (1994).

In addition to the ejecta nebulae surrounding LBV and WR stars, at least one Of star is also surrounded by an ejecta nebula. HD 148937 is a luminous Of star surrounded by the bipolar nebula NGC 6164/5 which is comprised of partially CNO processed material (Leitherer et al. 1987; Dufour et al. 1988). At present there are no tenable explanations in the literature as to how this nebula formed. Essentially this is because neither an LBV phase nor a RSG phase can be accomadated as a precoursor to an Of star phase, within the current evolutionary scenarios. HD 148937 is the subject of chapter 5 of this thesis, in which we offer an interpetation of this nebula in the context of a modified LBV phase.

1.5.1 η Carinae

We will close this introduction by commenting on the most exceptional LBV, η Carinae. η Car displays a number of fundamental differences from all other LBVs,

	Abundances	12+log(N(X)/N(H))			
Nebula	N/H	O/H	Log N/O	Sp Type	Refs
M1-67	8.45 ± 0.15	7.98 ± 0.27	0.47	WN8	a
NGC 6888	8.40 ±0.35	8.11 ±0.28	0.30	WN6	b
RCW58	8.07	8.49	−−0.4	WN8	c
S308	8.25	8.03	0.22	WN5	g
HII region	7.57	8.70	−−1.13		d
$60M_{\odot}$*model*	8.7	7.4	1.3	LBV	e
SN 1987A	8.3±0.2	8.2±0.2	0.14	RSG	f

Table 1.2: Abundance patterns determined for WR nebulae.

References: (a) Esteban et al. (1992), (b) Esteban et al. (1991) (c) Kwitter (1984), (d) Shaver et al (1983), (e) Langer et al. (1994), (f) Panagnia et al. 1997, (g) Esteban (thesis 1992).

which may well be indicative of it forming via a different evolutionary route. These differences raise questions about whether the variations seen in this luminous blue star arise for the same physical reasons as the variations seen in other LBV stars.

η Car is an extremely luminous star log $L/L_{\odot}$=6.6, this leads to an estimate of its initial mass as being more than $120M_{\odot}$, almost twice that of any other LBV. In section 1.2 we saw that there is strong observational evidence that the most massive stars evolve directly from the Of star phase into WN7 stars, without any intermediate LBV or RSG phase. Clearly η Car is not following this route, but why is η Car so exceptional? Furthermore η Car is surrounded by a nebula containing CNO equlibrium abundances (Dufour et al. 1997), as we will see this is quite different from the three LBV nebular abundance patterns that we derive in this thesis. From I.R studies of the dust in the nebula surrounding AG Car and HR Car, Waters et al. (1997) find that the dust particles have cooled slowly, allowing the formation of cystaline dust. This is in contrast to their study of the dust surrounding η Car which contains amorphous dust grains implying a faster rate of cooling. Dynamically the ejecta nebula surrounding η Car is also very different from that seen surrounding other LBV stars. η Car's nebula is expanding at almost an order of magnitude faster (600 km s^{-1}) than is typical for LBV nebulae. This leads us to question whether this nebula was ejected via the same mechanism as the other LBV ejecta nebulae.

Further doubt as to whether η Car is characteristic of the LBV class, is cast by the recently reported detection of periodicity in its photometry (Damineli et al. 1997). If confirmed this may suggest that η Car may be some kind of massive, close interacting binary system. Given the uncertainties in the evolutionary history of η Car and the stark physical and chemical differences between its ejecta nebula and those surrounding other LBVs , we will not assume that η Car is suffering the same instability as the other LBV stars. Since we aim to use the nebula properties to infer the physical conditions on the surface of the star when the nebula is ejected, it would not be helpful to include η Car in our sample of stars from the litterature

used to support our analysis.

Chapter 2

An abundance study of AG Car's nebula.

2.1 Introduction

Extensive multi-wavelength observations of AG Car have established it as the Rosetta Stone for the interpretation of LBVs. Despite the frequency of the investigations, AG Car continues to reveal many new insights into the LBV phenomena. The work presented here aims to throw new light on the previous evolutionary history of the star by studying the nebular abundance pattern and dynamics. In this chapter we will present the results of the abundance study, while a study of the dynamics will be deferred to a later chapter.

The abundance study is based on observations obtained at the Anglo-Australian Telescope in 1992 by L.J. Smith, C. Esteban and J.M. Vilchez. I undertook the abundance study, supervised by Dr Smith who presented the results as a paper in the Monthly Notices of the Royal Astronomical Society ("The AG Carine Nebula: An abundance of evidence for a RSG progenitor"; MNRAS, 290, 265-275, 1997).

The presence of a nebula surrounding AG Car was established by Thackeray (1950). A narrow band Hα image of the nebula is displayed in Figure 2.1. Thackeray notes that the nebula is not of uniform brightness, but rather is an elliptical ring nebula with angular dimensions of 39" by 30". The first spectroscopic observations of AG Car were made by Johnson (1976) and Thackeray (1977). These indicated an expansion velocity of 50 km sec $^{-1}$, which at the distance then assumed for AG Car of 2.5 kpc, implies a dynamical age of 3x10^{3}yrs. However, later determinations of distance to AG Car using the reddening method (Hoekzema et al. 1992) and its radial velocity combined with the Galactic rotation curve (Humphreys et al. 1989) established its distance as 6kpc. This implies a greater dynamical age of about 10^{4}yrs. At a distance of 6kpc, its projected dimensions of 39" by 30" equate to a size of 1.1$\times$1.0pc.

Johnson (1976) noted a large [NII]λ6584/Hα ratio, which suggested that the nebula could be comprised of CNO processed material. In addition to this he finds the spectra show moderate [SII] lines, weak [OII] and no detectable [OIII] lines indicating that the AG Car nebula is of a low excitation.

Resolving the detailed structure of the nebula surrounding AG Car is a challenging observational task, as it involves imaging faint features close to a bright central source. Such work has been undertaken by Paresce and Nota (1989) who used the STScI chronograph on the ESO 2.2m telescope to obtain multi-wavelength broad band images of AG Car's nebula. This revealed the presence of two bipolar outflows, one extending to the NE the other to the SW. Emission from these features arises through the scattering of stellar continuum by the dust present within them.

The first major infra-red study of AG Car's nebula was preformed by McGregor et al. (1988). They detected far-infrared emission from cool dust associated with AG Car's nebula. It was found that the dust emission is enhanced in a bar running

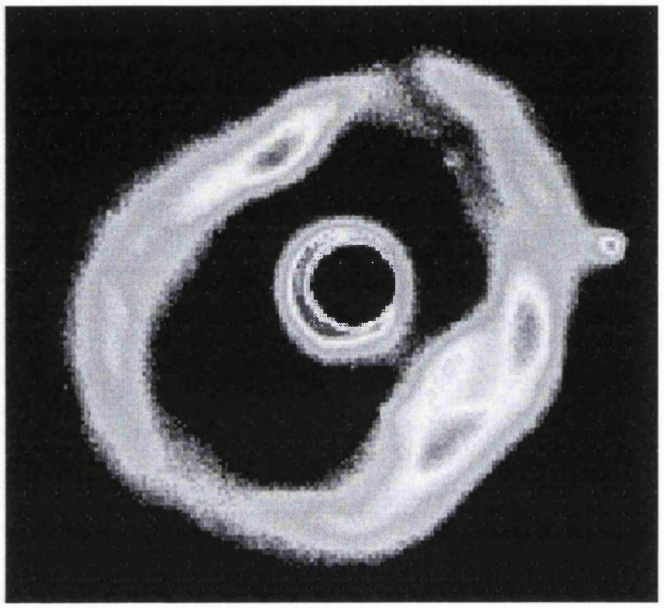

Figure 2.1: A deep Hα Chronographic image of AG Car (Nota et al. 1992).

NE-SW, providing clear evidence for asymmetric mass loss. However it is interesting to note that no evidence is found for any shells outside the visible nebula. If AG Car has ejected multiple shells they lay unresolved within the ionised optically visible shell.

ISO observations of AG Car were obtained by Lamers et al. (1996) using ISO's Short Wavelength Spectrometer (covering 2.4-45.2 microns). They found the spectra to consist of two components, the tail of the photospheric energy distribution and the emission from the circumstellar material. The former was modelled to yield the stellar parameters of T_{eff}=13000K, R_*=250$R_\odot$ and $\dot{M} = 9\times10^{-5}M_\odot$ yr^{-1}, while the emission from the nebula implied a dust mass of 0.03$M_\odot$. The solid state features revealed in these ISO observations were subsequently analysed by Waters et al. (1997). They identified emission bands from both crystalline olivine and Polycyclic Aromatic Hydrocarbons. The presence of crystalline olivine is particularly interest-

ing as it suggests a comparatively high temperature in the dust formation region.

A revealing piece of evidence in determining the evolutionary history of AG Car is the abundance pattern of the nebula. This can then be compared to stellar models to determine the evolutionary state of the star at the epoch of ejection. However the abundance determination requires the acquisition of deep spectroscopic images, in order to resolve weak diagnostic lines.

The first abundance study of the nebula surrounding AG Car was carried out by Mitra and Dufour (1990). Their data set did not detect the key temperature diagnostic line [NII] 5755, but did allow them to establish a 2σ upper limit on its possible line strength. Using this they infer an electron temperature of 9000^{+1000}_{-2000}K and a density of 800±200 cm^{-3}. Using these physical conditions in conjunction with the measured line fluxes they determined the total elemental abundances of nitrogen, oxygen and sulphur. These were found to have abundances (12+logX/H) of 7.5, 7.2 and 5.7 respectively, implying an under-abundance of oxygen and sulphur, but a normal nitrogen abundance with respect to galactic HII regions (Shaver et al. 1983).

This clearly demonstrated that the nebula is comprised of material ejected from the central star. However it presents us with several problems. Why is sulphur deficient when its abundance is not thought to be altered by any nucleosynthetic processes? Furthermore, if the depletion in the oxygen abundance is not mirrored by an enhancement in the nitrogen abundance, then where has the oxygen gone?

In light of these questions a second abundance study was preformed by de Freitas Pacheco et al. (1992). In this study the [NII] 5755 line was detected and yielded an electron temperature of 12400±100K. Considering the low ionization character of the nebula this is a surprisingly high temperature. From the sulphur lines the nebula was found to have a density of 1230±60 cm^{-3}.

Using these physical conditions de Freitas Pacheco et al. (1992) derive the ionic abundances for the singly charged species of nitrogen, oxygen and sulphur. In order to find the change in the nitrogen abundance they make the assumption that the sulphur abundance is cosmic, counter to the earlier result of Mitra and Dufour. Their N/S ratio then implies that nitrogen is enhanced by an order of magnitude, while their N/O ratio equals 7. Together these results imply that oxygen should be under-abundant by at least a factor of 6.

The ionised mass of the nebula has been determined by Nota et al. (1992). They estimated this using recombination theory to find the mass of hydrogen gas required to emit the the integrated Hα flux obtained in their chronographic images, under the physical conditions derived for the nebula. This implies an mass of $4.2M_{\odot}$.

In the light of the above discussion we see that AG Car's nebula abundance pattern remains uncertain. Given the pivotal role that AG Car has played in the study of LBVs, this situations appears in need of re-dress. Primarily, the uncertainties in the previous abundance studies are a consequence of not having established a reliable electron temperature. In the abundance study that follows we will use a new data set based on deeper exposures to address this problem.

2.2 Observations and Data Reduction.

The observations used in this abundance study were made using the Anglo-Australian Telescope (AAT) at the Siding Springs Observatory on the 20^{th} and 21^{st} March 1992. The data were collected by L.J Smith, C. Esteban and J.M Vilchez. They conducted deep long-slit spectroscopy of the nebula using the RGO spectrograph in conjunction with the 82cm camera and a blue Thomson CCD (see Table 2.1).

Date	Wavelength Range (Å)	Exposure Time (sec)
(a) slit position 1 PA= 131°		
1992 March 20	3578–4520	2000
1992 March 20	4417–5360	2000
1992 March 20	5282–6231	1000
1992 March 20	6180–7125	500
1992 March 21	8896–9772	1000
(b) slit position 2 PA= 30°		
1992 March 20	3578–4520	2000
1992 March 20	4417–5360	1000
1992 March 20	5282–6231	1000
1992 March 20	6180–7125	500
1992 March 21	8896–9772	1000

Table 2.1: Journal of Observations.

Observations were made using the 250B grating covering the wavelength range 3578-7125Å and the 270R grating covering the wavelength range 8896-9772Å. The latter being designed to detect the [SIII] 9531Å line. This then allowed us to determine the ionic abundance of S^{++}. However, this is based solely on the [SIII]λ9531 line which may well be affected by water absorption features. Consequently, this abundance represents a lower limit.

Long slit spectroscopic observations were taken at two offset positions from the star. The first had a position angle of 131^o and an offset of $\Delta\alpha$=7 arcsec west and $\Delta\delta$=8 arcsec south. The second had a position angle of 30^o and an offset of $\Delta\alpha$=6.3

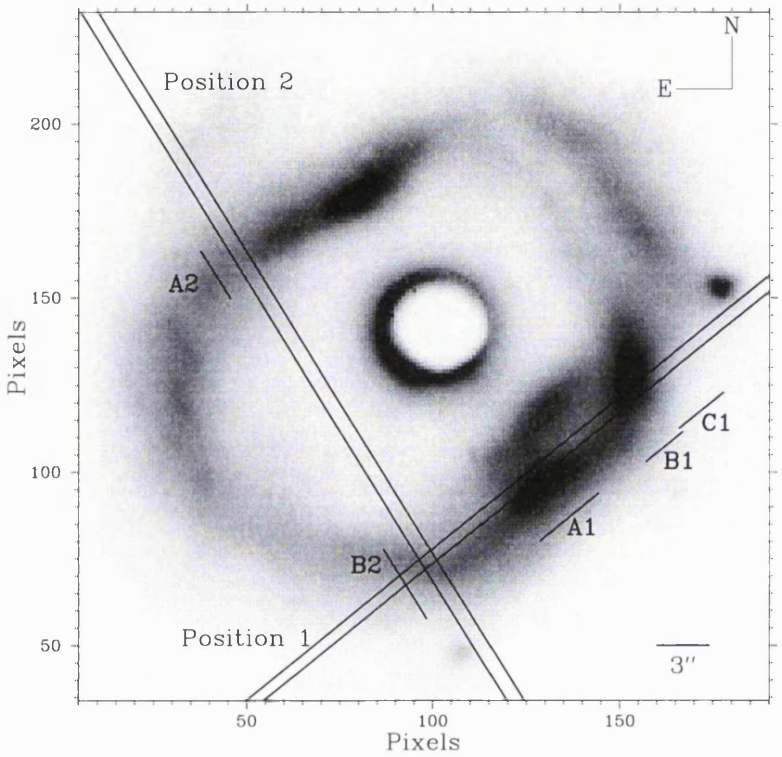

Figure 2.2: AG Car's nebula with the slit positions and extraction regions superimposed.

arcsec west and $\Delta\delta$=4 arcsec south. The slit used was 1" across and 180" long, giving a spatial resolution of 1pix=0.56 arcseconds and a spectral resolution of 4Å. During the observations the "seeing" conditions were typically 2". The slit positions used are shown in Figure 2.2.

The resulting spectral images were reduced using the STARLINK packages "FIGARO" and "DIPSO". The first stage in the reduction process was to remove the bias and divide through by a median flat field. Because of the deep exposures required to detect the [NII] 5755Å line, our images needed to be cleaned of cosmic rays. A region of sky was identified in each image allowing us to subtract the sky from the image. Finally the spectra were then corrected for atmospheric extinction.

To wavelength calibrate the spectra we used the Argon comparison arcs taken at regular intervals in between the nebula spectrum. First a spectrum is extracted from the long-slit image of the arc and the lines are identified over the whole wavelength range covered. A package within FIGARO is then used to trace the variation of pixel position of the identified lines at successive spatial positions up the 2-D arc image. This generates polynomial coefficients describing the variation in wavelength over the two dimensional image. The wavelength calibration is then done by mapping this wavelength grid onto the nebula images.

In order to flux calibrate the spectra, observations were made of the water vapor standard star CD -22°7696. The calibration of this star was done using spectrophotometric observations of the standard star LTT 4364 (Stone & Baldwin 1983). These were then used to construct flux calibration curves for our data set. Great care must be taken to ensure that the flux calibration curves were of the correct shape, any erroneous "kinks" could artificially strengthen a arbitrary line. To counter this we ensured the curves smoothness in the region of important lines, as well as repeating the procedure to produce several curves to check for consistency. To flux calibrate the 270B grating data, we scaled the continuum so that it was consistent with the flux calibrated continuum for the bluer spectral regions. An additional check was then made by ensuring that the extinction coefficient implied by the P8, P9 and P10 lines were consistent with that previously determined using the Hydrogen Balmer series.

Spectra were extracted from several spatial regions in order to test the chemical uniformity of the nebula, since any differences may shed light on its history. The bipolarity of the nebula is suggestive of shaping by a pre-existing equatorial density enhancement. However if material has been ejected from AG Car at different epochs, then they will have different chemical signatures. If an earlier phase of mass loss was asymmetric then this would lead to a difference between the polar and equatorial abundance pattern. By probing the chemical and physical uniformity we can place

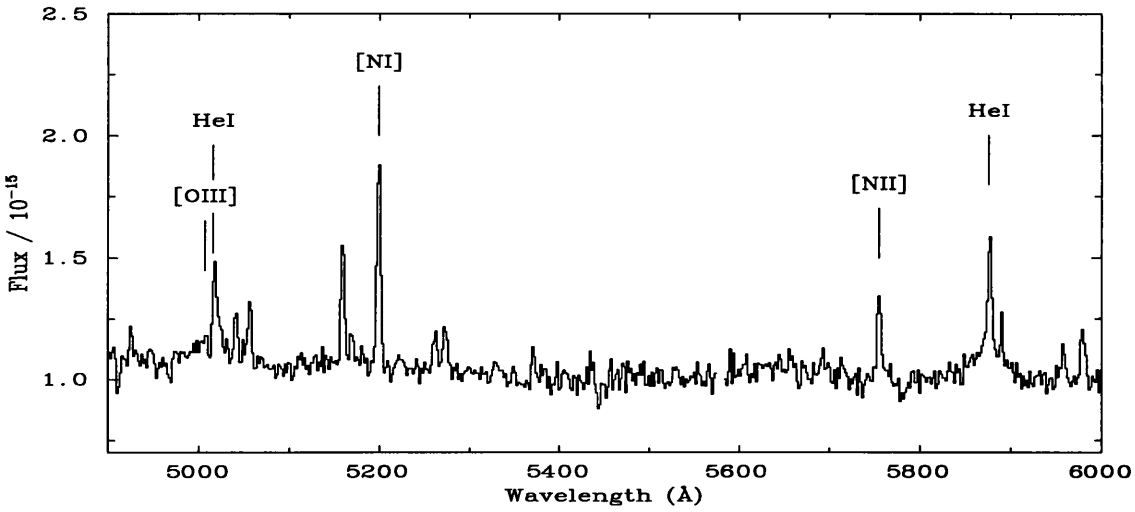

Figure 2.3: A spectrum from AG Car which includes the [NII]λ5755 line

constraints on such models.

From the first slit-position (P.A.=30) spectra were extracted over three regions; A1(extent 4.5 arcsec) covering the bipolar dust feature (Paresce and Nota 1989); B1(2.8 arcsec) covering a bright clump near the edge of the nebula and C1(3.4 arcsec) covering a region of emission next to B1. For the second slit position (P.A=130) two regions were chosen; A2(3.4 arcsec) and B2(5.0 arcsec) which cover the fainter outer regions of the nebula. The precise locations of these five regions are shown in Figure 2.2. In each position extracted the [NII]λ5755 line is clearly detected (see Figure 2.3). For the first time this allows an accurate determination of the temperature, to which the abundances are exponentially sensitive.

The nebula surrounding AG Car contains a great deal of dust which reflects light from the central star. Consequently we see the stellar continuum present in the nebula spectrum. This continuum rises steeply toward the blue, since this scattering process is more efficient at shorter wavelengths. In order to remove this continuum from our data, we fitted polynomials of a low order to it and subtracted it off.

Using the ELF package within DIPSO, we fitted Gausians to the line profiles. This allowed us to estimate the line flux, central wavelength and the rms errors associated with both. The resulting line fluxes (relative to H(β)=100) are given in Tables 2.2 and 2.3. By comparing the relative strengths of the Hα, Hβ, Hγ, Hδ and H line fluxes to those theoretically expected (Hummer & Storey 1987), we were able to determine the degree of interstellar reddening. In this way we found the extinction coefficient in the different regions ranged between $C(H\beta) = 0.76$ (A1) and $C(H\beta) = 1.25$ (C1) with a mean value of $C(H\beta) = 0.9 \pm 0.2$ (see Tables 2.2 and 2.3). The variation in extinction coefficient is attributed to extinction internal to the nebula. This is supported by recent HST imaging of the nebula (Nota et al. 1995) which shows that position C1 is particularly bright in continuum emission, suggesting the presence of a large quantity of scattering dust. Finally we note that our determinations of C(Hβ) agree well with previous determinations, $C(H\beta)$=0.71-0.75 (Mitra & Dufour 1990), $C(H\beta)$=0.81-0.91 (de Freitas Pacheco et al. 1992) and for the central star $C(H\beta)$=0.91 (Humphreys et al. 1989). The values of C(Hβ) that we derived were then used in conjunction with the formulae of Howarth (1983) to extinction correct the observed line intensities.

2.3 Analysis.

2.3.1 Description of the Spectra.

AG Car's nebular spectrum is characterised by a low degree of ionization (see Figure 2.4). This manifests itself through the absence of [OIII]λ5007 and clear presence of NIλ5200. The strength of the nitrogen and oxygen lines is indicative of the processed material from which the nebula is comprised. The [NII]λ6584 line is extremely strong, having typically two thirds the flux of the Hα line, while the only oxygen line

				A1		B 1		C1	
λ_{obs}	λ_{lab}	Ion	$k(\lambda)$	$F(\lambda)$	$I(\lambda)$	$F(\lambda)$	$I(\lambda)$	$F(\lambda)$	$I(\lambda)$
3727.1	3727.4	[OII]	0.257	4.94±0.53	7.75±0.82	3.10±0.23	5.31±0.38	1.67±0.16	4.41±0.43
3835.7	3835.4	H9	0.237	4.08±2.29	6.17±3.46	3.56±2.12	5.86±3.48	2.39±1.75	4.72±3.47
3889.2	3889.0	H8	0.226	7.32 ±2.36	10.88±3.51	6.09±2.10	9.79±3.38	5.51±1.8 8	10.57±3.61
3970.3	3970.1	Hϵ	0.210	11.06±2.31	15.97±3.33	10.02±2.16	15.55±3.36	8.94±1.86	16.37±3.41
4101.7	4101.8	Hδ	0.182	19.00±2.14	26.12±2.95	17.51±1.98	25.62±2.90	14.87±1.67	25.08±2.82
4340.6	4340.5	Hγ	0.127	35.86±1.33	44.76±1.67	35.47±1.13	46. 26 ±1.48	31.57±3.55	45.46±5.11
4474.7	4471.5	HeI	0.095					1.16±0.54	1.52±0.71
4861.5	4861.3	Hβ	0.000	100.00±0.59	100.00±0.59	100.00±1.53	100.00±1.53	100.00±6.36	100.00±6.36
5018.4	5015.7	HeI	−0.039	2.25±0.33	2.10±0.31	0.56±0.18	0.52±0.16	3.26±0.49	2.91±0.44
5198.9	5199.1	[NI]	−0.082	3.56±0.31	3.08±0.27	2.67±0.11	2.24±0.09	5.66±0.23	4.46±0.18
5754.9	5754.6	[NII]	−0.195	1.42±0.10	1.01±0.07	1.12±0.18	0.74±0.12	2.04±0.61	1.17±0.35
5876.9	5875.7	HeI	−0.215	1.65±0.30	1.13±0.20	1.37±0.29	0.87±0.18	3.85±0.59	2.07±0.32
6548.3	6548.0	[NII]	−0.318	145.51±3.45	83.40±1.98	138.45±3.61	70.92±1.85	185.38±4.86	74.22±1.95
6563.0	6562.8	Hα	−0.320	628.81±3.46	359.09±1.98	601.08±3. 63	307.34±1.86	957.45±4.94	381.03±1.96
6583.6	6583.4	[NII]	−0.323	472.16±3.41	268.26±1.94	435.21±3.60	221.15±1.83	570.18±4.79	225.01±1.89
6680.0	6678.2	HeI	−0.337	0.70±0.27	0.39±0.15			1.45±0.36	0.55±0.14
6716.6	6716.5	[SII]	−0.342	29.78±0.62	16.38±0.34	26.80±0.18	13.10±0.09	39.92±0.61	14.94±0.23
6730.9	6730.9	[SH]	−0.344	36.23±0.63	20.41±0.35	32.40±0.18	15.77±0.09	45.15±0.69	16.80±0.26
7066.5	7065.3	HeI	−0.388	2.41±0.34	1.22±0.17	1.49±0.23	0.66±0.10	5.85±0.61	1.91±0.20
9014.8	9014.9	P10	−0.599	5.43±0.83	1.99±0.10	6.56±0.98	1.94±0.10	10.02±1.70	1.88±0.23
9229.2	9229.0	P9	−0.596	7.17±0.83	2.56±0.29	9.19±0.98	2.63±0.28	15.06±1.78	2.71±0.32
9531.1	9531.0	[SIII]	−0.618	2.65±0.95	0.91±0.33	3.86±1.12	1.06±0.31	5.49±1.68	0.93±0.28
9546.3	9546.0	P8	−0.619	7.02±0.87	2.41±0.30	8.80±0.99	2.41±0.27	13.68±1.70	2.31±0.29
$C(H\beta)$				0.76		0.91		1.25	
$F_{obs}(H\beta)$[1]				1.35×10^{-13}		1.11×10^{-13}		5.27×10^{-14}	

[1] in ergs s^{-1} cm^{-2} integrated over the slit area given in the text for each position. (N.B. k(λ)is the extinction coefficient used, $F(\lambda)$ is the observed line flux and $I(\lambda)$ is the dereddened line flux.)

Table 2.2: Line fluxes for position 1.

				A2		B 2	
λ_{obs}	λ_{lab}	Ion	$k(\lambda)$	$F(\lambda)$	$I(\lambda)$	$F(\lambda)$	$I(\lambda)$
3727.1	3727.4	[OII]	0.257	4.00±0.55	6.42±0.87	4.38±0.38	6.90±0.61
3835.8	3835.4	H9	0.237	2.90±0.24	4.48±0.38	2.99±0.65	4.55±1.00
3889.5	3889.0	H8	0.226	5.60±0.37	8.50±0.56	6.35±0.76	9.49±1.08
3970.2	3970.1	Hϵ	0.210	10.70±4.73	15.75±6.95	10.64±0.81	15.44±1.19
4101.9	4101.8	Hδ	0.182	19.33±4.69	27.01±6.56	19.26±0.70	26.58±0.97
4340.3	4340.5	Hγ	0.127	35.15±4.77	44.39±6.03	36.48±0.71	45.68±0.88
4861.3	4861.3	Hβ	0.000	100.00±0.61	100.00±0.61	100.00±0.75	100.00±0.75
5017.4	5015.7	HeI	−0.039	1.79±0.26	1.67±0.24	1.51±0.39	1.41±0.36
5199.0	5199.1	[NI]	−0.082	5.68±0.27	4.88±0.23	4.69±0.15	4.05±0.13
5754.6	5754.6	[NII]	−0.195	0.82±0.24	0.57±0.17	0.98±0.29	0.69±0.20
5877.1	5875.7	HeI	−0.215	0.95±0.38	0.64±0.25	0.78±0.29	0.53±0.20
6548.0	6548.0	[NII]	−0.318	127.37±3.07	70.90±1.71	116.27±2.88	66.16±1.80
6562.8	6562.8	Hα	−0.320	610.43±3.05	338.49±1.69	564.45±3.15	320.53±1.78
6583.4	6583.4	[NII]	−0.323	394.72±3.05	217.70±1.68	370.36±3.15	208.88±1.78
6679.5	6678.2	HeI	−0.337	0.60±0.33	0.32±0.18	0.69±0.29	0.38±0.16
6716.4	6716.5	[SII]	−0.342	27.14±1.07	14.46±0.57	27.19±0.47	14.84±0.25
6730.7	6730.9	[SII]	−0.344	30.92±1.09	16.42±0.58	29.20±0.50	15.88±0.28
7066.6	7065.3	HeI	−0.388	1.45±0.30	0.71±0.15		
9014.8	9014.9	P10	−0.599	4.70±0.44	1.61±0.15	1.50±0.14	0.52±0.05
9229.2	9229.0	P9	−0.596	8.74±1.33	2.91±0.44	7.85±0.98	2.73±0.34
9531.1	9531.0	[SIII]	−0.618	4.81±1.04	1.54±0.33	3.38±1.23	1.13±0.41
9546.3	9546.0	P8	−0.619	9.87±0.92	3.16±0.29	10.25±1.20	3.42±0.40
$C(\mathrm{H}\beta)$				0.80		0.77	
$F_{obs}(\mathrm{H}\beta)$[1]				1.55×10^{-13}		2.08×10^{-13}	

[1] in ergs s^{-1} cm^{-2} integrated over the slit area given in the text for each position.
(N.B. k(λ)is the extinction coefficient used, $F(\lambda)$ is the observed line flux and $I(\lambda)$ is the dereddened line flux.)

Table 2.3: Line fluxes for position 2.

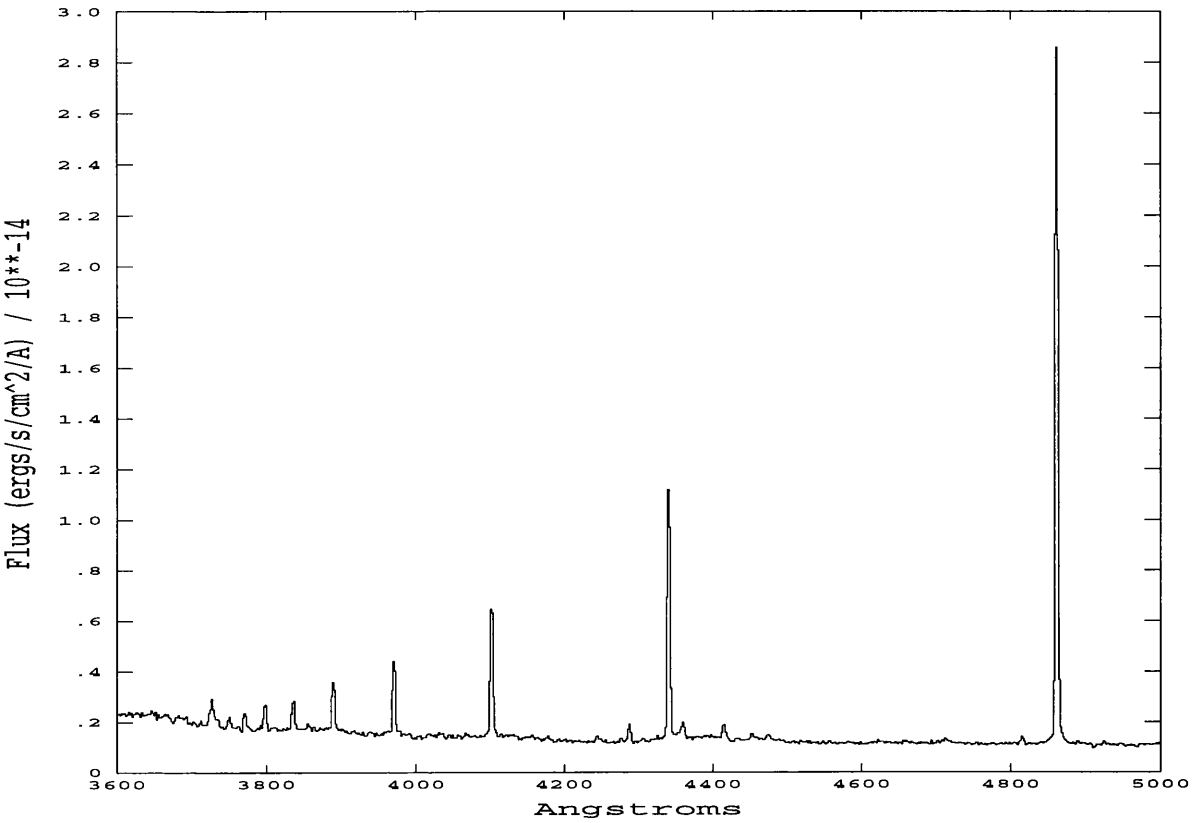

Figure 2.4: The H Balmer series emitted from AG Car's nebula.

detected is [OII]λ3727 with a flux of only 2% that of Hα (see Tables 2.2 and 2.3). While the [SII]$\lambda\lambda$6717,6731 are clearly detected having fluxes of about 15% Hβ, the [SIII] lines are surprisingly weak with [SIII]λ9531 having a flux of only 1.5% Hβ and [SIII]λ9069 not being detected at all. This may be a further manifestation of the nebula's low degree of ionization or an affect of the water absorption prominent at these wavelengths. Consequently we will regard our ionic abundance for S^{++} as a lower limit.

We note that in our spectra the nebular helium lines have an unusual line profile. This consists of a narrow emission line sitting upon a broad emission feature (see Figure 2.3). This profile can be understood in terms of the scattering of strong stellar helium lines by dust, to produce the broad components. The narrow component then represents the true nebular helium emission. Consequently when measuring

the helium line flux we fitted two Gausians to each line, allowing us to subtract off the broad component. There is no analogous problem for the hydrogen lines since the nebula component is dominant. A further peculiar feature of the helium lines is that they are all red-shifted by approximately 1.5Å with respect to the other nebula lines. In the case of HeIλ4471Å and λ5015Å this is explicable in terms of line blending with [FeII]λ4474.9Å and λ5018.4Å.

2.3.2 The Calculation of the Physical Parameters and Abundances.

In order to calculate the ionic abundances, we must first determine the physical conditions which prevail in the nebula. To determine the temperature we require two transitions with similar lifetimes, but which originate from different energy levels in the same ionic species. The similarity in life times means that the transitions will have the same probability of radiative decay and so the rate of decay will depend on the rate of pumping of each level. Since the energy of the levels differ, this will depend on the kinetic energy of the impacting electrons and so the electron temperature. Two lines with just these properties are [NII] 5755 and [NII] 6584. The ratio of these lines is strongly dependent on the temperature, with only a weak dependence on the density due to a slight difference in their decay lifetimes.

To diagnose the density we require two transitions originating from similar energy levels, but with a large difference in their transition probabilities. The similarity of the energy levels ensures that they are pumped equally, while the difference in transition probabilities means that collisional de-excitation is the dominant factor in determining the ratio of line fluxes. The most easily observed nebula lines with these properties are [SII]λ6717 and [SII]λ6731. By finding the physical conditions under which both the nitrogen and sulphur ratios can co-exist we determined the temperature and electron density at each of the positions analysed. To do this we utilised a program called "RATIO", which for a given line ratio this calculates the

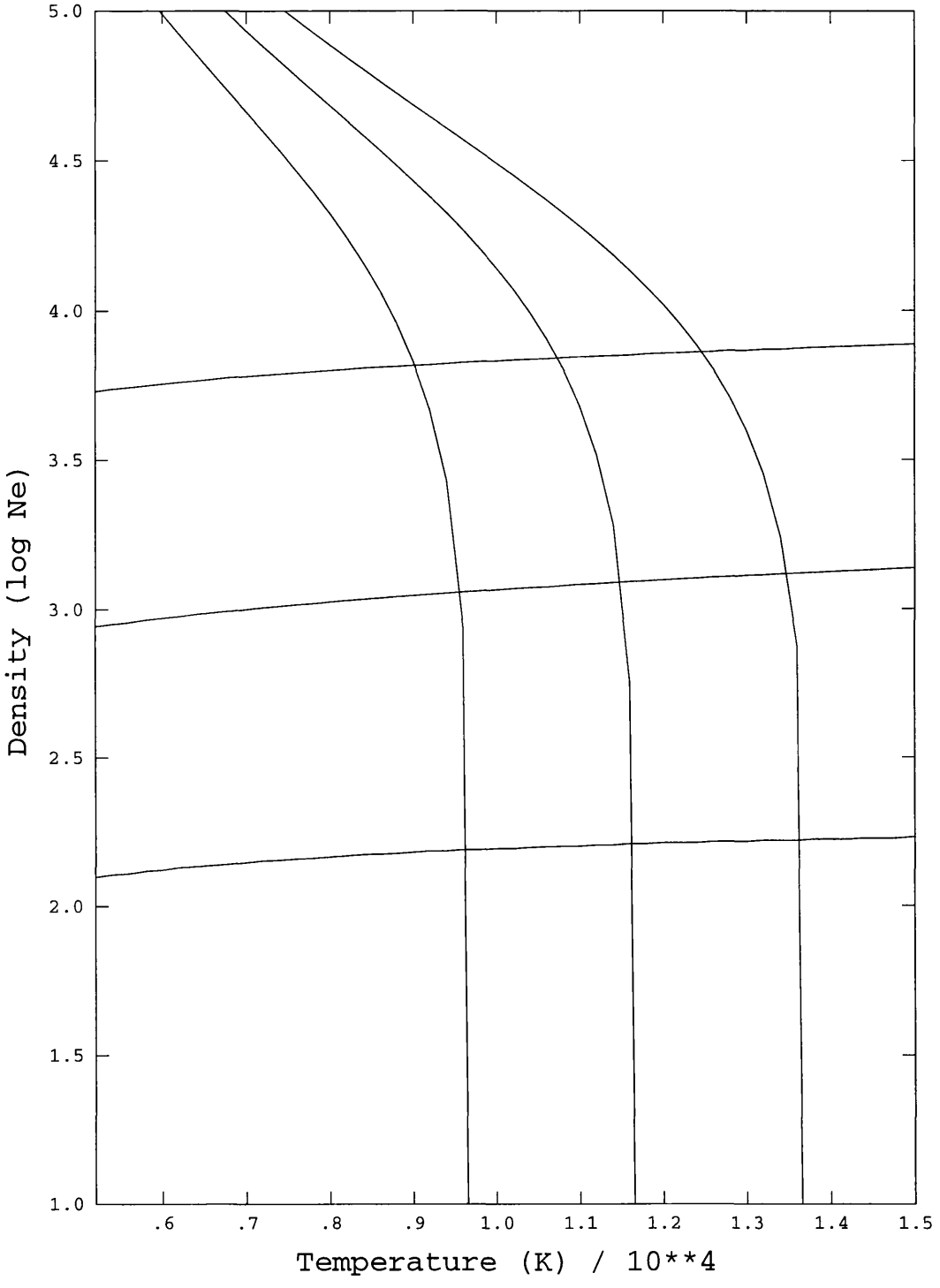

Figure 2.5: A diagram showing the variation of density with temperature implied by the observed line ratios (see text). The horizontal lines are the maximum, minimum and actual densities determined by the [SII] ratio and the vertical lines represent the temperature determined by the [NII] ratio.

implied electron temperature for a given electron density. By plotting such graphs for two line ratios we find under what unique physical conditions both line ratios are reproduced. An illustration of such a diagram is given in Figure 2.5, where the outlying lines are produced by using line ratios perturbed by the maximum error on the fluxes. This allows an assessment of the error on the electron temperature and density derived.

Once we have determined the temperature and density we can solve the equations of statistical equilibrium to find the ionic abundances. For collisionally excited lines the ionic abundance relative to hydrogen, is related to the ratio of de-reddened line intensities $I(\lambda)/I(H\beta)$ through the line emissivity of each ion $j(\lambda)$;

$$N(X^i)/N(H^+) = I(\lambda)j(H\beta)/I(H\beta)j(\lambda)$$

Where the line emissivity per ion is determined by

$$4\pi j(\lambda) = N_i A(\lambda) E(\lambda)$$

where N_i is the appropriate level population, $A(\lambda)$ Einstein transition coefficient and $E(\lambda)$ is the energy. In order to determine the level population, we use the electron temperature and density that we have previously derived. To then calculate the line emissivity we employed a program called "Equib" developed by M.J. Barlow. Using the line emissivity conjunction with the de-reddened line flux relative to $H\beta$, enables us to determine the ionic abundances. The errors on the resulting abundances were then assessed by recalculating the abundance implied by the maxium error on the electron temperature, density and the r.m.s error on the de-reddened line flux.

The ionic abundances were then summed to give the total abundance of each element. Since this is a low excitation nebula, we need only find the first couple of ionisation stages of each element. This is justified by the absence of HeII lines, which occur when HeI is ionised (I.P= 54ev). Consequently we would not expect any ionisation stages which require an ionising energy greater than this to be present and so we need only to find the ionic abundances of the following ionic species; N^+, N^{++}, O^+,O^{++}, S^+ and S^{++}. However our abundances are calculated with respect to H^+, emission from which comes from regions where no O^0 or N^0 could exist, since these species have a lower ionisation potential than hydrogen. This means that any emission detected from these ions must be emitted from a different spatial region that lies along our line-of-sight. Consequently we will not include these ionic abundances in the final elemental abundances.

2.4 Results.

This section will be comprised of three parts. Firstly we will report the results of our analysis of the physical conditions in the nebula. In the second part we will concentrate on the results of the abundance study, before finally placing these in context by comparing them with those derived for other nebulae.

From our analysis of the five extracted regions we find that the electron density varies between 600 e cm^{-3} (at B2) up to 1050 e cm^{-3} (at A1). This variation is probably associated with clumping in the nebula. The mean electron density, averaged over all the extraction regions, was found to be 820±170 e cm^{-3}. The range in density is similar to that found by Mitra and Dufour (1990) of 630-900 cm^{-3}, but the mean value is a little greater than that derived by Nota et al. (1992) of 500 cm^{-3}.

There existed no well established determinations of the electron temperature in

AG Car's nebula and so the temperature implied by our [NII]λ5755 detection is of some interest. Our results differ significantly from previous estimates. We find an average temperature of 6350$\pm$400 which indicates an exceptionally low degree of excitation, consistent with the ionisation stages observed. Previously Mitra and Dufour estimated a temperature range of 7500K to 9800K based on a two σ level detection of [NII] 5755, while de Freitas Pacheco et al (1992) derived a temperature of 12400$\pm$100K based on a [NII] 5755 line strength three times greater than our detection. The latter result is not consistent with the observed ionisation stages.

The temperature and density derived for each extraction region are presented in Table 2.4. From the variation in results we see a picture of a clumpy, low excitation nebula emerge. We also note that our derived density for the waist region is greater than that derived for the polar region.

Using the physical conditions derived above, we were able to solve the equations of statistical equlibrium to determine the ionic abundances. The ionic abundances of N^0, N^+, O^+, S^+ and S^{++} are presented in Table 2.4 together with upper limits on the abundances of O^0 and O^{++}. The upper limits have been calculated by finding the line strength which would rise 3σ above the noise level. This critera was applied to the [OI] 6300 line and the [OIII] 5007 line.

From these results it is apparent that the elemental abundances are dominated by N^+, O^+ and S^+. Since $O^+/O^{++}>100$, we find all the oxygen to be present in the singly charged state. The total elemental sulphur abundance is taken as the summation of the first and second ionization states, as mentioned before this represents a lower limit due to a possible under estimate of S^{++}. For nitrogen we equate the ionic abundance of N^+ to the total elemental abundance. The low upper limit on O^{++} also suggests that N^{++} does not make a significant contribution to the total nitrogen abundance. The abundances derived for each position in AG Cars nebula

Region	A1	B1	C1	A2	B2
N^0/H^+	$7.23\pm^{0.11}_{0.11}$	$7.12\pm^{0.06}_{0.09}$	$7.16\pm^{0.27}_{0.21}$	$7.61\pm^{0.28}_{0.22}$	$7.40\pm^{0.26}_{0.18}$
N^+/H^+	$8.27\pm^{0.05}_{0.04}$	$8.21\pm^{0.03}_{0.04}$	$8.06\pm^{0.16}_{0.13}$	$8.32\pm^{0.16}_{0.12}$	$8.22\pm^{0.16}_{0.10}$
O^0/H^+	<6.89	<6.89	<6.89	<7.06	<7.06
O^+/H^+	$7.57\pm^{0.12}_{0.12}$	$7.44\pm^{0.08}_{0.11}$	$7.08\pm^{0.31}_{0.26}$	$7.71\pm^{0.35}_{0.28}$	$7.60\pm^{0.30}_{0.22}$
O^{++}/H^+	<6.07	<6.07	<6.07	<6.36	<6.36
S^+/H^+	$6.60\pm^{0.06}_{0.05}$	$6.51\pm^{0.03}_{0.06}$	$6.38\pm^{0.18}_{0.14}$	$6.64\pm^{0.18}_{0.14}$	$6.55\pm^{0.16}_{0.13}$
S^{++}/H^+	>5.10	>5.19	>5.02	>5.44	>5.25
N/H	$8.27\pm^{0.05}_{0.04}$	$8.21\pm^{0.03}_{0.04}$	$8.06\pm^{0.16}_{0.13}$	$8.32\pm^{0.16}_{0.12}$	$8.22\pm^{0.16}_{0.10}$
O/H	$7.57\pm^{0.12}_{0.12}$	$7.44\pm^{0.08}_{0.11}$	$7.08\pm^{0.31}_{0.26}$	$7.71\pm^{0.35}_{0.28}$	$7.60\pm^{0.30}_{0.22}$
S/H	>6.61	>6.53	>6.40	>6.67	>6.57
log N/O	$0.70\pm^{0.17}_{0.16}$	$0.77\pm^{0.14}_{0.12}$	$0.98\pm^{0.42}_{0.44}$	$0.61\pm^{0.44}_{0.47}$	$0.62\pm^{0.38}_{0.42}$
$10^2 He^+/H^+(5876)$	0.71 ± 0.12	0.55 ± 0.11	1.30 ± 0.20	0.40 ± 0.16	0.33 ± 0.13
$10^2 He^+/H^+(6678)$	0.81 ± 0.31		1.14 ± 0.29	0.67 ± 0.38	0.79 ± 0.33
$10^2 <He^+/H^+>$	0.74 ± 0.18	0.55 ± 0.11	1.25 ± 0.23	0.49 ± 0.23	0.48 ± 0.20
T_e	$6403\pm^{147}_{149}$	$6306\pm^{173}_{91}$	$6969\pm^{581}_{648}$	$5900\pm^{412}_{500}$	$6155\pm^{400}_{499}$
n_e	$1049\pm^{159}_{132}$	$930\pm^{52}_{39}$	$767\pm^{118}_{105}$	$736\pm^{242}_{193}$	$603\pm^{102}_{90}$

Table 2.4: Abundances (12 + log X/H).

are presented in Table 2.4. The mean abundances are N=8.22±0.10, O=7.52±0.20 and S>6.57, where the sulphur abundance represents a lower limit.

A further test of the degree of chemical enhancement is to find the N^+/S^+ ratio. [NII]λ6584 and [SII]$\lambda\lambda$ 6717,6731 have very similar excitation energies (Johnson et al 1992). Consequently N^+/S^+ ratio only has a very slight dependence on temperature. Since the sulphur abundance is not altered by the CNO cycle, this ratio gives an indication of the change in the nitrogen abundance. We find an average value, in AG Cars nebula, of about 47, which is similar to the value of 33 found in P Cygni's nebula (Johnson et al. 1992), 79 found in M1-67, (Esteban et al. 1991) and 62 found in HR Car (Nota et al. 1996).

At the five positions analysed, within the errors, we find no difference in the abundances derived. The density varies, perhaps systematically increasing near the "waist", but the abundance pattern is uniform. This suggests that all parts of the nebula were "ejected" at the same time. It is unlikely that the "waist" represents an old object into which the main nebula erupted. The uniformity in abundances suggests that any equatorial density enhancement which might help shape the bipolar nebula, was composed of processed material and not hydrogen rich material such as that which would be expected in a proto-stellar disc.

Since no HeII recombination lines are observed, we infer that all the helium is present in the singly charged or neutral state. Using the recombination coefficients of Brocklehurst (1972), interpolated to the correct electron temperature and the observed HeI 5876 and 6678 line fluxes we have determined the ionic abundance of He^+. This results in a mean value of $He^+/H^+=0.57\pm0.12\times10^{-2}$. This is a remarkably low value particularly considering the degree of nitrogen enrichment. If AG Cars nebula were to contain a similar He/H ratio as that surrounding M1-67, then this would imply an ICF of about 40 (Esteban 1991). This is so large as to negate

the use of Ionisation Correction Factors (ICFs) to infer useful information about the helium abundance.

To better estimate the total elemental helium abundance we ran a series of photo-ionization models using the Harrington code (1982). We took from the literature all the input parameters, bar three unknowns, the filling factor, the nebula thickness and the helium abundance. These parameters were then varied through their feasible ranges and the best fit of the output parameters to the observations was searched for. The result of this effort was inconclusive, as fits of similar"goodness" could be achieved using quite different sets of parameters.

The only light that we could shed on the AG Cars helium abundance is through inference from the other nebula abundances. We note that the nitrogen abundance in AG Cars nebula is identical to that in M1-67 (Esteban et al 1991). If the helium enrichment is tied to the nitrogen enrichment then this would suggest a similar helium abundance as M1-67, implying $Y = 0.47$.

We will conclude this section by placing the abundances that we have derived in the context of the abundances found for other ejecta nebula surrounding evolved stars. In Table 2.5 we present the abundance pattern of a number of WR ring nebulae, the probable RSG material surrounding SN 1987A, the surface composition of a number of Of-stars and the surface composition of different evolutionary tracks in the LBV and RSG phases.

The abundance pattern that we have derived for AG Cars nebula is not consistent with the CNO equilibrium composition, which is predicted by evolutionary models for the surface composition of LBV stars (Langer et al. 1994). These models suggest that at CNO equilibrium an N/O ratio of 26 is achieved, this compares with an N/O ratio of only 5.7±2.2 found in AG Car's ejecta nebula. However, the

Nebula / Star	N/H	O/H	Log N/O	Y_{neb}	Y_{star}	Sp Type	Refs
AG Car	8.22±0.11	7.52±0.20	0.76		0.62	LBV	a
He3-519	8.21±0.10	7.57±0.15	0.64		0.66	LBV(?)	b
M1-67	8.45 ± 0.15	7.98 ± 0.27	0.47	0.47	0.87	WN8	c
NGC 6888	8.40 ±0.35	8.11 ±0.28	0.30	0.43		WN6	d
RCW58	8.02 ±.08	7.44 ± 0.15	0.5	0.48	0.84	WN8	e
NGC 6164-5	8.38 ±0.02	7.95 ±0.03	0.12			O6.5f?p	f
HII region	7.57	8.70	-1.13	0.29	–	–	g
SN 1987A	8.34±0.2	8.2±0.2	0.16	0.44	–	RSG	i
ζ Pup	9.0			–	0.50	O4n0f	k
α Cam				–	0.46	O9.5Ia	l
HD 192639				–	0.45	O7Ib(f)	n
HD 151804				–	0.50	O8Iaf	m
η Car	8.93	<7.19	1.7			LBV	j
$60M_{\odot}$*model*	8.7	7.4	1.3	–		LBV	h
$35M_{\odot}$ model						RSG	o

Table 2.5: Abundance patterns determined for LBV/WR nebulae and some stellar surface compositions.

References: (a) Chapter 1, this thesis; (b) Chapter 4, this thesis; (c) Esteban et al (1990); (d) Esteban & Vilchez (1992); (e) Chapter 4, this thesis; (f) Chapter 5, this thesis. (g) Shaver et al (1983); (h) Langer et al. (1994). (i) Panagia et al. (1997); (j) Dufour et al. (1997); (k) Bohannan et al. (1990); (l) Voels et al. (1989); (m) Crowther et al. (1996); (n) Herrero et al. (1992); (o) Langer et al. (1994).

nebula is clearly nitrogen enriched. AG Car lies at a galactocentric distance of 8.6 kpc, which is close to the galactocentric distance of the Sun which lies at 8.5 kpc. Consequently, the abundance pattern of the unprocessed material in the vicinity of AG Car is well represented by the abundance pattern of HII regions in the solar neighbourhood, which have been determined by Shaver et al. (1983) and are given in Table 2.5. From this we see that AG Cars nebula abundance pattern is consistent with *partially CNO processed material.* From Table 2.5 we see that this abundance pattern is found in the surface material of stars late in the RSG phase (Panagia et al. 1997) and on the surface some of Of-stars (Meynet et al. 1994; Bohannan et al. 1990). However, caution is required when comparing AG Cars nebular abundance pattern to that found in the RSG material surrounding SN 1987A, since the LMC N and O abundances are 0.3dex below typical galactic values. Taking this into account when assessing the degree of enrichment which has occurred implies that this RSG material is more enriched in nitrogen (by 0.2 dex), but less depleted in oxygen (by 0.7 dex) than the material in AG Cars nebula. In the next section we will look at the implications of these observations for the evolutionary history of AG Car.

2.5 Discussion.

2.5.1 Introduction.

AG Car is a prototype object for the LBV class, through studying it numerous advances have been made in the understanding of general LBV properties. However in some ways AG Car is an unusual LBV, the most important being that it lies above the HD limit. Of the thirty or so known LBVs this is only true of AG Car, R127, P Cygni and η Car (if the latter is really an LBV).

The initial mass of an LBV plays an important role in determining its evolutionary history. If as suggested by Lamers & Fitzpatrick (1987) the LBV phenomena

is connected with the star impinging on its Eddington limit, then LBVs above the HD-limit will encounter this on their first red-ward excursion, while those below the HD limit are more likely to encounter it during the blue-ward part of the loop, after the heavy mass loss in the RSG phase. The possible association of the LBV phenomenon with the modified Eddington limit means that we need to establish the evolutionary histories of the high and low mass LBVs separately.

In the discussion that follows we will address a number of issues, with the ultimate aim of establishing the conditions which prevailed on the stellar surface during the nebula forming epoch. The purpose of this being to discriminate between the different theoretical mechanisms that have been proposed to explain the formation of LBV ejecta nebulae. This theme will run through all the chapters in this thesis and the conclusions will be presented in the final chapter.

In the first subsection of the discussion we will look at the possibility that AG Car originally ejected a nebula with CNO equilibrium abundances which were subsequently diluted through mixing with hydrogen-rich material from the previous O-star wind. In the second subsection we will use the derived abundance pattern in conjunction with dynamical properties of the nebula to isolate the parts of AG Car's evolutionary track consistent with both. This leads to an uncertainty as to whether AG Car ejected its nebula close to the H-D limit or whether it could have continued its red-ward evolution, with a luminosity in excess of its modified-Eddington limit, to eject the nebula during a RSG phase. The critical factor in discriminating between these two possibilities is the mass loss rate as the star exceeds its modified-Eddington limit. This is addressed in the third subsection. Finally, in the fourth subsection we will review the stellar evolutionary models and highlight the inability of some which use very enhanced mass loss rates (Langer et al. 1994, Meynet et al. 1994) to explain the LBV nebular properties.

2.5.2 Dilution of the Nebular Abundance Pattern?

In this section we will explore the possibility that, when ejected the nebula contained material with a CNO equilibrium abundance, but that this composition has since been diluted by swept up wind material. This is not tenable for two reasons. Firstly all nebulae surrounding LBV and WR stars have very similar abundance patterns, despite a wide range of dynamical ages (see Table 2.5.2 and Table 2.5). There is no correlation between nebula age and enrichment of the abundance pattern, as would be expected if swept up material was acting as a diluting agent. Secondly, the nebula could not have swept up enough material to cause the required dilution. During the main sequence phase the powerful O-star wind carves a cavity in the surrounding ISM, leaving the nebula to erupt into a hot, low density WBB. If the total observed mass of the nebula M_{neb} includes the ejected mass M_{CNO} plus the swept up mass M_{sw}, then the ratio of M_{sw}/M_{CNO} is given by:

$$\frac{M_{sw}}{M_{CNO}} = \frac{X_{CNO} - X_{neb}}{X_{neb} - X_{sw}}$$

Letting X_{neb} represent AG Car's observed nebular nitrogen abundance, while setting X_{CNO}=0.013, and X_{sw}=0.001 (García-Segura et al. 1996a), we find the mass of swept up wind material has to be about six times the amount ejected with CNO-equilibrium abundances. Taking the total nebula mass as $4.2\,M_\odot$ (Nota et al. 1992) we find $3.6\,M_\odot$ of wind material is required. This mass is many orders of magnitude more than was present in the portion of the WBB contained in the nebula. Hydrodynamical modelling (Garcia-Segura et al. 1996a) suggests that during the O-star phase $32M_\odot$ of wind material will be deposited in a 100pc WBB. The diameter of AG Cars nebula is 1pc, which implies that if the density of the WBB is uniform, then the nebula has only swept up $3.2\times10^{-5}M_\odot$ of O-star wind material.

This mass is considerably short of the $3.6M_{\odot}$ required to dilute CNO material to the observed abundance pattern. We conclude that the partially processed nebular abundances are not explicable in terms of dilution by swept up wind material.

Consequently we find that the nebula surrounding AG Car consists of partially CNO processed material. This conflicts with the idea that the nebula was ejected during the present LBV phase. Atmospheric modelling of AG Car by Smith et al. (1994) found that it has a surface helium abundance (Y=0.62) which is expected to arise when CNO equilibrium material is present on the stellar surface. This is consistent with the evolutionary models (Meynet et al. 1994) which predict a CNO equilibrium surface abundance during the LBV phase. Consequently the nebula must have been ejected from the star before CNO equilibrium surface abundances were achieved. The fact that most LBVs are surrounded by nebulae, also provides support for the idea that the nebula ejection occurs near the beginning of the LBV phase.

2.5.3 The Physical Conditions at the Stellar surface During the Epoch of Nebular Formation.

We will begin this section by looking at the implications of the nebular dynamics (see Table 2.5.2) before identifying which type of stars, of a comparable mass to AG Car have been observed to achieve the observed nebular abundance pattern on their surface.

The high mass LBV instability strip lies close to the HD limit. From atmospheric modelling it is believed that the HD limit is coincident with the locus of modified Eddington Limits (Lamers and Fitzpatrick 1987). This means that as the star starts to approach the HD limit, its effective surface gravity will start to decline, which implies that high mass stars (initial mass $> 60M_{\odot}$) must achieve a low surface gravity

Nebula	Radius (pc)	Expansion velocity (Km sec^{-1})	Dynamical timescale (x10^3yrs)	Nebular mass ($M_\odot$)	Spectral Type
R127	2.2[3]	53[3]	40[3]	3.1	LBV
RCW 58	2.6/3	87/100[1]	30[1]	1.5	WN8
He3-519	1.4[2]	61[2]	20[2]	2	LBV(?)
NGC 6888	1.7	85[1]	20[3]	9	WN6
WRA 751	0.4[5]	26[5]	15[5]	–	LBV(?)
M1-67	0.5[1b]	42[1b]	13[1b]	0.8	WN8
AG Car	0.6[2b]	70[2b]	8.4[2b]	4.2	LBV
NGC 6164/5	1.0[4]	350[4]	3.5[4]	2	Of6.5p
HD 168625	0.15	40[3b]	1[3b]	0.03	LBV(?)
HR Car	0.06[3c]	110[3c]	0.8[3c]	2.1	LBV
P Cygni	0.2[3]	140[3]	0.4-0.8	0.01	LBV

Table 2.6: A review of the dynamical properties of LBV and WR nebulae.

references: (1)Esteban et al. 1991 (b=1990 c=1992), (2)Smith et al. 1994 (b=1996), (3)Nota et al. 1995 (b=1996 c=1996), (4) Leitherer et al. 1987, (5) Hutsemekers et al. 1991.

while still in the blue. Since the expansion velocity is expected to be broadly correlated with the escape velocity, this suggests that the low nebula expansion velocities could be a reflection of the low surface gravities of the stars from which they were ejected. That is, AG Car's nebular expansion velocity of 70 km s^{-1} is incompatible with ejection from a BSG, which has an escape velocity of about 800 km s^{-1}, unless the star were near or in excess of its modified Eddington limit.

The other piece of evidence that we must consider is the partially CNO processed nebula abundance pattern. Where in the HRD have stars of a comparable mass to AG Car been observed to have such a surface composition? Evidence that evolved Of stars can attain the observed nebula abundance pattern on their surface comes from the application of atmospheric models. Voels (1989) found a helium Y=0.46 for α Cam, while Bohannan et al. (1990) found Y=0.50 for ζ Pup and Crowther et al. (1996) found Y=0.50 for the O8Iaf star HD 151804. These references also include deterimations of the helium abundance in other Of stars which display both more and less processed material on their surfaces. Since we would expect helium and the CNO elements to become enriched in parallel, these helium abundances are indicative of partially CNO processed material. Furthermore, we note that the helium abundance (Y) in M1-67 is 0.47 (Esteban et al. 1991), 0.48 in RCW58 (Rosa 1987) and 0.43 in NGC 6888 (Esteban & Vilchez 1992). These nebular abundance studies also found nitrogen and oxygen abundances similar to those we have determined for AG Car's nebula. This supports our inference that the partially CNO processed material seen in the nebula occurs with a characteristic helium abundance. The characteristic helium abundance is observed to occur in Of stars.

Further evidence that partially CNO processed material, consistent with the nebular abundance patterns can occur on the surface of Of stars comes from abundance studies (Dufour et al. (1988); Chapter 5, this thesis) of the ejecta nebula surrounding the Of star HD 148937. They find an oxygen and nitrogen abundance very similar to that found in the nebula surrounding AG Car (this Chapter), He3-

519 (Chapter 4) and RCW 58 (Chapter 4). Observationally Of stars can achieve the observed nebular abundance pattern, when this is achieved near the H-D limit the star will have a low surface gravity and so be able to eject a nebula with a low expansion velocity.

2.5.4 The Effect of Supra-Eddington Limit Mass Loss.

Toward the end of the Of-phase the star will start to evolve red-ward, as it approaches its Eddington limit it can achieve both the correct surface gravity and abundance pattern to explain the observed nebula properties. However it has been suggested (Smith et al. 1997) that the star may continue to evolve red-ward inside the HD-limit becoming a RSG before ejecting the nebula. This does not seem necessary on the basis of nebula studies, since it has been demonstrated by Voels et al. (1989), Herrero et al. (1992), Crowther et al. (1995) and Bohannan et al (1996) that partially CNO processed material does occur on the surface of Of-stars. However the feasibility of a RSG scenario rests on the mass loss rates incurred while the star passes through the Eddington limit. If a large rate of mass loss is encountered during or after the modified Eddington limit is reached, then the red-ward evolution may be halted, if not the star may evolve into a RSG.

A star trying to exceed its Eddington limit must over come at least two major sources of mass loss, the first driven by angular momentum and radiation as the star hits its Omega-limit (Langer 1997), the second driven by strange mode pulsations, to which stars impinging on their Eddington limits are extremely unstable (Cox 1997; Soukup et al. 1994; Glatzel & Kirakidis 1993). We will now look at the significance of these mechanisims and assess their likely affect on the red-ward evolution of a star like AG Car.

As discussed in Chapter 1 the CAK theory suggests a dependance of the terminal

velocity and mass loss rate on the stellar temperature and effective surface gravity. Indeed as the effective surface gravity reduces to zero (corresponding to the star reaching its Eddington limit) the terminal velocity goes to zero while the mass loss becomes arbitarally large. In practice this must be averted by the process of photon tiring (Owocki & Gayley 1997). In this process the apparent stellar luminosity is diminished as the radiation field is doing work lifting the mass from the stars gravitational well. Consequently the luminosity sets a limit to the maximum rate of mass loss. For a $23M_{\odot}$ star with a radius of $30R_{\odot}$ and luminosity of log L/L=6.0, photon tiring implies a maximum mass loss rate of $10^{-2}M_{\odot}$ yr^{-1}. If the mass loss rate is too great and the photons tire, the flow will stagnate (Owocki & Gayley 1997). This might lead to some type of mass circulation which would tire the photons and reduce Γ to unity at the stellar surface. Consequently, as the star evolves toward its Eddington limit we would expect to see the terminal velocity fall, while the mass loss rate rises, reaching a maximum value at the limit given by photon tiring. Once the Eddington limit is reached, the mass loss could be halted by a process of mass circulation (Owocki & Gayley 1997), although the details of such a process have not been worked out.

Langer (1997) has pointed out that the correct criteria for the stability of massive stars is not the Eddington limit, but rather the Omega limit. For a rotating star to be hydrostatically stable there must be a momentum balance at its surface which includes a contribution from the centrifugal acceleration. Consequently, if the star exceeds some critical angular velocity (the Omega limit) then mechanical forces will help generate mass loss. As the star evolves toward its Eddington limit its effective surface gravity will drop, which in turn will cause the critical angular velocity to drop. This means that the star will suffer heavy mass loss before the Eddington limit is reached. Outflow is triggered when V_{crit} is attained, but it is still the radiation field which lifts the material out of the gravitational well and so the mass loss rate is still limited by photon tiring. The actual mass loss rate depends on the evolutionary speed of the star in the HR diagram. This means that the faster

the star evolves toward the Eddington limit, the greater the mass loss rate and so the larger the tendency to halt its red-ward evolution. For a $60M_{\odot}$ track Langer (1997) predicts that after the critical velocity is attained and the star is impinging on the Eddington limit, a mass loss rate of the order of 10^{-3}–$10^{-2}M_{\odot}$ yr^{-1} will result. This means that when a star approaches and then exceeds its Eddington limit, it will suffer a rate of mass loss greater than that needed to halt the stars red-ward evolution in the stellar models (Meynet et al. 1994).

As discussed in section 1.4.1 the mass loss at the Ω limit occurs primarily from the stars equatorial regions. However the radiation field at the equator is not sufficent to lift this rate of mass loss out of the stars gravitational well. However, the balance of forces at the stellar surface dictates that the mass must leave the star. This will lead to the formation of a circumstellar disk. The mass deposited in the equatorial region will then act to scatter the photons toward the polar regions and increase the mass loss rate there (Owocki and Langer privt comm 1997). Consequently the mass loss predicted to arise through the stars interaction with the limit is a lower limit, since it does not include radiatively driven mass loss from the poles.

A second source of mass loss is driven by stellar pulsations. Highly luminous stars with low surface gravities are unstable to many forms of pulsational instability (Cox et al 1997). Most of these involve comparatively low radial velocities and so cannot eject material from the star without aid from the radiation field. Consequently attention has focused on strange mode pulsations since some modes can reach large radial velocities. These have been investigated by Glatzel & Kiriakidis (1993) and Cox et al. (1997) who find that radial velocities of 200 km s^{-1} can be achieved allowing the ejection of material. Using hydrodynamic models Cox et al. (1997) conclude that "alot of mass loss can indeed occur during the many outbursts blue-ward of the HD-line".

We conclude that a star evolving toward its Eddington limit will incur a sustained period of heavy mass loss. These mass loss rates are so large that it would seem unlikely that its red-ward evolution could continue. Accordingly the formation of the LBV nebula is expected to occur near the HD-limit where the LBV will have a low effective surface gravity and can have a surface composition identical to the observed nebula abundance pattern. This conclusion is supported by the bipolar character of LBV nebulae, which naturally asises if the mass loss occurs near the limit.

2.5.5 Implication for the Evolutionary Models.

An interesting problem arises if we examine the stellar models of Meynet et al. (1994) to see when they predict the nebula abundance pattern should arise on the surface of the most massive stars. They predict that this is *always* achieved comparatively early in the Of star phase, which causes two problems. Firstly this is $4x10^5$ years premature, before the star reaches the LBV instability strip. This problem is not acute as the ejection of a massive nebula will alter the model predictions. Secondly, when the observed nebular abundance pattern is reached the star is not impinging on the Eddington/HD limit, and so it has a high surface gravity. This would imply a high escape velocity and so a large expansion velocity, contrary to what is observed. Clearly the standard evolutionary models are not compatible with the observations of LBV nebulae. What revisions to the models are possible?

These models use an artificially high mass loss rate to remove enough mass to reproduce the WR luminosities. A consequence of this is that the stars red-ward evolution is slowed and finally halted before the HD limit is reached. To do this they use a mass loss rate of double the observed value. For a $60M_\odot$ track, $10M_\odot$ needs to be removed to obtain the correct resulting WR luminosities. However this mass loss rate is not tenable observationally, but if the observed mass loss rates were used in

the models then they will fail to reproduce the WR luminosities. This problem may partly arise because the mass loss rates used are time averaged values which ignore any brief large scale mass loss (like an LBV eruption), which if they were included, would allow a lower time averaged mass loss rate to reproduce the WR luminosities. If, like AG Car the star bulk ejects a nebula of at least $4M_{\odot}$, then the continuous mass loss need only remove $6M_{\odot}$ and so need not be so high. Indeed the remaining $6M_{\odot}$ can be removed in the same time with only a slightly enhanced mass loss rate.

The effect of the lower mass loss rate, would be to make the star evolve faster to the red and reveal the processed material at the surface more slowly. That is, the high mass loss rates used in the models help maintain the star in the blue by revealing hotter material, in doing so they also reveal deeper more processed material faster. A lower mass loss rate, compatible with the observed values would serve to lessen these effects and so cause the enriched abundances to be achieved at a lower surface temperature closer to the LBV instability strip. The enhanced surface compositions found in some Of-stars (Crowther et al. 1996) would then be attributed primarily to rotational mixing or them lying in a different mass range.

These issues have been explored quantitively by Pasquali et al. (1997), who have run a series of models, which incorporate standard mass loss rates, enhanced mass loss and rotational mixing. They conclude that strongly enhanced main sequence mass loss rates (as in Langer et al. 1994 and similar to Meynet et al. 1994) is not viable since it predicts an absence of luminous ($\log L_*/L_{\odot}=5.8$) main-sequence stars with an effective temperature below 30,000K, contrary to observations. Instead they find that best agreement between the models and observations can be attained if the mass loss rate is more modestly enhanced and the affects of rotational mixing are incorporated. Under this scheme, the point at which the nebular abundance pattern is achieved on the surface of the star is dependent on the initial angular momentum of the star. Consequently these models predict stars with the correct nebular abundance pattern on their surface in the vicinity on the modified Eddington limit and

so there need be no conflict between theory and observations of LBV nebulae.

2.5.6 Conclusions.

On the basis of the preceeding arguments, we have shown that the nebula surrounding AG Car is comprised of partially CNO processed material. Reviewing the determinations of the stellar surface compositions found in the literature (Crowther et al 1995; Bohannan et al. 1991; Herrero et al; 1992 and Voels et al. 1989) we conclude that such an abundance pattern occurs on the surface of massive stars early in their redward loop. From the models of Pasquali et al. (1997) we find that the exact position in the HRD at which this abundance pattern is achieved, depends on the stars mass loss rate and angular momentum.

AG car's nebula has a low expansion velocity of only 70 km s^{-1}, which is indicative of an ejection from a star with a low effective gravity. Such a low effective gravity can only be achieved while the star is near its modified Eddington limit or during a RSG phase. We have reviewed the mass loss rate which is expected to arise when a star above the HD limit encounters its Ω limit and found that these far exceed those needed to halt the stars redward evolution in the models of Meynet et al. (1994). Consequently we conclude that AG Car must have been on the part of its evolutionary track which lies near its Eddington limit when the circumstellar nebula was ejected. This conclusion is supported by the bipolar character of the LBV nebula. Such asymmetry is a natural consequence of mass loss form a star near its Ω limit.

Finally we note that the abundance pattern and expansion velocity of AG Car's nebula are incompatible with the nebula being ejected from a star described by evolutionary tracks which use very enhanced mass loss rates (Langer 1994, Meynet et al. 1994), since these *always* achieve the abundance pattern while the star has a

high surface gravity. This is inconsistent with the observed low nebular expansion velocity.

Chapter 3

The nebula surrounding HR Carinae.

3.1 Introduction

This work was carried out in collaboration with Antonella Nota, Anna Pasqulai and Mark Clampin of the Space Telescope Institute. They obtained extensive observations of the bipolar nebula surrounding HR Car. Primarily these were designed to allow a comprehensive analysis of the nebular dynamics. The observations were obtained by them at the European Southern Observatory using the New Technology Telescope in May 1995. The data were then independently reduced at U.C.L. and STScI. We at U.C.L subsequently derived abundances from the spectroscopic observations, while the dynamical analysis was conducted at the STScI. The results of this work are presented as a paper which is in press in The Astrophysical Journal.

Interest in HR Car was first aroused in 1912 by Fleming who reported that its spectra contained emission lines. This was confirmed by Henize (1952) who took detailed optical spectra showing hydrogen, helium and iron lines to be in emission. He also noted that these lines displayed, what we now call, P-Cygni type profiles. Confirmation of the unusual nature of HR Car came when Hoffleit (1940) found, us-

ing the Harvard Patrol plates, indications that its visual magnitude had fluctuated by 1.5 mags.

To better understand the nature of HR Car, it became important to ascertain its fundamental stellar parameters. The most pertinent of these was its luminosity, but this requires knowledge of the distance, which was then poorly known. Initially membership of the Carina OB association was assumed, resulting in a distance of 2.5kpc. This value was always treated with caution since the Carina spiral arm is tangential to our line of sight and so stars within it may have a considerable range of distances. Initial indications that HR Car may in fact lie at a greater distance than this first came when Van Genderen (1990) applied the amplitude-luminosity relation of Wolf (1989) to HR Car. This suggested a distance of 6kpc.

This inference was confirmed by a study of the reddening of the field stars surrounding HR Car (Van Genderen 1991). A sample of main sequence stars nearby was taken and their absolute luminosity determined from their spectral type. Each star's distance could then be found. Since we can also determine each star's reddening, this allows us to plot distance verses reddening. Using this method HR Car's reddening (E(B-V)=0.9±0.1) corresponds to a distance of 5±1 kpc. This distance implies a luminosity of log(L/L)=5.5 for HR Car, making it comparable to the luminosity of the other LBVs.

Further confirmation of this distance estimate comes from a study of the kinematical distance to HR Car made by Hutsemekers and Van Drom (1991). They derived a systemic velocity for HR Car of 22±4 km sec^{-1}, implying a distance of 5.4 ± 0.4 kpc. They also note that this is consistent with the very strong interstellar Na I D lines seen in the stellar spectra. Using this revised distance they go on to rescale the mass loss rate determined by McGregor et al. (1988) finding it to be of the order of $2x10^{-6}$ $M_{\odot}$ yr^{-1}.

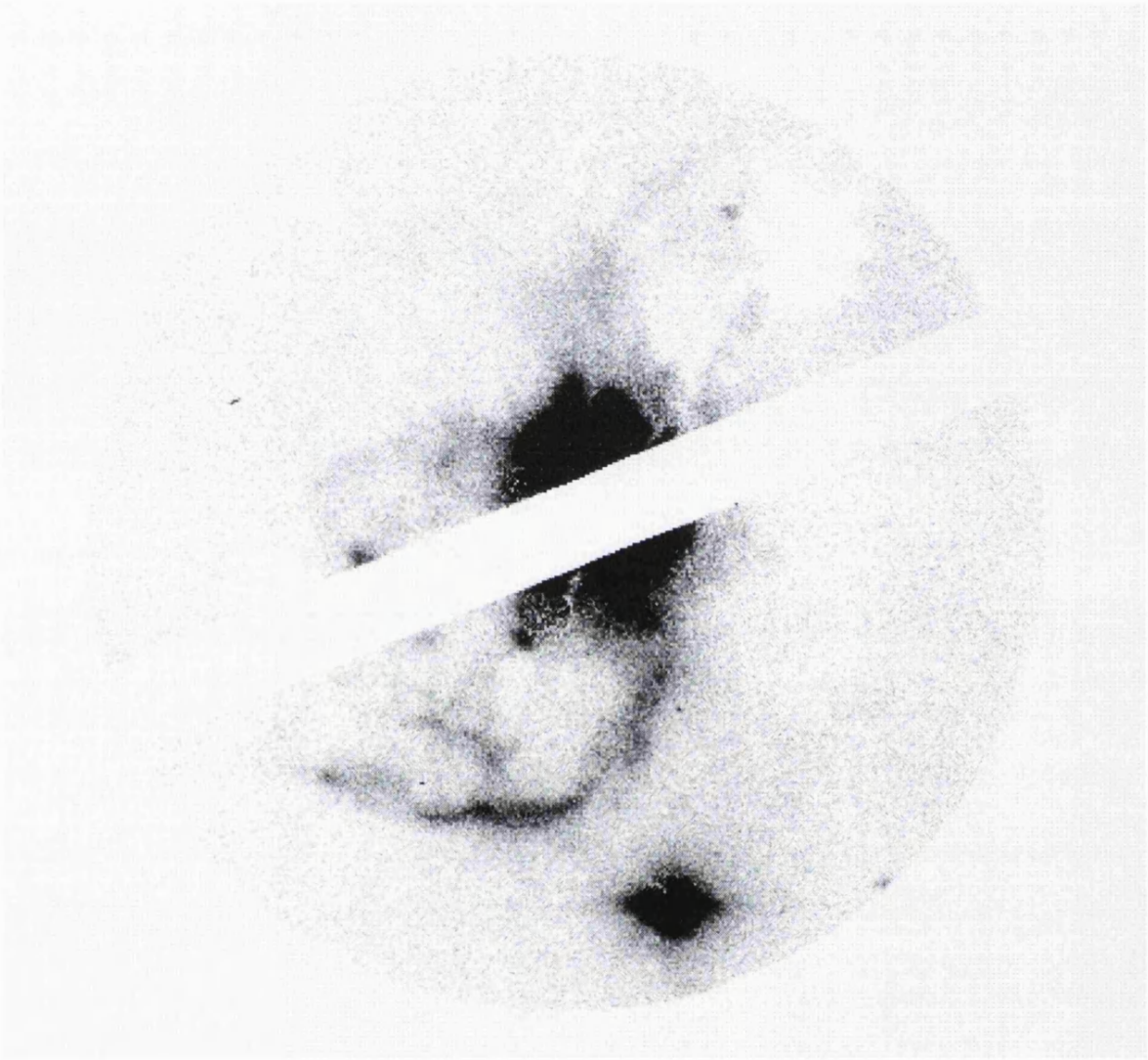

Figure 3.1: A deep Hα Chronographic image of HR Car's nebula (Clampin et al 1995).

An unusual feature of HR Car's stellar spectrum is the presence of extremely wide emission features (FWZI=3000 km sec^{-1}), upon which the Balmer emission lines are situated. The origin of these features is not clear. It has been suggested that they could be caused by electron scattering, as in the case of P Cygni (Bernat and Lambert 1978). However, Hutsemekers and Van Drom (1991) suggest the features are more likely to be the result of high velocity motions in the atmosphere of HR Car and point out that similar features are seen in WR and extreme Of-stars. Both these classes of star are thought to be closely related to LBVs.

In recent years it has become increasingly clear that a nebula ejection phase is an integral part of the LBV phenomena. As our imaging techniques have improved, increasing numbers of LBVs have been found to have associated nebulae. The detection of LBV nebulae presents a challenging observational task, as the nebulae are often faint and close to the bright central star.

The first detection of a nebula surrounding HR Car came in 1991 when Hutsemekers and Van Drom used narrow band filters centred on nebula emission lines, in conjunction with a chronograph, to obtain deep unsaturated images. From their observations Hutsemekers and Van Drom find that the nebula surrounding HR Car has a bipolar geometry, with arched structures being observed to the south-east and north-west (see Figure 3.1).

Further imaging has been conducted by Clampin et al. (1995) using the STScI chronograph in conjunction with ESOs New Technology Telescope. In addition they took spectropolarimetric observations of the central star. These observations confirm the bipolar character of the nebula and discovered a wealth of smaller scale detail. They note that HR Car's nebula is nearly point symmetric, implying that the shape of the nebula is unlikely to be determined by the surrounding ISM. In-

stead they suggest its shape could be an intrinsic feature of the outburst mechanism which formed the nebula. In their observations Clampin et al. (1995) find evidence for new nebular structure close to the central star, which they termed the "inner nebula". Within this inner nebula they identify a number of spherically distributed emission blobs.

The most recent investigation of HR Car's nebula has been carried out by Weis et al. (1996). They obtained both imaging and high dispersion, long-slit echelle data. This revealed the presence of two main kinematic components in the nebula structure. The first being the expanding bipolar lobes, the second being slow moving, bright [NII] emission blobs. They confirm that the bipolar lobes are aligned along an axis at a position angle of 125^o and find a line-of-sight expansion velocity of 75-150 km sec^{-1}. However the data did not allow a full analysis of the nebula dynamics, since the three dimensional orientation of the polar axis was not known. However by assuming that the radial expansion velocity is no more than twice the line of sight velocity and taking the extent of the lobes to be 0.63pc and 0.67pc, they derive a dynamical age of between 4200-8400yrs.

In addition to studying the geometry of the bipolar nebula, Clampin et al. (1995) took spectropolarimetric observations of HR Car, designed to yield information about the structure of the material close to the central star. These observations were partly motivated by the earlier spectropolarimetric observations of Serkowski et al. (1975), which suggested polarimetric variations. Any variation in polarization would indicate that it is intrinsic to the star, rather than having an interstellar origin, which would not vary with time. Clampin et al find that the observed polarisation is confined to a narrow range of position angles $30^o \pm 1^o$. They note the similarity of this alignment with that of the major axis of HR Car's inner nebula and suggest that it maybe indicative of some asymmetric time dependent mass loss process. If we assume that HR Car is not a binary, then these results indicate that the stellar wind is asymmetric within a few stellar radii of the central star. Similar results have

been obtained for AG Car and R127 (Schulte-Ladbeck et al. 1994; Leitherer et al. 1994 and Schulte-Ladbeck et al. 1993).

In the literature a number of estimates of HR Car's nebular mass have been made. The first estimate of the total nebular mass was made by Hutsemekers (1994) who used both the observed Hα flux method and the electron density method, to independently derive the nebula mass. This yields an ionised gas mass of $0.12M_{\odot}$. While IR estimates of the dust mass yielded $0.001M_{\odot}$. A second estimate of the mass of HR Car's nebula was made by Clampin et al. They take a higher surface brightness region to be representative of the nebulae as a whole and so derive a greater nebula mass of $2.1M_{\odot}$. This is more consistent with typical LBV nebula masses, such as those surrounding AG Car, He3-519 and R127.

Among the first infrared observations of HR Car were those made by McGregor et al. (1988). These revealed the presence of cool dust and the signature of CO. However they find no infrared continuum excess characteristic of hot dust. This suggests that the dust present is either shielded or at some distance from the hot central star. A more recent analysis of the dust emission, using ISO data, has been carried out by Waters et al. (1996). They find evidence for the presence of Iron oxides, Magnesium oxides and silicate dust. They note that no crystaline olivine dust is present, in contrast to that observed in the nebula surrounding AG Car.

Using the Infrared Space Observatory, Lamers et al. (1996) have obtained IR observations of HR Car between 2.4 and 45 microns. They find the spectrum to consist of two components, one from the photosphere/stellar wind, while the other originates from dust in the circumstellar nebula. They note the presence of a discrepancy in the flux levels obtained with different instrumental apertures. This indicates that cooler dust emission is present outside the nebula seen at optical wavelengths, since this lies inside both the apertures used. By modelling the free-free emission

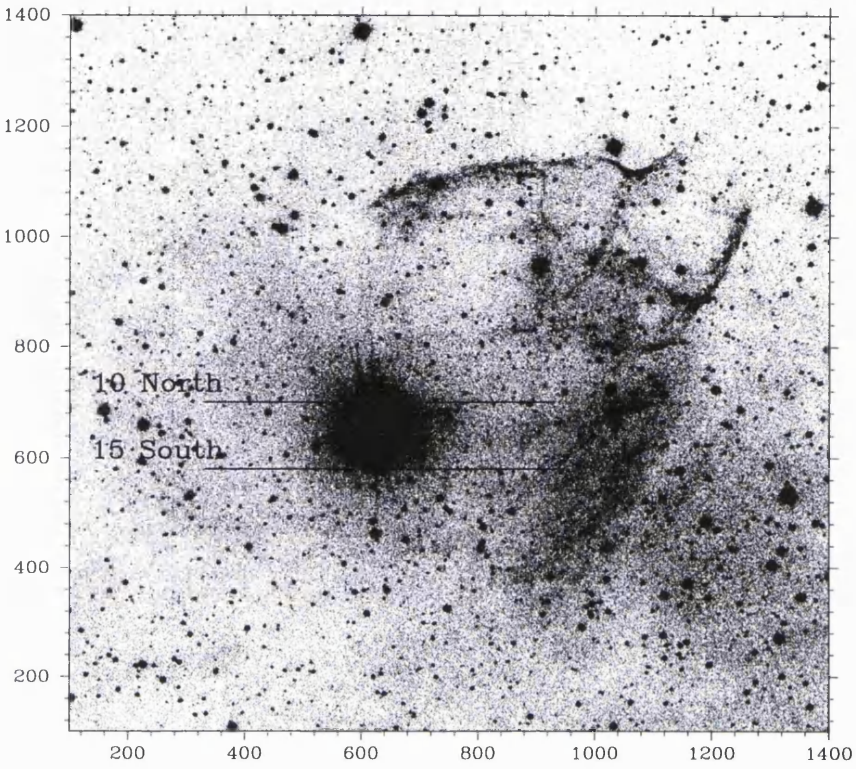

Figure 3.2: An Hα image of the HII region encompassing HR Car's nebula (Clampin et al. 1995).

they find that it is best reproduced by a star with a temperature of 8000-10000K and an effective radius of 220-340$R_{\odot}$.

ISO has also been employed by Trams et al. (1996) to image HR Car using its ISO-CAM instrument. The images were taken at 8.5 and 16 microns. They find that the spectral flux increases at longer wavelengths in contrast to the stellar spectrum which remains more or less flat. This is indicative of emission from a surrounding nebula. However because of its faint nature in comparison to the bright central star, they were unable to resolve the nebular structure.

The bipolar nebula surrounding HR Car is itself embedded in an extensive HII region (see Figure 3.2). Naturally the question arises as to whether it is a line-of-sight relation or whether they are actually cospatial. As observed by Weis et al. (1996), the outer HII region has a "funnel-like" structure to the north-west, centred on HR Car. A natural inference is that the HII region has been shaped by outflow from the central star, either through an ejection of material or through the action of the stellar wind. Weis et al. (1996) favor an ejection of material. This is because a wind-blown bubble with the characteristics of the funnel would be comparatively young, they estimate about $2x10^5$yrs. This they suggest is too brief a time for the star to have evolved from the main sequence to the LBV phase.

An important piece of evidence when determining the origin of HR Car's nebula is the abundance pattern. This has not been determined for HR Car's nebula, but a number of authors have drawn attention to a probable over-abundance of nitrogen. Weis et al. (1996) note that the [NII] bright knots that they detected have a [NII]λ 6583 to Hα ratio of 0.9, in comparison to a value of 0.3 for the nearby HII region. However they found no nitrogen enhancement in the material comprising the bipolar lobes, where they found a ratio comparable to that of the HII region. This inference must be treated with caution since the temperature is ill constrained (T_e<12500K) and so abundance and ionisation effects are not separable. However, the nitrogen over abundance is confirmed by Hutsemekers et al. (1991), who show that the N^+/O^+ ratio, which for low excitation nebulae is insensitive to temperature, is greater than 0.4. This compares to that of galactic HII regions, which is about 0.07 (Shaver et al 1983). This clearly demonstrates that the bipolar nebula surrounding HR Car is comprised of CNO processed material and therefore testifies as to the evolved status of HR Car. However this study was not able to establish the nebular abundance pattern.

In summary, HR Car is surrounded by a bipolar nebula, the orientation and precise dynamics of which are unknown. This nebula contains CNO processed ma-

Date	Wavelength Range (Å)	Resolution (Å)	Exposure Time (sec)
Slit position 3: 5″S			
1995 May 22	3390–5278	6.3	4000
1995 May 22	5080–6423	2.3	2000
1995 May 22	6244–6876	1.2	2000
Slit position 4: 10″S			
1995 May 24	3390–5278	6.3	4000
1995 May 24	5080–6423	2.3	2000
1995 May 24	6244–6876	1.2	2000

Table 3.1: Journal of Observations.

terial, but its actual abundance pattern has not been determined. The aim of our observations is to address these questions. In the sections which follow, I will give a detailed account of my abundance study. In addition to this I will outline the conclusions reached by Antonella Nota, Anna Pasquali and Mark Clampin as to the dynamical properties of the nebula. This chapter will then close with a discussion of the implications for HR Car and LBVs in general.

3.2 Observations

The observations used in this abundance study were made using the New Technology Telescope (NTT) at the European Southern Observatory (ESO) between 22-24 May 1995. The data were collected by Nota et al, primarily for an analysis of the nebula dynamics. They conducted deep imaging of the nebula using the STScI chronograph, in addition to extensive long-slit spectroscopic observations.

Date	Wavelength Range (Å)	Resolution (Å)	Exposure Time (sec)
Slit position 5: 15″S			
1995 May 24	3390–5278	6.3	4000
1995 May 24	5080–6423	2.3	2000
1995 May 24	6244–6876	1.2	2000
Slit position 1: 5″N			
1995 May 22	3390–5278	6.3	4000
1995 May 22	5080–6423	2.3	2000
1995 May 22	6244–6876	1.2	2000
Slit position 2: 10″N			
1995 May 22	3390–5278	6.3	4000
1995 May 22	5080–6423	2.3	2000
1995 May 22	6244–6876	1.2	2000

Table 3.2: Journal of Observations...cont

The spectroscopic observations were carried out using the high resolution spectrograph EMMI in conjunction with a Tektronix CCD. The observations covered a wavelength range of 3400-6900Å (see Table 3.1) with a wavelength resolution of 6.3Å in the blue and 1.0Å in the red. The spatial resolution obtained was about one third of an arcsecond. During the observations the "seeing" conditions were extremely good, ranging from 0.5" to 0.6". Long-slit spectroscopic observations were taken at six positions off-set from the star by 15", 10", 5" north and 15", 10" and 5" south. The slit used was 1" across and 180" long. The slit position ran from east to west in all cases.

In order to flux calibrate the spectra, observations were made of the standard stars Kopff27 and G93-48 (Stone & Baldwin 1983). The subsequent data reduction and calibration was carried out independently at U.C.L and the STScI using STARLINK and IRAF packages respectively. The resulting calibrations were consistent.

3.3 Analysis

In this section we will describe the steps taken to extract information about the nebula from our long-slit spectroscopic images. The first stage in the reduction process was to remove the bias and divide through by our median flat field. Because of the deep exposures required for HR Car's faint nebula, our images needed to then be cleaned of cosmic rays.

The next step was to subtract away the sky emission from our images. However, the location of HR Car presented us with a challenge, since it is embedded in an HII region. Our aim is to remove both the sky emission and the emission from the HII region, leaving just the flux from HR Car's bipolar nebula. The flux from the HH region was greater to the west of HR Car than to the east. An HII region spectra

(including the sky emission) was then extracted. This spectra was then scaled to the interpolated strength of the HII region flux over the region of the bipolar nebula. This was then subtracted from the long-slit images.

The success of this method depends on the assumption that the emission from the HII region varies smoothly. The resulting images can be used to test this assumption in two ways. Firstly, is the resulting nebular continuum plausible? Secondly what does the [SII]λ6717/[SII]λ6731 line ratio imply about the bipolar nebular density? Since HII regions have lower densities than observed in LBV nebulae, the HII region will have a higher [SII]λ6717/[SH]λ6731 ratio. Consequently if we remove too little HII region emission then our derived nebular density will be too low. Where as if we over estimate its contribution and remove too much, then the resulting nebular density will be too high. The nebular density which resulted from the subtraction of the interpolated HII region flux was very similar to that found in other LBV nebulae. This suggests that our assumption was valid and the flux from the HII region does indeed vary smoothly from east to west.

At this point we were able to wavelength calibrate the spectra. This was done using the Argon comparison arcs taken at regular intervals in between the nebular images. First a spectrum is extracted from the long-slit image of the arc and the lines are identified over the whole wavelength range covered. A package within FIGARO is then used to trace the variation of pixel position of the identified lines at successive spatial positions up the 2-D arc image. This generates polynomial coefficients describing the variation in wavelength over the two dimensional image. The wavelength calibration is then done by mapping this wavelength grid onto the nebula images. Each image was then corrected for atmospheric extinction.

To flux calibrate the data two standard stars were observed, Kopff27 and G93-48. Since we were aiming to determine the nebula abundances, it became very important

to obtain the right shape flux calibration curves. Any error in these would translate directly into an error on the relative flux measured for individual lines, leading to incorrect abundances. To counter this, we derived two sets of calibration curves, one from each of the standard stars. The resulting calibration curves were very similar, the discrepancies would not introduce significant errors into our results. The curves derived from Kopff27 were then applied to our data.

From the reduced images we chose the regions over which to extract nebular spectra. Using the ELF package within DIPSO, we fitted Gausians to the line profiles. This allowed us to estimate the line flux, central wavelength and the rms errors associated with both. By comparing the relative strengths of the Hα, Hβ, Hγ, Hδ and Hϵ line fluxes to those theoretically expected (Hummer & Storey 1987), we were able to determine the degree of interstellar reddening. In this way we find an extinction coefficient of C(H$_\beta$)=1.6 for the bipolar nebula surrounding HR Car. It is interesting to note that we derived an extinction coefficient of 1.4 for the surrounding HII region. This supports the conjecture that the HII region and HR Car lie at the same distance and are physically connected. In Table and 3.3 we present the observed and de-reddened line intensities.

The nebular spectrum is characterised by a low degree of excitation, with [OIII] being absent, while [NI]λ5200 is present at 5" north and [OII]λ3727 is present at all positions bar 10"north. At 5" and 10" north we note that Hα has a well defined P Cygni profile. An interesting feature of these spectra is the existence of the [NiII]λ 6667 line (see Figures 3.4 and 3.5). This feature grows weaker as we move away from the central star, being well resolved at both 5" north and south, but being faint or unresolved further out than this. Lucy (1995) has argued that this line arises via a fluorescence mechanism, in regions of high density with a strong UV field. In principle, this line could be used as a density diagnostic and may well be indicative of nebular clumping close to the central star.

Position + Extent			15″S: 11″		10″S: 21″		5″S: 10″	
λ_{lab}	Ion	$k(\lambda)$	$F(\lambda)$	$I(\lambda)$	$F(\lambda)$	$I(\lambda)$	$F(\lambda)$	$I(\lambda)$
3727	[O II]	0.257	<20.8	<76.5	<25.7	<68.1	<10.7	<27.7
4340.5	Hγ	0.127	25.1 ± 3.0	47.3 ± 5.7			28.6 ± 3.7	45.7 ± 5.9
4861.3	Hβ	0.000	100.0 ± 6.5	100.0 ± 6.5	100.0 ± 10.3	100.0 ± 10.3	100.0 ± 7.4	100.0 ± 7.4
5199.1	[N I]	−0.082	22.6 ± 5.8	14.9 ± 3.9	<4.4	<3.2	18.1 ± 2.1	13.4 ± 1.6
5754.6	[N II]	−0.195	<10.4	<3.9	<7.0	<3.4	3.6 ± 1.0	1.8 ± 0.5
6312.1	[S III]	−0.287	<4.1	<1.0	<1.3	<0.5	<1.3	<0. 5
6548.0	[N II]	−0.318	189.4 ± 8.1	38.7 ± 1.7	100.6 ± 6.2	30.1 ± 2.1	74.5 ± 16.8	23.1 ± 5.2
6562.8	Hα	−0.320	1539.8 ± 9.2	311.1 ± 1.9	1021.9 ± 6.8	301.9 ± 2.3	895.4 ± 18.6	275.4 ± 5.7
6583.4	[N II]	−0.323	631.6 ± 8.2	125.8 ± 1.6	352.7 ± 7.4	103.4 ± 2.3	277.9 ± 17.8	84.5 ± 5.4
6666.8	[Ni II]	−0.335					22.3 ± 1.1	6.5 ± 0.3
6716.5	[S II]	−0.342	39.6 ± 0.3	7.2 ± 0.1	22.9 ± 2.6	6.2 ± 0.7	9.3 ± 1.0	2.6 ± 0.3
6730.9	[S II]	−0.344	37.2 ± 3.0	6.7 ± 0.5	23.9 ± 2.3	6.5 ± 0.6	13.8 ± 1.1	3.9 ± 0.3
C (Hβ)			2.2		1.6		1.6	
F_{obs}(Hβ)				1.73×10^{-15}		3.29×10^{-15}		1.59×10^{-14}

Table 3.3: The fluxes and intensities measured for the nebular lines.

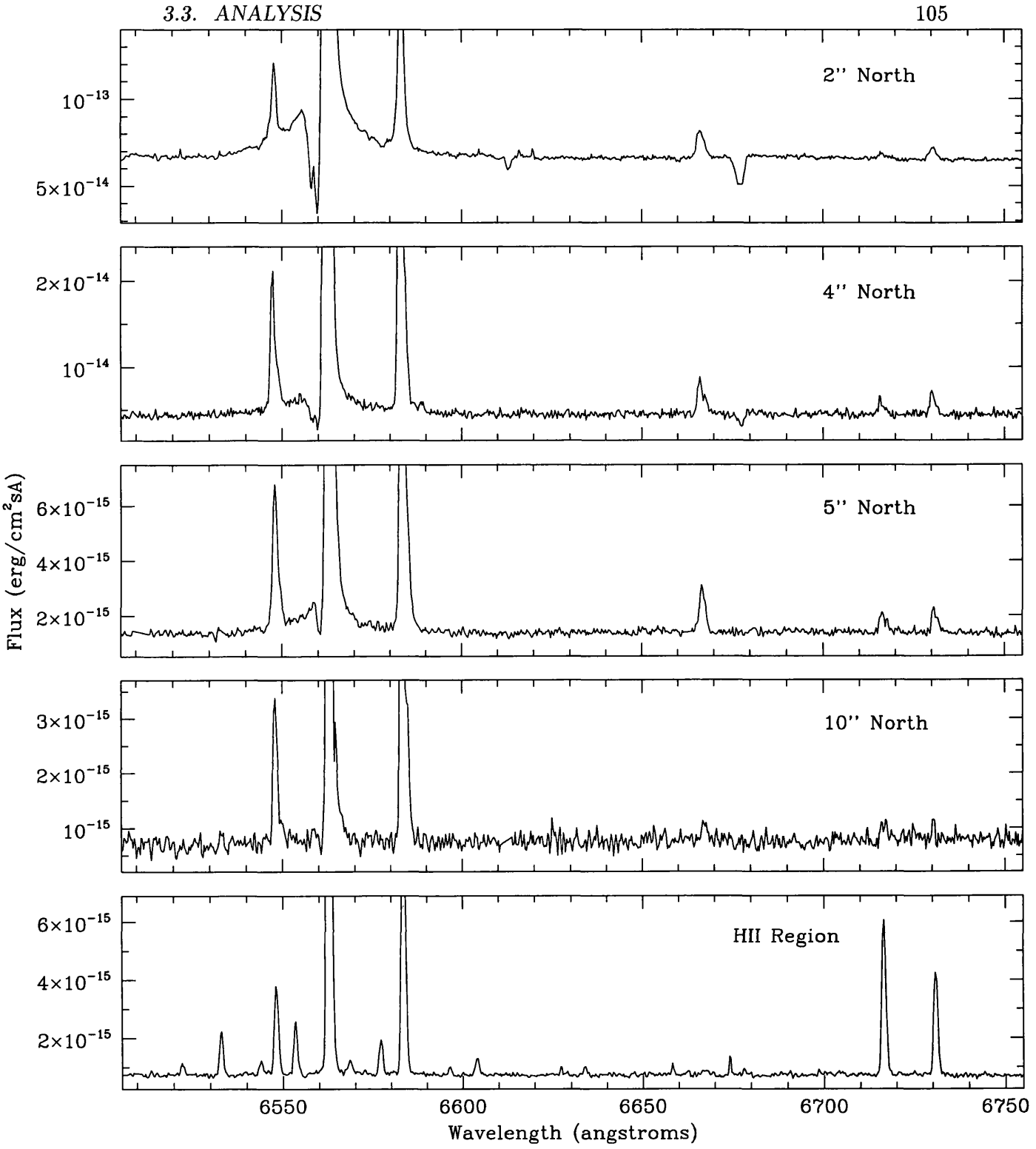

Figure 3.4: Spectra extracted from the northern lobe.

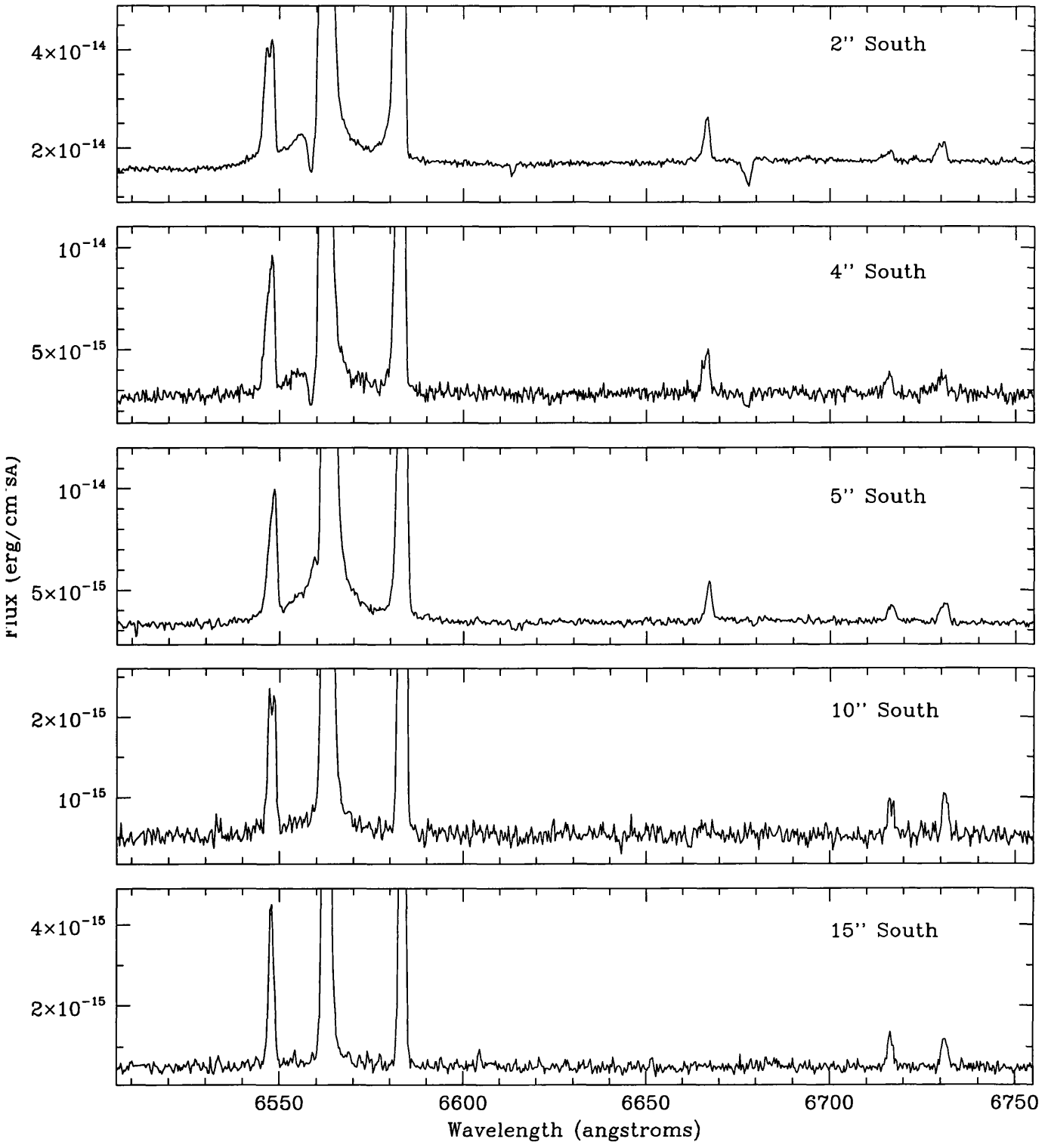

Figure 3.5: Spectra extracted from the southern lobe.

At 5" north and 5" south the key temperature diagnostic line [NII]λ5755 is resolved, being 3σ above the noise level. However the [NII]λ6584/[NII]λ5755 ratio implies an electron temperature of 11500$\pm$2000K. This is unlikely to be due to shock excitation since [SII]$\lambda\lambda$6717, 6731 indicate a density typical for LBV nebulae and so do not appear affected by shocks. This temperature is too high to be compatible with the low ionisation stages observed and suggests that our spectra are contaminated by scattered stellar light. Assuming a temperature of 10000K, we can use the ratio of the sulphur lines at 6716Å and 6731Å to estimate the density (see Table 3.4). For the inner nebula regions this ratio is at its high density limit, implying a density greater that 10^4 cm^{-3}. While in the outer reaches of the nebula the ratio is at its low density limit implying a density of less than 100 cm^{-3}. This variation swamps any possible errors due to our assumed temperature and clearly indicates a line-of-sight density gradient moving radially out from the central star.

While the abundance calculation is linearly dependent on our density estimate, it is exponentially dependent on our assumed temperature. Consequently, in order to determine HR Car's nebula abundance pattern we must constrain the temperature. To do this we will assume that any alteration of the nebular abundance pattern is due to CNO processing of the material. Under this assumption, we would not expect the abundance of sulphur to be modified, since it not created or destroyed in any of the nuclear reactions. We therefore constrain the temperature by demanding that our abundance calculation yield sulphur at a cosmic level.

To do this we must first determine what the cosmic abundance of sulphur is at this point in the Galaxy. Using the empirically derived formula of Shaver et al (1983);

- $12+\log(S/H)=7.23-0.005R_G$
- $R_G=(d\ \cos\ b)^2 - 2dR_0\cos b\cos l + R_0^2$

and assigning HR Car the Galactic co-ordinates of b=-2.2, l=285.8, a distance of d=5.4kpc and R_0=8.5kpc, yields a sulphur abundance of 12+log(S/H)=7.23.

If we now derive the sulphur abundance for the HII region surrounding HR Car, we find that a cosmic abundance is obtained if we assume a temperature of 8000K. At this temperature both the nitrogen and the oxygen abundances also have cosmic abundances. This confirms that this method of constraining the temperature works reliably. Furthermore, it indicates that the HII region is composed of unprocessed material, as this is the only way a single temperature could cause all three abundances to appear cosmic.

Applying this technique to HR Car's nebula, we derive the sulphur abundance at 11500K, 8000K and 6000K (see Table 3.6). These results imply that a cosmic sulphur abundance will be realised at a little over 6000K. We note the similarity of this to the temperature derived for M1-67 (Esteban et al. 1991), AG Car (Smith et al. 1997) and P Cygni's nebula (Johnson et al. 1992).

This temperature, in conjunction with the [SII]λ6716/[SII]λ6731 sulphur line ratio, can be used to determine the electron density at each of the positions analysed. The resulting densities (see Table 3.4) confirm that the nebular electron density tends to decrease as we move away from the central star.

Following the procedure described above, we determined the physical conditions in the nebula at the locations where spectra were extracted. This information is required to solve the equations of statistical equilibrium and so derive the abundances. It should be noted that the uncertainty in our derived temperature is likely to be the dominant source of error in the resulting abundances.

Position	n_e (cm^{-3})	T_e (K)
15″S	430^{+190}_{-160}	
10″S	660^{+740}_{-410}	
5″S	2240^{+2970}_{-1110}	$11\,310^{+2180}_{-2020}$
4″S	2400^{+4180}_{-1290}	
2″S	4260^{+5480}_{-2430}	
2″N	$> 12\,000$	
4″N	2570^{+2220}_{-1020}	
5″N	1200^{+6020}_{-1050}	$11\,470^{+2450}_{-2150}$
10″N	400^{+1440}_{-400}	
H II	< 100	

Table 3.4: The physical conditions at each slit position.

Nebula	N^+/S^+
HR Car 15″S	49
HR Car 10″S	55
HR Car 5″S	74
HR Car 5″N	68
HR Car 10″N	148
HR Car H II	7
P Cyg[1]	33
AG Car[2]	47
M1–67[3]	79
⟨H II⟩[4]	3

Table 3.5: Variations in the N^+/S^+ ratio.

References; 1. Johnson et al. (1992); 2. Smith et al. (1996)

3. Esteban et al. (1991); 4. Shaver et al. (1983).

A second method of evaluating the degree of chemical enhancement is to find the N^+/S^+ ratio. [NII]λ6548 and [SII]λ6717,6731 have similar excitation energies (Johnson et al. 1992) and so the resulting N^+/S^+ ratio has only a very slight dependence on temperature. Since the sulphur abundance is not altered by the CNO cycle, this ratio gives an indication of the change in the nitrogen abundance. The N^+/S^+ determined at each slit position is given in Table 3.5, along with that found in a number of other WR and LBV nebulae. This shows an average value, in HR Car's nebula, of about 60. This is very similar to that found in M1-67 and AG Car.

3.4 Results

This section will begin with a presentation of the abundance study results, placing them in the context of other recent nebula abundance studies. We will then outline the dynamical results obtained by Antonella Nota, Anna Pasquali and Mark Clampin for the HR Car nebula, since this information is relevant to the final interpretation and discussion of the nebula abundance pattern.

The results of our abundance study are presented in Table 3.6, where three elements are considered: sulphur, nitrogen and oxygen. No evaluation of the carbon abundance is made as it has no detectable lines in the optical. Using our data we have calculated the implied abundances under a number of assumed temperatures, 11400K, 8000K and 6000K.

Primarily we will consider the spectra obtained at -5" south and +5" north, since these are our highest signal to noise data. In these spectra we observe two ionic species of nitrogen, N^0 and N^+. These have abundances (12+log(N/H) of 8.13 and 7.89 at 5" south and 8.26 and 7.97 at +5" north, assuming an electron temperature of 6000K. Summing these to give an elemental nitrogen abundance yields

8.33 and 8.44 respectively. Neutral nitrogen has not been clearly detected at slit positions further out than 5". This is due to the faintness of the nebula and so lower resulting signal to noise ratio of these spectra.

From these data it was not possible to determine the oxygen abundance, as no oxygen lines were clearly detected. However we were able to determine an upper limit for the flux of [OII] 3727 and so determine the maxium oxygen abundance consisitent with the data. To do this we estimated the flux which would be three sigma greater than the level of the noise and so would count as a line detection. This places an upper limit of $12+\log(O^+/H^+)$ =8.52 at 5"north and $12+\log(O^+/H^+)$=8.38 at 5"south. If the temperature were any greater than 6000K these abundances will fall rapidly. Because of oxygen and nitrogen have similar first stage ionisation potentials, it is unlikely that a significant quantity of oxygen is present in the neutral state. Consequently we take O^+/H^+ >8.4 as an upper limit on the elemental oxygen abundance. Since the cosmic oxygen abundance is 8.70 we conclude that there is evidence for oxygen being deficent in this nebula. The ionic and elemental abundances derived at each position are presented in Table 3.6.

Finally we note that the elemental sulphur abundance is comprised of two contributions one from S^+ and the other from S^{++}. The only S^{++} line in the wavelength range covered by our data is [SIII] 6312, which is weak and not detected in our observations. Consequently this is of little help in constraining the S^{++} abundance. However S^{++} is not expected to be present in a significant quantity in low excitation nebulae such as this. In light of this we take the abundance derived using the [SII]6731 line to be representative of the total sulphur abundance.

For the dynamical analysis of HR Car's nebula further observations were obtained, in addition to those used for the abundance study. Using ESOs NTT between 26-29^{th} of January 1996, images were taken at five further slit positions. These were

Ion	Abundances (12+log X/H)									
	$T_e = 11\,400$ K			$T_e = 8\,000$ K			$T_e = 6\,000$ K			Average
	5″N	5″S	H II	5″N	5″S	H II	5″N	5″S	H II	H II*
N^0/H^+	6.98	6.89		7.60	7.48		8.26	8.13		
N^+/H^+	7.10	7.04	6.98	7.52	7.44	7.40	7.97	7.89	7.84	
N/H	7.34	7.19		7.86	7.76		8.44	8.33		7.57
O^+/H^+	< 7.06	< 6.93	8.05	< 7.76	< 7.62	8.75	< 8.52	< 8.38	9.50	8.70
S^+/H^+	5.32	5.21	6.13	5.72	5.59	6.54	6.14	6.02	6.97	
S^{++}/H^+	< 5.60	< 5.84	< 6.60	< 6.30	< 6.51	< 7.29	< 7.02	< 7.26	< 8.05	
S/H	< 5.78	< 5.93	< 6.73	< 6.40	< 6.56	< 7.36	< 7.07	< 7.28	< 8.08	7.06

* Shaver et al. (1983)

Table 3.6: The results of the abundance analysis.

at off sets from the star of 0, 2"and 4" south and 2" and 4" north, again with an east-west orintation. This new data was used to study the dynamics of the innermost parts of the nebula. Gaussians were then fitted to the line profiles and the wavelength shifts determined.

The first feature to emerge from this dynamical study was the markedly different dynamics of the two lobes. The line profiles from the eastern lobe were blueshifted, while those from the western region were redshifted. This is consistent with two outwardly expanding bipolar lobes. Under the assumption of a bipolar geometry it is possible to determine the nebular orientation. The orientation is characterised by two parameters. Firstly, the angle between the major axis of the nebula and the line of sight-right ascension plane. Secondly, the angle between the nebula's major axis and the line of sight-declination plane. By applying a least-squares fitting procedure to the velocity distributions a best fit is found to occur with an angle of about 50^o between the nebula's major axis and the right ascension axis and an angle of approximately 30^o between the major axis and the declination axis.

With this determination of orientation we can de-project the velocities implied by the line profile shifts to find the true expansion velocity. Doing this we derive a maxium expansion velocity of 115 km sec^{-1}, which assuming a distance of 5.4kpc implies a dynamical age of the order of 5000 yrs.

3.5 Discussion

HR Car is one of the few Galactic LBVs and accordingly has been the target of many observations. Dispite this effort, it is only recently that a clear picture of this object has started to emerge. HR Car displays many facets in common with other LBV nebulae, the bipolarity, the expansion velocity and the nebular abundance pat-

tern. However, it also has some properties with differ from those seen in other LBV nebulae. Most interesting of these are the density enhancement toward the nebula "waist", the extensive cool dust laying outside the nebula and the lack of any crystaline silicate dust, seen in nebula like AG Car. Any complete model of LBVs must embrace both the features common to all the LBV nebula and the excentricities of the individual nebulae.

We will begin by considering the implications of the abundance study. Under the assumption that sulphur should have a cosmic abundance, we derived an electron temperature of a little over 6000K for HR Car's nebula. This in turn implies a nitrogen abundance of 12+log(N/H)=8.4 and an oxygen abundance of less than 8.4. First we note that this is consistent with the nebular abundance pattern found for M1-67 (Esteban 1991), AG Car (this thesis), RCW 58 (this thesis), He 3-519 (this thesis) and NGC 6164/5 (this thesis). We conclude from this that the nebula surrounding HR Car has an abundance pattern which is typical for ejecta nebula surrounding massive stars. Furthermore this fact suggests that stars on the same evolutionary track eject their nebula at a common point.

The question naturally arises as to which evolutionary phase encompasses the nebula-forming event? By comparison with the evolutionary models of Meynet et al (1994) we see that a star of HR Car's luminosity achieves this nebula abundance pattern on the stellar surface toward the end of the Red Supergiant phase. However the blueward evolution of a post-RSG star is extremely rapid, crossing the HR diagram in about 100 yrs (we see this happening with IRC+10420; Kastner & Weintraub 1995). However, theoretoical predictions for the surface abundances in massive post-main sequence stars are not totally reliable since they do not predict the observed range of the helium abundance seen in Of stars. The models should be used as a guide, but employed with caution. The implication of this is that the abundance pattern testifies to the nebula being ejected close in time to the end of the RSG phase, but cannot distingush how far, if at all, the star had evolved blueward.

Further evidence that HR Car ejected its nebula near the end of the RSG phase comes from the ISO observation of Lamers et al. (1996), who find emission from dust extending well beyond the visible nebula. They find that the dust emission has two components, one from comparatively hot dust at a location consistent with the optically visible nebula and a second component which is from cooler dust, extending to a greater distance from the central star. A natural interpretation of this cool dust emission is to suggest that it originates from dust formed in the wind of a RSG star. We argue against the dust being formed in previous LBV outbursts on two grounds. Firstly, the uniformity of LBV nebulae abundance patterns, in conjunction with the large nebula masses, suggest that only one ejection event occurs. Secondly, Hutsemekers (1994) found a relationship between the nebula mass and stellar luminosity, but no relation beetween the nebula mass and dynamical age, which also implies the nebulae are formed in a single event.

A second diagnostic that we can use to determine the epoch of nebula ejection is the nebula dynamics. It is expected that the nebula expansion velocity will broardly reflect the stellar escape velocity when the nebula was ejected. Now HR Car's nebula is expanding with a velocity of about 100 km s^{-1}, suggesting that it originated from a star with a low surface gravity. To place this in context we note that a $35M_{\odot}$ RSG has an escape velocity of about 80 km s^{-1}, while a $35M_{\odot}$ BSG has an escape velocity of 500-800 km s^{-1}. Naivly this supports our inference that the HR Car's nebula was ejected during a RSG phase, however a second possibility exists which is also consistent with both the abundance pattern and the dynamics.

The modified Eddington limit is dependent on the effective opacity, which peaks at 12000K (Lamers&Fitzpatrick 1987). This means that the star's effective surface gravity will decrease as it approches this temperature. During a RSG phase the star will loose a great deal of mass. For example a star with an initial mass of $60M_{\odot}$

will loose about $10M_{\odot}$ (Jones et al. 1993). Consequently, when it returns to the blue it will be over-luminous, which may cause it to exceed its modified Eddington limit and so have an extremely low surface gravity (Humphries and Davidson 1994). Under these circumstances we would expect a very high rate of radiatively-driven loss of mass to occur at a low outflow velocity. Furthermore, since the evolution blueward is rapid, such a star would have surface abundances which are effectively the same as those at the end of the RSG phase. From this we conclude that there are two regions of the HR diagram from which HR Car could have ejected its nebula, the end of the RSG phase and the region of its track around 12000K.

Observationally it is hard to distinguish between these two senarios. One approach may be through an analysis of the dust present in the nebulae. Some chemical pathways are suppressed more than others by a strong UV radiation field and so it is likely that nebulae ejected from a stars with effective temperatures of 3000K and 12000K contain different molecules. To model these differences requires a knowledge of the hydrodynamics involved, which are at present unclear. We will return to the potential observational differences between these two senarios later, in particular we will focus on the significance of the nebular bipolarity.

The dynamical work of Antonella Nota, Anna Pasquali and Mark Clampin clearly demonstrates the bipolar nature of HR Car's nebula. Asymmetry is a feature common to all well-resolved LBV nebula. This is an important fact and one which is telling us something fundamental. What is the cause of the LBV nebula bipolarity?

To address this we must look at the possible mechanisms which have been proposed for the shaping of LBV nebulae. There are two basic routes by which the asymmetry can be introduced, through rotation and through magnetic fields. The latter is unpopular since the presence of magnetic fields has not been established observationally and there is some doubt as to whether they could avoid decaying

by the post main sequence phase. The former, rotation is the route en vogue. Rotation could potentially introduce bipolarity into the LBV nebulae in two ways. It could cause earlier stages of stellar evolution to create asymmetries in the surrounding circumstellar medium, which then shape the intially spherically expanding LBV nebula. The earlier asymmetry might be caused by an asymmetric RSG wind or the remnants of a protostellar disc, an affect of rotation acting in the collapsing gas cloud (Nota et al. 1995). Alternatively, rotation might lead to the star ejecting an intrinsically asymmetrical nebula (Frank 1997).

In this context, HR Car is an important object as there is evidence that it is, and always has been, losing mass asymmetrically. Firstly we note that the "funnel-shaped" structure in the HII region to the west of HR Car is likely to have formed as a result of the impact of the wind. However the shape of the funnel is too closed to form part of a spherically symmetrical bubble. Indeed the centre of the "funnel" is aligned with the major axis of HR Car's bipolar nebula. Under the assumption that the "funnel" is a wind-blown bubble Weis et al. (1996) estimate its age at 1-2x10^5yrs. This suggests that HR Car has had an asymmetric wind for at least this time.

Further evidence of asymmetric mass loss comes from the spectropolarimetric observations of Clampin et al (1995). They show that emission close to the star is intrinsically polarised and conclude that asymmetries are present in the wind within a few stellar radii of HR Car. Furthermore, they note that the absorption lines in HR Car's spectra are narrow. If these lines have a photospheric origin, then this would imply a low vsini, since our line of sight is not parallel to the major axis.

How are we to reconcile the spectropolarimetric observations, which show intrinsic polarisation, with the inference from the photospheric absorption lines that the star now has a low rotation rate? One possiblity is that the presence of a circum-

stellar disk may have resulted from rotation at an earlier epoch. If a dense disc were to dissipate over a long timescale, the spectropolarimetric results would then be a consequence of scattering from this disk. Further evidence for a disk surrounding HR Car comes from the presence of CO overtone and [NiII]λ6667 emission, both of which require the presence of very high densities. In addition to this we note the trend of increasing densities at slit positions closer to the central star. All of these factors support the inference that a circumstellar disk may be associated with HR Car. The presence of a disk may be explicable if HR Car lies near its Ω limit. If this were the case then its mass loss would be inherently asymmetric, even if its Vsin(i) were comparatively low. There is some evidence that heavy mass loss from near the Ω limit may lead to the formation of a disk (see Chapter 6 and Section 1.4.2).

Chapter 4

The Common Origin of Ejecta Nebulae.

4.1 Introduction

In this chapter we will present abundance studies of two nebulae, one surrounding a WR star (RCW 58), the other surrounding an LBV (He3-519). Deep long-slit spectroscopic observations were made by L.J Smith and myself using the Anglo-Australian Telescope (AAT) in the April of 1996. Images were taken at one slit position, where we ensured that they were of sufficiently long exposure to clearly detect the [NII]λ5755 line. An accurate abundance analysis of these nebulae allows a direct comparison to be made of the abundance pattern in a nebula surrounding a WR star to that in a nebula surrounding an LBV star. The depth of the spectroscopic images allowed very tight constraints to be placed on the nebular electron temperature, yielding small errors on our resulting abundances. This in turn allowed a comparatively rigorous test of the suspected uniformity of abundance pattern between the two nebulae. This work is being prepared for publication in MNRAS.

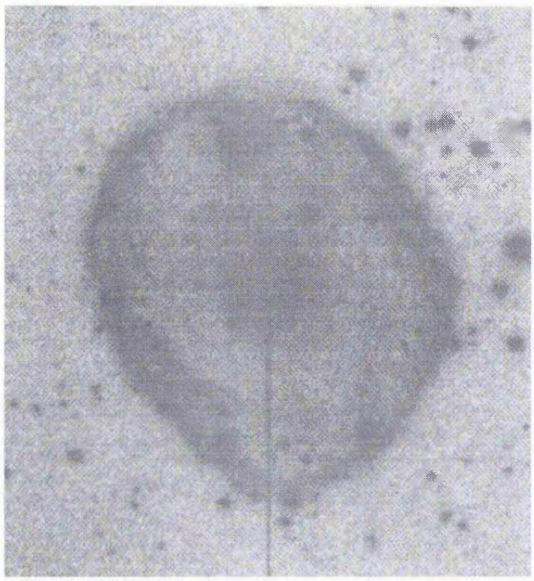

Figure 4.1: A Hα image of the nebula surrounding He3-519.

4.1.1 He3-519.

The presence of a nebula surrounding He3-519 (see Figure 4.1) was first detected by Hoffleit (1953). In addition to which He3-519 and AG Car are spectroscopically very similar (Henize 1976; Stahl 1986; and Walborn 1990). Despite this He3-519 has received little investigation in comparison to other LBV candidates. This omission was corrected by two papers, Davidson et al. (1993) and a more extensive work by Smith et al. (1994). In this section we will review these papers in some detail. Firstly we wish to establish the basis on which the LBV candidacy for He3-519 has been proposed, since we are classifying this as an LBV nebula. Then we will give an overview of the previous work on the nebula.

Davidson et al. obtained UV spectra covering 2000-3300A using the IUE satellite, and made U,B,V and R photometric observations using the 0.9m Cerro Tololo telescope. To estimate the stellar temperature they argued that the helium λ4471 line is probably formed by ionization and recombination in the stellar wind. From the strength of this line they estimate the flux of helium-ionising photons required, which is then used to constrain their choice of black-body . In this way they infer

an effective temperature of between 35000-40000K.

Using this stellar temperature they were able to determine the degree of reddening. To do this Davidson et al. de-reddened a 35000K black body curve for a range of reddenings (E(B–V)=1.2-1.6). The resulting continua were then compared to the observed photometric magnitudes in order to determine the best fit. In this way they found E(B-V)=1.4 for He3-519. However we note that their estimation of the line contribution to the photometric magnitudes were most uncertain, particularly for the V-band were they had to "guess the brightness of HeIλ5876, Hα and other emission lines" (Davidson et al. 1993).

The distance to He3-519 was then determined using the reddening distance method. This involves taking a sample of stars near to the line-of-sight of He3-519, deducing their luminosity on the basis of their spectral type and then measuring their reddening. The result is a plot of reddening verses distance. By carrying out this procedure for He3-519 Davidson et al. derive a minimum distance of 6kpc and estimate the true value is probably nearer 8kpc. On the basis of this distance they infer a luminosity of $2\times10^6 L_\odot$, a little brighter than AG Car and well above the HD-limit. In the light of the luminosity, the spectral characteristics of He3-519 and the presence of a ring nebulae, Davidson et al. (1993) proposed its LBV candidacy.

The second paper published in 1994 on He3-519 was by Smith et al. based primarally on observations made with the Anglo Australian Telescope (AAT) using the UCL echelle spectrograph. Stellar and nebular spectra were obtained of sufficiently high resolution to allow the application of a non-LTE model atmosphere code (Hillier 1990) to the central star. The results of this analysis differ significantly from those of Davidson et al.

The absence in the spectra of NHI and SiIV, prevent He3-519 being classified

as a Ofpe/WN9 star. Closest agreement is found between the He3-519 spectra and those of AG Car just after minimum in 1990/1991. However it is difficult to assign either case a unique spectral type within the present classification scheme. Consequently Smith et al. introduce new WN subtypes to incorporate these stars. In this scheme He3-519 is classified as a WN11 star due to the absence of NIII and NIV, but strong NII lines.

Both the nebular spectra and the detected interstellar bands were employed to calculate the interstellar reddening. By comparing the observed Hα to Hβ ratio to that theoretically expected (Hummer & Storey 1987), an E(B–V) of 1.14 was deduced. While the interstellar bands observed in the UCLES spectra also imply an E(B–V) of 1.14.

He3-519 lies towards the Carina nebula, which itself is at a distance of 2.5kpc, accordingly this is the distance adopted by Stahl (1986) for He3-519. However, it has since been established that LBVs like AG Car lay on the far side of the nebula (Humphreys 1989) a conclusion also reached by Davidson et al. for He3-519, based on the reddening method. Using their nebula spectra, Smith et al. derive a systemic velocity of 27.6 km s^{-1}. It is not possible to do this with stellar lines since they are either blended or have P Cygni profiles. By using the Galactic rotation curve of Fich et al. (1989) it is found that this systematic velocity corresponds to a distance of 8$\pm$1kpc. This is in excellent agreement with the distance derived by Davidson et al. (1993). Combining the reddening, the distance and the visual magnitudes (Stahl 1986), implies an absolute visual magnitude of M_v=-7.1 with an intrinsic E(B–V) colour of -0.12.

Using the wind velocity with a β=1 velocity law as a constraint, the non-LTE model atmosphere code of (Hillier 1990) was applied to derive the stellar temperature, luminosity, radius, mass loss rate and hydrogen to helium ratio. He3-519

is found to have an effective temperature of 27500K, luminosity of $L/L_{\odot}$=5.66, $R/R_{\odot}$=30, X=0.33 and a mass loss rate of $1.3\times10^{-4}M_{\odot}$ yr^{-1}. Both the derived temperature and luminosity are very different from those found by Davidson, the discrepancy being due to the latter using a black body approximation for the continua. This new estimate of the luminosity places He3-519 below the HD-limit and so may well imply a different evolutionary history. While this more detailed analysis finds a lower luminosity for He3-519 than infered by Davison et al (1993), the luminosity is still within the range found for other LBVs (Crowther et al. 1997).

The combination of the derived mass loss rate, hydrogen abundance, spectral characteristics, luminosity and the presence of a ring nebula, all of which are comparable to other LBVs, make a powerful case for He3-519 being also being an LBV. The key factor missing which would definatively allow its classification as an LBV, is the lack of observed long-term variability in its temperature. This is not unique amongst LBVs since no such variability has been observed in prototype objects like P-Cygni. While He3-519 remains in a dormant phase it represent a very plausible LBV candidate.

Turning now to the nebula surrounding He3-519, we find that it has been subject to relatively little investigation. The first analysis of the ejecta nebula, based on a realistic distance to He3-519 has been made by Davidson (1993). He assumed that the ring nebula is an ejecta nebula with a density and filling factor typical of those seen around other LBVs. A estimate of the nebula mass was then made based the observed Hα flux. Because of the numerous uncertainties this is thought to be between 1-10$M_{\odot}$.

A more rigorous study of the ring nebula was undertaken by Smith et al (1994) who made spectroscopic observations of the nebula. These were made at two slit position with position angles of 45° and 119°. High resolution two dimensional spectral

images were taken covering Hα and [NII]. In addition to this the RGO spectrograph was employed to obtain nebula spectra covering the wavelength range $\lambda\lambda$3560-7125, allowing a fairly detail analysis.

The spatio-wavelength images revealed a complex velocity structure, with the FHWM of the lines varying from 30 km s^{-1} upto 60 km s^{-1}, while over all retaining an elipsoidal geometry. From the line splitting an expansion velocity of 61 km s^{-1} is derived. If the nebula lies at 8kpc then it has a radius of 1.14pc and so a dynamical age of 1.8×10^4yrs.

Assuming an electron temperature of 8000K, the [SII]λ6731/[SII]λ6717 line ratio indicated an electron density of 300 cm^{-3}. Under the assumption of these physical conditions the Hα flux requires a nebula mass of the order of $2M_\odot$. This is an aproximate value since it assumes that the electron density derived is typical of the whole nebula and that the helium abundance is not significantly enhanced, which is probably untrue.

4.1.2 RCW 58.

The nebula RCW 58, surrounding the Wolf-Rayet star WR40 (HD 96548), has proved a favoured testing ground for dynamical models. There exists strong evidence that the nebula consists of a system of two shells. Deep narrow band optical imaging, centered on H α 6563A and [OIII] 5006A was under taken by Chu et al. (1982). This revealed the presence on two distinct nebulae, one seen at each band pass, which were not co-spatial. It was suggested that this system of shells corresponds to an ejecta nebula interacting with a wind blown bubble. More recently Marston et al. (1994) obtain simarly elegant images (see Figures 4.2 4.3).

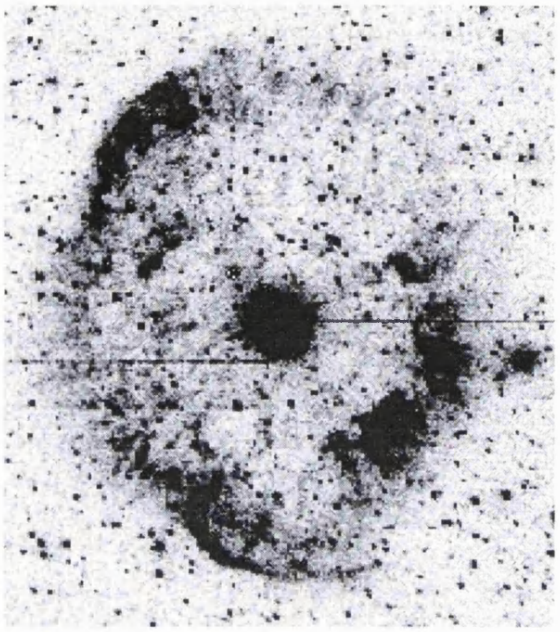

Figure 4.2: A deep H alpha image of RCW58 (A.P.Marston)

The dynamics of the nebula have been studied by Smith et al. (1984) who found that the nebula expansion velocity, as traced by different ionic species, is correlated to the ionization potential of each species. This work was developed by Arthur et al. (1992) who modelled the interaction of a mass loaded wind with the highly clumpy nebula structure. They found that this velocity dispersion could be explained by the entrainment of clump material by the impacting wind. In a second paper by Smith et al. (1988) the dynamical properties of the nebula were further investigated in a spatially resolved spectroscopic study using a number of emission lines. This revealed that RCW 58 is a well defined, regular shell, expanding at 87 ± 3km s^{-1}.

Confirmation of the ejecta nature RCW 58 came from the nebula abundance pattern. This was first investigated by Kwitter (1984), however they did not detect the [NII]λ5755 temperature diagnostic line. Instead they used the temperature which made the oxygen abundance cosmic. Under this assumption they found the nebula abundance pattern to be enriched in both nitrogen and helium.

A more comprehensive nebula abundance study was undertaken by Rosa et al (1987). A photoionisation code was used to model the ionisation balance of a number

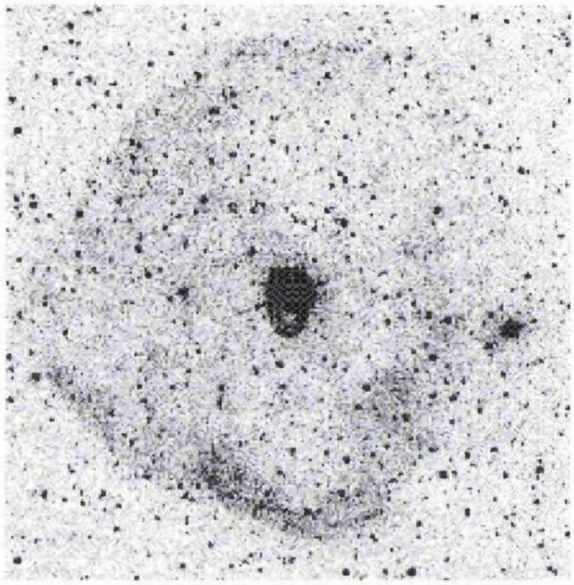

Figure 4.3: A deep [OIII] image of RCW58 (A.P.Marston)

of ionic species, yielding the temperature and abundance pattern. The abundances found were log(O/H)+12=8.72, log(N/O)=−0.30, log(He/H)+12=11.37. This study concured with that of Kwitter (1984), in finding that both helium and nitrogen were over abundant. In addition to which they find oxygen to be over abundant relative to Orion, which they take to represent unprocessed material. They do not discuss this surprising result.

It is not clear whether RCW 58 originated through a bulk ejection of material from the stellar surface or through the interaction of different stellar mass loss phases. The latter possibility has been investigated by Garcia-Segura et al. (1996) using a hydrodynamical code, taking its input from the tracks of Langer et al. (1994). Garcia-Segura finds that the dense, thin LBV shell is unstable to "nonlinear thin shell instabilities". This causes the nebula to break up in to clumps with a small, but regular angular frequency, in contrast to "Vishnic" instability which arises when a WR wind impacts onto the reminants of a RSG wind, resulting in clumping with a longer angular frequencey. Furthermore, as the nonlinear thin shell instability develops the clumps take on a cometary appearence due to the entrainment of material from them. They concluded that this picture is broadly consistent with RCW 58.

However we note that these conclusions rest on the detailed mass loss history used in Langer's tracks being correct for the LBV outburst phase. Since the outburst mechanism is not known, this should perhaps be considered an illustration of a new important techneque, rather than giving a definitive description of the mass loss from RCW 58.

4.2 Observations of He3-519 and RCW 58

The observations were made on 26^{th}&27^{th} April 1996 using the 3.9m Anglo-Australian Telescope. The data were acquired specifically for this abundance study and so designed to detect the important diagnostic lines [NII]$\lambda\lambda$5755,6584 and [SII]$\lambda\lambda$6717,6731. The RGO spectrograph was used in conjunction with a Thomson CCD to obtain very deep spectral images at one slit position on each of the two nebula. This configuration yielded a spectral resolution of 0.80Å and a spatial resolution of 0.5". During the observations the seeing was typically one arc second.

Deep long-slit spectroscopic images were taken covering five spectral regions between 3643Å and 9689Å (see Table 4.1). The primary aim being to resolve the [NII] 5755Å line with the minimum error on the flux. The slit positions were chosen to include the brightest region of each nebula, so as to maximise the signal to noise ratio. For He3-519 we chose a slit position with a position angle of P.A.=33^o and an off set of $\Delta\delta$=21"south and $\Delta\alpha$=11"west. While the slit position used for RCW 58 had a P.A.=23^o and an off set of $\Delta\delta$=3.6' south and $\Delta\alpha$=14.6" west. To flux calibrate the data we observed two standard stars HD 60753 and LTT 6248. In both cases the slit had the dimensions of 2" by 4.2".

The data were reduced using the FIGARO and DIPSO packages on STARLINK. We subtracted the bias, wavelength calibrated and cleaned the images of cosmic rays.

Date	Wavelength Range	Exposure Time (sec)
Slit position 3 PA=45		
1996 Apr 26	3643-4452	300
1996 Apr 26	4409-5221	300
1996 Apr 26	5593-6405	700
1996 Apr 26	6389-7199	200
1996 Apr 26	8904-9689	500
Slit position 2 PA=0		
1996 Apr 27	3643-4452	2000
1996 Apr 27	4409-5221	1000
1996 Apr 27	5593-6405	2000
1996 Apr 27	6389-7199	500
1996 Apr 27	8904-9689	500

Table 4.1: Journal of observations.

The sky was subtracted and the images extinction corrected. Spectra were then extracted over regions of apparent uniform temperature and density. The ELF routine in DIPSO was used to fit Gaussians to the emission line profiles, enabling the line fluxes and associated RMS errors to be determined. By comparing the observed ratio of H β to H α, H γ, H δ, H ϵ, H 9 and H10 to that theoretically expected, we then determined the interstellar extinction coefficient (Hummer & Storey 1987). This yielded a value of C=1.55 for He3-519, which compares well to the value of C=1.65 found by Smith et al. (1994). For RCW 58 we obtain an extinction coefficient of C=0.33. This is a little lower than the previous value of C=0.64 derived by Kwitter et al. (1984). Figures 4.4 & 4.6 show examples of the reduced spectra obtained for He3-519, while Tables 4.2 & 4.3 show the observed and de-reddened line fluxes for both RCW 58 and He3-519.

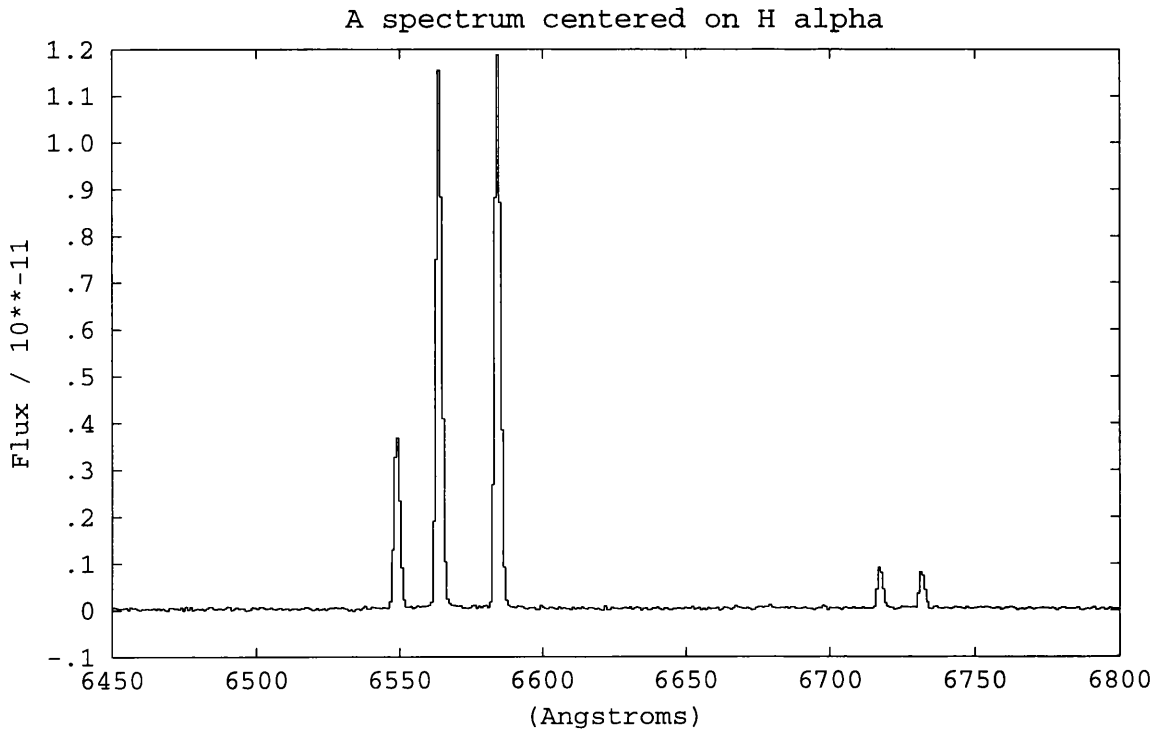

Figure 4.4: An example of the Hα, [NII]$\lambda\lambda$6548,6584 and [SII]$\lambda\lambda$6717,6731 emission lines from He3-519

4.3 Results.

In this section we will present the results of our abundance study and set the stage for the discusson that follows. These observations were reduced and analysed in the same way as those for AG Car and HR Car. Consequently, we will not describe this process in full, but instead only draw attention to eccentricities encountered in these new data sets.

Our first task was to find the physical conditions in the nebulae. In the case of He3-519 no complications arose and so the analysis proceeded as described in Chapter 2.3. However, RCW 58 presented a greater challenge, due to its more complicated dynamical structure. A further complicating factor for RCW 58, was that the sulphur and oxygen density diagnostics gave conflicting results.

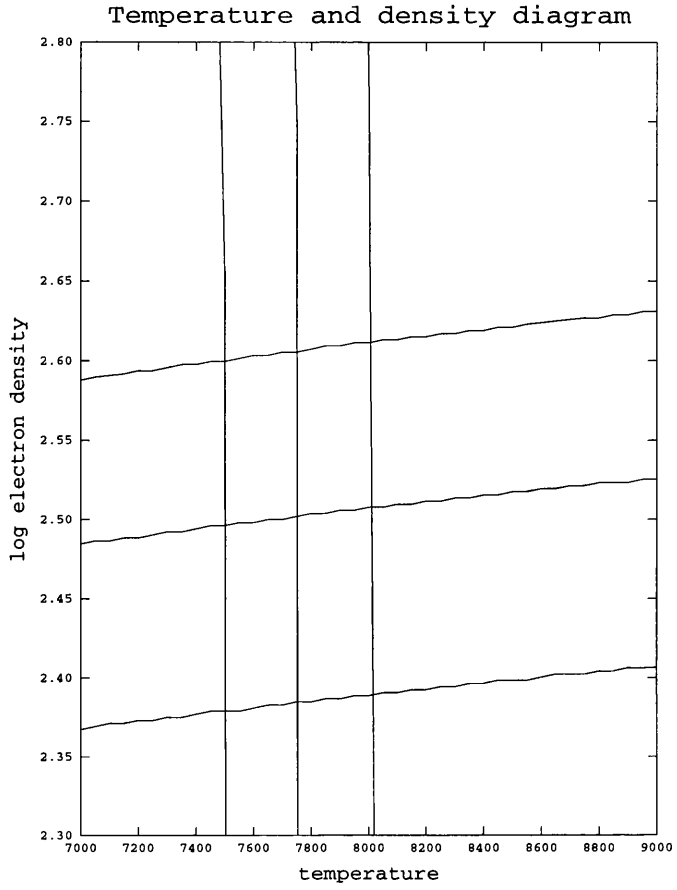

Figure 4.5: A diagnostic diagram showing the temperature and density implied by the sulphur and nitrogen line ratios for He3-519. The outlying line represent the maxium errors due to the uncertinty on the line ratios.

In He3-519 the oxygen density diagnostic lines 3726A and 3729A are blended and so only the sulphur lines [SII] 6717 and [SII] 6731 were employed. These lines in conjuction with the [NII]λ5755 and [NII]λ6584 temperature diagnostic lines imply an electron temperature of 7751^{+267}_{-250}K and an electron density of 316^{+108}_{-78} cm^{-3}. A diagnostic diagram is displayed in Figure 4.5, this illustrates the physical conditions under which both the line ratios can co-exist. This density is in excellent agreement with that found by Smith et al. (1994), who determined an electron density of 300^{+135}_{-105}. However they were forced to assume an electron temperature of 8000K.

For RCW 58 our sulphur and oxygen diagnostic lines gave differing electron densities. The sulphur ratio indicating an extremely low value, near the low density

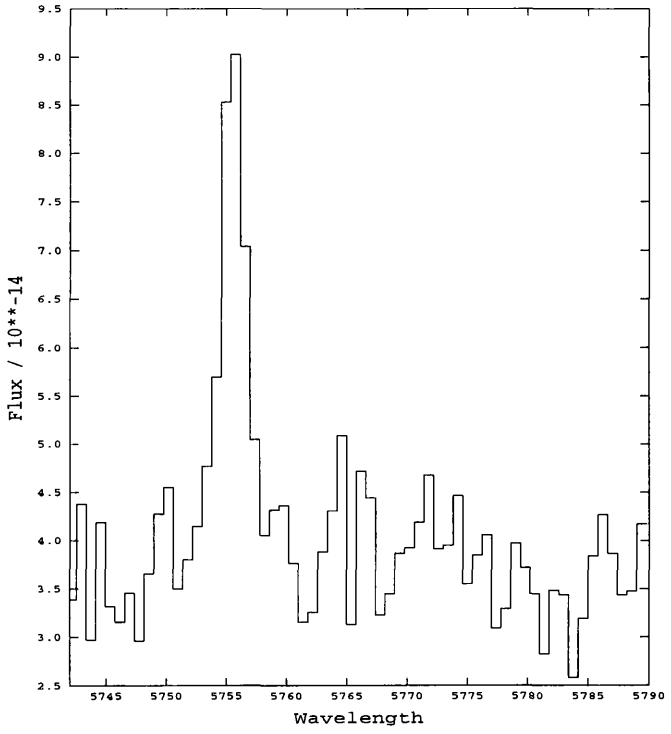

Figure 4.6: The Nitrogen 5755 line from He3-519.

limit. This is unusual for both an ejecta nebula and a wind-blown bubble (WBB). The oxygen line ratio implies an electron density of about 500 cm^3. Given the highly clumpy nature of the nebula, we treat these values with caution. However, the final abundance pattern has little dependance on the electron density, since it is mainly dependent on the electron temperature. Given these uncertainties we will assume an electron density of 300 cm^{-3}. Using the oxygen and nitrogen lines we derive an electron temperature of 8160^{+267}_{-250}. These physical conditions are typical of those found in other ejecta nebulae and so are unlikely to be in serious error (see Table 4.3). While the electron temperature is very similar to that assumed by Kwitter (1984), the electron density is somewhat greater than their value of 190 cm^{-3}.

An additional problem arose for RCW 58, since the nebula consists of two largely concentric shells, which may have different compositions and physical conditions

(Chu 1982). These two shells have been interpreted by Marston (1996) as a WBB sweeping up a previous RSG wind and a LBV second shell ejected during the LBV phase. Our spectra were not of sufficiently high resolution to dynamically separate these shells. This raises the question as to what extent the blending of the line profiles from different physical regions is important? To tackle this question we took advantage of high resolution spectra taken at the same slit position by Smith et al. (1985). These archive spectra show the presence of the two shells, but indicates that the flux from the WBB is about one third that of the LBV ejecta. This means that it is the emission from the ejecta nebulae will dominate that of the WBB and so we do not expect the line blending to effect our results significantly. Further support for the view that the blending of line profiles from RCW 58 has not seriously affected our results is the remarkable consistency of the physical conditions derived for both RCW 58 and our other nebula He3-519 as well as the nebula surrounding AG Car (Smith et al. 1997) and M1-67 (Esteban et al. 1990).

Once the physical conditions have been derived, we are able to model the plasma through the equations of statistical equilibrium and so relate the relative abundances to observed emission line ratios. This calculation is done using collisionally excited lines of each ionic species, finding the abundance relative to hydrogen of each. The ionic abundances were then summed to give the total elemental abundance (see Table 4.4).

We directly observed line fluxes from S^+, N^0, N^+, O^+, O^{++} and in the case of He3-519 S^{++} (see Tables 4.2 & 4.3). However a quantity of N^{++} may also be present and so must be taken into account using an ionization correction factor (I.C.F. see Chapter two). In both nebulae HeI, but not HeII lines are observed. This suggests that the ionising flux is not sufficiently energetic enough to doubly ionise helium (I.P 54.4 eV). Consequently we would not expect O^{+++} to significantly contribute to the oxygen abundance since O^{++} has an I.P of 54.9eV. This means that we are directly observing all the ionization stages that directly contribute to the final oxy-

λ_{obs}	Ion	k(λ)	F(λ)	I(λ)
3726.5	[OII]	0.257	11.8±3.0	14.4±3.7
3729.0	[OII]	0.256	11.1±3.0	13.5±3.7
4340.5	Hγ	0.127	34.6±1.6	38.1±1.8
4471.7	HeI	0.095	9.9± 2.5	10.6±2.7
4959.0	[OIII]	-0.024	9.7±1.0	9.5± 1.0
5007.2	[OIII]	-0.036	30.6±1.3	28.6±1.2
5755.1	[NII]	-0.195	2.9±0.2	2.5±0.2
6300.0	[OI]	-0.282	3.1±1.0	2.5± 0.8
6548.2	[NII]	-0.318	116.8±5.6	91.7±4.4
6562.6	Hα	-0.320	359.4±16.4	281.8±12.9
6583.1	[NII]	-0.323	371.2±1.7	290.4±1.3
6678.7	HeI	-0.336	9.6±0.8	7.5±0.6
6716.5	[SII]	-0.342	12.1±0.7	9.4±0.5
6731.7	[SII]	-0.344	7.4±0.7	5.7±0.5

$F_{obs}(H(\beta)) = 8.674\times10^{-12}\pm1.315\times10^{-13}$ergs/cm^2/str/s

Table 4.2: The observed and de-reddened line fluxes from RCW 58.

λ_{obs}	Ion	k(λ)	F(λ)	I(λ)
3727.5	[OII]	0.256	9.8±1.6	24.4±4.0
3970.5	Hϵ	0.210	8.6±0.5	18.1±1.1
4100.5	Hδ	0.182	14.1±1.9	27.0±3.7
4340.7	Hγ	0.127	32.6±1.7	51.3±2.7
5006.2	[OIII]	-0.036	4.7±1.1	4.2±1.0
5200.3	[NI]	-0.083	19.4±1.9	14.4±1.4
5755.0	[NII]	-0.195	5.0±0.4	2.5±0.2
5875.1	HeI	-0.214	5.1±0.4	2.4±0.2
6312.8	[SIII]	-0.283	1.0±0.2	0.4±0.1
6547.8	[NII]	-0.318	333.9±7.1	107.3±2.3
6562.6	Hα	-0.320	1002.8±7.0	320.0±2.2
6583.2	[NII]	-0.323	1062.2±6.8	335.4±2.2
6716.5	[SII]	-0.342	74.5±1.9	22.0±0.5
6730.7	[SII]	-0.344	66.8±1.7	19.6±0.5

$F_{obs}(H(\beta)) = 2.795\times10^{-12}\pm2.713\times10^{-14}$ergs/cm^2/str/s

Table 4.3: The observed and de-reddened line fluxes from He3-519.

gen abundance . This is important as the ICF used is based on the abundance of oxygen ionic species and its total elemental abundance. The ionization correction factors use are (Kingsburgh & Barlow 1994);

$$\mathrm{ICF(N)} = \mathrm{O/O^+}$$
$$\mathrm{A(N)} = \mathrm{ICF(N)} \times \mathrm{N^+ \ / \ H^+}$$
$$\mathrm{ICF(S)} = (1\text{-}(1\text{-}(\mathrm{O^+ \ / \ O})^3))^{(-1/3)}$$
$$A(N) = ICF(S) \times (\mathrm{S^+ + S^{++}})/\mathrm{H^+}$$

In this way we derived the abundances presented in Table 4.3. We see that in addition to the two nebulae having almost identical physical conditions they have very similar oxygen and nitrogen abundances. What is even more remarkable is the fact that this abundance pattern is also indistinguishable from that of AG Car (Smith et al. 1997), M1-67 (Esteban et al. 1990) and NGC 6164/5 which surrounds an Of-star (Dufour et al. 1988 and Chapter 5). That is, all ejecta nebulae surrounding massive stars which have had accurate abundances studies performed upon them, have yielded essentially the same abundance pattern, regardless of whether the central star is a LBV, WR or Of star (see Table 4.5).

In Table 4.5 we give the abundance pattern of unprocessed material found in a typical HII region (Shaver et al. 1983), along with the abundance pattern expected on the surface of a $60_\odot$ LBV star, which consists of CNO equlibrium material (Langer et al. 1994). We see from this that the nebulae abundance patterns is intermediate between the two. That is, the *abundance pattern found in nebulae surrounding massive stars is that of partially CNO processed material.* Also in Table 4.5 are the results of an abundance study of the equatorial ring material surrounding SN 1987A. This circumstellar material is believed to have been deposited during a previous RSG phase (Panagia et al. 1997). We note that while the nitrogen abundance found for this material is, within errors, indistinguishable from that found in the

	Abundance (12+log X)	
	He3-519	RCW 58
S^{++}/H^+	$6.47^{+0.12}_{-0.15}$	$5.68^{+0.03}_{-0.05}$
S^+/H^+	$6.31^{+0.07}_{-0.05}$	$5.34^{+0.11}_{-0.07}$
N^+/H^+	$8.07^{+0.05}_{-0.04}$	$7.67^{+0.05}_{-0.06}$
N^0/H^+	$7.65^{+0.15}_{-0.39}$	—
O^{++}/H^+	$6.61^{+0.14}_{-0.16}$	$7.10^{+0.12}_{-0.06}$
O^+/H^+	$7.52^{+0.15}_{-0.16}$	$7.18^{+0.21}_{-0.21}$
S/H	$6.70^{+0.10}_{-0.11}$	$5.84^{+0.11}_{-0.05}$
N/H	$8.21^{+0.08}_{-0.11}$	$8.02^{+0.07}_{-0.09}$
O/H	$7.57^{+0.15}_{-0.16}$	$7.44^{+0.17}_{-0.13}$
ρ_e	316^{+108}_{-78}	$300^{+2377}_{-l.d.l}$
T_e	7751^{+267}_{-250}	8160^{262}_{-451}

Table 4.4: The derived ionic and total abundances.

ejecta nebula, the oxygen abundance is less depleted. This may be due to the lower mass of SN 1987A progenitor than the LBV progenitors. This leads to lower core temperatures in the former case and so the ON cycle, which is initiated at a higher temperature than the CN cycle, plays a less important role. On this basis we might expect more massive RSGs to have a greater degree of oxygen depletion. Over all the nebular abundance pattern that we have derived for the ejecta nebulae are similar to the abundance pattern found for the SN 1987A RSG material. This strongly suggests that the ejecta nebula were ejecta during or soon after the RSG phase. We note that the models of Meynet et al. (1994) suggest that for the most massive stars, this abundance pattern will arise at the very end of the period spent as a RSG.

	Abundances 12+log(NX/NH)				
Nebula	N/H	O/H	Log N/O	Sp Type	Refs
AG Car	8.22±0.11	7.52±0.20	+0.76	LBV	a
He3-519	8.21±0.10	7.57±0.15	0.64	LBV(?)	b
M1-67	8.45 ± 0.15	7.98 ± 0.27	+0.47	WN8	c
NGC 6888	8.40 ±0.35	8.11 ±0.28	0.30	WN6	d
RCW58	8.02 ±.08	7.44 ± 0.15	0.5	WN8	e
NGC 6164/5	8.38 ±0.02	7.95 ±0.03	+0.12	O6.5f?p	f
HII region	7.57	8.70	7.06		g
$60M_{\odot}$*model*	8.7	7.4		LBV	h
SN 1987A	8.34±0.2	8.2±0.2		RSG	i

Table 4.5: Abundance patterns determined for other LBV/WR nebulae.

References: (a) Chapter 1, this thesis; (b) Chapter 4, this thesis; (c) Esteban et al. (1990); (d) Esteban & Vilchez (1992); (e) Chapter 4, this thesis; (f) Chapter 5, this thesis. (g) Shaver et al. (1993); (h) Langer et al. (1994). (i) Panagia et al. (1994).

4.4 Discussion

In this discussion we will focus on ejecta nebulae surrounding stars evolving below the HD limit. That is, those with a luminosity of less than about log $(L_*/L_\odot)$=5.8. Of the abundance studies carried out for such nebulae, the most accurate are those presented in this chapter and in the next chapter covering NGC 6164/5. These latter results confirm a detailed abundance study made by Dufour et al. (1989). In addition to this robust nebula abundance patterns for M1-67 (Esteban et al. 1992) and AG Car (Chapter 2) have been derived. Other reasonable, but less reliable abundance studies have been carried out on HR Car (Chapter 3) and NGC 6888 (Esteban & Vilchez 1992). There are other similar nebulae for which abundance studies have been attempted but these are subject to very great uncertainties. Consequently in Table 4.5 we have presented details of only the most reliable abundance studies and will base our discussion on these.

From these abundance studies two main results emerge.

- *Within a factor of two the nebula abundance patterns are identical*

- *The nebulae abundance pattern is partially CNO processed*

In this discussion we will work through the implications of these results for the low mass LBVs (i.e those below the H-D limit), in the light of dynamical infomation taken from the literature. We find four main conclusions are reached, each is outlined in its own subsection.

4.4.1 LBV nebulae as the precursors of WR ring nebulae.

Initially we will consider what implications the uniformity of nebula abundances has for the distinction between WR and LBV nebulae. Since the LBV candidate He3-519 has a luminosity of log $(L_*/L_\odot)$=5.66 (Smith et al. 1994), while WR40 has log $(L_*/L_\odot$=5.1) (Crowther et al. 1995), we would expect that they lie on similar evolutionary tracks since both are below the H-D limit.

As discussed in Chapter 2, the dilution of the nebula abundances by swept up material, does not have a significant effect. This is because the earlier O-star phase carves out a low density cavity which contains too little material to significantly dilute the nebula material. Any wind material from the end of a previous RSG phase will have an abundance pattern very similar to the ejecta nebula and so will not effect the nebula abundance pattern. The fact that both nebulae have the same abundance pattern would then imply that they were ejected when their respective central stars were in the same evolutionary state.

Furthermore, from a survey of the literature we note that the dynamical ages of LBV nebulae are systematically lower than those of WR ejecta nebulae, the only exception being R127 (see Table 2.6). This strongly suggests *that LBV and some WR ejecta nebulae are the same objects, with the central stars being observed at different points in its evolution.*

4.4.2 The ejecta origin of the nebulae.

A key point in understanding the formation of LBV nebulae is to determine whether they result from a bulk ejection of material from the star or from the sweeping up of a slow wind phase by a subsequent fast wind. Of central importance to this issue are the nebula dynamics.

LBV nebulae typically consist (see Table 2.5) of a few solar masses of ionised material expanding at 70 km sec^{-1}. Now considering the relative amounts of momentum carried by the stellar wind and the LBV nebula we find that the expansion velocity is insensitive to the impact of the stellar wind. This point is corroborated by the lack of correlation between the nebula expansion velocity and dynamical age. That is, if the stellar wind significantly accelerates the ejecta nebula we would expect that the older nebulae would have higher expansion velocities. This is not the case (see Table 2.5).

The character of nebulae formed by a fast WR wind sweeping up an earlier slow RSG wind has been modelled by Garcia-Seguria (1996) (see section 1.5). It is found that the RSG wind builds up at a point where the wind's ram pressure is balanced by the thermal pressure of the hot main sequence bubble, into which it is flowing. When a subsequent fast wind phase begins (the model uses a WR wind, but the logic applies equally to an LBV wind) the comparatively little RSG wind mass between the star and the build up of RSG is swept up in a nebula which is expected to be too weak to detect. It is not until the fast wind reaches the build up of RSG wind material, that the emission measure increases and nebula becomes optically visible. The radius at which this occurs primarily depends, in their model, on the RSG terminal wind velocity. They computed two limiting cases, one with a RSG terminal wind velocity of 15 km s^{-1} and the other with 75 km s^{-1}. They found that the nebula becomes visible at a radius anywhere between 3-10 pc. Furthermore, at this point virtually all the mass lost in the RSG phase is visible, implying a nebula mass in excess of $10M_{\odot}$. These nebular radii and masses are quite different from nebulae surrounding LBV stars or indeed RCW 58, but they do bear a close resemblance to nebulae like NGC 6888 and S 308. Consequently we conclude that the nebulae formed from swept up RSG wind are larger and more massive than the nebulae seen around LBV and some WR stars.

From the above considerations it would seem unlikely that the nebulae consist of swept up relic RSG wind material. Instead the nebula dynamics and masses offer evidence of an ejecta origin. A large number of possible ejection mechanisms have been proposed. These fall into two main categories, hydrodynamic and thermodynamic. Into the former category fall strange mode pulsations, interaction with the omega limit and interaction with the Eddington limit, while the latter category includes instabilities connected with changes in ionization state like the Stothers and Chin model. In this context it becomes important to establish the physical conditions which prevail in the star at the epoch of nebula ejection. This can then be used to place constraints on the proposed ejection mechanisms.

4.4.3 The point of nebula ejection from LBVs below the HD limit.

The abundance pattern seen in LBV nebulae is similar to that predicted by the model tracks (Meynet et al. 1994) toward the end of the RSG phase. This is also supported by an abundance study of the material in the ring of SN1987A. This ring of is believed to consist of material lost in an earlier RSG phase (Panagia et al. 1997: see Table 4.5). From this we conclude that low mass LBVs eject their nebulae close, in time, to the the end of the RSG phase. However at the end of the RSG phase the star evolves rapidly blue-ward, passing through a range of spectral types on a time scale too short for the abundances to significantly evolve. This blue-ward evolution is halted as the star enters the LBV instability strip. From atmospheric modelling of LBVs we know that their surface abundance pattern is about CNO equilibrium (Lennon et al. 1994) and so more evolved than that of the nebula. Consequently, the nebula must have been ejected between, near the end of the RSG phase and the LBV phase.

An additional constraint comes from the nebula kinematics. If the nebula material was bulk ejected then the key factor determining its velocity is the surface

gravity, not the star's temperature. The escape velocity for a initial mass of $35M_{\odot}$ RSG is about 80km s^{-1}, while that from a BSG with an initial mass of $35M_{\odot}$ is about 700 km s^{-1}. If the nebula had been ejected from a BSG phase then the initial velocity must have been very fast, making it surprising that all the nebulae we observe have low expansion velocities, with little variance 20-140 km s^{-1} (the exception being η Car). That is, if the nebula were ejected from a BSG then this implies that the ejection velocity is sensitively tied to the escape velocity. However it would seem more likely that the ejection was from a star with a low surface gravity, where the ejection velocity simply has to be of the same order of magnitude as the escape velocity.

What regions of the stellar evolutionary tracks, below the HD limit, satisfy this criteria? From the above discussion it is clearly compatible with the escape velocity from a bloated RSG. However it may also be compatible with a blue supergiant impinging on its modified Eddington limit. High mass stars evolve through the blue loop at a constant luminosity. However during the RSG, OH/IR and YSG phases they can lose almost half their original mass (Jones et al. 1993). It has been suggested by Humphreys et al. (1994), that this combined with an increasing surface opacity as the star tends toward 12000K, could cause the star hit its modified Eddington limit and become unstable. This would occur in the approximate region low mass LBV instability strip leading to a very low effective surface gravity and a period of heavy mass loss. Since the transit time between these locations is brief the abundances at both will be the same. How then can we distinguish between them?

One indication may come from the bipolarity of the LBV nebulae. All LBV nebula are bipolar (bar the very low mass nebula around P Cygni), two broad mechanisms have been proposed to explain this. Either the star ejects an intrinsically bipolar nebula or it ejects a spherical nebula into a circumstellar media with an equatorial density enhancement. The origin of this is thought to be either a protostellar disc or a previous asymmetric RSG wind. Nota et al. (1995) argue

that a protostellar disc would represent a very high density contrast in a thin disc. This would lead to an extreme bipolarity, perhaps consisitant with HR Car but not He3-519 or the RCW 58 nebula. Consequently we will focus on an asymmetric RSG wind as a possible cause of a equatorial density contrast in the circumstellar medium.

It is a surprising fact that some massive RSG do have asymmetric winds, despite the effects of rotation being greatly diminished in the bloated RSG phase. This has led Martin and Garnett (1994) to raise the possibility that binarity may have played a role in shaping the RSG wind prior to SN 1987A. Considering the three well imaged massive RSG and post-RSG IRC +10420, HD 179821 and μ Cep we see only the latter has evidence of bipolarity (Mauron et al. 1986), while the former two have circular dust envelopes (Kastner et al. 1995). From this we conclude that bipolar outflows are not an endemic feature of RSGs. Which raises the question of why virtually all LBV nebula are bipolar? Unless one was to assume that the cause of the asymmetry is also responsible for the great outbursts, then it would seem hard to form consistently bipolar nebula from an ejection into a relic RSG wind.

In contrast, mass loss near the Ω limit is intrinsically bipolar regardless of the initial rotation rate (Langer 1997). Accordingly we would expect virtually all LBV nebulae to be bipolar, as observed. In addition to this there is some observational support for the nebula forming outbursts occurring in the blue. Goodrich et al. (1989) have argued that SN 1961V was actually a misidentified LBV eruption. The progenitor to this outburst was a BSG. More recently Drissen et al. (1997) have identified in LBV in outburst in NGC 2363. From colour band imaging they suggest that it was previously a blue star. However there is no clear evidence linking this brightening of several magnitudes to a large increase in mass loss. At the present time the weight of evidence seems to favour the nebula forming event occurring toward the blue.

4.4.4 Constraints on the Outburst Mechanisium.

What are the physical causes of the outbursts which form the nebula? The nebulae themselves are relics from this era and represent our only direct observational link to this early phase. It is through these nebula that we can analyse the physical conditions prevailing in the star during outburst and so shed light on the underlying mechanisium.

From Table 4.5 we can see that all the LBV nebulae have remarkably uniform abundance patterns. The nebula compositions are that of partially processed CNO material. From atmospheric analysis (Crowther&Bohannan 1997) it has been found that a number of Of stars (log $L_*/L_\odot$=5.7-5.9) have surface material more evolved than this. Consequently if they went on to become LBVs and form nebulae they would have quite different nebula abundance patterns than that which is observed. This implies that not all stars of a given mass go on to form LBVs.

From the combination of uniform abundance patterns and low expansion velocities, seen in all LBV nebulae (bar η Car), there would seem to be two factors common to all stars ejecting LBV nebulae. Firstly that they must have a low surface gravity. Secondly that the star must be at a particular point in it evolution, in terms of its surface composition. When a star achieves one of these factors but not the other no nebula is ejected. This is supported by the fact that some Of stars have already surpassed this surface abundance pattern without ejecting a nebula. While some WR stars which should have passed through a RSG phase and so had a phase of low surface gravity also do not have nebulae. This suggests that the conjunction of abundances and low surface gravity is not coincidental, but rather both are necessary for the ejection mechanism to operate.

Finally we note the physical conditions under which strange mode pulsations

arise. These occur in low density envelopes where there are large non-adiabatic effects. Strange mode pulsations are terminated if the surface helium abundance exceeds approximately Y=0.4, since this reduces the opacity and so increases the effective surface gravity. Consequently strange mode pulsation are expected to arise in both RSGs and blue-ward of the HD limit (Cox 1997). The influence of the helium abundance on the opacity may also be significant in deciding if the post-RSG star exceeds its Ω limit while evolving blue-ward. If the star has a too greatly enhanced surface composition then its modified Eddington limit will be greater and so it may not encounter the Ω limit and so avoid an LBV phase.

The interplay between the enhanced helium abundance and the acquisition of a low surface gravity is interesting for two reasons. Firstly it offers an explanation of why not all stars in a given mass range suffer an LBV phase leading to the ejection of a nebula. If the star had a too high helium composition on the blue-ward leg of the loop then it wouldn't impinge on its modified Eddington limit, wouldn't suffer strange mode pulsations and is less likely to exceed its Ω limit. Secondly if the abundance pattern controls whether the modified Eddington limit plays a significant role, then this would offer a natural explanation of the uniformity in nebula abundance patterns. The atmospheric studies of Of-stars suggest that stars of a similar mass in the same evolutionary phase have a wide spread in their surface compositions. We note that if this is true for stars at the end of the RSG phase, then we would not a priori expect a uniformity in the nebula abundance patterns. Allowing the surface composition to control the instability mechanism, makes this coincidence inevitable.

4.5 Summary

We will conclude this chapter by re-iterating our main conclusions.

• Both LBV and WR ejecta nebulae originate from stars within the same mass range. Both have the same abundance pattern and a comparable range of nebula expansion velocities. However WR ejecta nebulae tend to have greater dynamical ages. From this we infer that *LBV and WR ejecta nebula are the same objects with the central star at different points in its evolution.*

• We find that LBV nebula do not consist of RSG wind swept up by the faster LBV wind, since there is no correlation between nebula age and expansion velocity. Consequently we conclude that the nebula have an ejecta origin, by which we mean an extended period of very enhanced mass loss.

• All the nebula in our sample are comprise of partially CNO processed material. All display low expansion velocities, in the range 20-110 km s^{-1}, indicating ejection from a star with a low surface gravity. We conclude that these two criteria are necessary, if not sufficient criteria for the outburst instability to operate. These criteria are met both by evolved RSG and post-RSGs impinging on their modified Eddington limit. On the balance of evidence we favor the latter hotter location as the site of nebula ejection.

Chapter 5

The Evolutionary History of HD 148937.

5.1 Introduction

The star HD 148937 together with its nebular complex, represents one of the most enigmatic objects in the southern sky. Over the years it has been identified as a pre-main sequence star (Bruhweiler et al. 1981), a post-main sequence star (Leitherer et al 1987 and Dufour et al. 1988), a planetary nebulae (Henize 1959) and a massive star (Leitherer et al. 1986 and Dufour et al. 1987). However, recent abundance studies show that the surrounding nebula NGC 6164/5 contains processed material, demonstrating the evolved nature of HD 148937. In this chapter we present an abundance study of this nebula and propose a scenario by which it may have formed. This work is being prepared as a paper for MNRAS.

The first spectroscopic classification of HD 148937 was made by Westerlund (1960) who classified it as a O6f star. This classification was refined in 1972 when Walborn gave it a O6.5fp classification because of the CIII and NIII emission. Assuming membership of the Ara OB1 association suggests a distance of 1300pc. This implies that HD 148937 has M_V=-6 which suggests that it is a luminous O-star and excludes the possibility that NGC 6164/5 (a surrounding HII region) is a planetary

nebula.

The circumstellar medium surrounding the HD 148937 has a complex structure, reflecting the mass loss history of the central star. The dominant feature of this complex is the bipolar nebula NGC 6164/5 (see Figure 5.1). Encompassing this structure is a large wind blown bubble (semi-major axis 5pc) caved out by the stellar wind. This system is contained within the Stromgrem sphere ionised by HD 148937 which extends 25pc terminating in a dusty neutral shell (Leitherer et al. 1987). Naturally, the question arises as to how this system of nebulae have formed?

The wind blown bubble (WBB) encompassing NGC 6164/5 consists of filamentary structures, forming an ellipsoidal geometry. Based on the work of Weaver et al. (1977) we can relate the luminosity of the central star and the size of the WBB to the duration of the main sequence stellar wind and so stellar age. While this relation is designed for spherical WBBs, the oval character of this WBB should not lead to a significant error. Bruhweiler et al. (1981) found that the radius of the WBB implied an age of 1.4×10^5yrs for HD 148937. This very short duration has led them to suggest that it could be a pre-main sequence star.

Turning our attention to the inner nebulae NGC 6164/5, we note its highly bipolar geometry with bright emission from the polar regions (see Figure 5.1). Two previous abundance studies have been undertaken for NGC 6164/5. The first was by C.Leitherer and C.Chavarria-K (1987), the second by Dufour et al. (1988). From the Hα/Hβ ratio and the Whitford extinction law Leitherer et al determined an interstellar extinction of E(B–V)=0.6 toward NGC 6164/5. At two of the nebula positions analysed the temperature diagnostic line [NII]λ5755 was detected. Using the [NII]λ6584/ [NII]λ5755 ratio in conjunction with the [SII]λ6731/[SII]λ6717 ratio they found an electron density of 10 000 cm^{-3} and an electron temperature of 6700K. Using these physical parameters and by assuming that all the nitrogen was

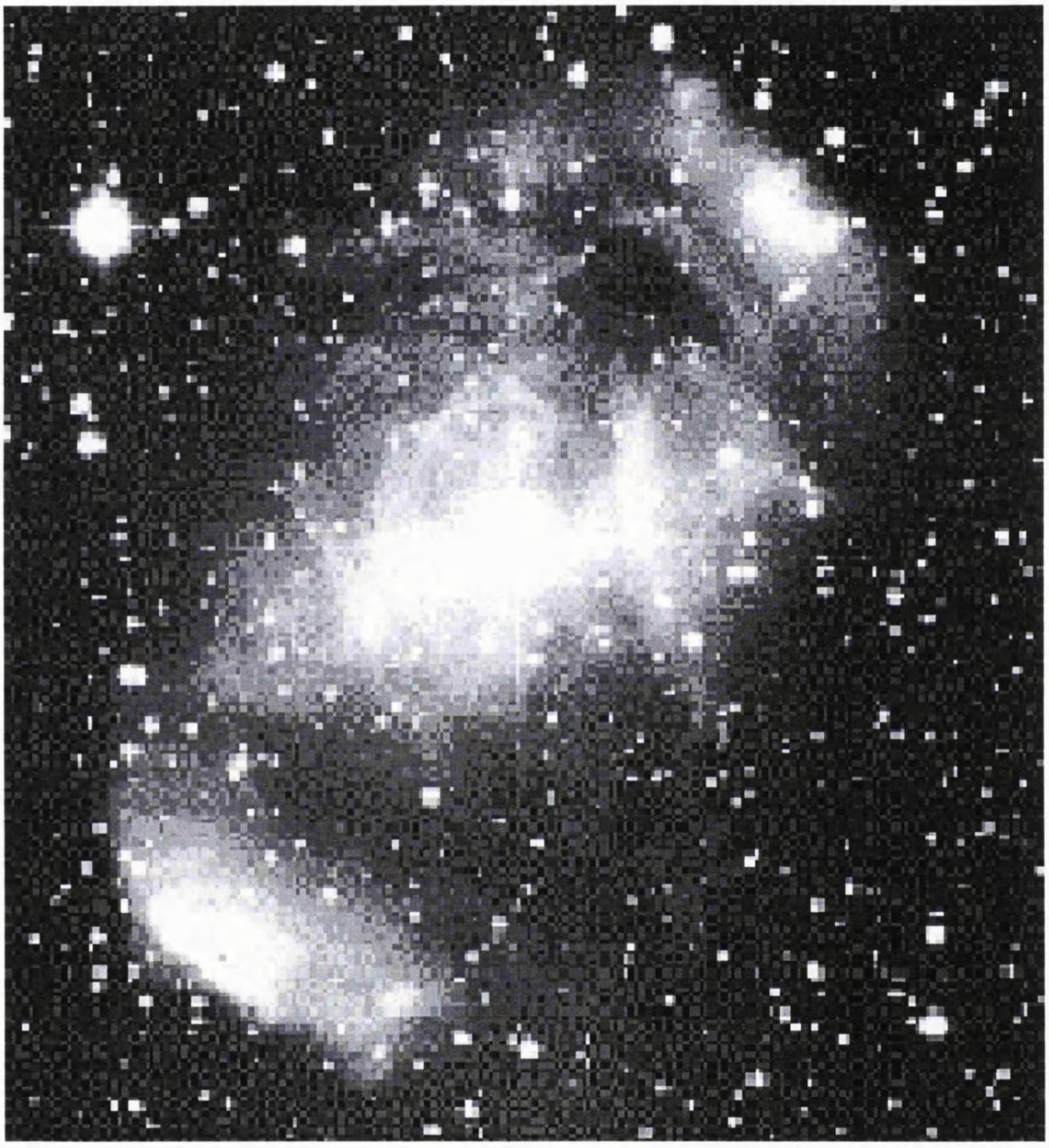

Figure 5.1: An image of the nebula NGC 6164/55 and the central star HD 148937.

present in the singly charged state, they determined the abundance of nitrogen in NGC 6164/5. They found that nitrogen is over abundant by a factor of five relative to the Sun.

In addition to this Leitherer et al. (1987) took spectroscopic images at a number of other positions, both of NGC 6164/5 and the WBB which encompasses it. Although the nitrogen temperature diagnostic line [NII]λ5755 was not detected at these positions an alternative approach was used to test for variations in the nitrogen abundance. This exploited the similarity between the N^+/S^+ ratio and the N/S ratio (see Chapter 3.3). Now since sulphur does not partake in any nucleosynthesis processes, then its abundance should remain unchanged. Consequently any variation in the N/S ratio is due to an alteration in the nitrogen abundance, irrespective of the temperature. The log N^+/S^+ ratio in the WBB was found to be a little less than unity, which is typical for Galactic HII regions. However it was found that over NGC 6164/5 this ratio was of the order of 1.6 in broad agreement with the nitrogen enhancement previously derived.

The second more comprehensive abundance study was conducted by Dufour et al. (1988) based on observations made using the 4m CITO telescope, taken at several slit positions across the nebula. Using the Hα/Hβ ratio in conjunction with the Seaton extinction law (1979) they found an average extinction coefficient of about C(Hβ)=1.1. Within the errors this appeared to be uniform at all the positions analysed. As both the temperature and density diagnostic lines were detected, the physical conditions were well established. This revealed that both the electron density and the electron temperature were quite variable across the nebula. The former ranged from N_e=200 to N_e=7000 cm^3, while the latter ranged from 6400K to 8800K. The temperature variation was not found to be correlated to the density variation and both were well above observational errors.

Using these physical conditions the equations of statistical equilibrium were solved to derive the ionic abundances. The most reliably derived elemental abundance is that of oxygen, since in this low excitation nebula all the oxygen is expected to be in the singly or doubly ionised state, both of which have observable lines in the optical. The elemental nitrogen and sulphur abundances were equated with those of singly charged state, which Dufour et al. note establishes a minimum abundance. They confirmed the nitrogen enhancement found by Leitherer et al. (1987), but in addition found oxygen to be depleted by a factor of three.

Because of the low ionization state of the nebula a large quantity of He^0 is thought to be present consequently no estimate for its elemental abundance could be made.

In conclusion Dufour et al. find that the lobes of NGC 6164/5 are chemically uniform, although they find some evidence that the waist is comprised of less processed material. The degree of oxygen depletion found for NGC 6164/5 is incompatible with it being a planetary nebula. Instead Dufour et al. suggest that it maybe analogous to objects like η Carinae. This is because it is only in nebulae surrounding the most massive stars, that we see such a severe oxygen depletion. The scatter in the abundances found by Dufour et al. (1988) for the different nebula regions that were studied are considerable 12+logN/H=8.04-8.66 and O/H=7.93-8.60. However they conclude that this does not represent a genuine variation of the abundances. Consequently the abundance pattern for NGC 6164/5 remains quite uncertain.

The second informative facet of NGC 6164/5 is that of its kinematics. The only detailed study of the global dynamics was made by Leitherer et al. (1987). Using high resolution spectra obtained with ESOs 1.4 coude altazimuth telescope. They find that the line emission from one lobe is blue shifted, while the other is red-shifted, both having an un-de-projected line-of-sight expansion velocity of about 30

km s^{-1}. Since NGC 6164/5 is highly bipolar it was necessary to find its angle of orientation, before a full dynamical study could be made. Using the line profiles and the observed vsini as constraints, Leitherer et al. find the angle between the nebular major axis and our line of sight to be 85^o. This is consistent with the line widths and the need for the rotational velocity to be beneath the break up velocity (since HD 148937 has a Vsin i of 200 km s^{-1}). Using this angle to de-project the observed line-of-sight velocity implies that NGC 6164/5 has an expansion velocity of 350 km s^{-1}. Given its semi-major axis of 1pc this implies a dynamical time scale of 3000yrs.

The small scale dynamical properties of NGC 6164/5 have been recently investigated by Scowen et. al. (1995). They used the H.S.T to image the outer polar reaches of the nebula's southern lobe. These images reveal it to have a highly clumpy structure, with the clumps themselves having a cometary appearance. Scowen et al interpret this as an effect of the stellar wind and UV field striking the clumps. The UV radiation photoevaporates material, which then becomes entrained in the stellar wind. While the stellar wind strikes the clumps forming bow shocks at the head of the clump before enveloping it and streaming out behind, creating cometary tails. Scowen et developed an analytical model of the interaction between the wind, clump material and UV field. This allows them to make an independent estimate of the mass loss from HD 148937, which yields $2.2\times10^{-5}M_{\odot}$ yr^{-1}. This is a factor of three greater than the value derived by Hutchings (1976).

HD 148937 is the only Of star known to be surrounded by an ejecta nebulae (although there are two other possible candidates, HD 108 and HD 193612). Why did it eject such a nebula? What type of instability did it suffer? To help answer these questions we have carried out an abundance study of of NGC 6164/5 using deep images. This allows us to accurately determine the fluxes of faint diagnostic lines like [NII] λ 5755 and so obtain a highly accurate temperature determination, which significantly reduces the errors on our abundance determination. The aim of this

work is two fold: to determine a single accurate nebular abundance pattern and to test for differences between this abundance pattern and that found in the LBV/WR nebulae. We note that to date that the abundance pattern in NGC 6164/5 has not been accurately determined, as Dufour et al. interpret the scatter in their abundance determinations (12+log(N/H=8.04- 8.66, 12+log(O/H)=7.93-8.60) as due to errors rather than a genuine variation.

5.2 Observations

The observations were carried out on the 26^{th} and 27^{th} of April 1996 using the 3.9m Anglo-Australian Telescope. Deep long slit spectroscopic images were taken covering five spectral regions between 3643A and 9689A (see Table 5.2). The RGO spectrograph was used in conjunction with a Thomson CCD. Images were taken at a slit position which crossed a bright knot in the outer edge of the nebular major axis, with a P.A.=45^o and an offset of $\Delta\delta$=112" north and $\Delta\alpha$=150" west. In order to flux calibrate the data we observed two standard stars CD-32^{o}9927 and LTT 6248.

The data were reduced at the U.C.L STARLINK node using the "FIGARO" and "DIPSO" packages . The images were bias subtracted, flat fielded, wavelength calibrated and cleaned of cosmic rays. The sky was subtracted and the images extinction corrected. Spectra were then extracted from the region emitting the greatest flux. The resulting images had a spatial resolution of 0.75"/pix and a wavelength resolution of 0.8Å/pix. During the observations the "seeing" was typically one arcsecond.

The "Elf" routine in "DIPSO" was used to fit Gaussians to the emission lines, enabling the line fluxes and wavelengths to be determined, along with the RMS errors. By comparing the observed ratio of Hβ to Hα, Hγ, Hδ, Hϵ, H9 and H10, to that theoretically expected (Hummer & Story 1987), we determined the interstellar

Date	Wavelength Range	Exposure Time (sec)
Slit position 3 PA=45		
1996 Apr 26	3643-4452	300
1996 Apr 26	4409-5221	300
1996 Apr 26	55593-6405	700
1996 Apr 26	6389-7199	200
1996 Apr 26	8904-9689	500
Slit position 2 PA=0		
1996 Apr 27	3643-4452	2000
1996 Apr 27	4409-5221	1000
1996 Apr 27	55593-6405	2000
1996 Apr 27	6389-7199	500
1996 Apr 27	8904-9689	500

Table 5.1: Journal of Observations.

extinction coefficient. This yields an extinction coefficient of C=1.0, which agrees well with the value of C=1.1 obtained by Dufour et al. (1988).

5.3 Results

In this section we will present the abundance pattern and the physical conditions that we have derived for NGC 6164/5. This work does not aspire to be a comprehensive multi-slit position abundance study of the type carried out by Dufour et al. (1988), but rather has been undertaken with a very specific purpose in mind. In light of our results for AG Car, He3-519 and RCW 58 we find they all contain a very similar abundance pattern. The aim of this work is to accurately determine the abundance pattern of NGC 6164/5, in order to rigorously test whether the abundance pattern in this ejecta nebula surrounding an Of-star is really the same as those, in our sample, surrounding WR and LBV stars.

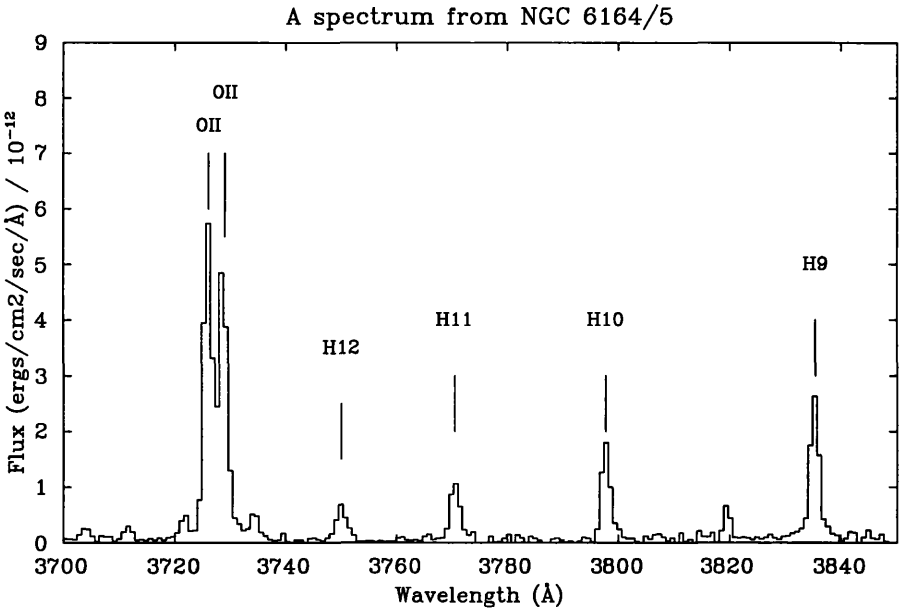

Figure 5.2: An example spectrum showing part of the H Balmer series and the [OII]$\lambda\lambda$3727,3739 lines.

The line fluxes and dereddened intensities are shown in Table 5.2. The combination of the nitrogen lines [NII]$\lambda\lambda$6584, 5755 with sulphur lines [SII]$\lambda\lambda$6731, 6717 allow us to derive the electron temperature and density of the nebula in the usual way. This yields an electron temperature of 7830^{+78}_{-58}K and an electron density of N_e=1404^{+106}_{-94} cm^{-3}. The accuracy of the final abundance determination rests largely on the accuracy of our temperature determination, which we have been able to constrain very tightly. Both the temperature and density we have derived fall well within the range found by Dufour et al. (1988). We note the errors on their temperature determination is typically about $\pm$500K, while the error on their density was of the order of $\pm$300 cm^{-3}.

Solving the equations of statistical equilibrium for these physical conditions we derived the ionic abundances, which are presented in Table 5.3. We note that this nebula is considerable hotter than that of AG Car, accordingly we see that a significant quantity of sulphur is present as S^{++}. Consequently we need to account for the presence of N^{++} through the use of an ionisation correction factor. Following

λ_{obs}	λ_{lab}	Element	k(λ)	F(λ)	I(λ)
3725.8±0.3	3726.0	[OII]	0.25	9.43±0.33	16.93±0.60
3728.6±0.3	3728.8	[OII]	0.25	8.25±0.33	14.79±0.6
3798.1±1.3	3797.9	H10	0.244	3.09±0.02	5.39±0.03
3835.7±1.2	3835.4	H9	0.237	4.35±0.01	7.46±0.02
3868.2±0.3	3868.8	[NeIII]	0.25	1.56±0.15	2.64±0.25
3889.2±0.7	3889.0	H8+HeI	0.226	14.75±0.14	24.72±0.24
3970.3±0.4	3970.1	Hϵ	0.210	10.12±0.22	16.33±0.35
4068.7±0.4	4068.6	[SIII]	0.210	0.55±0.09	0.85±0.12
4101.7±0.2	4101.8	Hδ	0.182	16.93±0.09	25.63±0.13
4340.6±0.1	4340.6	Hγ	0.127	33.94±0.42	45.28±0.56
4474.7±0.5	4474.9	HeI	0.095	3.95±0.05	5.26±0.07
4713.1±0.7	4713.2	HeI	0.036	0.43±0.23	0.48±0.25
4861.5±0.01	4861.3	Hβ	0.000	100.00±	100.00±
4925.1±0.7	4924.6	HeI	-0.016	1.44±0.03	1.38±0.03
4958.3±0.7	4958.9	[OIII]	-0.024	17.31±0.25	16.39±0.24
5006.2±0.7	5006.8.6	HeI	-0.036	53.07±0.39	48.94±0.36
5018.4±13.6	5015.7	HeI	-0.039	2.84±0.03	2.60±0.03
5198.9±0.2	5197.9+5200.3	[NI]	-0.082	0.98±0.12	1.09±0.13
5754.9±0.2	5754.6	[NII]	-0.19	2.87±0.03	1.84±0.02
5876.9±1.2	5875.7	HeI	-0.215	22.84±0.09	14.00±0.06
6312.2±0.7		[SIII]	-0.283	0.80±0.02	0.42±0.01
6548.3±0.6	6548.0	[NII]	-0.318	212.83±1.89	103.10±0.92
6563.0±0.1	6562.8	Hα	0.320	596.21±9.17	287.42±4.42
6583.6±0.1	6583.4	[NII]	-0.323	690.88±5.95	330.84±2.94
6677.0±0.7	6678.2	HeI	-0.337	8.60±0.06	4.00±0.02
6716.6±2.9	6716.5	[SII]	-0.342	14.85±0.17	6.82±0.08
6730.9±2.3	6730.9	[SII]	-0.344	19.74±0.07	9.02±0.08
7066.5±0.3	7065.3	HeI	-0.388	4.57±0.05	1.89±0.02
7135.6±0.3	713.9	[ArIII]	-0.396	13.85±0.15	5.61±0.06
9014.8±0.3	9014.9	P10	-0.599	6.46±0.40	1.72±0.11
9068.0±0.2	9068.0	[SIII]	-0.59	46.34±0.23	12.23±0.06
C (Hβ)			1.30	1.30	1.00
F_{obs}(Hβ)			1.138e-13		1.105e-10

Table 5.2: Observed line fluxes and de-reddened line intensities.

Kingsburgh & Barlow (1994);

$$ICF(N)=O/O^{+}$$

$$A(N)=ICF(N)\times N^{+}/H^{+}$$

This implies that about half the nitrogen is present in the doubly charged state. Surprisingly we detect nitrogen in the neutral state which given our derived electron temperature must come from a different physical region from that in which N^{+} and N^{++} is found. Possibly this is formed in clumps or in a neutral shell outside the ionised nebula. Consequently we do not include the neutral nitrogen abundance in our final determination of the elemental nitrogen abundance. The ionic abundances were then summed to give the total elemental abundance, which are presented in Table 5.3

We find that NGC 6164/5 has the following abundance pattern (12+logX/H), $N/H=8.38^{+0.02}_{-0.02}$, $O/H=7.95^{+0.03}_{-0.03}$ and $S/H=6.60^{+0.03}_{-0.03}$. This abundance pattern is within the range of values found by Dufour et al., our oxygen abundance being at the very bottom of this range. The errors on these abundances are exceptionally small for a nebula abundance study. This is because of the instrumentation used to observe an intrinsically bright nebula. Surprisingly this abundance pattern is consistent with that found in our abundance studies of WR and LBV nebulae.

5.4 Discussion

In this discussion we will try to use the nebula characteristics to place constraints on the evolutionary history of HD 148937. We will draw parallels between this evolved Of-star and the LBV class of stars. Can HD 148937 be understood in terms of a

Abundances	12+log(Nx/NH)
S^+/H^+	$5.96\pm^{0.01}_{0.02}$
S^{++}/H^+	$6.49\pm^{0.03}_{0.03}$
N^+/H^+	$8.07\pm^{0.02}_{0.02}$
O^0/H^+	<
O^+/H^+	$7.64\pm^{0.04}_{0.04}$
O^{++}/H^+	$7.65\pm^{0.02}_{0.02}$
N/H	$8.38\pm^{0.02}_{0.02}$
O/H	$7.95\pm^{0.03}_{0.03}$
S/H	$6.60\pm^{0.03}_{0.03}$
T_e	$8400\pm^{115}_{155}$
N_e	$1404\pm^{106}_{94}$

Table 5.3: A Table giving the ionic and elemental abundances.

modified LBV phase? Furthermore in the light of work on Sher 25 (Weis 1997) and HD 108 (Underhill 1994), how unique is HD 148937?

5.4.1 The Location of Nebula Ejection in the HRD.

The luminosity of HD 148937 is $\log L/L_\odot = 5.3\times10^5$ (Leitherer et al. 1986), which is comparable to that of LBVs like HR Car. By comparison with evolutionary tracks (Meynet et al. 1994) we infer a ZAM of $40M_\odot$. However we note that HD 148937 is a comparatively fast rotator, with a Vsini=200 km s^{-1} (see Figure 5.3). In the recent calculations by Langer et al. (1997) we find that fast rotators of a given initial mass evolve at a higher luminosity than more slowly rotating stars. Consequently we might expect HD 148937 to have an initial mass somewhat lower than the $40M\odot$ previously inferred.

From our abundance study we find that the nebula is comprised of partially CNO processed material. This raises the question; at which evolutionary epoch would HD 148937 have such a surface composition? From the models of Meynet et al (1994) we see that this composition is achieved at the end of the RSG phase. However, evolutionary models which include rotation indicate that rotation has the effect of bring processed material to the surface faster (Pasquali et al. 1997). This suggests that the nebular abundance pattern can be interpreted in two ways, either it indicates that HD 148937 is a post-RSG object or that the processed abundances were achieved earlier than the standard models predict, perhaps due to rotation, while the star was still in the blue. In some ways this is reminiscent with the dilemma we encountered with AG Car.

Next we will consider the implications of the nebula dynamics. Leitherer et al (1987) found that NGC 6164/5 has an expansion velocity of 350 km s^{-1}. Using the physical parameters quoted there (T_{eff}=37 800K, R=17$R_{\odot}$, L=5.3$\times 10^5$) we find an escape velocity from HD 148937 of 1000km s^{-1}, which is considerably higher than the nebula expansion velocity. We note that an effective temperature of 15 000K implies a radius which would make the expansion comparable to the escape velocity. This suggests that the star probably ejected the nebula in a previous cooler phase. However it does not seem compatible with ejection from a RSG, where the expansion velocity would be an order of magnitude greater than the escape velocity. We note that the implied location for nebula ejection is close to the low mass LBV instability strip, which maybe related to the opacity maxima at 12 000K causing blueward evolving stars with a high L/M ratio to exceed their modified Eddington limit.

In light of the abundance and dynamical evidence from the nebula, it appears possible that the HD 148937 ejected NGC 6164/5 from one of two possible evolutionary states. Either while *evolving redward prior to a RSG phase or while evolving blueward after the RSG phase.*

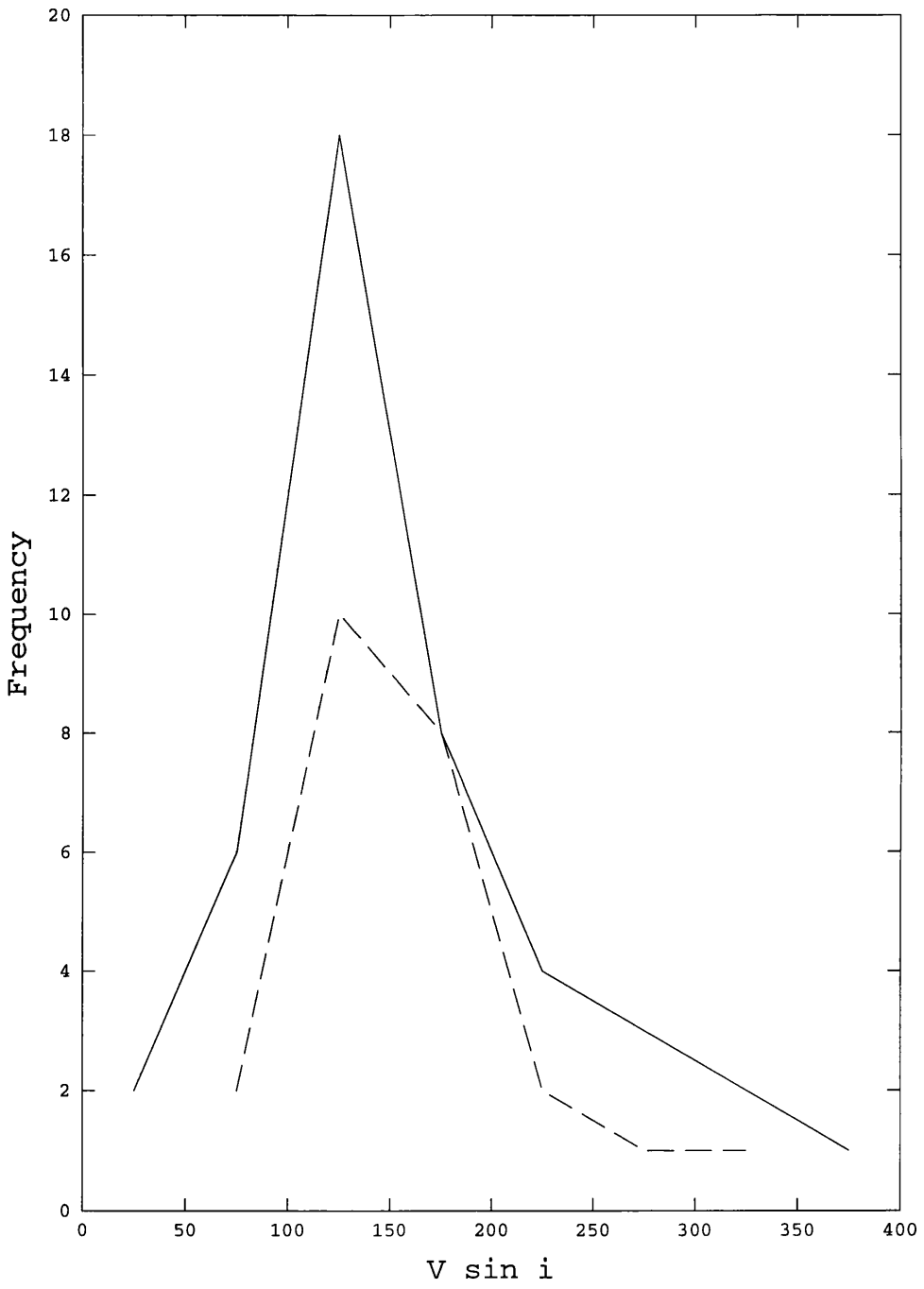

Figure 5.3: Two graphs of vsini verses frequency of occurrence, compiled from Prinja and Howarth 1989. The solid line is for stars less luminous than log $L_*/L_\odot$=5.8, while the dashed line is for stars more luminous than this.

5.4.2 The Mechanisim of Nebula Ejection?

Next we will compare and contrast NGC 6164/5 to those nebulae surrounding WR and LBV stars. NGC 6164/5 is comprised of $2M_{\odot}$ of material (Leitherer et al. 1987). This mass is typical of LBV nebulae which usually contain a few solar masses of ionised material (see Section 1.5). Like LBVs HD 148937 has ejected a great deal of mass to form a shell nebula, without destroying the star. This can be done in essentially two ways, either in some discrete ejection event or though a fast wind sweeping up a previous slow wind phase. This latter possibility is clearly ruled out by the combination of large expansion velocity (350 km s^{-1}) and short dynamical time (3000 yrs). That is, the low velocity, high mass loss phase in which $2M_{\odot}$ can be lost is the RSG phase, which has terminal wind velocities of about 40km s^{-1} for the most massive RSGs. There is no way this mass could be accelerated to 350 km s^{-1} within the 3000yrs available. Consequently NGC 6164/5 must have been ejected in some discrete event. The only known instability which causes the ejection of this quantity of mass in a discrete event without destroying the central star, is the LBV instability. This instability occurs in massive, hydrogen deficient post-main sequence stars, which are criteria met by HD 148937.

From our previous abundance studies we have found a uniformity of nebular abundance patterns in nebulae surrounding WR and LBV stars. This in conjunction with dynamical arguments led us to the conclusion that LBV and some WR nebulae are the same objects with the central star at different points in its evolution. Put another way, we infer that they are a product of a common physical mechanism, which operates when this characteristic abundance pattern is present on the stellar surface. To within a small margin of error, this abundance pattern is identical to that found in the ejecta nebula surrounding HD 148937. This abundance uniformity between NGC 6164/5 and LBV/WR nebulae is, on its own, strong evidence that a

common mechanism is at work.

The central difference between NGC 6164/5 and LBV/WR nebula is its dynamics. NGC 6164/5 has an expansion velocity of 350 km s^{-1}, which is much faster than any other LBV nebula (bar, as usual, Eta Car). Typically LBV nebulae have expansion velocities of 70 km s^{-1} (see Section 1.5), with the fastest being HR Car (110 km s^{-1}) and P Cygni (140km s^{-1}). Any satisfactory account of NGC 6164/5 must explain its dynamics.

If a star's evolutionary path were uniquely determined by the initial composition and mass, then the fact that HD 148937 is a galactic star with a luminosity comparable to that of LBVs like HR Car implies that it will undergo an LBV phase. A characteristic of the LBV phase is the initial high mass loss phase resulting in the formation of a nebula. This occurs when a certain chemical composition is present on the stellar surface. HD 148937 has already achieved this surface composition, as witnessed by the abundance pattern of NGC 6164/5. When HD 6164/5 achieved the abundance pattern it ejected a nebula. This means that in terms of nebula ejection HD 148937 has behaved in a very similar way to an LBV star.

The flaw in this argument is that a stars evolutionary track is not uniquely determined by just the initial mass and composition, but also by angular momentum. Since HD 148937 is a fast rotator this point needs to be assessed carefully. To do this we will look at how the evolutionary models are modified by the introduction of rotation. The two key points that emerge are that the mixing is enhanced, bringing the processed material to the surface faster and secondly, that a fast rotating star evolves at a higher luminosity than a slower rotator of the same mass. The latter point means that fast rotators intrinsically have a higher L/M ratio and therefore need to lose less mass before they encounter their Eddington limit (or Ω limit).

On the basis of the nebula abundances and dynamics we previously concluded: *the epoch of nebula ejection either occurred during a slightly cooler phase while evolving redward or during its blueward post-RSG evolution.* On the basis of the above discussion it is likely that physical cause of the ejection of NGC 6164/5 is also responsible for the formation of LBV nebulae. In the previous chapter we concluded that the location of LBV nebula ejection is either at the end of the RSG phase or as the LBV encounters its modified Eddington limit at about 12,000K while evolving blueward. This latter location is consistent with both of the possible locations of nebula ejection from HD 148937. If HD 148937 is a post-RSG star, then it is surprising that despite losing a great deal of mass ($8M_{\odot}$ - Jones 1993) it still has a comparatively high rate of rotation for an O-supergiant. In addition, having lost mass in the RSG phase and being a fast rotator would lead us to expect that HD 148937 should have an exceptionally high L/M ratio. If this were the case and the star was evolving blueward when it ejected its nebula we would expect the ejection to occur at cooler temperature than is usual for LBVs, implying a lower expansion velocity than is observed. Consequently we conclude that HD 148937 is not a post-RSG, but rather a star which encountered its modified Eddington limit while evolving redward. This is in contrast to normal LBV behavior in which nebula forming LBV instability is encountered on the blueward leg of the excursion.

If the nebula was ejected on the redward leg of the blue loop, then HD 148937 is approaching the instability region from the opposite direction than is usual for LBVs. This implies that it will become unstable at a higher temperature. At this higher temperature the star will have a harder radiation field. Consequently each particle in the wind is in motion because it has been struck by a higher energy photon than if it were in the wind from a cool star. This implies that even if a star has a zero effective gravity, the wind out flow velocity still has some dependence on the stellar temperature. Since what ever the LBV instability is the material is likely to be lifted out of the stars gravitational well by the radiation field, then we would expect the stellar temperature to influence the nebular expansion velocity as

a second order effect. The high expansion velocity of NGC 6164/5 could then be attributed to its ejection from a hotter star, lying on the left hand side rather than the right hand side of the instability region.

Our proposed scenario also has implications for the present spectral type of HD 148937. Since it has not passed through a RSG phase it will not have suffered the associated mass loss and so will be more massive than a comparable LBV which has undergone a RSG phase. Consequently it will have a higher surface gravity. In this context we note that HD 148937 has log $g_*/g_\odot$=3.5 (Leitherer et al. 1987) compared to a typical value of log $g_*/g_\odot$=3.0 for Ofpe/WN9 stars (Crowther private comm. 1997). This could lead to it lying dormant not as a slash star or a B supergiant, but rather as an Of star. Since the mass loss characteristics are dependent on both the temperature and the surface gravity, the high value of the latter will serve to reduce the mass loss rate, preventing evolution into a slash star which requires a denser, slower wind. We suggest that the presence of HD 148937 as an Of star with a low mass loss rate is supporting evidence for our scenario, independent from the evidence provided by the nebula.

5.4.3 Is HD 148937 Unique?

Finally we will compare HD 148937 to other BSG which have recently been found to be surrounded by ejecta nebulae. Sher 25 in NGC 3603 has been imaged by Brander et al. (1996) revealing bipolar lobes with an equatorial ring. Sher 25 is classified as a B1.5Iab star with a luminosity of M_{bol}=9.1. We note immediately the similarity to P Cygni which is classified as a B1Ia$^+$ star and has a luminosity of M_{bol}=-8.3 (Nota et al 1995). Sher 25s nebular lobes are comprised of material which is enriched in nitrogen and have a de-projected expansion velocity of 80 km s^{-1}. This ring and lobe structure is reminiscent of the lobes and waist seen in NGC 6164/5. Brandner et al suggest an analogy between Sher 25 and Sk 69 202, the progenitor star of SN

1987A. However this was thought to be only half as massive as Sher 25 and so not susceptible to any LBV instability. Consequently they interpret the nebula as RSG wind material swept up by a fast BSG wind.

However we suggest that the presence of an ejecta nebula with an expansion velocity of 80 km s^{-1} around a star of a similar spectral type and luminosity as P Cygni, is more naturally explained by an LBV eruption. The expansion velocity of this nebula is much slower than that of NGC 6164/5 suggesting that Sher 25 followed a more normal LBV evolutionary track. We conclude that Sher 25 is not directly analogous to HD 148937. Rather its significance, along with P Cygni, lies in the fact that two stars which have probably experienced nebula forming LBV outbursts, lay dormant not as slash stars but as normal B supergiants which are showing no unusual variability associated with LBVs. If stars which have ejected a nebula in a LBV outburst can lie dormant in this way then we should not necessarily expect HD 148937 to always display LBV variability after ejecting NGC 6164/5.

We will close by briefly mentioning HD 108, which has been classified as a O6:f?pe star by Walborn (1972), suggesting a close link with HD 148937. The most thorough investigation of HD 108 has been made by Underhill (1994), who suggests a connection with LBV and B[e] stars. Historically HD 108 has shown variability in its emission and absorption line profiles and radial velocities (Plasket & Pearce 1931; Beals 1951; Hutchings 1975; Vreux & Conti 1979). Underhill suggests that emission features seen in the visible spectrum are incompatible with emission from a spherically symmetric wind, but instead could originate from a polar jet and equatorial disk. Clearly further high resolution spectroscopic observations are needed to help clarify the nature of this interesting object. At present the situation is too confused to to allow helpful analogies between HD 108 and HD 148937.

5.5 Conclusion.

In this chapter we have presented the results of an abundance study which to within a factor of two, shows that NGC 6164/5 contains material with the same abundance pattern as observed in LBV/WR nebulae. From the nebula expansion velocity and dynamical age we conclude that NGC 6164/5 was ejected in a discrete event, without destroying the central star. This in conjunction with the similarity of mass and evolutionary state of HD 148937 compared to LBV progenitors, leaves the LBV nebula forming instability as the only known candidate. Consequently we conclude that NGC 6164/5 and LBV/WR nebulae have been ejected through the action of a common physical mechanism.

We then sought to find the periods in the evolution of HD 148937 during which a nebula could be ejected with the abundance pattern and dynamical properties of NGC 6164/5. This was found to be possible only during the redward evolution toward a RSG phase or during the blueward post-RSG evolution. Both these regions incorporate one of the two locations we have previously found to be possible locations for the LBV giant out bursts. We note that the nebula dynamics of NGC 6164/5 makes it unlikely that it originates from a RSG. This further strengthens our earlier belief that LBV eruptions occur at the hotter site (toward the low mass LBV instability strip) rather than during the RSG phase.

The next step is to determine whether HD 148937 was a post-RSG object. We noted that due to its comparatively fast rotation it will have an intrinsically high L/M ratio. Firstly, if it has lost a great deal of mass in a RSG phase then it is surprising that HD 148937 is still such a fast rotator. Secondly, if it ejected NGC 6164/5 during a phase of blueward evolution then its intrinsically high L/M ratio should cause it to become unstable earlier when the star is cooler and more bloated than is usual for LBVs. This would lead to a smaller not greater nebula expansion velocity, contrary to what is observed.

From these considerations and interpreting HD 148937 within the framework that we have previously developed for the ejection of LBV/WR nebulae, the following picture emerges. HD 148937 begun a blue loop excursion reducing in temperature until reaching the vicinity of the low mass LBV instability strip. As it cooled its surface opacity would have increased which may have caused it to impinge on its modified Eddington limit. Since the rotation of HD 148937 causes it to have an intrinsically high L/M ratio this may have triggered the LBV eruption on its first passage through this zone. In addition to which HD 148937 is comparatively close to its break up velocity and so any further reduction in its surface gravity is likely to make it unstable. HD 148937 is then interpreted to be in a dormant state as an Of star, which maybe analogous to slash stars for objects which have followed this rather different evolutionary path.

This scenario also offers explanations of the central stars unusual Of spectral type and the high expansion velocity of NGC6164/5. The high post eruption mass of the star leads to a comparatively high surface gravity. This will lower the mass loss rate reducing the prominence of the wind lines preventing a slash star classification, but favoring an Of spectral type. While the ejection of the nebula from an unusually hot star leads to a faster terminal wind velocity even in the low gravity limit.

Chapter 6

The dynamics of AG Car's nebula: On disks and shells.

6.1 Introduction

The presence of an optical nebula surrounding AG Car was first detected by Thackery (1950). This nebula has an elliptical appearance with the major axis lying at a position angle of 130°. Dynamical studies of the nebula show that in three dimensions the ring morphology is bipolar. This implies that either the mass loss was intrinsically asymmetric or that the circumstellar media surrounding the star had a toroidal density enhancement. A number of methods of breaking the spherical symmetry have been investigated, these include binarity (Gallagher 1989), protostellar discs, wind compressed discs, magnetic fields, asymmetric flow from a RSG progenitor (Nota et al. 1995) and interaction with the Omega limit (Langer 1997).

Resolving the detailed structure of the nebula surrounding AG Car is a challenging observational task, as it involves imaging faint features close to a bright central source. Such work has been undertaken by Paresce and Nota (1989) who used the STScI chronograph on the ESO 2.2m telescope to obtain multi-wavelength broad band images of AG Car's nebula. This revealed the presence of two bipolar

outflows, one extending to the NE the other to the SW. A further investigation of the geometry of AG Car's nebula was carried out by Nota et al. (1992) using the Johns Hopkins Adaptive Optic chronograph with the 1m Swope telescope at Las Campanas. The Hα+ [NII] image they obtained is shown in Figure 6.1. They also made spectroscopic observations centered on Hα to study the nebula dynamics. They concluded that nebula has an elliptical structure in three dimensions.

No measurable colour difference (B-I) was found between this "jet" like outflow and the central star. This implies that the emission from the jet is likely to be stellar light scattered by dust. An intriguing feature of these dusty jets is their constant surface brightness as we move radially out from the star. Paresce and Nota (1989) suggest that this may be caused by the density increasing outward through the jet, perhaps as the material piles up against the inner edge of the nebula. Finally they estimate the total mass of dust in the features to be $10^{-3}M_{\odot}$.

A second technique to analyse the nebular structure was employed by Smith (1991), who obtained high resolution long-slit spectroscopic images. These confirmed that the nebula was indeed ellipsoid in shape. However the images also revealed collimated high velocity flows inside the nebula at position angles of 0^{o} and 180^{o}. This is displaced by an angle of approximately 45^{o} from the dust "jets" found by Paresec and Nota. At present the relationship between these two features is unclear. From these spectroscopic images Smith (1991) found an average expansion velocity of 70 km sec^{-1}.

Spectropolarimetric observations of AG Car (Schulte-Ladbeck et al. (1993) and Leitherer et al. (1994)) have shown that the star has a very large intrinsic polarisation. Furthermore this polarisation is variable changing by 0.5 percent over a period of two months (Leitherer et al. 1994). From the results of Schulte-Ladbeck et al (1993) the polarisation is found to have a preferred axis laying at a position angle

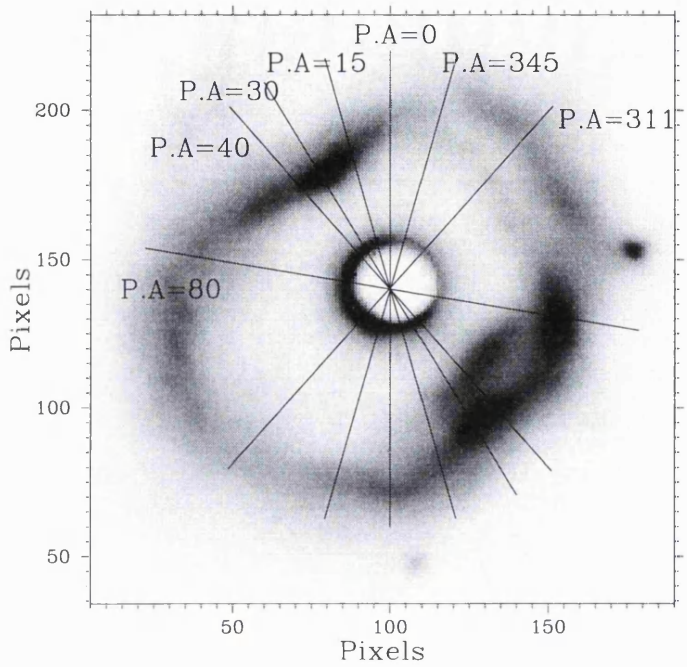

Figure 6.1: AG Car's nebula with the slit positions indicated.

of $145^o \pm 10^o$. This is aproximately perpendicular to the dust jet found by Paresce and Nota (1989) and parallel to the nebula major axis. Spectropolarimetry probes the inner most reaches of the nebula, close to the central star. Consequently these results suggest that the geometry seen on the large scale, in the circumstellar material, is established early in the stellar wind.

In this chapter we present the analysis of dynamical data taken at seven radial slit positions over AG Car's nebula (see Figure 6.1). A preliminary analysis of four of these slit positions (0^0,30^0, 131^0 and 80^o) has been presented by L.J.Smith in "Wolf-Rayet stars and their interrelations with other massive stars in Galaxies." In this work she finds evidence for a low velocity jet, attaining a maximum velocity of a little over 100 km s^{-1}. This jet-like feature appears at position angles of both 0^o and 30^o and so a preferred axis at a position axis of about 15^o is identified. We note that this position angle is not aligned with either the major or minor nebula axis.

6.2 Observations

The dynamical data were obtained during two observing runs using the Anglo-Australian Telescope (AAT) in conjunction with the UCL echelle spectrograph. The first observing run was in April 1989 and the second in January 1991. The same instrumental configuration was used on both occasions. This yielded a spectral resolution of 7 km s^{-1} and a spatial resolution of 1.1" (the seeing averaged 1.7"). In total images were taken at seven slit positions, covering the Hα and [NII] $\lambda\lambda$ 6548,6584 lines. The slit used had dimensions of 1" arcseconds wide by 57" arcseconds long. The first two slit positions chosen are aligned with the major and minor nebular axies at position angles of 30° and 311°. A third was taken at a position angle of 40°, which falls along the dust jet found by Paresce & Nota (1989). A further two slit positions P.A=15°, and 345° were taken to investigate the angular extent of the velocity jet at P.A.=0°. Finally the seventh slit position, taken for completness, lies at P.A=80 which is approximately perpendicular to the velocity jet. This slit positions are shown in Figure 6.1 projected onto an image (Nota et al. 1992) of the nebula. The images have been bias-subtracted, flat fielded and wavelength calibrated, but not sky-subtracted or flux calibrated. To dynamically calibrate the data we have compensated for the motion of the Earth and Sun to produce velocities relative to the local standard of rest.

6.3 Results

In this section we will present the results obtained in two formats. Firstly we will present the images, then a series of high resolution spectra extracted over a few pixels slicing through the images in the spatial direction. This format has been chosen because, while the spectra allow the identification of the faintest features, the images are required to place each extraction region in the context of the overall data set. The velocity scales on the spectra have a resolution of 7 km s^{-1}. The images

shown are those of [NII]λ6584, our Hα images are not displayed as they have a lower dynamical resolution due to the greater thermal broadening of the lighter H atoms.

6.3.1 Position angle 311°: image 1, spectra 1→12

This slit position lies along the major axis of the nebula. From image one we see that the nebula extends further to the south-east of the star than the north-west. While the SE part of the shell displays a regular symetrical apperance, the NW sector is more complex containing a bright clump inside the overall ring of the nebula. At the extremity of the NW nebular region we see an extended plume of emission.

Examining the extracted spectra from the SE (spectra 1) working NW (spectra 12) we see a broadly Gaussian line profile centered on 0 km s^{-1}, splits into two components. By midway into the north-western half (pixels 11-15) of the nebula these two split components have themselves developed substructure, with shoulders appearing in the highest velocity side of each line. Close to the central star, where the line-of-sight velocity is most de-projected we see the main emission peaks have expansion velocities of $\pm$70 km s^{-1}. At this position (pixels 16-20) the blue-shifted shoulder has separated becoming a discrete dynamical component with an velocity of -105 km s^{-1}.

The next spatial regions over which spectra were extracted incorporate strong stellar continuum emission. These spectra show many terrestrial water absorption features. As we move into the north-western part of the nebula we re-acquire the nebular lines clearly split (pixels 28-29). We note that the emission from the back of the shell is considerably weaker than from the front. Furthermore the red-shifted component is at a significantly higher velocity than the blue-shifted component (70 km s^{-1} v.s 105 km s^{-1}). This indicates that the nebula is not symetrical in our line of sight along the south-eastern part of its major axis. In neither component is

there any indication of substructure. As we move a little further SE (pixels 30-31) the blue-shifted component dramatically splits. This splitting is not apparent in either the spectra before or after, indicating the splitting is not due to an extended feature. Moving to the outer part of the SE axis (pixels 32-37) we see the velocity of the line components drop, merging into a single line centered on the stellar rest frame. We note that this line profile tends to sit on emission wings extending up to approximately 75 km s^{-1}. At the extremity of the SE axis we see the merged line profile split once again. This can be identified with the emission plumes seen in image one. These plumes have a velocity of about 40 km s^{-1} and extend beyond the dominant ring nebula.

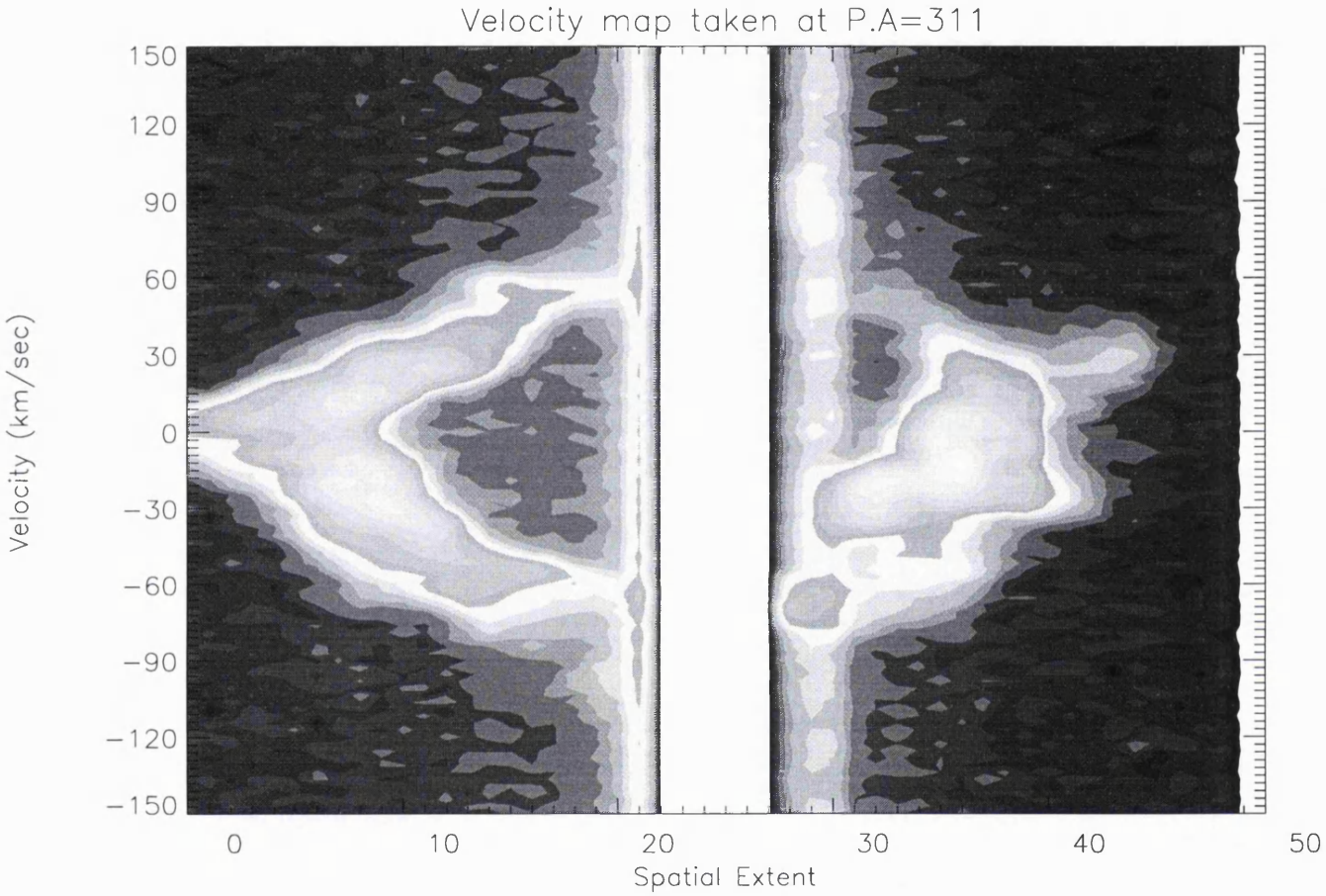

Figure 6.2: Image 1: position angle 311°. Spatial extent is in pixels where one pixel is approximately 0.01pc

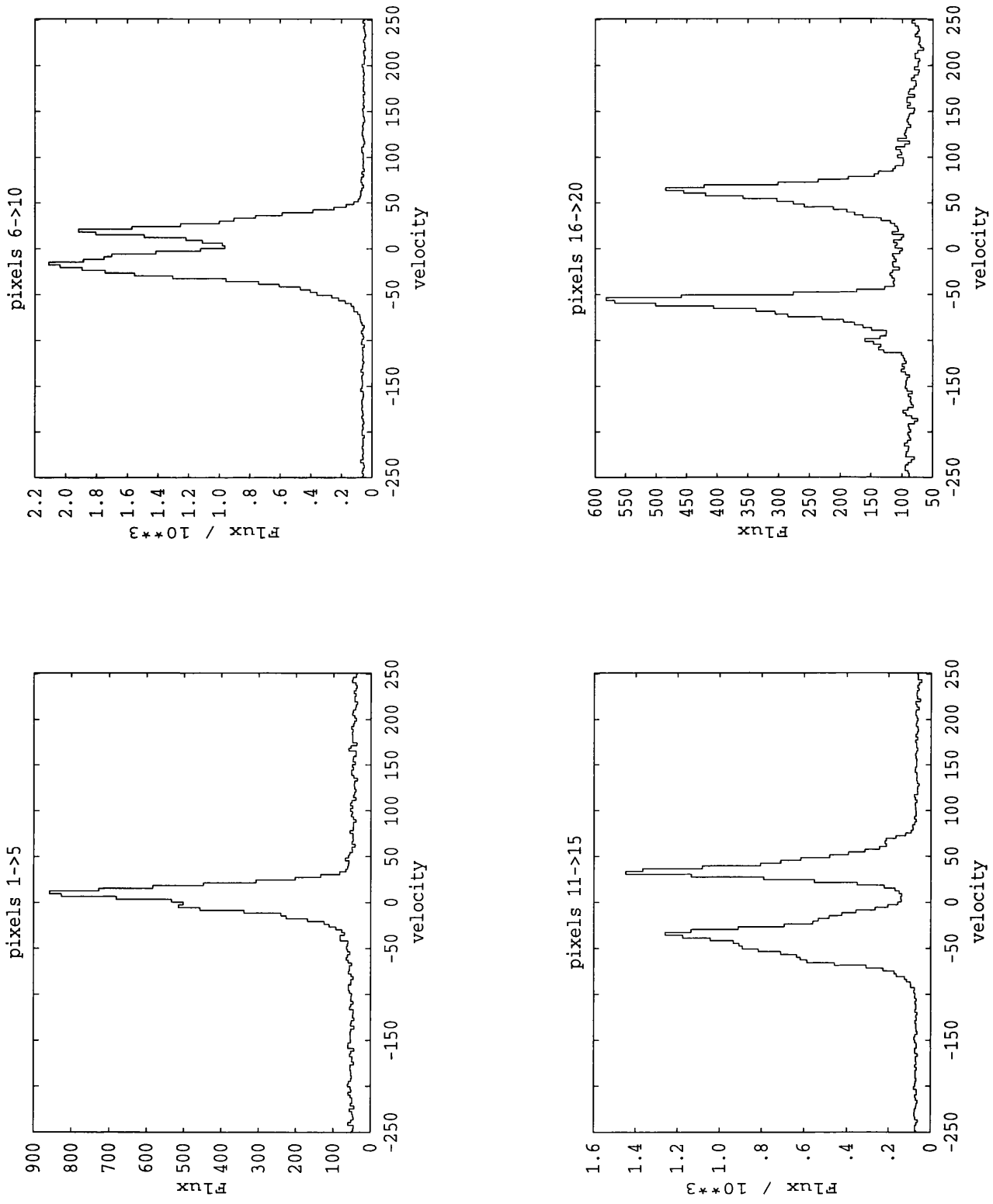

Figure 6.3: Extracted spectra 1→4

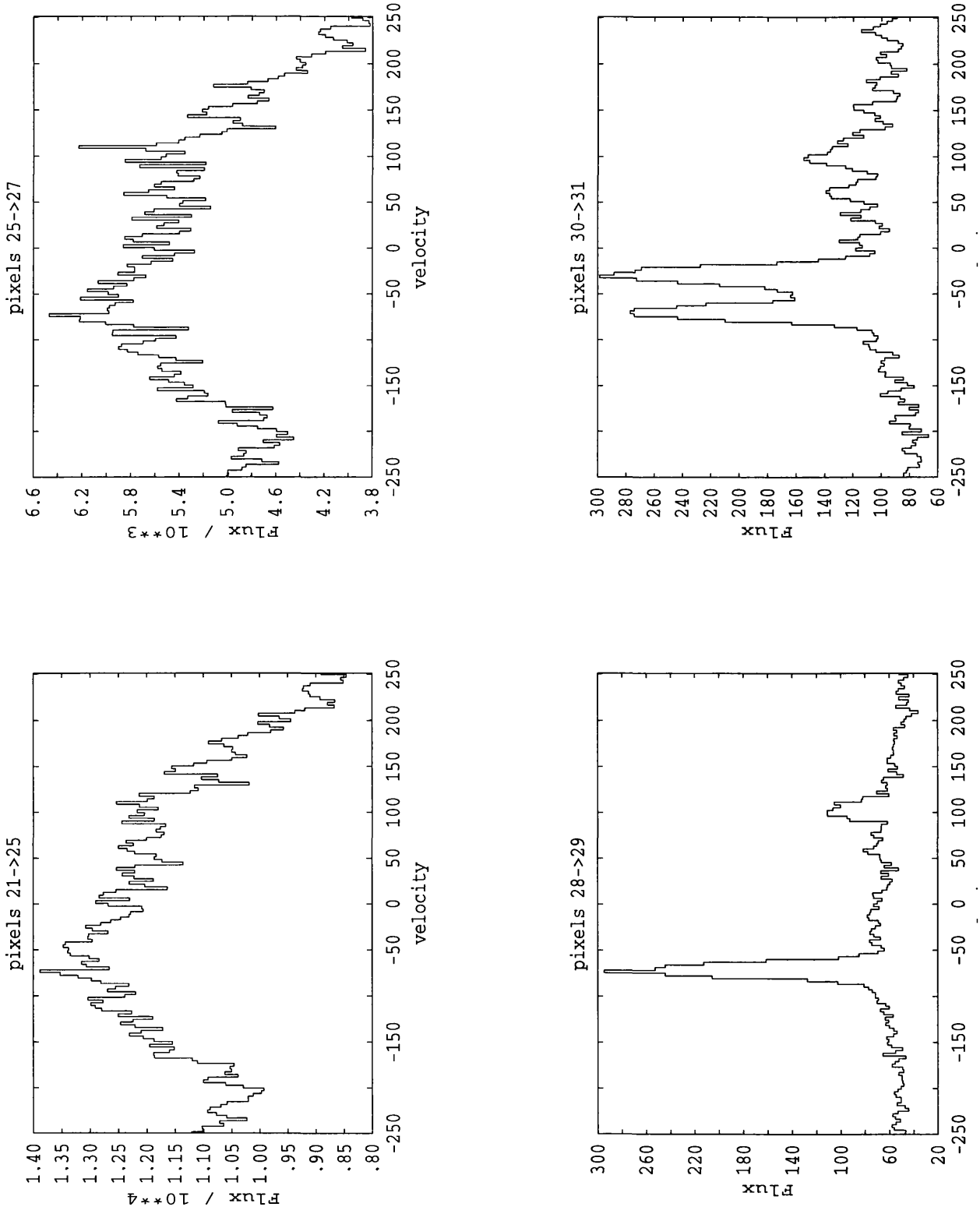

Figure 6.4: Extracted spectra 5→8

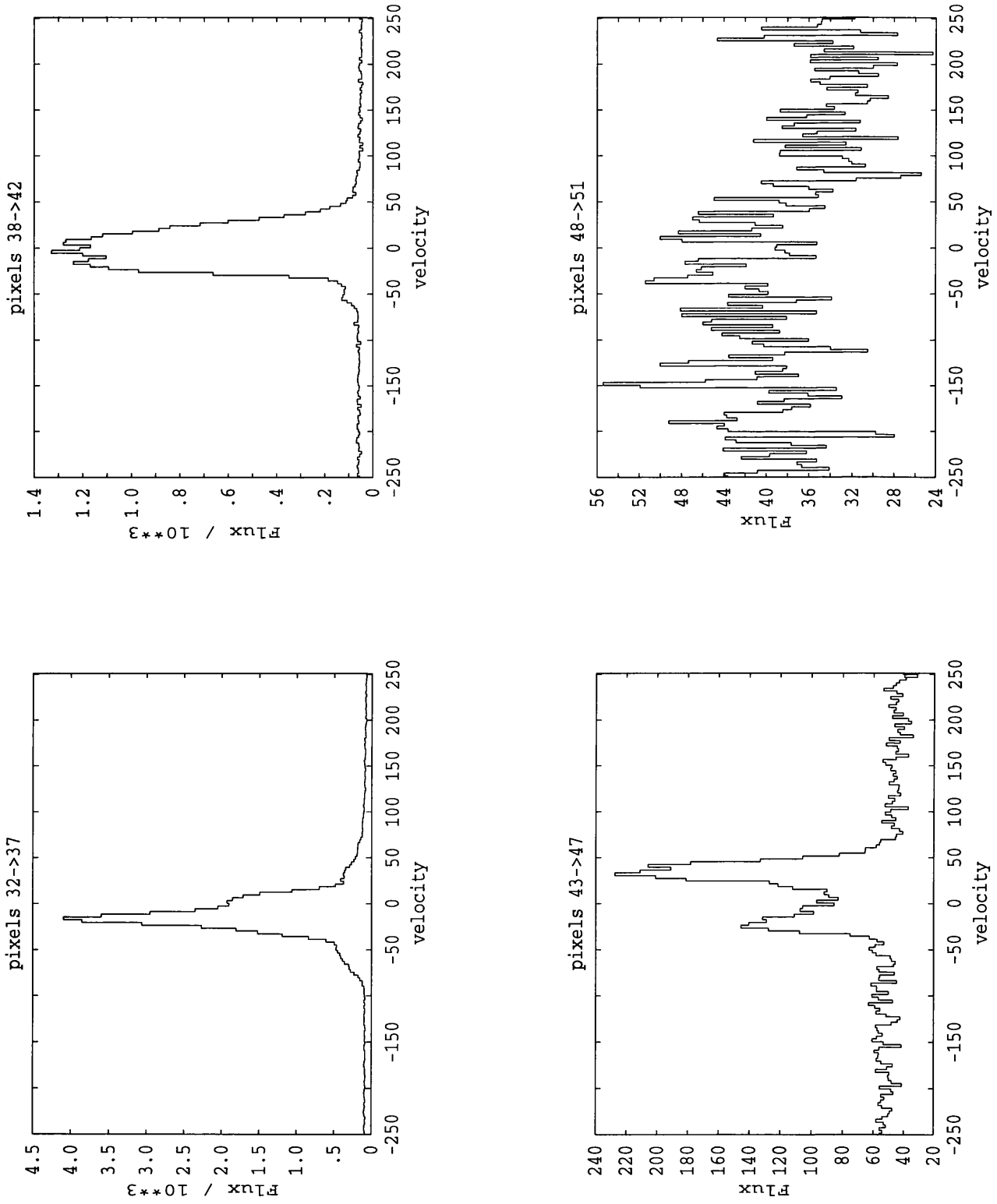

Figure 6.5: Extracted spectra 9→12

6.3.2 Position angle 345°: image 2, spectra 13→24

Image two is most remarkable for its high degree of symmetry, having bright emission features at both extremities of the slit position. The north-western emission maxima is blue-shifted (-50km s^{-1}), while the SE maxima is slightly red-shifted (20 km s^{-1}). The simplest 3-dimensional shape compatible with the elliptical appearance of the ring nebula is that of an ellipsoid. We also note the faint detection of high velocity blue and red-shifted material seen in this image close to the central star.

We note the presence of two regions of emission outside the nebular ring. One is red-shifted on the NW side of the slit position, the other blue-shifted on the SE part of the axis. However the south-eastern emission region appears have a lower expansion velocity than its north-western counter part.

We will now look at these trends in more detail using the extracted spectra, starting from the south-eastern end of the slit position. The nebula emission begins with a broad, complex line profile (pixels 6-12), from which a dominant blue-shifted (-25 km s^{-1}) peak emerges (pixels 12-18). Progressing north this line splits and the blue shifted component develops a shoulder (pixels 18-24). As we move closer to the central star this shoulder develops into a separate dynamical feature with a blue-shift of more than 100 km s^{-1} (pixels 30-36), while the line splitting of the original peak becomes more pronounced. Through this progression the initial emission peak becomes progressively less blue-shifted. Close to the central star a remarkable change occurs, the two component red-shifted line reverts to a Gaussian profile, while the more blue-shifted peak splits into two components (pixels 30-36).

As we pass through the region contaminated by stellar continuum, neither the red-shifted or blue-shifted lines appear to have multiple components. This maybe an effect of the line-to-continuum ratio being much lower here. However the red-shifted

line continues to increase in velocity through this region. Moving to the northern extremity of this slit position, we find a dramatic weakening of the red-shifted component, making it hard to detect (pixels 54-60). This feature maybe identified with the faint northern plume seen in image two. The nebular emission terminates with the blue-shifted line profile splitting (pixels 60-66). It would seem that this occurs because of a new less blue-shifted emission feature, rather than the line merging with the original red-shifted component.

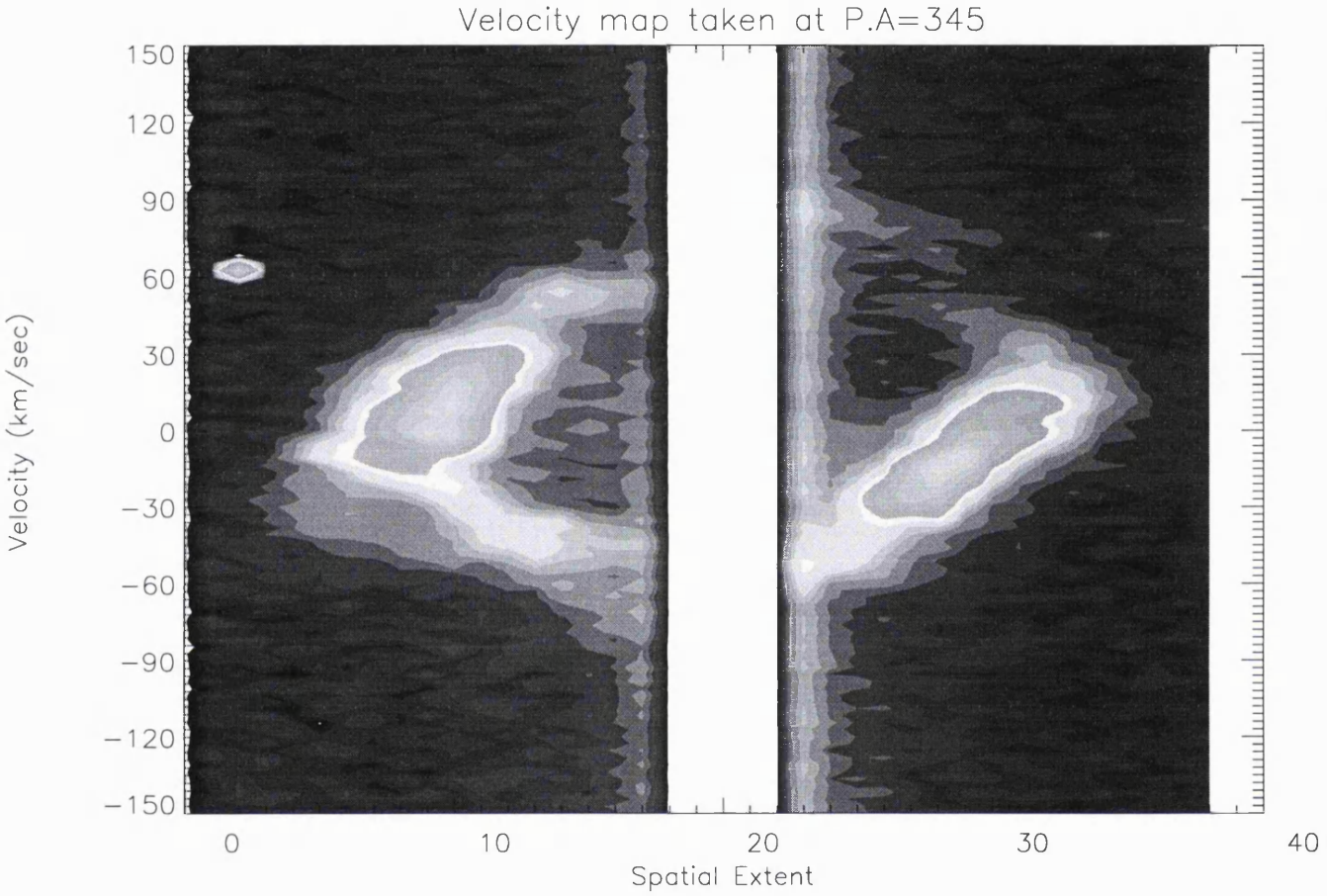

Figure 6.6: Image 2: position angle 345^o

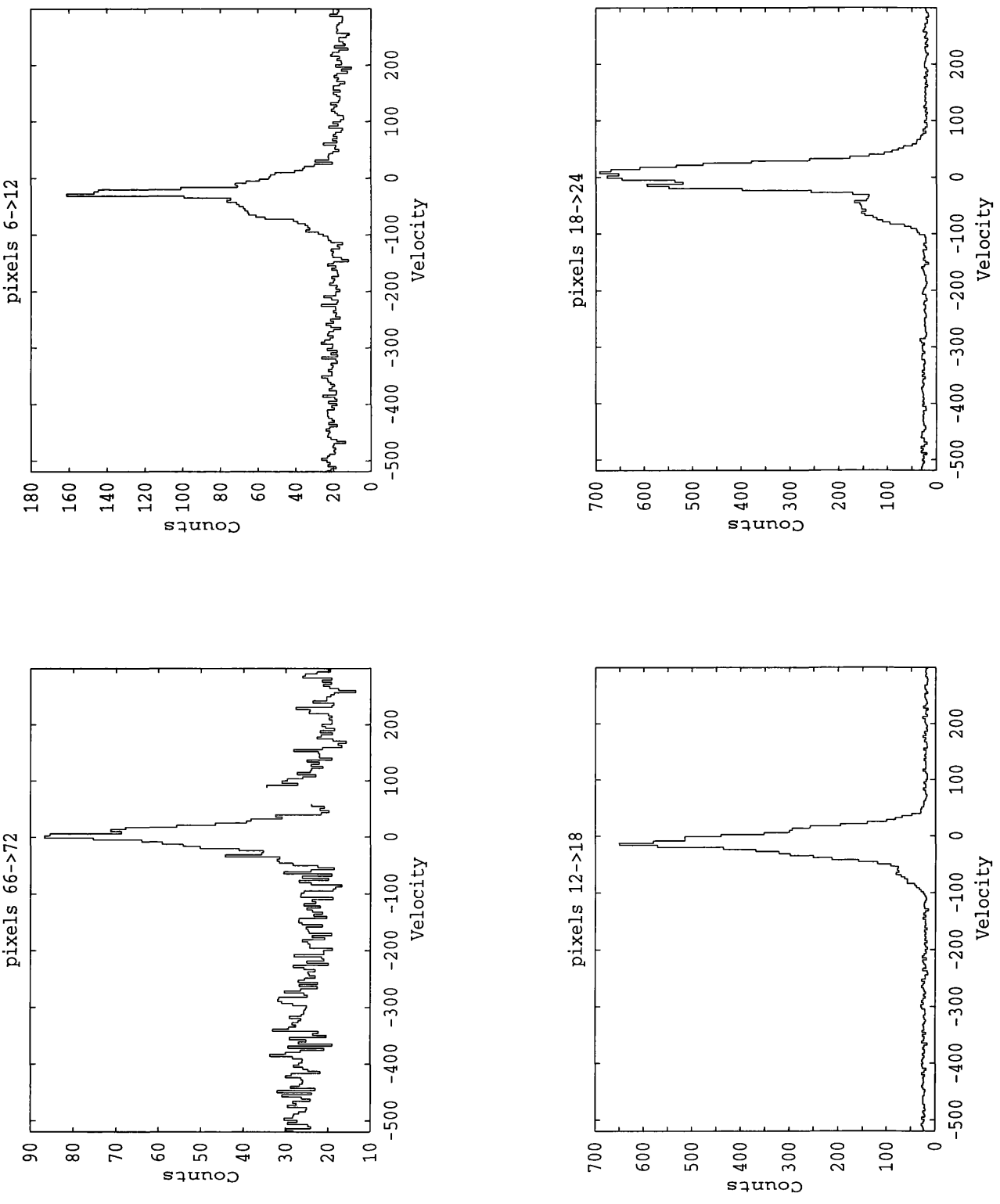

Figure 6.7: Extracted spectra 1→4

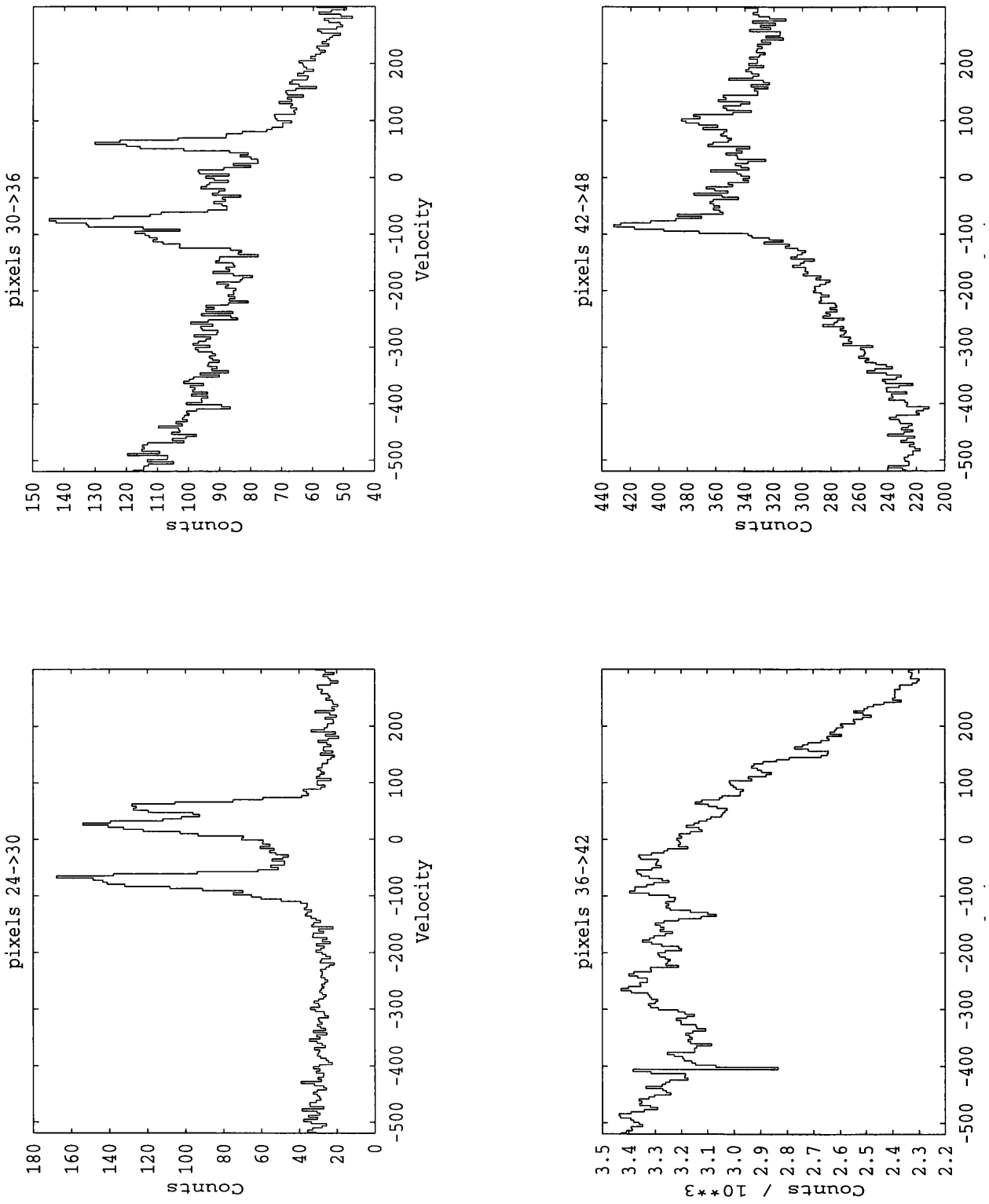

Figure 6.8: Extracted spectra 5→8

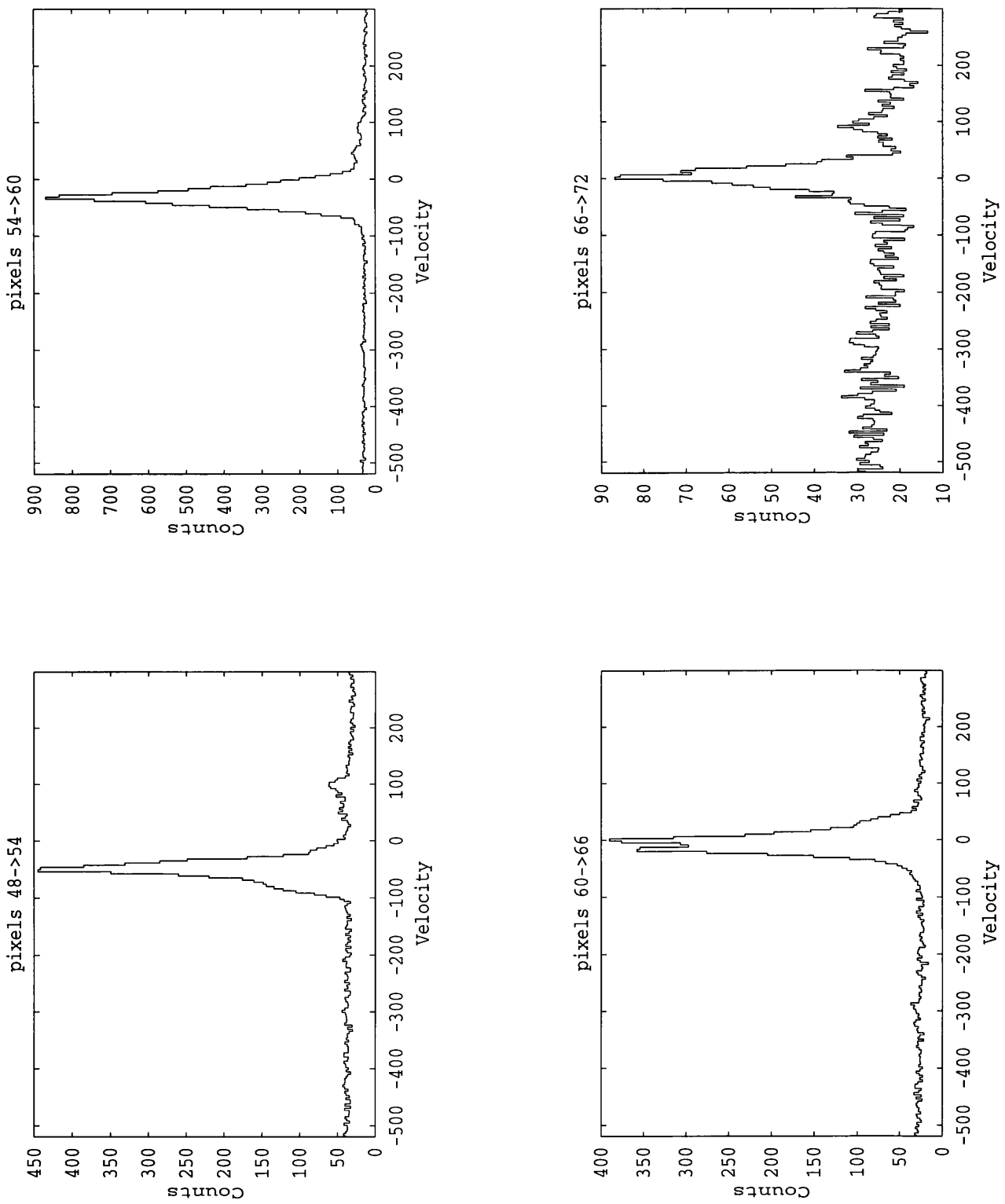

Figure 6.9: Extracted spectra 9→12

6.3.3 Position angle 0°: image 3, spectra 25→36

Image three presents a highly complex dynamical picture. Fundamentally we see an asymmetric ring nebula which is more extended, both spatially and in terms of velocity in the north than the south. In addition to this there exists a high velocity (100 km s^{-1}) red-shifted plume to the north and a similar high velocity blue-shifted plume to the south. We note the presence of a discrete emission feature located in the southern part of the ring nebula, since this feature is multi-cored we infer that it is most probably a nebular condensation, rather than a field star. Finally, we see the presence of lower velocity emission extending from the north and south ends of the ring nebula.

For a more detailed picture we turn, once again, to the extracted spectra. In the Southern region, nebula emission is first identified as a single blue-shifted emission line at 75 km s^{-1} (pixels 1-3). This grows in strength as we move north and is joined by a stronger less blue-shifted component (30km s^{-1}). The more blue-shifted of the components is associated with the southern high velocity plume (pixels 5-10), while the stronger, lower velocity component appears to correspond to the lower velocity plume emerging from the southern end of the ring nebula. We note the emission from the low velocity plume has broad wings in velocity space, while the emission from the higher velocity plume is sharper, suggesting a narrower velocity distribution.

Moving north, we see the emission from the plume strengthens and develops a second component which becomes progressively more red-shifted, together these represent emission from the front and back of the optical nebula. Briefly the spectra cover the detached southern emission feature, which having a projected red-shifted velocity of only 20 km s^{-1}, (pixels 11-15) creates a second component in the dominated red-shifted line. As we move closer to the central star these features acquire an expansion velocity of $\pm$ 60 km s^{-1} (pixels 16-20) and envelop the emission from

the high velocity plume in their wings.

Continuing our progression north, the nebular lines emerge from the stellar continuum with a velocity approaching ± 100 km s^{-1} (pixels 29-32). This velocity very rapidly drops to about± 50 km s^{-1}, revealing the presence of a northern high velocity plume $+80$ km s^{-1} (pixels 38-44). In the northern part of the slit position the red-shifted emission from the ring nebula is very weak, being comparable in strength to the high velocity plume. Accompanying this the blue-shifted line develops a high velocity shoulder, which fades as we move further north. At the northern edge of the nebula the emission lines from the ring nebula drop in velocity and begin to merge at a velocity of 0 km s^{-1}. At the northern extremity (pixels 45-50) the high velocity plume persists maintaining a velocity of close to 100 km s^{-1}.

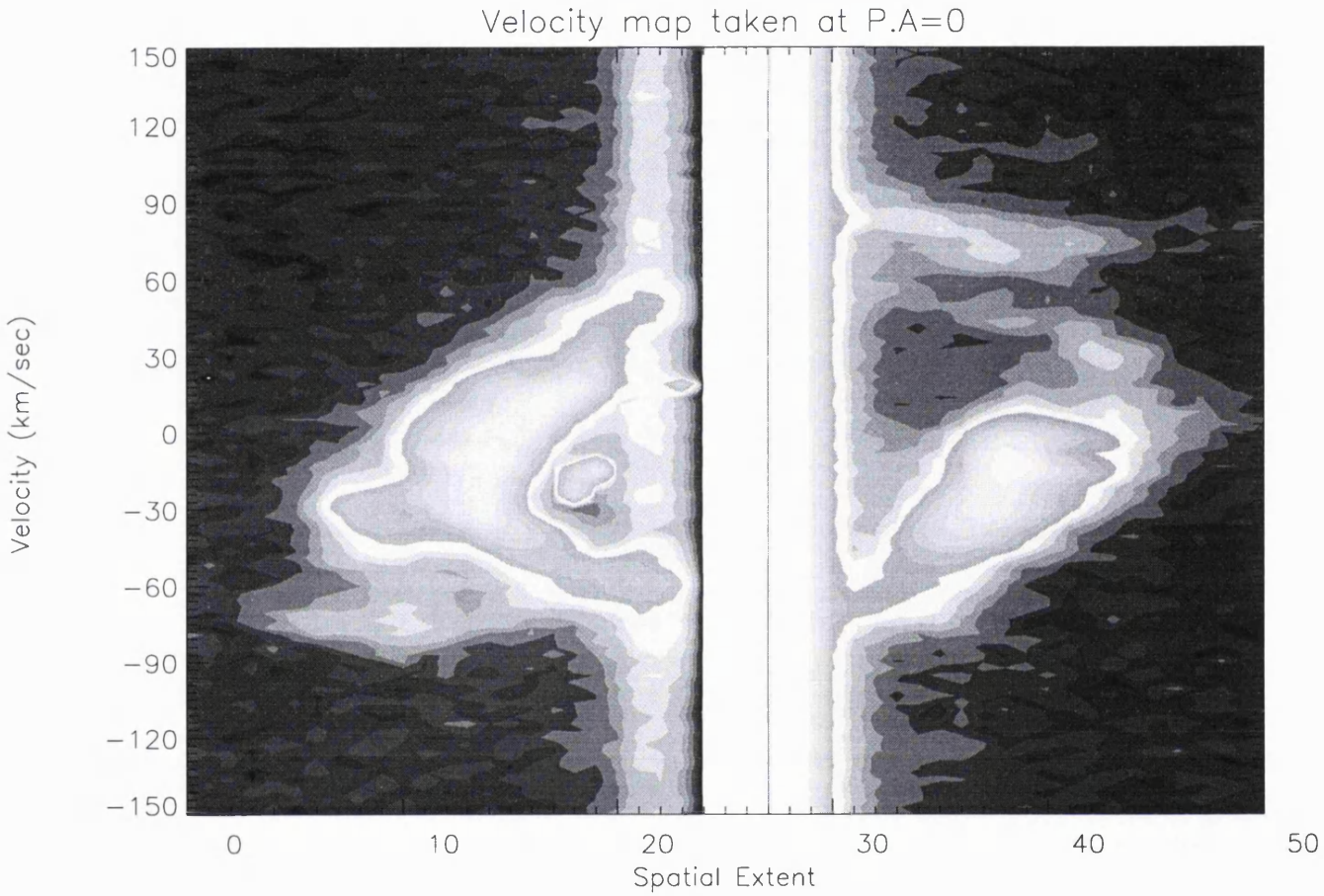

Figure 6.10: Image 3: position angle 0^o

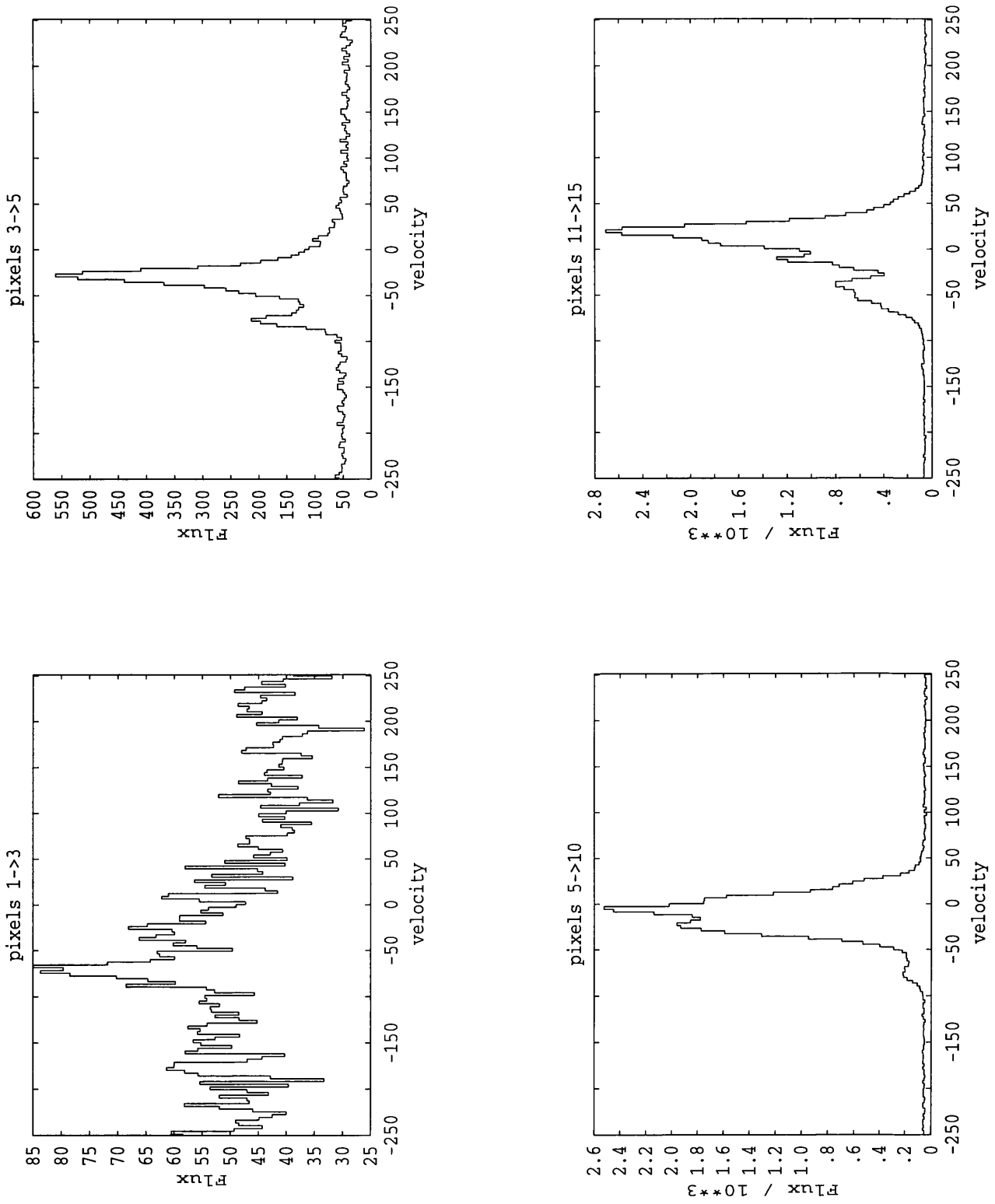

Figure 6.11: Extracted spectra 1→4

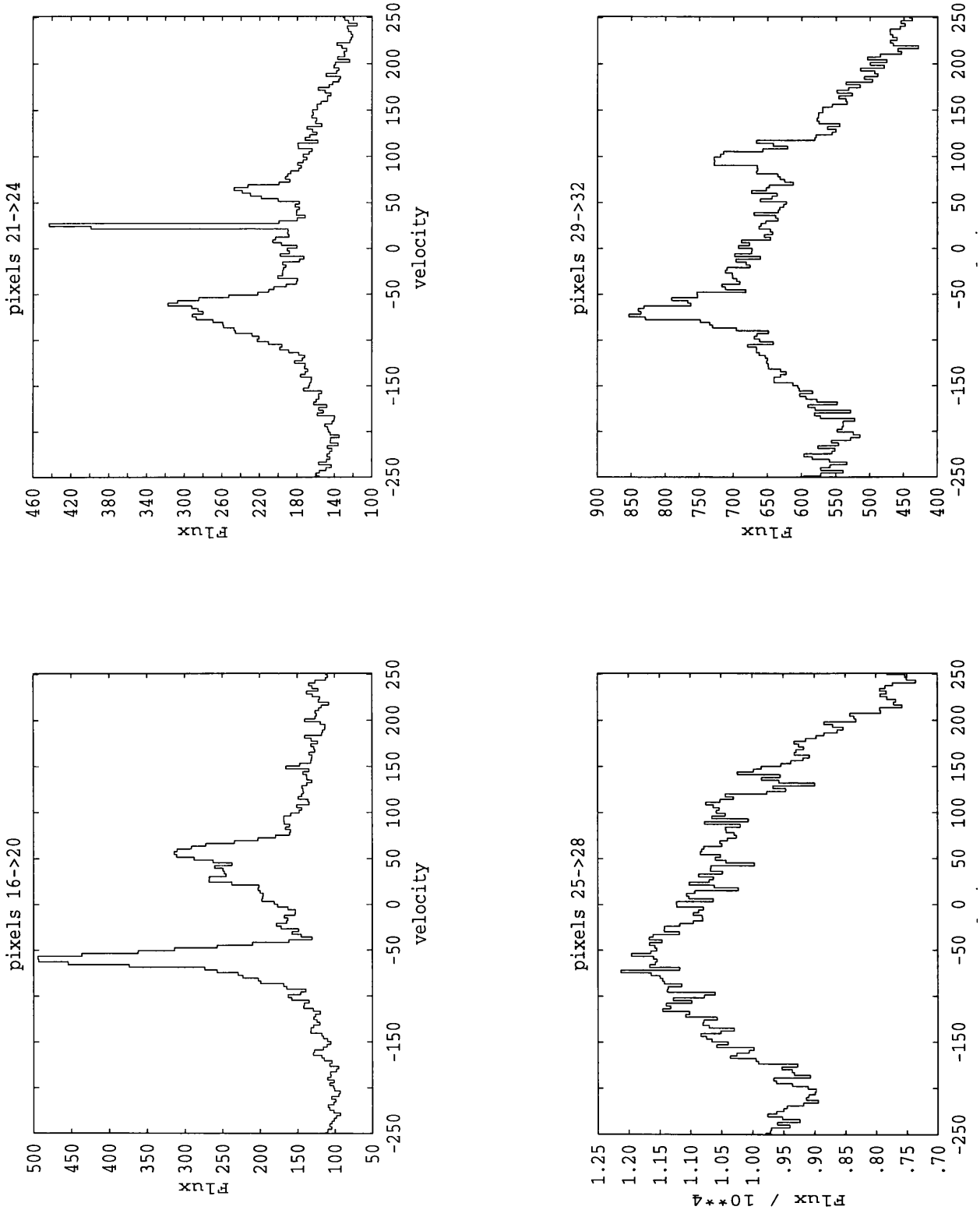

Figure 6.12: Extracted spectra 5→8

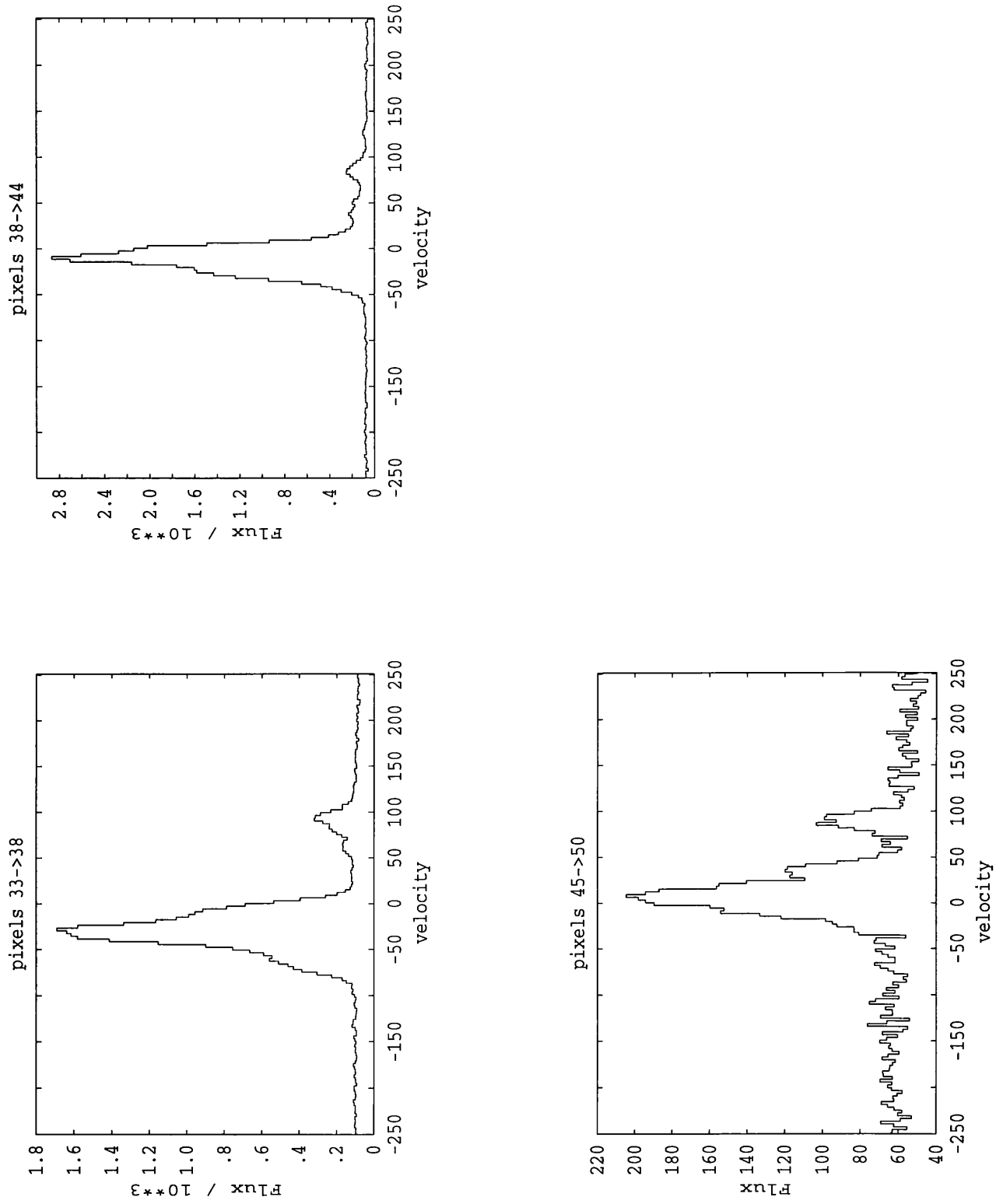

Figure 6.13: Extracted spectra 9→12

6.3.4 Position angle 15°: image 4, spectra 36→48

Image four retains many features in common with image three, being essentially a ring nebula with a red-shifted high velocity plume emerging from north and a high velocity blue-shifted plume emerging from the south. However image 4 shows a lower degree of symmetry than image 3. As in image three the back of the northern part of the shell produces only weak emission. Furthermore we note that the dominant emission from the southern region is blue-shifted, to a much greater extent than the bulk of the emission from the north region.

We will briefly comment on the accompanying spectra, which show a progressive increase in line splitting as we move toward the central star. Nebula emission is first detected with a blue shifted velocity of 40 km s^{-1} (pixels 6-12). The spectra which include the dominant southern emission region, confirm that it has a clumpy structure, through the red-shifted component becoming briefly split. The southern high velocity plume attains a maximum velocity of 90 km s^{-1} (pixels 12-18). There is some evidence that this velocity decreases as we move toward the central star.

Close to the central star a maximum line splitting of 90 km s^{-1} is observed (pixels 42-48). As we move north a high velocity plume emerges from the red- shifted line component. This begins with a velocity of 50 km s^{-1}, increasing to 80 km s^{-1} at the northern extremity (pixels 60-66). In this region the line components merge at a blue-shifted velocity of 20 km s^{-1}.

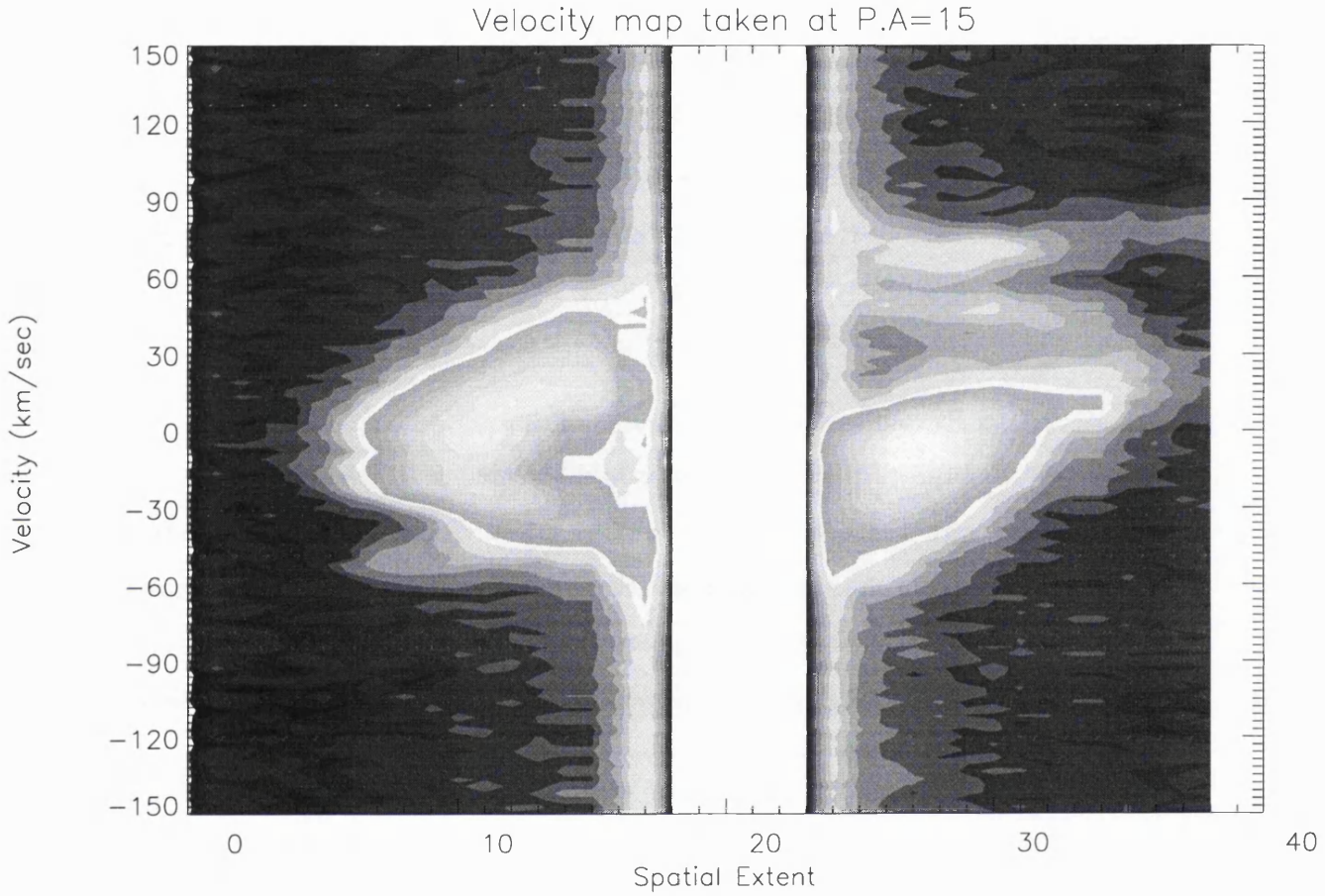

Figure 6.14: Image 5: position angle 15°

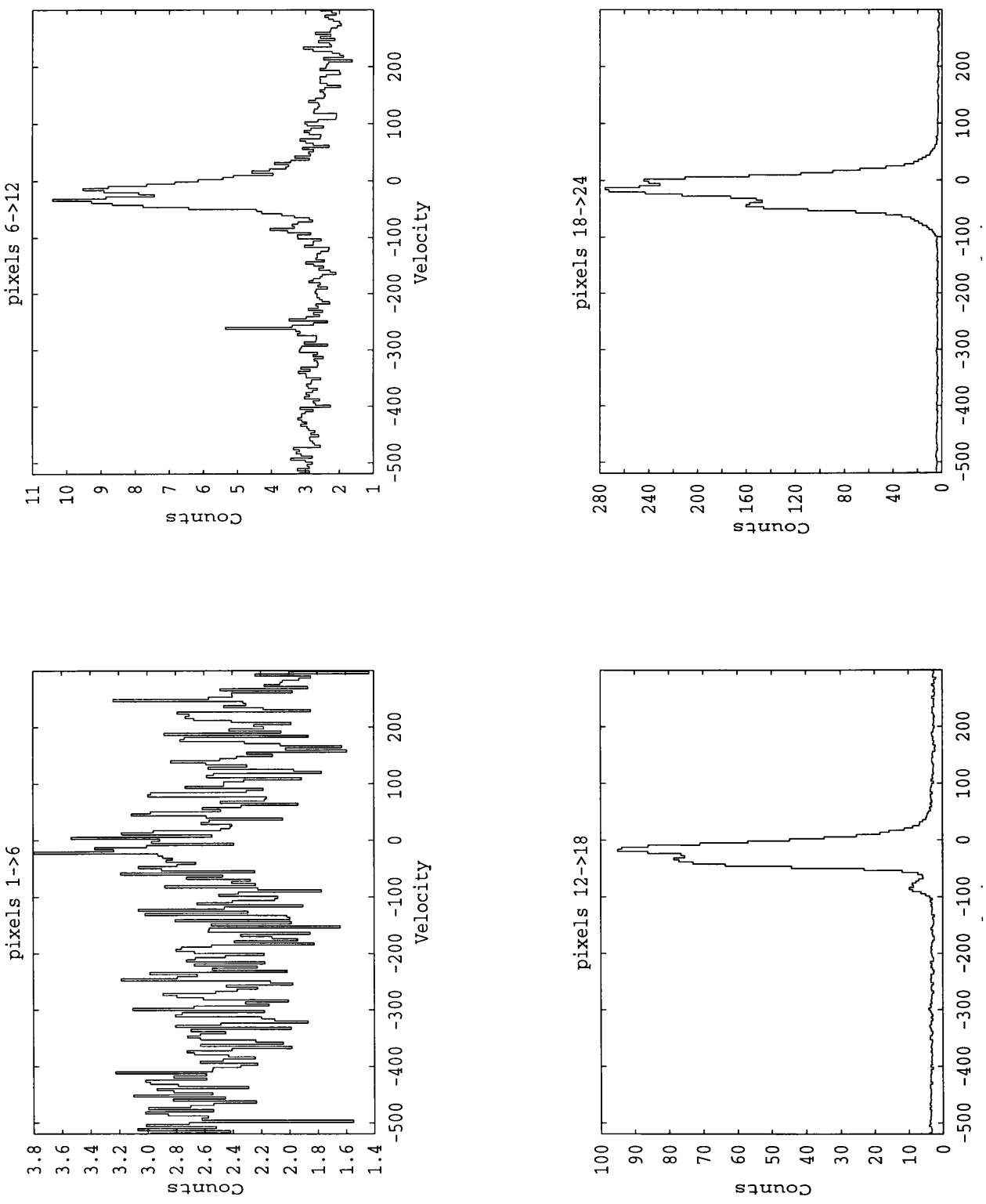

Figure 6.15: Extracted spectra 1→4

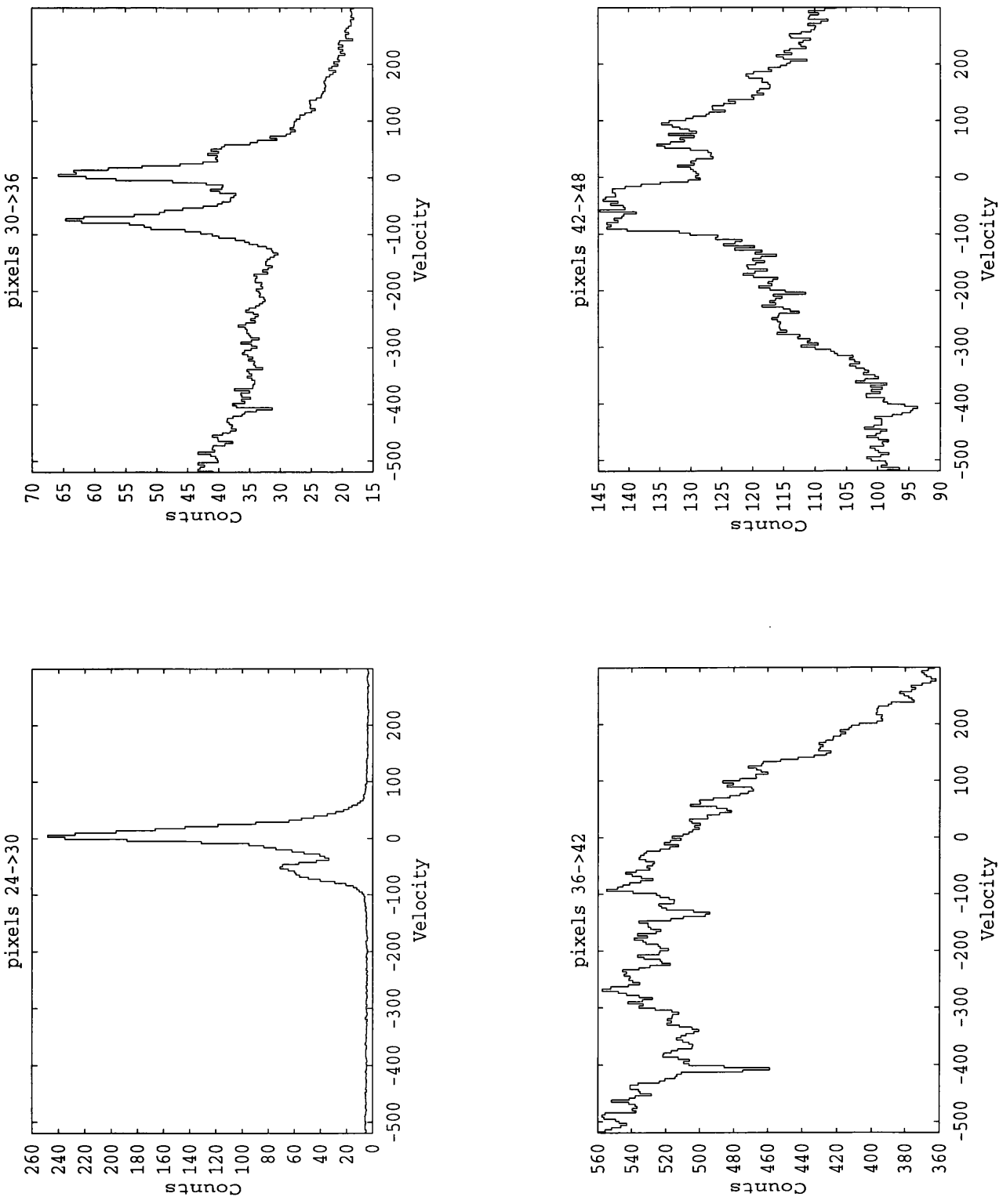

Figure 6.16: Extracted spectra 5→8

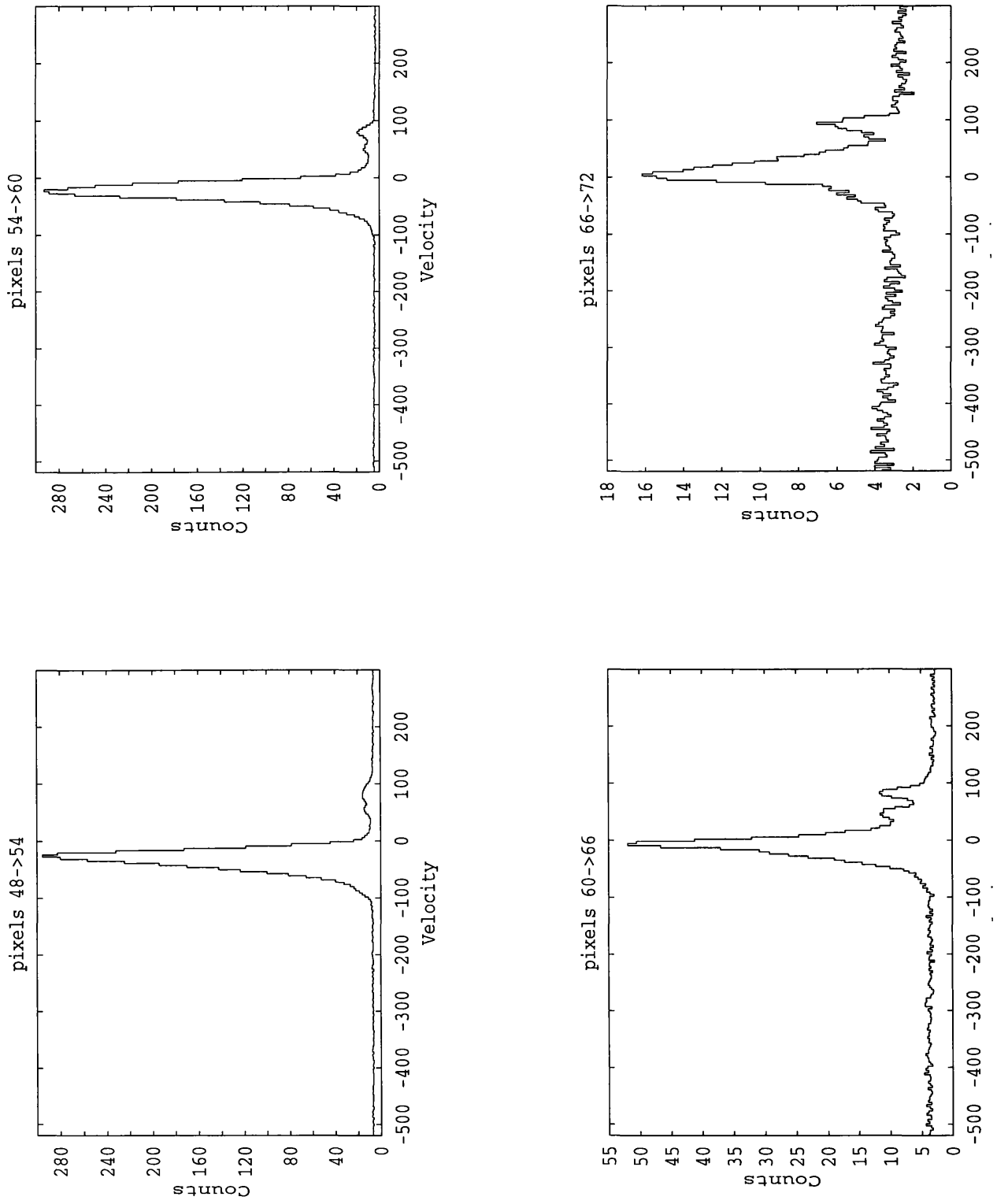

Figure 6.17: Extracted spectra 9→12

6.3.5 Position angle 30°: image 5, spectra 49→51

Image five lies along the minor axis of the observed ring nebula. This coincides with the "dust jet" imaged by Paresce & Nota (1992). The broad structure of image five is very similar to that seen in the previous two images. Spatially it is more extended than image four and so in this respect bears a greater similarity to image three. We note that while the northern high velocity plume is still prominent, its southern counterpart is is largely absent at all but the closest position to the central star

Turning to our extracted spectra, we find that from the southern region the emission smoothly splits into two peaks (pixels 11-15). A maximum line splitting of 45 km s^{-1} occurs near the central star, where the blue shifted component acquires a high velocity shoulder (70 km s^{-1}), corresponding to the faint southern high velocity plume. As the nebular emission emerges from the stellar continuum to the north a four component line profile is observed (pixels 31-33). Within these line profiles it is the emission from the higher velocity components that dominate. The origin of this complicated line profile is not clear, but it may represent the ring nebula in conjunction with the base of both the north and south high velocity plumes.

Moving further north a bright blue-shifted emission feature is encountered, while the emission from the back of the nebula is weak. The four component emission profile disappears (pixels 34-39). In this region the northern high velocity plume attains 85 km s^{-1}. As we continue the progression north the blue-shifted emission splits, once again creating a four peaked line profile (pixels 40-44). This is transitory. Moving further north the high velocity plume fades and the other line components merge into a single line profile centered on a red-shifted velocity of 20 km s^{-1}.

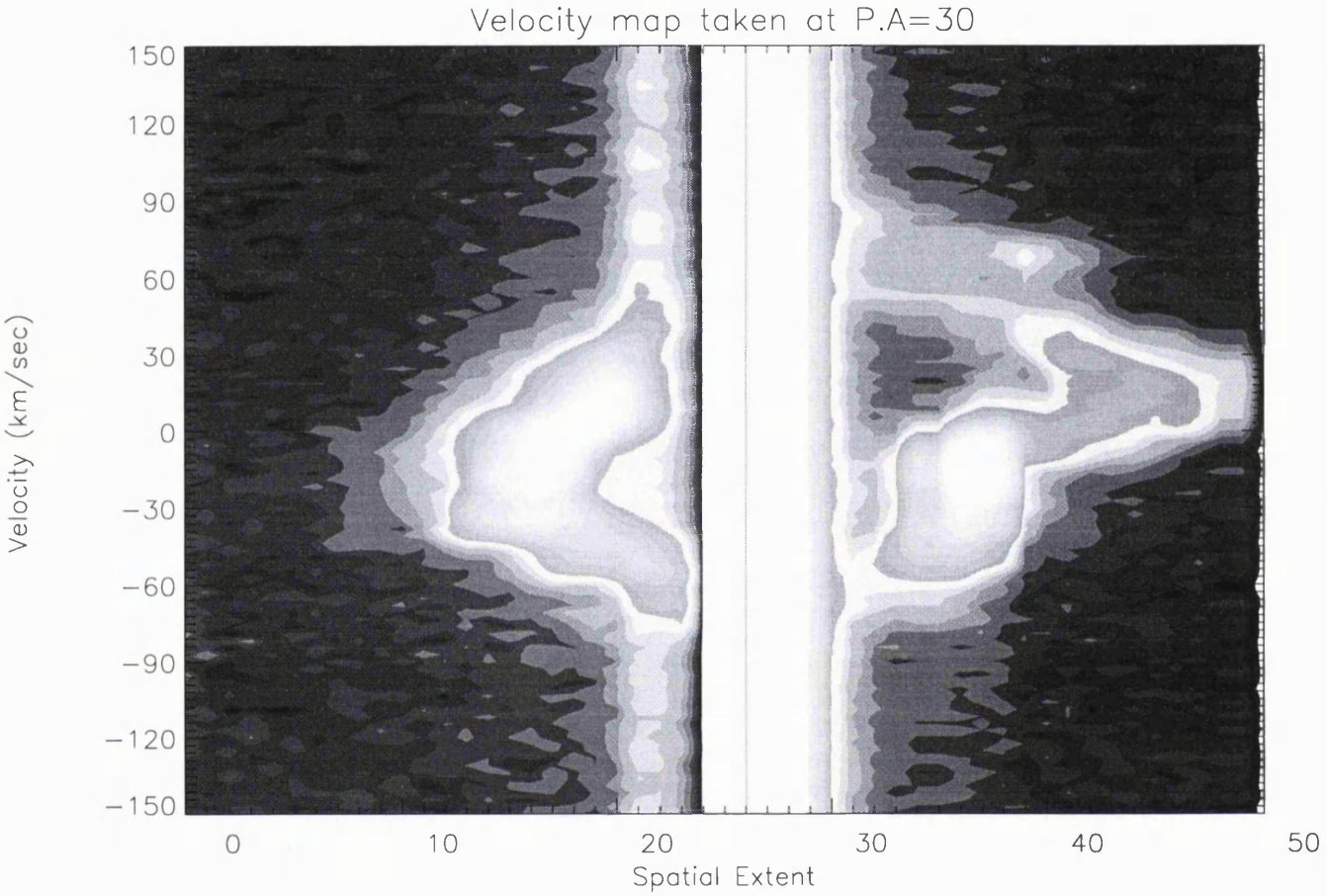

Figure 6.18: Image 5: position angle 30°

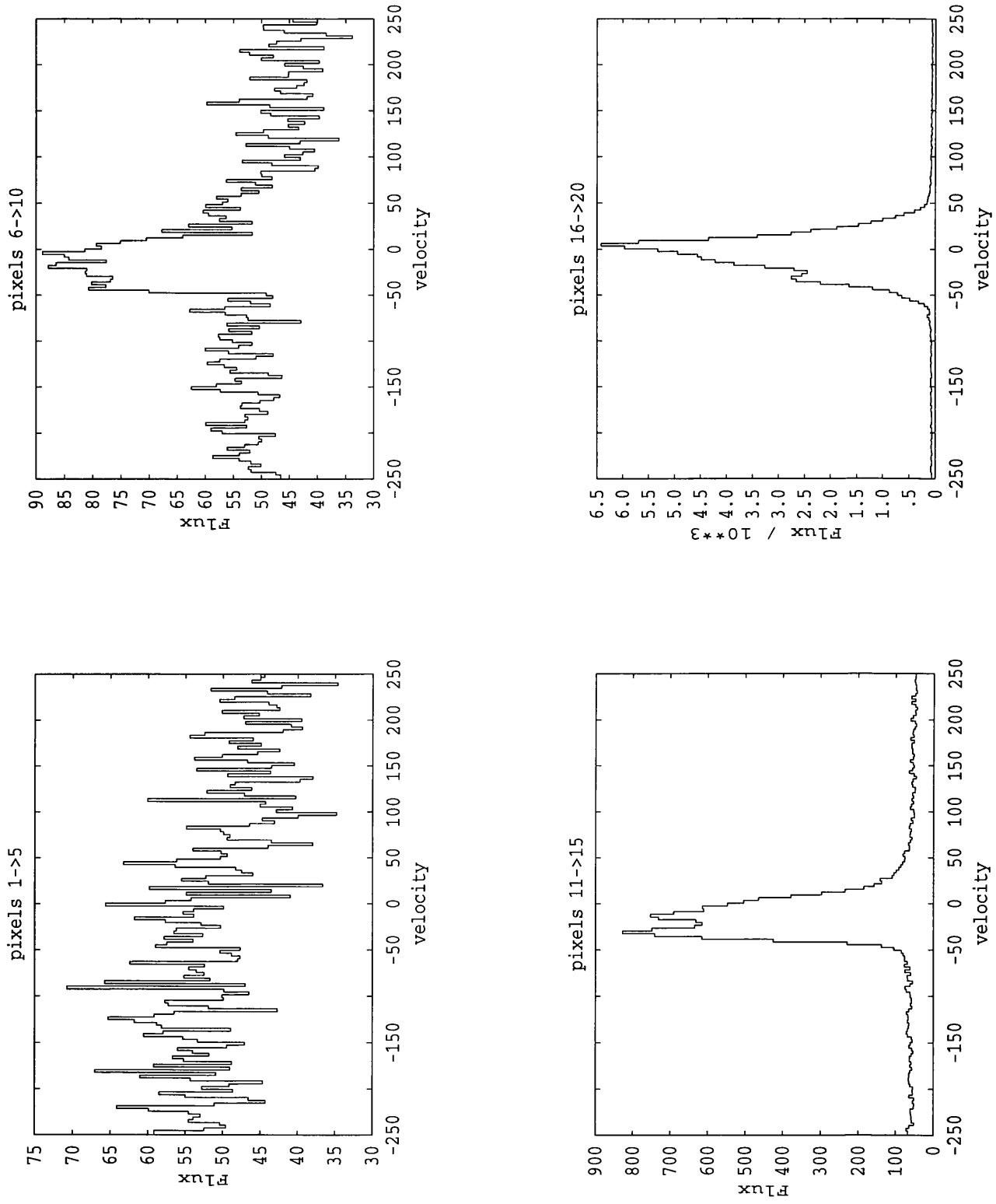

Figure 6.19: Extracted spectra 1→4

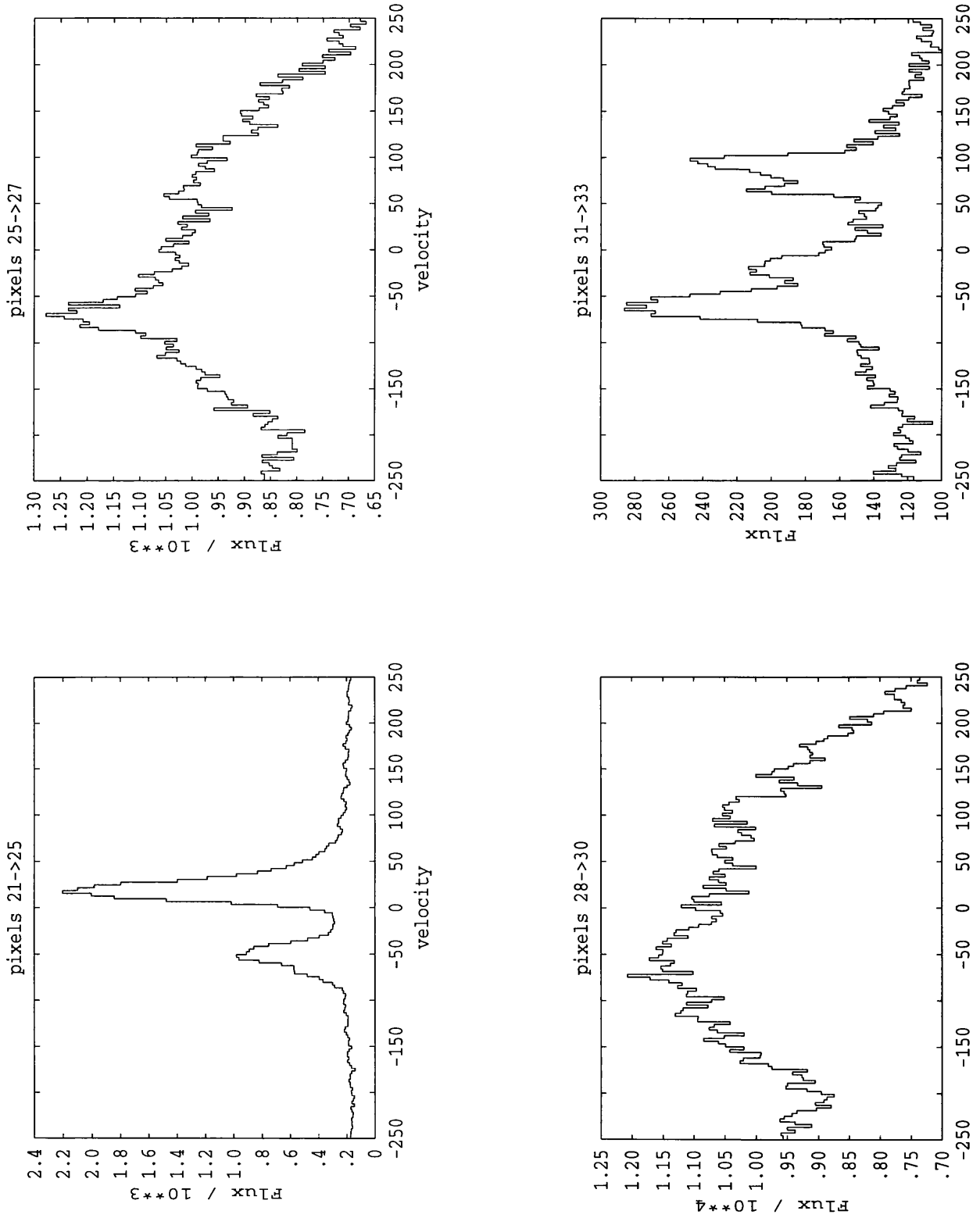

Figure 6.20: Extracted spectra 5→8

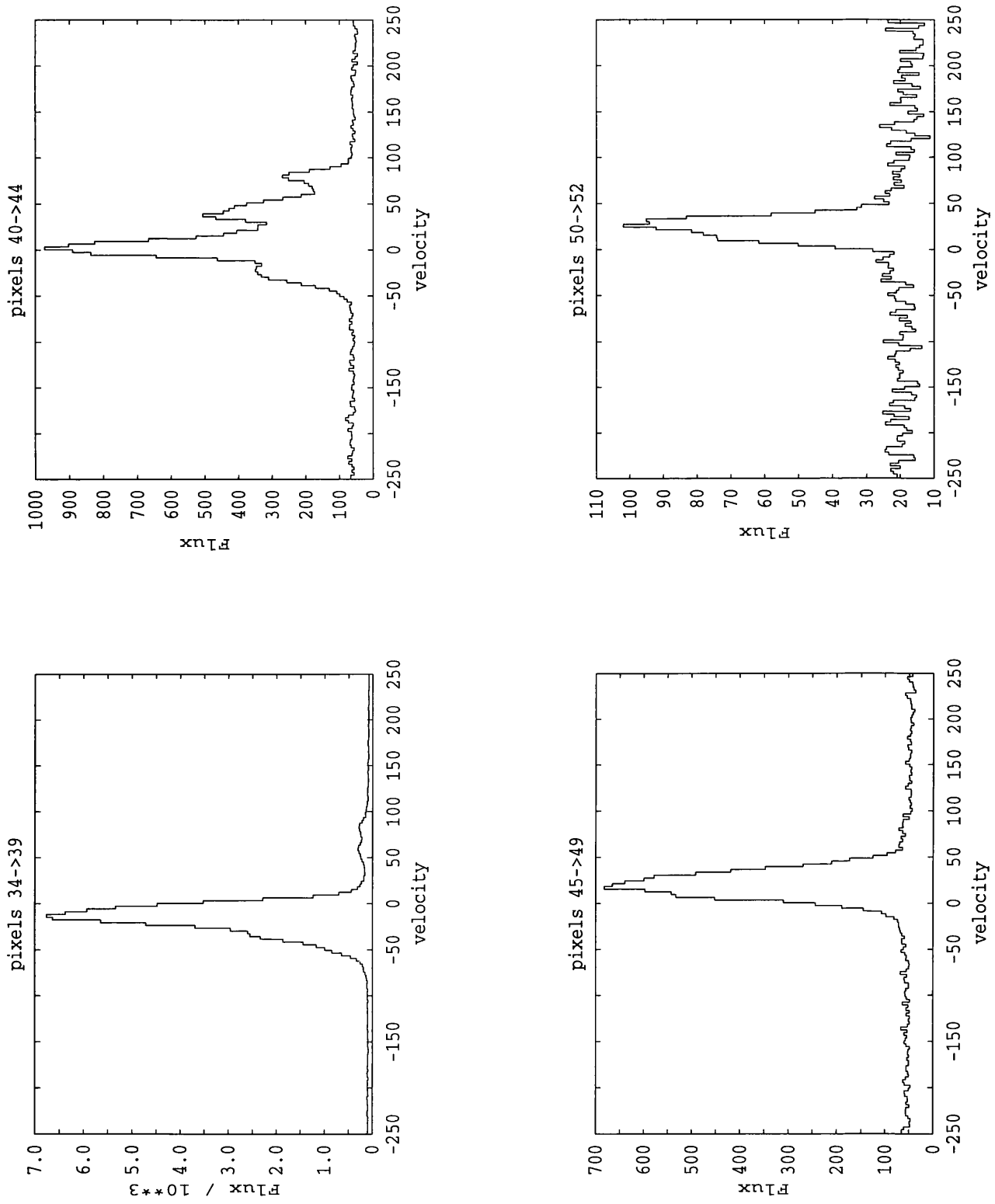

Figure 6.21: Extracted spectra 9→12

6.3.6 Position angle 40: image 6, spectra 52→64

In image six we see a return to a more symmetric nebular cross section, we note the similarity to image four. Although the symmetry is somewhat broken by northern emission maxima. This slit position passes through a region of faint emission outside of the ring nebula to the north (see figure 6.1). The origin of this material is not known. It also intersects the "dust jet", which is at a P.A. of 30°-40°. In these image there is no clear evidence of any high velocity plumes to either the north or south. This slit position also lies along the "dust jets" found by Paresce & Nota (1989).

The first detection of nebular emission at the southern end of this slit position comes with a quite broad line profile (pixels 6-12), which from image six, appears to be due to an extended smooth distribution of material, or multiple unresolved clumps. As we move north this profile is slow to split, achieving a line separation of 60 km s^{-1} close to the star (pixels 30-36). At this point we note that the blue-shifted component develops a high velocity shoulder. It is not clear if this corresponds to a blue-shifted high velocity plume. If it does, its projected velocity is comparable to the nebular expansion velocity in this region. As we move north from the central star the shoulder on the blue-shifted line component fades and a new high velocity shoulder appears in the red- shifted line component (pixels 54-60). Toward the northern extremity the two peaks merge (pixels 60-72), with the resulting Gaussian having a velocity of 10 km s^{-1}.

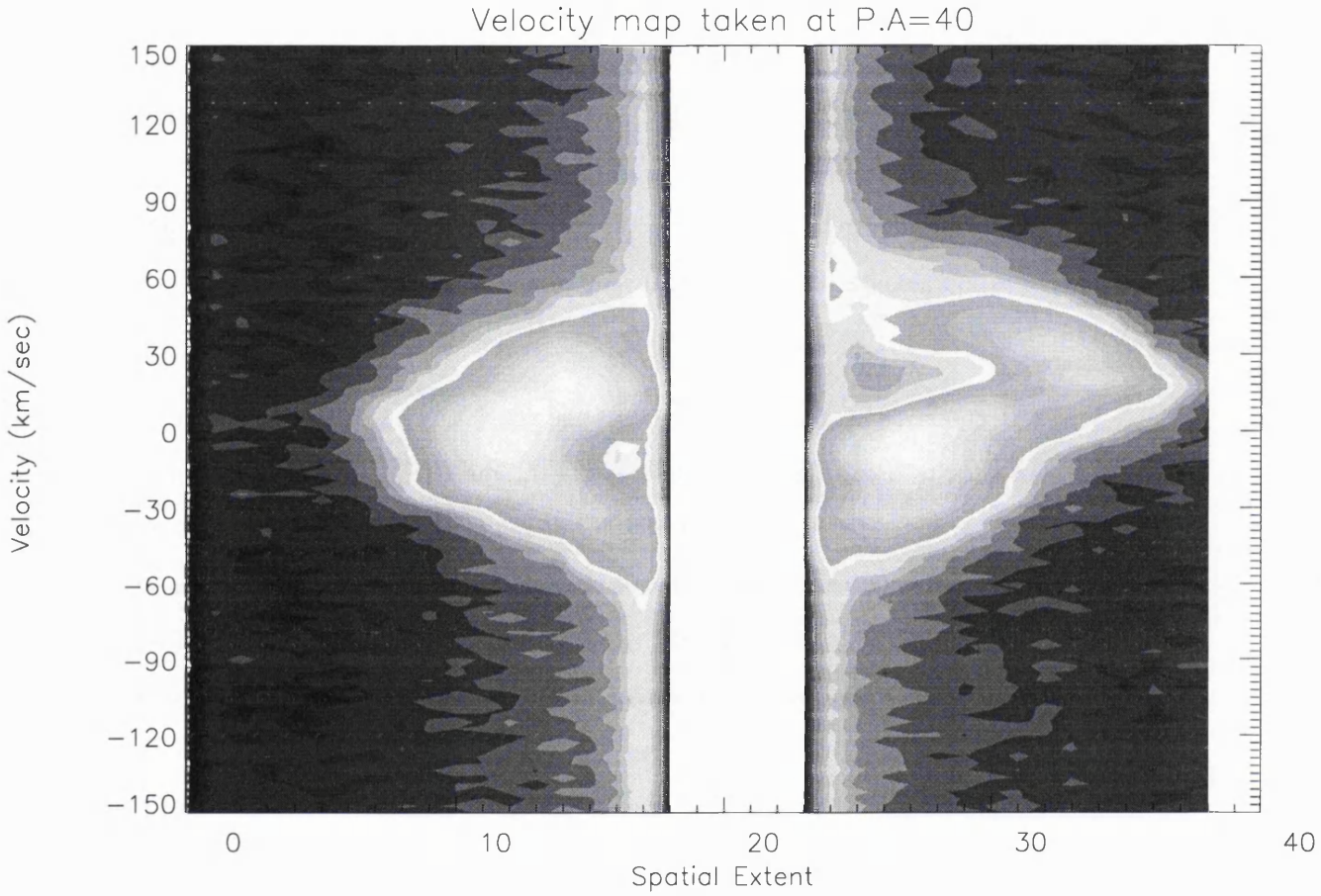

Figure 6.22: Image 6: position angle 40°

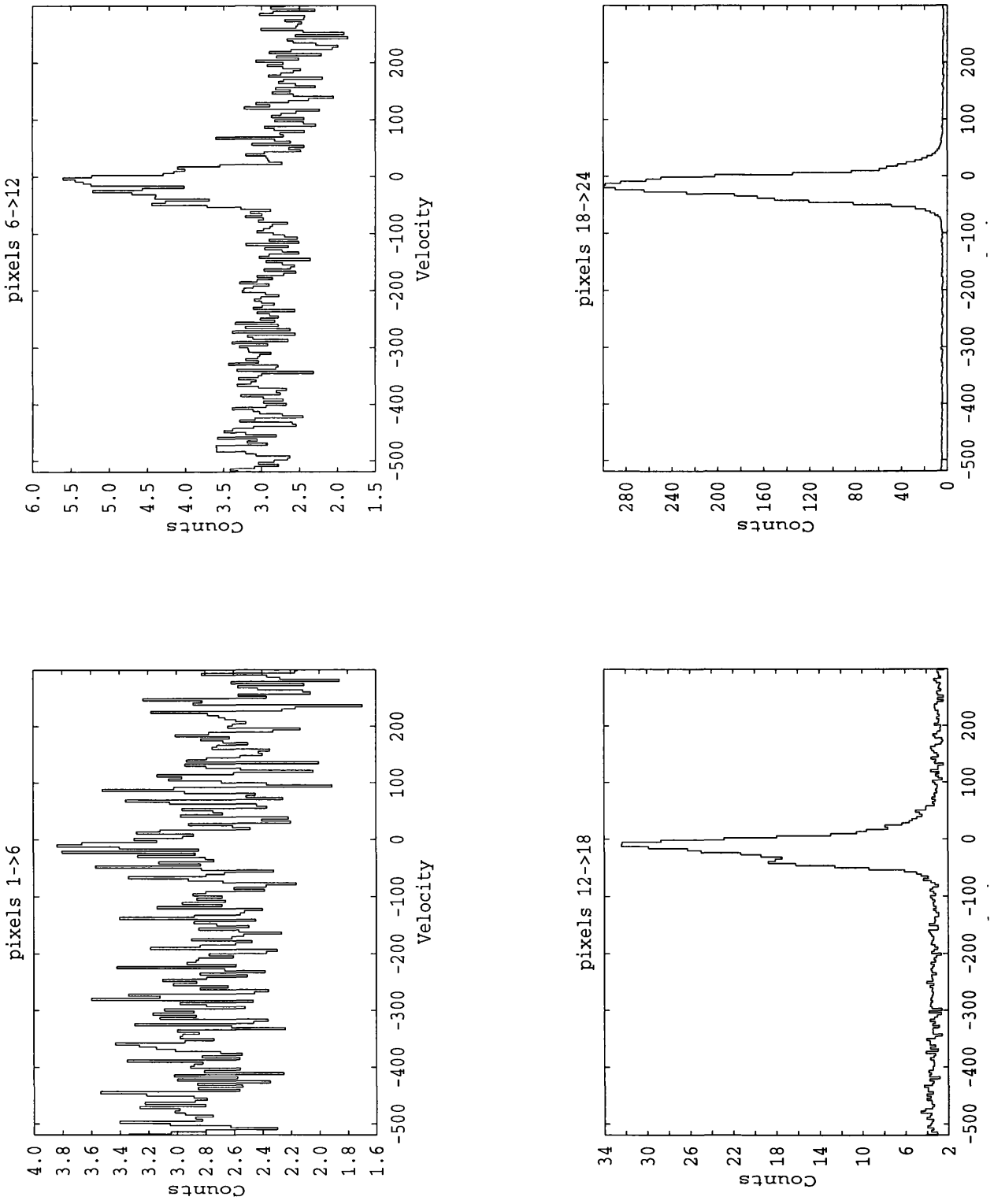

Figure 6.23: Extracted spectra 1→4

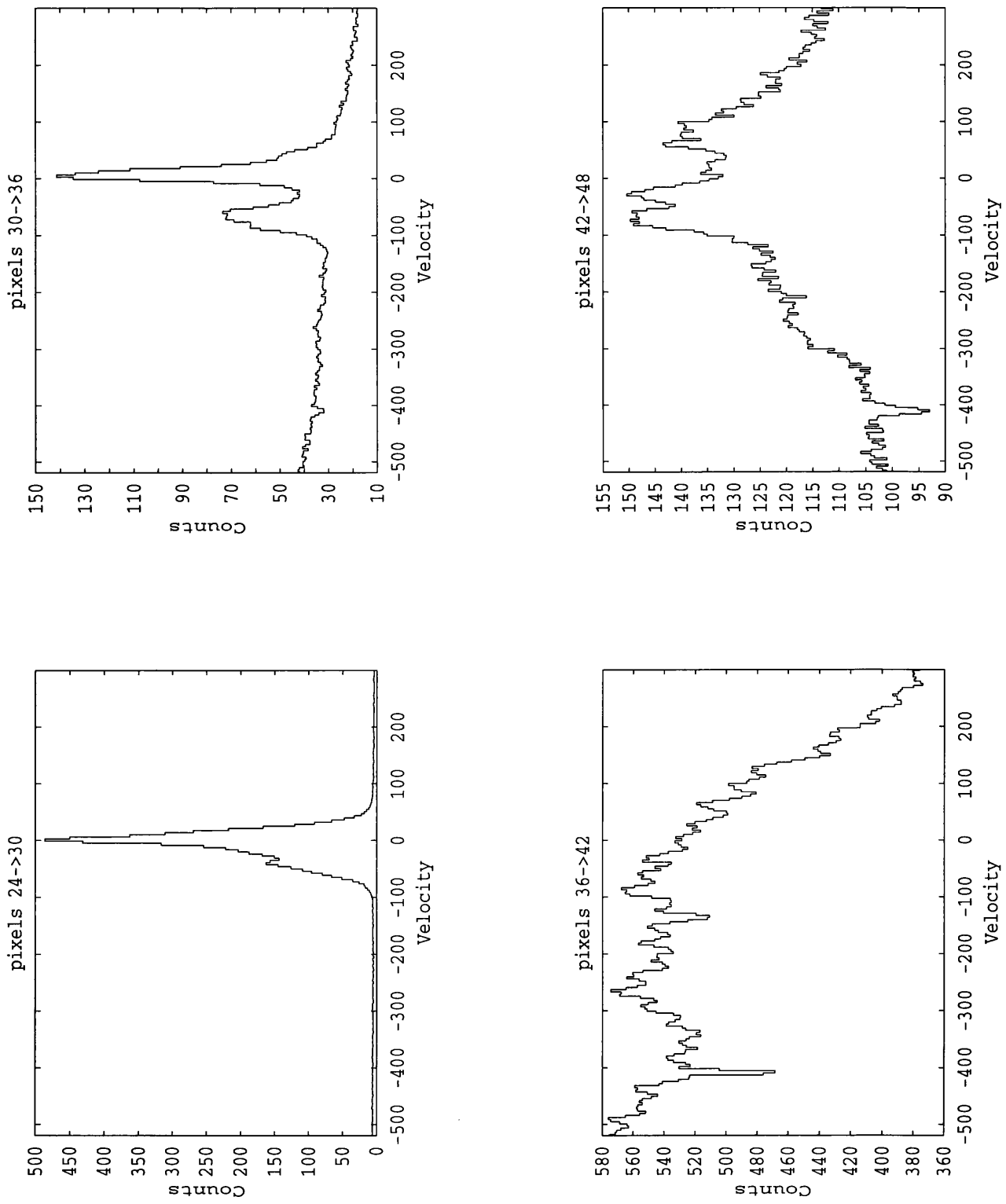

Figure 6.24: Extracted spectra 5→8

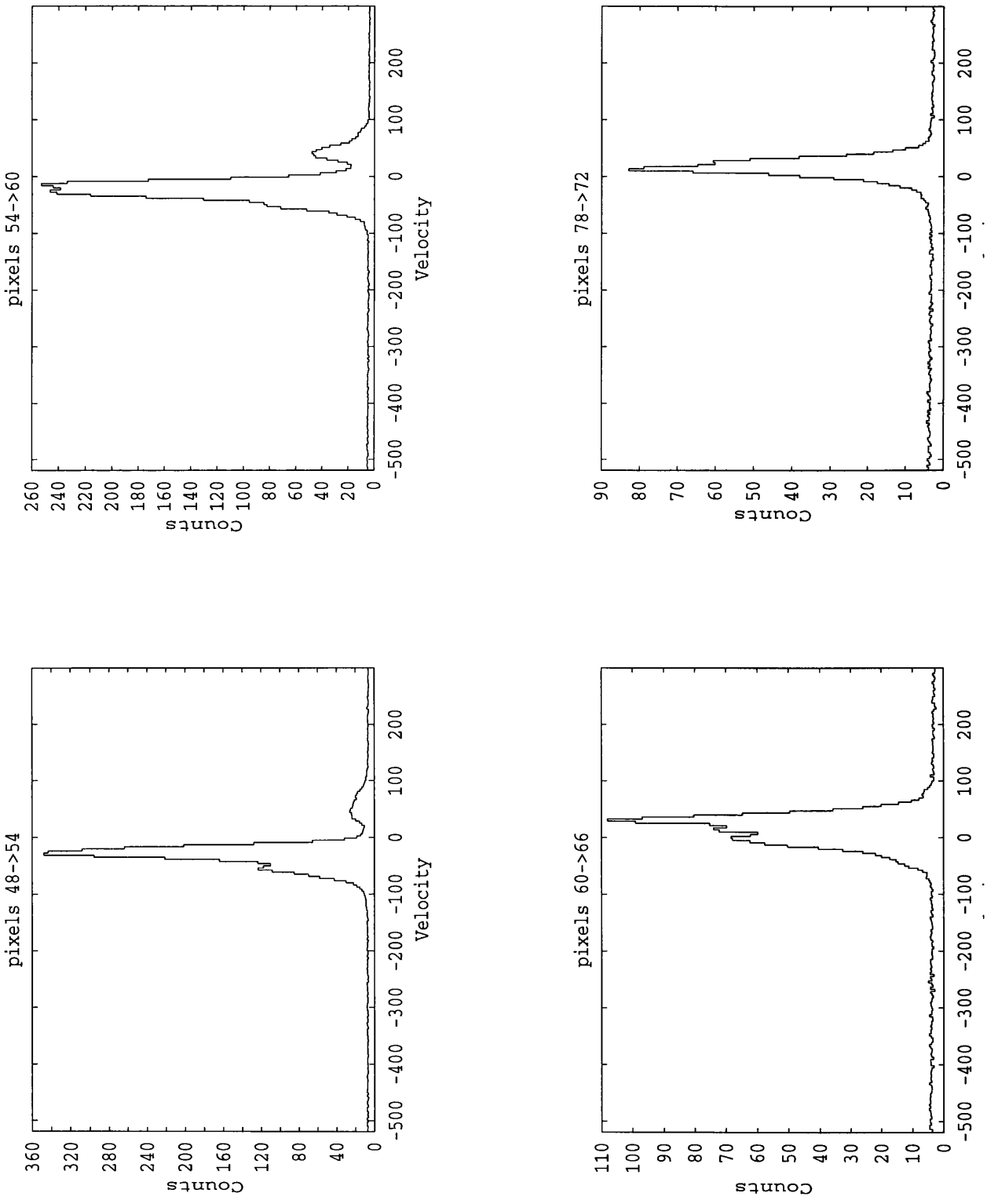

Figure 6.25: Extracted spectra 9→12

6.3.7 Position angle 80°: image 7, spectra 65→77

Our final image is image seven. This has a regular and symetrical appearance. Since this position angle is approaching the major axis of the nebula, the ring of the nebular emission has a large spatial extent, although the maximum line (60 km s^{-1}) splitting (pixels 21-25) is comparable to that seen at the other slit positions. We note, particularly to the north, that the nebula emission extends well beyond the main ring nebula shell. In this image we see some evidence for clumping, mainly toward the east. If the high velocity plumes are in this image, they are not present as distinct dynamical feature. We note that there exists symetrical emission enhancements close to the central star, blue-shifted to the west and red-shifted to the east.

The picture outlined above is supported by the corresponding spectra. Generally the spectra are indicative of line splitting due to a symetrical, clumpy nebula. They also illustrate that the symmetric, higher velocity, density enhancements, close to the star, are rather more distinct from the ring nebula than we might initially infer from the image (pixels 16-25). The spectra suggest that their velocity is close to 50 km s^{-1}.

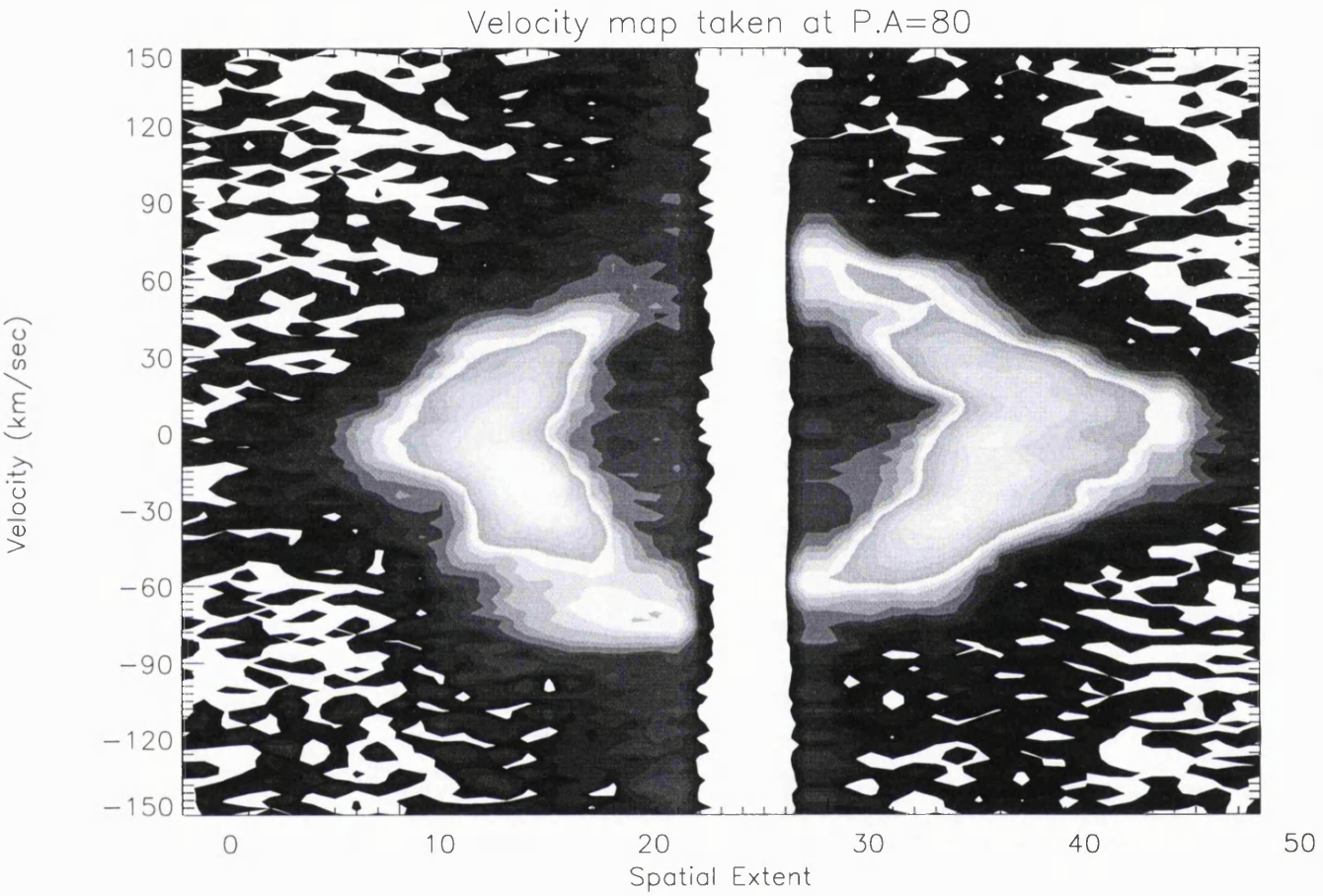

Figure 6.26: Image 7: position angle 80°

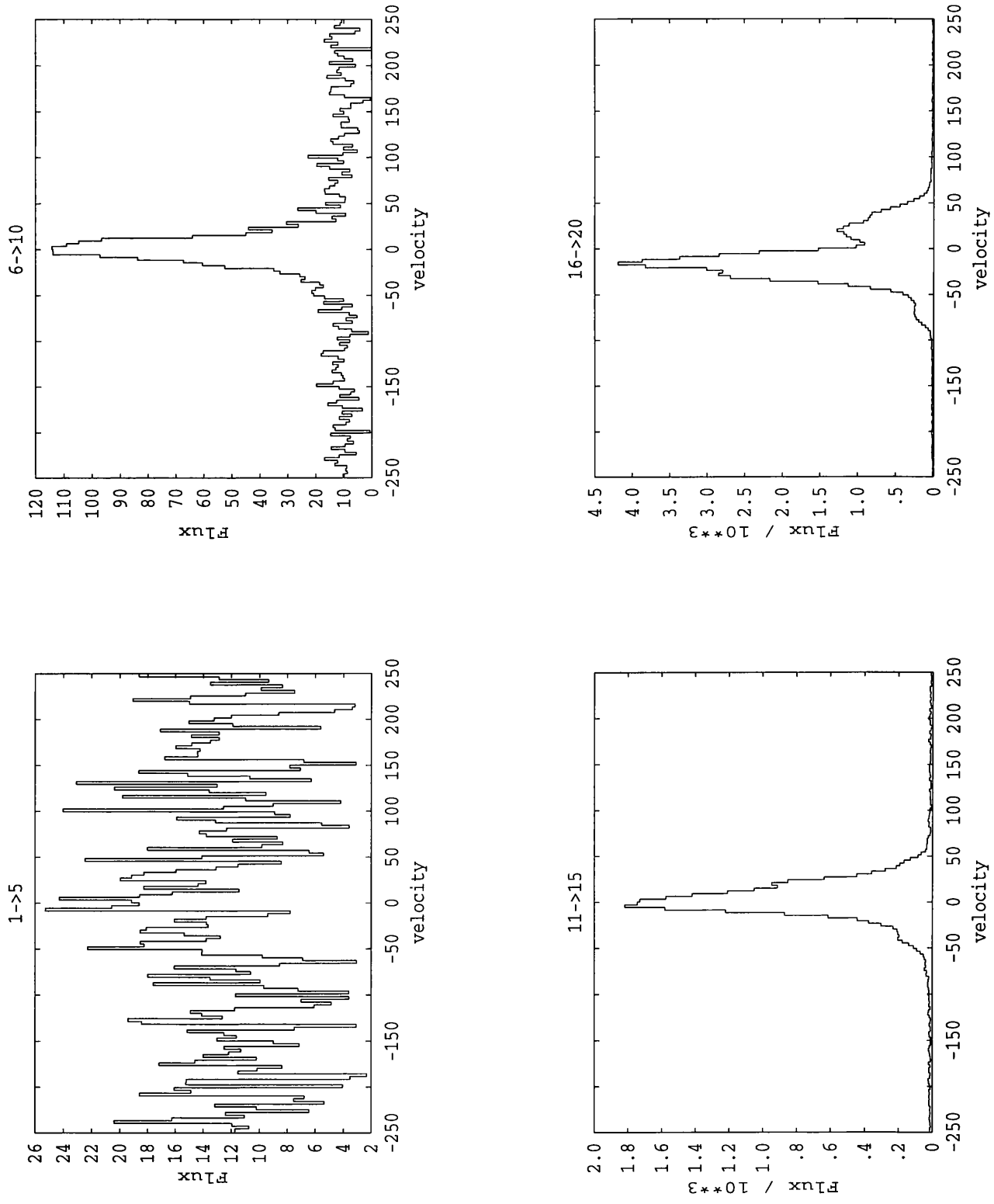

Figure 6.27: Extracted spectra 1→4

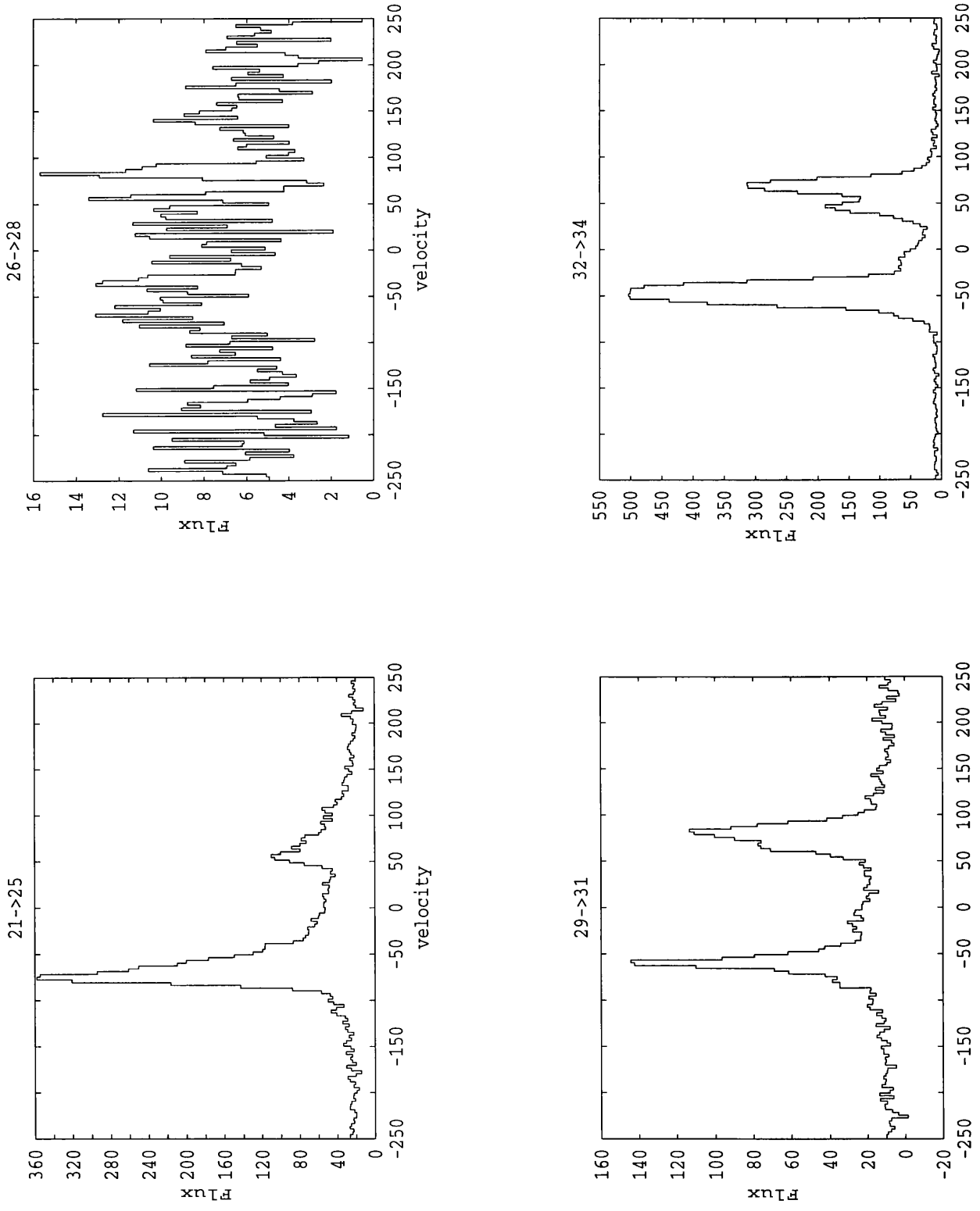

Figure 6.28: Extracted spectra 5→8

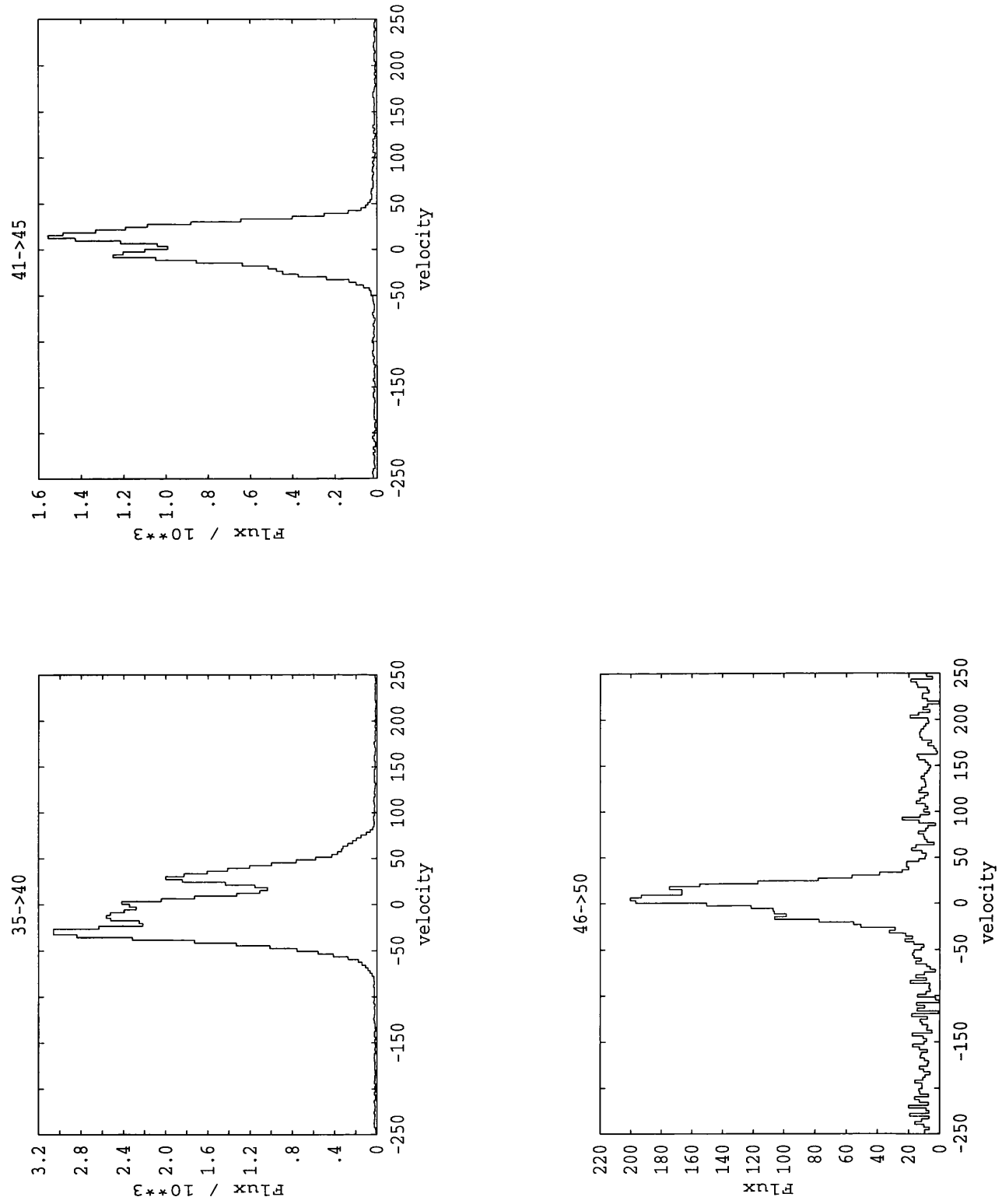

Figure 6.29: Extracted spectra 9→12

6.4 Analysis

In this section three questions will be addressed. What is the shape and orientation of the ring nebula? What is the global structure of the high velocity plumes? Is there evidence for more than one shell having been ejected?

The projection of AG Car's nebula onto the sky results in an elliptical ring, consequently we will assume its three dimensional shape is that of an ellipsoid. This means that we need to determine if it is a oblate or prolate ellipsoid. Closely connected with this question is that of the ellipsoids orientation, that is the angle between our line of sight and the nebulars major axis. If we examine images 2→6, we note a general trend of the brightest emission features in the north to be blue-shifted while those in the south are red-shifted. This "tilt" is a consequence of not viewing the ellipsoid along an axis of symmetry.

However at a position angle of 80^o no such tilt is observed implying the edge material here is moving perpendicular to our line of sight. Consequently, if the nebula is an oblate ellipsiod, then a P.A of 80^o corresponds to its major axis (since the ellipse cannot be edge or face on as would not allow a tilt to occur at any P.A.). The position angle of the major and minor axies of an ellipsoid, projected onto the sky, are not altered by the ellipsoids orrientation and so we know that the major axis lies at a P.A.=311^o. This is incompatible with a P.A=80^o required by an oblate ellipsoid to explain the lack of tilt at this position angle and so the nebula must be a prolate ellipsoid.

If we now consider the case of a prolate ellipse, we find that a position angle with no tilt will occur at a P.A. offset from the minor axis. If the nebulars major axis is perpendicular to the line of sight then no tilt will occur at any position angle. As we make this angle acute then the material along the plane formed by the minor

axies becomes red and blue shifted and the plane of tangentially moving material migrates. The angle of inclination neutralises the line-of-sight motion of some previously red and blue-shifted material. The position angle at which neither edge is red or blue shifted depends on both the angle of inclination of the major axis to the line of sight and the angle between the major axis and P.A=0 (i.e the angle of the nebula's rotation in the plane of the sky).

We note that in the images that we have presented, the emission maxima in the southern region of the nebula (below P.A.=80^o) are red- shifted, while those in the northern region are blue-shifted. This suggests that the major axis of the elipsoid is oriented away from us in the southern region and accordingly, toward us in the northern region. The angle of this inclination may be estimated on the basis that tangentally moving material occurs at a position angle of 80^o, while the minor axis lies at P.A.=30^o and the major axis of the nebula lies at 311^o. The angle between the P.A. of the minor axis and that of the tangentally moving material, is a function of the angle of inclination between our line of sight and the nebula's major axis, the P.A of the major axis and the three dimensional shape of the nebula. However since the latter is not known and so we cannot deduce the nebula's angle of inclination.

The expansion velocity of the nebula, as determined by the maxmium line splitting is about 70 km s^{-1}. However, given that the nebula's major axis is inclined to our line of sight, then this represents a velocity intermediate between the maxium expansion velocity, which occurs along the major axis and the minium expansion velocity which occurs along the minor axis. Whether this implies an upward or downward revision to the nebula's dynamical age depends on the angle of inclination.

Next we will look at the global distribution of the high velocity plumes. Examining the images we see that they are most extended at position angles 0^o and

15^o, as we move away from these position angles their spatial extent decreases. It is only at P.A.=40^o that no plumes are observed, although we note our detection at P.A.=80^o is weak. Generally, the velocity of the plumes is fairly constant at the different position angles, ranging from 72 km s^{-1} at P.A.=15^0 up to 103 km s^{-1} at P.A=311^o for the red-shifted plume and -73 km s^{-1} at P.A.=80^o to -105 km s^{-1} at P.A=311^o for the blue-shifted plume. The length of the red and blue-shifted plumes at a given position angle do appear well correlated, although an exception to this is P.A.=30^o where only the red-shifted plume is prominent.

A significant feature of these high velocity plumes is the reduced emission from the part of the ring nebula where they originate. This is evident at all slit positions (bar, P.A.=30). This may be indicative of the high velocity plumes having removed material from the ring nebula.

A further characteristic of the plumes is that they are velocity shifted in the opposite sense to the emission maxima in the same part of the nebula. This occurs for all position angles at which the plumes are seen, regardless of the nebula's orientation, if the plumes are perpendicular to the major axis. We note that the fact that the high velocity plumes are observed at all but one of the position angles means that the global structure of which the plumes are part, must have a very large angle of out flow. This suggests that they are unlikely to have a jet or fan-like appearence. This is an indication that the high velocity plumes could be part of some kind of out flowing disk (see Figure ??).The interpetation of the plumes as components of a disc is further supported by the observation that the highest velocity plumes are observed at a position angle of 311^o which lies along the nebular's major axis. This is to be expected if the plumes form a disk-like geometry, since it would be along the major axis that the largest component of their velocity is directed along our line of sight.

Each plume also has a companion plume in the opposite hemisphere with the

opposite velocity shift. This further supports the idea of an out flowing disk, since it would seem to require that the plumes are point symmetric about the central star, with half the structure moving toward us and the other half receding.

Based on the spectropolarimetic observations, Schulte-Ladbeck et al. (1994) and Leitherer et al. (1994) suggest that AG Car may have a two component wind. This would consist of a fast component emanating from the polar regions, while a slower denser wind originates from the equatorial region. This latter component must have a disk like geometry, on the grounds of symmetry. To explain the amount of intrinsic polarisation they suggest that the equatorial wind must be at least twice as dense as the polar wind. They find that the intrinsic polarisation varies along a preferred axis, with a position angle of 145^o. This position angle is roughly co-aligned with the major axis of the nebula, implying that the slower, dense wind flows out along the nebula's minor axis. This offers a natural origin for the disk like outflow that we observe as the high velocity plumes, since they would be a manifestation of the winds asymmetry at a large radius. That is, the spectropolarimetric observations probe the asymmetric outflow afew hundred solar radii from the star, while the dynamical nebular study is observing the affects of the outflow a parsec from the star.

In this context in is interesting to note that the "dust jets" found by Paresce & Nota also lie along the minor axis of the nebula. In our interpetation this co-incides with the position angle of the dense outflowing wind, which may provide a suitible enviroment for the formation of dust. Furthermore, it is at P.A.=30^o and 40^o that the high velocity plumes are hardest to detect. This would result from the motion along our line of sight, being a minimum along the minor axis. Consequently, it would be at this position angle that we are looking through the greatest depth of disk, which might then appear as the dust jets.

Further evidence for a two component wind comes from a multi-wavelength study

of AG Car's wind geometry by Leitherer et al. (1994). They identify a slow wind which varies on the time scale of years and a faster wind component, which showed no variablity during the period of their monitoring (Dec 1990 to Jun 1992). The slow wind component manifested itself through absorption conponents in the Hα profile. This recombination line tends to form in comparatively dense regions, where as the fast wind component appears as absorption features in collisionally excited UV lines like Si IV$\lambda\lambda$1393,1402 which tend to form in less dense regions. During the period of the observations the fast wind component maintained a constant velocity of about 900 km s^{-1}, while the slow wind component decreased its velocity from 275 km s^{-1} in December 1990 to 137 km s^{-1} in July 1991 and then to 59 km s^{-1} in March 1992. Consequently we note that the velocity of the slow wind component during the epoch of our observations (Jan 1991) is comparable to the velocity of our high velocity plumes.

In the light of the above discussion, the similarity between the geometry of AG Car's nebula and the geometry of the mass loss predicted to occur when a star impinges on its Eddington limit is striking (see section 1.4). In this disscussion we reviewed the competition between the mass loss from the equator caused by the star exceeding its limit and the process of photon tiring. This leads to the prediction that a disk will form around the equarorial region of the star, while the main mass loss occurs from the polar regions. This implies that the nebula will be prolate possibly with some manifestations of a disk. If the disk were to survive the 8000 years since the nebula formation, then our disk like outflow may be a consequence of this relic.

Finally we will address the issue of whether AG Car's nebula consists of a single or multiple shells. A distinct shell would lead to the presence of an extended coherent dynamical structure, varying continuously and smoothly in velocity space. In this data set we have identified two coherent dynamical structures, the main ring nebula and the out flowing disk. Emission from such a structure could require the

fitting up to four Gaussians. Consequently we must ask, do we see any line profiles which have more components than this?

When considering this, we must also remember the highly clumpy structure of the nebular revealed by recent HST imaging (Nota et al. 1995). The large scale clumping will tend to introduce discrete dynamical components into some line profiles. These can easily be distinguished from additional components due to shells, since they will lack any spatial coherence on the larger scale. From the 77 spectra extracted we see only two which require more than four gausians to be fitted, spectra 4 and 9 from image 3 which was taken at a position angle of 0°. The detection of these components is, at best marginal. Close to the central star, where the line splitting is stronger they are no longer detected. From this we conclude that this data set contains no evidence that AG Cars ring nebula contains multiple shells. Since the data set is both high resolution and spatially extensive, this places tight constraints on the nature of any shells which might be present.

6.5 Conclusions

On the basis of the dynamical data presented here three primary conclusions have been reached. From the eliptical projection of the nebula on to the sky, we inferred that it is likely to have an elipsoidal structure. Based on the "tilt" observed in the position of the emission maxima at the different slit positions we concluded that AG Cars nebula has a prolate elipsoidal form. Furthermore the velocity shift of these maxima indicate that the southern part of the major axis is orientated toward us, while the northern part is orientated away.

In our dynamical dataset we identify two large scale dynamical structures, the main ring nebula and high velocity plumes which we interprt as an outflowing disk.

The disk-shaped outflow appears as a series of high velocity plumes seen at all slit positions, bar P.A.=40 and attains a maxium velocity of 105 km s^{-1} along the major axis. Each plume is velocity shifted in the opposite sense to the emission maxima seen in the region of the plume. This suggests that the plumes are orientated perpendicular to the major axis. Most of the southern plumes observed have a counter part in the northern half of the nebula, with an opposite velocity shift. This implies that the plumes are point symmetric and are centered in a plane. In the data set we observe a general tendency for the ring nebula emission to be weak in the region of a plume. This may result from higher velocity plumes stripping material from the ring nebula in the form of a mass loaded flow.

Finally we note that this data set provides evidence of only one shell forming the observed ring nebula. This data set covers the regions close to the central star, out to the limits of the ring nebula with a spatial resolution of 1.1" and a velocity resolution of 7 km s^{-1}. No evidence of multiple shells has been found.

Chapter 7

Conclusions

7.1 Introduction.

LBVs represent a key phase in the transition of massive O stars into WR stars. To understand the LBV phenomena, two central questions must be addressed: How does the LBV phase fit into the evolutionary sequences? Is there evolutionary structure within the LBV phase? Since different evolutionary phases have different mass loss characteristics, we can in principle, shed light on these questions by studying the circumstellar medium. By developing an observationally based description of the LBV phase, we may hope to constrain the range of theoretical mechanisms which have been proposed to explain the phenomena. It is only when we have a full observational description in conjunction with a knowledge of the underlying physical mechanisium, that we can truly claim to understand LBVs.

A ubiquitous feature of LBVs is the presence of circumstellar nebulae. A number of different mechanisms for their formation have been proposed, but at the present time *even the gross picture is basically unknown.* In this thesis we have used the chemical and dynamical properties of the nebulae to infer the physical conditions on the surface of the star during the epoch of nebula ejection. This in turn has allowed us to discriminate between the different theoretical mechanisms for the formation of

Nebula / Star	N/H	O/H	Sp Type
AG Car	8.22±0.11	7.52±0.20	LBV
He3-519	8.21±0.10	7.57±0.15	LBV(?)
HR Car	8.4	<8.4	LBV
RCW58	8.02 ±.08	7.44 ± 0.15	WN8
NGC 6164-5	8.38 ±0.02	7.95 ±0.03	O6.5f?p

Table 7.1: The abundance patterns of ejecta nebulae surrounding massive stars determined in this thesis.

the nebulae.

7.2 A Review of the Observational Results

In the preceeding chapters we have presented abundance studies of three LBV, one WR and one Of star nebula. We have found in all cases, that they contain material with essentially the same abundance pattern (see Table 7.1). Given the wide range of surface abundance patterns determined for stars at similar points in their post-main sequence evolution, this uniformity in the nebular abundance pattern is surprising. The uniformity suggests that the chemical composition of the surface layers of the star is physically important to the operation of the ejection mechanisium.

The abundance pattern that we have found in the LBV nebulae is that of partially CNO processed material. However, from the model of Meynet et al. (1994) LBV stars are expected to have CNO equilibrium compositions. This expectation is confirmed by the atmospheric modelling of R71 (Lennon 1994) and AG Car (Smith et al. 1994). Consequently the nebulae cannot have been formed by a series of small outbursts during the LBV phase. Instead they must have been ejected at the beginning or before the LBV phase.

In Chapter 3 we find circumstantial evidence for the presence of a disk around HR Car. The detection of nebular [NiII]λ6667 in increasing strength towards the star, suggests there exists a region of high density. This is reinforced by our finding that the nebular density increases away from the polar regions. Furthermore, spectropolarimetric observations (Clampin et al. 1995) show that there is asymmetry in HR Car's mass loss close to the central star. If there is a disk around HR Car then we would expect the strong stellar radiation field to strip material from it and so have manifestations at the nebular scale. In Chapter 6, we believe that we are directly observing such manifestations in the nebula surrounding AG Car, where we find material out-flowing in the plane of the nebula's minor axis. If this represents the large scale affects of an inner disk, then this would explain the bipolar-polar dust jets imaged by Paresce & Nota (1989) and the spectropolarimetric observations of Schulte-Ladbeck et al. (1994) which reveal asymmeteric mass loss close to the central star.

7.3 Nebula Ejection from Stars Evolving Above the H-D Limit.

It is a well established observational fact (Humphreys & Davidson 1979) that the region of the HRD immediately below the H-D limit has a very different appearance from that above it. This suggests that in making this transition in luminosity we encounter some new physical process which modifies the evolutionary tracks. From the work of Lamers & Fitzpatrick (1987) we find that the H-D limit is coincedant with the locus of modified Eddington limits in the HRD, implying that the "new physics" is intimately connected with this. Consequently we will not assume that stars above and below the H-D limit evolve on similar evolutionary tracks. This means that we need to establish the point of nebula ejection from high and low mass LBVs independently.

Of the thirty or so LBVs known, only four (AG Car, R127, η Car and possibly P Cygni) are evolving on tracks above the H-D limit. Consequently these stars represent a rare subsection within the already scarce LBV class. In this thesis we have carried out an abundance study on the nebula surrounding AG Car. The resulting abundance pattern was found to be identical, within the errors, to that we have derived for nebulae surrounding the lower luminosity LBVs He3-519 and HR Car.

When during the evolution of these most massive stars does such an abundance pattern arise on their surface? From the work of Voels et al. (1989), Herrero et al. (1992), Crowther et al. (1996) we find that O and Of stars display a wide range of surface abundances, some having abundance patterns which are more processed than those found in LBV nebulae. This range may be a manifestation of mixing due to rotation (Pasquali et al. 1997). That is, a star at a given point on its evolutionary track does not have a unique surface abundance, because this is also influenced by the star's angular momentum.

The second facet of the nebulae which bares witness to the the physical conditions on the surface of the star at the time of ejection are the dymanics. The expansion velocity of a nebula is broadly correlated to the escape velocity of the star from which it was ejected. This is especially true if the material has been lifted from the star's gravitational well by the radiation field since the terminal velocity of a wind is dependent on the star's effective temperature and effective gravity. Like other LBVs AG Car's nebula has a low expansion velocity of only 70 km s^{-1}, which is indicative of ejection from a star with a low surface gravity. By contrast a massive BSG (initial mass $60M_{\odot}$) has an escape velocity of over 1000 km s^{-1}. How then has AG Car achieved a period of low surface gravity? From the calculations of Lamers & Fitzpatrick (1987) we see that the H-D limit is coincident with the locus of modified Eddington limits in the HRD. As a star approaches its modified Eddington limit its effective surface gravity will decline. Consequently, if the mass loss which formed the nebula surrounding AG Car occurred while the star was near its modified Ed-

dington limit then this would explain the low nebular expansion velocity. Given the range in Of star surface abundance patterns, it is also possible that the abundance pattern seen in the nebula could be present on the surface of the star during this period. That is, the ejection of a nebula while a massive BSG is impinging on is modified Eddington limit could form a nebula with the same abundance pattern and dynamics as that seen in the nebula around AG Car.

At this point we must consider a second possibility. It has been suggested by Smith et al. (1997) that the mass loss which occurs when the Eddington limit is exceeded is not sufficient to halt the red-ward evolution of the most massive stars and so they continue to evolve inside the HD-limit to become RSGs. This would then offer a second phase in which a nebula with a low expansion velocity could be ejected. In this thesis we have argued against this possibility for a number of reasons.

From the work of Langer (1997) we see that stars approaching the Ω limit must lose whatever mass is needed to prevent Ω=1. As discussed in Chapter 6 this may lead to the formation of a disk, in which case the mass loss rate is unrestricted by photon tiring. The time scale over which the envelope must be lost is much less than the time scale over which it expands due to core contraction. This conclusion ignores the effects of strange mode pulsations which will further enhance the mass loss rate, inhibiting continued red-ward evolution. Furthermore, while the mass loss may redden a star evolving inside the H-D limit, making it hard to detect in the optical, it would be a very bright source in the I.R. However IRAS surveys have found no such candidate objects.

In contrast, ejection of the nebula from near the modified Eddington limit carries a number of advantages in explaining the geometry of the nebula. As discussed in Chapter 2, as a star approaches its modified Eddington limit, it will first encounter the Ω limit. This will cause a very large mass loss from the equator, which due to

photon tiring could lead to the formation of a disk. This mass loss would then serve to redistribute the radiation field toward the poles causing the greatest mass loss to occur there (Owocki & Gayley 1997) and so will form a prolate nebula. In Chapter 6 we presented a dynamical study of AG Car's nebula in which we found evidence for it being a prolate ellipsoid surrounded by an out-flowing disk-like structure. We suggest that these are the hallmarks of mass lost from a star nearing its modified Eddington limit.

In the light of this, ejection of the nebula from a massive RSG inside the H-D limit, would seem the more problematic of the two possible locations for nebula ejection. In contrast, ejection from near the modified Eddington limit suffers none of these problems and carries with it great explanatory power concerning the geometry of the nebula. That is, ejection from a RSG inside the H-D limit is capable of explaining fewer of the nebular properties and suffers both theoretical and observational difficulties. Consequently we favour the hotter site for the ejection of the nebula.

7.4 Nebula Ejection from Stars Evolving Below the H-D Limit.

In this thesis we have carried out abundance studies on nebulae surrounding two LBVs evolving below the H-D limit, HR Car and He3-519. We have found that they are comprised of partially CNO processed material. The abundance pattern that we have determined is consistent with that which arises at the end of the RSG phase in the models of Meynet et al. (1994). We also find close agreement between the abundance pattern that we have derived for the LBV nebulae and that determined for the ring surrounding SN 1987A, which is thought to consist of RSG material (Panagia et al. 1997). This contrasts sharply with the abundance pattern, determined by the application of atmospheric models to the surface of LBV stars, which

find a CNO equilibrium abundance pattern. Consequently, the nebulae must have been ejected at the beginning or before the LBV phase. This excludes the possibility that the nebulae are formed by a series of ejections through the LBV phase, since this would form nebulae comprised of material which is more processed than RSG material.

Next we we consider the information that can be gleaned from studying the nebular dynamics. Reviewing the literature we find that LBV nebulae typically have expansion velocities in the range 40-140 km s^{-1}. This is similar to the escape velocity from the RSG phase of a star with an initial mass of $35M_{\odot}$, since this has an escape velocity of about 80 km s^{-1}. However we find that it is incompatible with an ejection from the BSG phase which would have an escape velocity of about 700 km s^{-1}.

The nebular properties offer evidence that the nebula was ejected from a star with a low surface gravity, close in time to the end of the RSG phase. Clearly ejection from a RSG would satisfy these criteria. However, a second possibility exists. At the end of the RSG phase the star evolves very rapidly back toward the blue, over this brief period (10^2yrs) the surface abundances do not have time to significantly change. A low effective surface gravity will then arise during this period as the star approaches its modified Eddington limit.

High mass stars evolve through the blue loop at a constant luminosity. During the red-ward part of this evolution they can loose almost half of their mass (Jones et al. 1993). This combined with an increasing surface opacity as the star tends toward the iron opacity bump, could cause the star to hit its modified Eddington limit and become unstable. Either way, the low expansion velocities of the nebulae strongly argues that *low luminosity LBVs are post RSG objects.* This is because a RSG phase is required either to provide the period of low surface gravity or to lose

sufficient mass so that the star subsequently encounters its modified Eddington limit.

Consequently we find that there are two regions of the evolutionary track from which the nebula may have been ejected. How then can we distinguish between them? One indication comes from the ubiquitous bipolarity of LBV nebulae. It has been suggested that the nebulae may be shaped through interaction with an asymmetric RSG wind. However a survey of the literature shows that while some RSG outflows are asymmetric, many are not. Accordingly, if this were the shaping mechanisium then we would expect to see many spherical LBV nebulae. In practice the only spherical nebula surrounding an LBV is P Cygni's, which has an exceptionally low mass of $0.01M_{\odot}$ (Barlow et al. 1994). In contrast mass loss from a star impinging on its modified Eddington limit is inherently bipolar. This is because, before encountering the modified Eddington limit, the star will exceed the Ω limit which causes a heavily asymmetric mass loss. Accordingly this offers a natural explanation of the bipolar character of LBV nebulae. In addition to this there is also some weak observational support for the nebulae being ejected while the star is in the blue. Goodrich et al. (1989) have argued that SN 1961V was actually a misidentified LBV eruption. Earlier colour band imaging establishes the progenitor as a blue star. More recently Drissen et al. (1997) have identified an LBV in outburst in NGC 2363, brightening by several magnitudes over a period of a few months. Again, colour band imaging has shown the progenitor to have been a BSG. However we note that in this latter case there is insufficient observation to show if the giant outburst is accompanied by a large ejection of mass.

Consequently we conclude that LBVs evolving below the HD limit are post-RSG stars, which eject their nebulae while evolving blue-ward. There are two possible site for this to occur, at the end of the RSG phase and as the star approaches its modified Eddington limit toward the blue. Because of the bipolar character of LBV nebulae, we favor the hotter site.

While, in general we conclude that LBVs evolving below the H-D limit must be post-RSG objects, because mass loss is needed to create the high L/M ratio causing the star to impinge on the modified Eddington limit, leading to the observed low nebular expansion velocities (unless you argue the nebulae are ejected from RSG, which rather makes the point moot!). We suggest that some fast rotating stars may be an exception to this. If a star is rapidly rotating then less mass need be lost to make it hit its Ω limit. Accordingly it may become unstable during the red-ward phase of its loop. We suggest that HD 148937 may be such a star. Furthermore, this may explain why the post eruption object is an Of star. Since HD 148937 would have lost less mass than a post RSG-LBV, it will have a higher surface gravity when it moves away from the modified Eddington limit. This will reduce the mass loss rate and prevent the slash star classification which requires wind lines. Indeed atmospheric modelling of HD 148937 (Leitherer et al. 1987) suggests that it does have a greater effective surface gravity than slash stars.

7.5 Constraints on the Outburst Mechanism.

What is the physical mechanism which causes the ejection of the nebulae? The nebulae themselves are relics of an earlier era of mass loss and represent our only direct observational link to this phase of an LBVs evolution. Taking archeology into a new realm we have analysed these relics to infer some of the physical conditions which prevailed on the surface of the star during the epoch of nebula formation.

The combination of nebular dynamics and chemical composition are incompatible with the idea that the nebulae were formed by mass loss due to the instability found in the models of Stothers & Chin. Their models first phase of instability occurs when the star first becomes a RSG. This would produce nebulae with too great a dynamical age. The second phase, results in a series of smaller mass loss events and occurs in the blue, being identified with the LBV phase. This would produce

nebulae comprised of too highly processed material.

We have found that the nebulae surrounding LBV, some WR stars and NGC 6164/5 around the Of star HD 148937, have very similar abundance patterns, corresponding to partially CNO processed material. From the atmospheric analyses (Crowther & Bohannan 1997) it has been found that a number of Of stars (log $L/L_{\odot}$=5.7-5.9) have a surface abundance more processed than this. Consequently if they were to go on to become LBVs, ejecting a nebula, they would have quite different nebular abundance patterns from the one that is observed. This implies that not all stars above a given mass go on to become LBVs.

From the uniform abundance pattern and low nebular expansion velocity seen in all LBV nebulae (bar η Car), it would seem that there are two factors common to all stars ejecting LBV nebulae. Firstly, they must have a low surface gravity. Secondly, the star must be at a particular point in its evolution, in terms of its surface composition. When a star achieves one of these factors but not the other no nebula is ejected. This is supported by the fact that some Of stars have already surpassed this surface abundance pattern without ejecting a nebula. This suggests that the combination of low surface gravity and a particular abundance pattern is not coincidental, but rather both are necessary for the ejection mechanism to operate.

In light of this, we note the physical conditions under which strange mode pulsations arise. These occur in low density envelopes where there are large non-adiabatic effects. Strange mode pulsations are terminated if the surface helium abundance exceeds approximately Y=0.4, since this reduces the opacity and so increases the effective surface gravity. Consequently strange mode pulsation are expected to arise in both RSGs and blue-ward of the HD limit (Cox 1997). The influence of the helium abundance on the opacity may also be significant in deciding if the post-RSG star exceeds its Ω limit while evolving blue-ward. If the star has a too greatly enhanced

surface composition then its modified Eddington limit will be greater and so it may not encounter the Ω limit and so avoid an LBV phase.

The interplay between the enhanced helium abundance and the acquisition of a low surface gravity is interesting for two reasons. Firstly it offers an explanation of why not all stars above a given mass suffer an LBV phase leading to the ejection of a nebula. If the star had a too high helium composition on the blue-ward leg of the loop then it wouldn't impinge on its modified Eddington limit, wouldn't suffer strange mode pulsations and is less likely to exceed its Ω limit. Secondly if the abundance pattern controls whether the modified Eddington limit plays a significant role, then this would offer a natural explanation of the uniformity in nebula abundance patterns. The atmospheric studies of Of-stars suggest that stars of a similar mass in the same evolutionary phase have a wide spread in their surface compositions. We note that if this is true for stars at the end of the RSG phase, then we would not a priori expect a uniformity in the nebula abundance patterns. Allowing the surface composition to control the instability mechanism, makes this coincidence inevitable.

7.6 Summary.

New Results.

• In this thesis we have determined the first accurate abundance pattern for a nebula surrounding an LBV (AG Car). This has been consolidated by two further abundance studies of nebulae surrounding the LBVs He3-519 and HR Car. We have shown, contrary to expectations that LBV nebulae are not comprised of CNO equilibrium material, but rather only partially CNO processed material.

• We have carried out an abundance study of the ring nebula RCW 58 surrounding the star WR40. We have found that this is comprised of partially CNO processed material. The abundance pattern that we have derived for RCW 58 is very similar

to that found in our sample of LBV nebulae. This suggests that some WR nebulae are relic LBV nebulae.

• We have also undertaken an abundance study of the nebula NGC 6164/5 surrounding the Of star 148937. We find that this nebula is comprised of partially CNO processed material. Furthermore, the abundance pattern is very similar to that found in AG Car, HR Car, He3-519 and RCW 58. This strongly suggests that the surface abundance pattern of a massive star plays a crucial role in controlling the ejection mechanism.

• Finally, in this thesis we have presented a dynamical study of the nebula surrounding AG Car. We concluded that the nebula is a prolate ellipsoid. Furthermore, we find evidence for a disk like out-flow extending from the minor axis of the ellipsoid. This is the first such outflow to be detected around an LBV nebula, and may be a large scale manifestation of disk-like structures, suggested by spectropolarimetric results, close to the central star.

Inferences

• On the basis of our abundance determinations and in conjunction with the results of atmospheric analyses of LBV surface compositions, we conclude that LBV nebulae are ejected at the beginning or prior to the LBV phase.

• We find two factors common to all LBV nebulae, that is a common abundance pattern and ejecta nebulae from a star with a low surface gravity. We therefore suggest that these two factors are necessary requirements for the nebula ejection mechanism to operate.

• On the basis of the nebular dynamics and chemical composition, we identify two possible sites of the nebula ejection from stars evolving on tracks above the H-D limit. One site lies near the modified Eddington limit, while the other occurs during a RSG phase inside the H-D limit. The latter site suffers theoretical and obser-

vational objections, while the former site naturally explains the nebular geometry found in Chapter 6 for the nebula surrounding AG Car.

• Applying the same reasoning to stars evolving on tracks below the H-D limit, we find a similar situation, and again favor the hotter site as this makes the bipolar character of the nebulae explicable. We conclude that in general that low mass LBVs must be post-RSG objects, in order to achieve the low surface gravities implied by the low nebular expansion velocities. An exception to this may exist in the case of fast rotating stars which would require less mass to be lost to make them hit their Ω limit. We suggest that HD 148937 may be such a star and note that such a scenario offers a natural explanation for why the post eruption star is an Of star.

Bibliography

[1] Appenzeller, I., 1988, In:"Physics of Luminous Blue Variables" 133 IAU coll, 195

[2] Arthur, S.J., Dyson, J.E., Hartquist, T.W., 1993, MNRAS, 261, 425

[3] Arthur J., Henney W., 1996, A&A,

[4] Barlow, M.J., Drew, J.E., Meaburn, J., Massey, R.M., 1994, MNRAS, 268, 29

[5] Beals, C.S., 1951, Pub Dom Astrophys Obs Victoria, 9, 1

[6] Bernat, A.P., 1981, ApJ, 246, 184

[7] Bernat, A.P., Lambert, D.L., 1978, PASP, 90, 520

[8] Bohannan, B., Walborn, N.R., 1989, PASP, 101, 95

[9] Bohannan, B., Voels, S.A., Hummer, D.G., Abbott, D.C., 1990, Astrophys. J., 365, 729

[10] Bowers, P.F., Claussen, M.J., Johnston, K.J., 1993, AJ, 105, 284

[11] Brandner, W., Grebel, E.K., Chu, Y.-H., Wris, K., 1996, ApJ, 475, L45

[12] Brocklehurst M., 1972 MNRAS, 157, 211

[13] Bruhweiler, F.C., Gull, T.R., Henize, K.G., Cannon, R.D., 1981, Astrophys J, 251, 126

[14] Chu Y.-H., 1982, ApJ, 254, 578

[15] Chu, Y.-H., 1988, PASP, 100, 986

[16] Chu Y.-H., 1991, in van der Hucht, K.A., Hidayat, B., eds, Proc. IAU Symp. 143, Wolf-Rayet Stars and Interrelations with other Massive Stars in Galaxies, Kluwer, Dordrecht, p.349

[17] Clampin, M., Schlute-Ladbeck, R., Nota, A., Robberto, M., Paresce, F., Clayton, G., 1995, AJ, 110, 251

[18] Clegg R.E.S., 1987, MNRAS, 221 31

[19] Conti P.S., 1984, in Meader A., Renzini A., eds, Proc. IAU Symp. 105, Observational Tests of the Stellar Evolution Theory. Kluwer, Dordrecht, p.233

[20] Crowther, P.A., Bohannan, B., 1997, A&A, 317, 532

[21] Crowther, P.A., 1995, A&A, 293, 172

[22] Crowther, P.A., 1997, "Luminous Blue Variables: Massive Stars in Transition", PASP conf series, 120, 51

[23] Crowther, P.A., Hillier D.J., Smith, L.J., 1994, A&A, 293, 172

[24] Crowther, P.A., Smith, L.J., Hillier, J.D., Schmutz, W., 1995, A&A, 293, 427

[25] Crowther P.A., Smith L.J., 1996, A&A, 305, 541

[26] Crowther P.A., Smith L.J., Hillier D.J., Schmutz W., 1994, A&A, 293, 427

[27] Cox, A., Guzik, J.A., Soukup, M.S., 1997, "Luminous Blue Variables: Massive Stars in Transition", PASP conf series, 120, 133

[28] Damineli, A., "Luminous Blue Variables: Massive Stars in Transition", PASP conf series, 120, 272

[29] Davidson, K., 1987, ApJ, 317, 760

[30] Davidson K., Dufour R.J., Walborn N.R., Gull T.R., 1986, ApJ, 305, 867

[31] Davidson K., Humphreys R.M., Hajian A., Terzian Y., 1993, ApJ, 411, 336

[32] de Koter A., Lamers H.J.G.L.M., Schmutz W., 1996, A&A, 306, 501

[33] Drissen, L., Roy, J.R., Robert, C., 1997, ApJ, 474, L35

[34] Dopita, M.A., Bell J.F., Chu Y.-H., Lozinskaya T.A., 1994, ApJS, 93, 455

[35] Dufour, R.J., Glover, T.W., Hester, J.J., Currie, D.G., van Orsow, D., Walter D.K., 1997, "Luminous Blue Variables: Massive Stars in Transition", PASP conf series, 120, 225

[36] Dufour R.J., Parker R.A.R., Henize K.G., 1988, ApJ, 327, 859

[37] Eichler, D., Shalom, A.B., Oreg, J., 1994, ApJ, 448, 858

[38] Esteban C., Rosado, M., 1995, ApJ, 304, 491

[39] Esteban C., Smith, L.J., Vílchez J.M., Cleg, R.E.S., 1993, A&A, 272, 299

[40] Esteban C., Vílchez J.M., 1992, ApJ, 390, 536

[41] Esteban C., Vílchez J.M., Smith L.J., Manchado A., 1991, A&A, 244, 205

[42] Esteban C., Vílchez J.M., Smith L.J., Clegg R.E.S., 1992, A&A, 259, 629

[43] Fairall, A.P., Parker, R.A.R., Henize, K.G., 1985, PASP, 97, 780

[44] Fich, M., Blitz, L., Stark, A.A., 1989, ApJ, 342, 272

[45] Figer, D.F., Mclean, I.S., Morris, M., 1995, ApJ, 447, L29

[46] Filippenko, A.V., et al., 1995, AJ, 110, 2261

[47] Fitzsimmons A., Dufton P.L., Rolleston W.R.J., 1992, MNRAS, 259, 489

[48] Fleming, W.P., 1912, Harvard Annals, 56, 181

[49] Frank, A., 1997, "Luminous Blue Variables: Massive Stars in Transition", PASP conf series, 120, 338

[50] Frank, A., Balick, B., Livio, M., 1996, ApJ, 471, L56

[51] de Freitas Pacheco, J.A., Damineli, N.A., Costa, R.D.D., Viotti, R., 1992, A&A, 266, 360

[52] Gallagher, J.S., 1989, In:"Physics of Luminous Blue Variables.", IAU coll 113, 185

[53] Garc´ ia-Segura G., Mac Low M.-M., Langer N., 1996a, A&A, 305,229

[54] Garc´ ia-Segura G., Langer N., Mac Low M.-M., 1997, "Luminous Blue Variables: Massive Stars in Transition", PASP conf series, 120, 133

[55] Garc´ ia-Segura G., Langer N., Mac Low M.-M., 1996b, A&A, 316,133

[56] Gautschy, A., Glatzel, W., 1990, MHRAS, 245, 597

[57] van Genderen, A.M., Robijn, F.H.A., van Esch, B.P.M., Lamers, H.J.G.L.M., 1991, A&A, 246, 407

[58] van Genderen, A.M. et al., 1992, A&A, 264, 88

[59] van Genderen, A.M., Robijn, F.H.A., van Esch, B.P.M., Lamers, H.J.G.L.M., 1991, A&A, 246, 407

[60] Goodrich, R.W., Stringfellow, G.S., Penrod, G.D., Filippenko, A.V., 1989, ApJ, 342, 908

[61] van Genderen, A.M., et al., 1990, A&A sup, 82, 189

[62] Glatzel, W., 1994, MHRAS, 271,66

[63] Glatzel, W., Kiriakidis, M., 1993, MNRAS, 264, 50

[64] Glatzel, W., Mehren, S., 1995, MHRAS, 282, 1470

[65] McGregor, P.J., Finlayson, K., Hyland, A.R., Joy, M., Harvey, P.M., Lester, D.F., 1988, ApJ, 329, 874

[66] Hamann W.-R., Koesterke L., Wessolowski U., 1993, A&A, 274, 397

[67] Harrington, J.P., Seaton, M.J., Adams, S.,Lutz, J.H., 1982, MNRAS, 199, 517

[68] Herrero A., Kudritzki R.P., V´ ilchez J.M., Kunze D., Butler K., Haser S., 1992, A&A, 261, 209

[69] Hillier, D.J., 1990, A&A, 231, 116

[70] Hinze, K.G., 1952, A&A, 115, 133

[71] Henize, K.G., 1959, AJ, 64, 51

[72] Henize K.G., 1976, ApJS, 30, 491

[73] Hoekzema, N.M., Lamers, HJ.G.L.M., van Genderen, A.M., 1992, A&A, 257, L17

[74] Howarth I.D., 1983, MNRAS, 203, 301

[75] Howarth, I.D., Prinja, R.K., 1989, ApJs, 69, 527

[76] Hoffleit D., 1953, Ann. Harvard Coll. Obs., 119, 37

[77] Hoffleit D., 1940, Harvard Bull, 913, 4

[78] Hu, J.Y., de Winter, D., The, P.S., Perez, M.R., 1990, A&A, 227, L17

[79] Hummer D.G., Story P.J., 1987, MNRAS, 224, 801

[80] Huphreys R.M., Davidson K., 1979, ApJ, 232, 409

[81] Huphreys R.M., Davidson K., 1994, PASP, 106, 1025

[82] Huphreys R.M., Lamers H.J.G.L.M., Hoekzema N., Cassatella A., 1989, A&A 218, L17

[83] Hutchings, J.B., 1976, ApJ, 203, 438

[84] Hutchings, J.B., 1975, ApJ, 200, 122

[85] Hutsem´ ekers D., 1994, A&A, 281, L81

[86] Hutsem´ ekers D., van Drom, E., 1991, A&A, 251, 620

[87] Johnson, H.M., 1976, ApJ, 206, 469

[88] Johnson D.R.H., Barlow M.J., Drew J.E., Brinks E., 1992, MNRAS, 255, 261

[89] Jones T.J. et al., 1993, ApJ, 411, 323

[90] Justtanont et al., 1996, A&A, 315, 217

[91] Kastner J.H., Weintraub D.A., 1995, ApJ, 452, 833

[92] Kilian J., 1992, A&A, 262, 171

[93] Kingsbrugh R.L., Barlow M.J., 1994, MNRAS, 271, 257

[94] de Koter, A., Lamers, H.J.G.L.M., Schmutz, W., 1996, 306, 501

[95] Kwitter K.B., 1984, ApJ, 287, 840

[96] Lamers, H.J.L.M., Fitzpatrick, E.L., 1987, ApJ, 324, 279

[97] Lamers H.J.G.L.M, Snow T.P., Lindholm D.M., 1995, ApJ, 455, 269

[98] Lamers H.J.G.L.M. et al, 1996, A&A, 315, L225

[99] Langer, N., 1997, "Luminous Blue Variables: Massive Stars in Transition", PASP conf series, 120, 83

[100] Langer N., Hamann W.-R., Lennon M., Najarro F., Pauldrach A.W.A, Puls J., 1994, A&A, 290, 819

[101] Leitherer, C., C.Chavarria, -K., 1987, A&A, 175, 208

[102] Leitherer, C., 1997, "Luminous Blue Variables: Massive Stars in Transition", PASP conf series, 120, 58

[103] Leitherer, C., Shmutz, W., Abbot, D.C., Hamann, W.R., Wessolowski, 1989, ApJ, 346, 919

[104] Leitherer C. et al., 1994, ApJ, 428, 292

[105] Lennon, D.J., Wobig, D., Kudritzki, R.P, Stahl, O., 1994, In:"Evolution of massive stars." Space Science Reviews, 66, 207

[106] Lucy, L.B., 1995, ApJ, 294, 555

[107] Lucy, L.B., Abbott, D.C., 1993, Astrophys J, 255, 286

[108] Marston A.P., 1991, ApJ, 366, 181

[109] Marston A.P., 1994, ApJ, 109, 1839

[110] Marston A.P., 1996, AJ, 112, 2828

[111] Marston A.P., 1997, ApJ, 475, 188

[112] Marston, A.P., Chu, Y.-H., Garc´ ia-Segura G., 1994, ApJ sup, 93, 229

[113] Marston, A.P., Yocum, D.R., Garc´ ia-Segura G., Chu, Y.-H., 1994, ApJ sup, 95, 151

[114] Martin, C., Arnett, D., 1995, ApJ, 447, 378

[115] Mathis, J.S., Cassinelli, J.P., van der Hucht, K.A., Prusti, T., Wesselius, P.R., Williams, P.M., 1992, 384, 197

[116] Mauron, N., Cailloux, M., Tilloles, P., le Fevre, O., 1986, A&A, 165, 66

[117] Meader, A., Meynet, G., 1987, Astr ap, 181, 243

[118] Meynet G., Meader A., Schaller G., Schaerer D., Charbonnel C., 1994, A&A, 103, 97

[119] Miller, G.J., Chu, Y.-H., 1993, ApJ sup, 85, 137

[120] Mitra P.M., Dufour R.J., 1990 MNRAS, 242, 98

[121] Moffat, A.J.F., 1989, ApJ, 347, 373

[122] Morris, P.A., Eenens, P.R.J., Blum, R.D. 1996 ApJ, 470, 597

[123] Nedoluha, G.E., Bowers, P.F., 1992, ApJ, 392, 249

[124] Nota A., Clampin M., Garc´ ia-Segura G., Leitherer C., Langer N., 1996, in Benvenuti P., Macchetto F.D., Schreier E.J., eds, Science With The Hubble Space Telescope- II Space Telescope Institute, in press.

[125] Nota A., Leitherer C., Clampin M., Greenfield P., Golimowski D.A., 1992, ApJ, 398, 621

[126] Nota A., Livio M., Clampin M., Schulte-Ladbeck R., 1995, ApJ, 448, 788

[127] Nota A., Pasquali, A., Drissen, L., Leitherer, C., Robert, C., Moffat, A.F.J., Schmutz, W., 1996, ApJ sup, 102, 383

[128] Nota A., Smith L.J., Pasquali A., Clampin M., Stroud M.P., 1996, ApJ, 486, 338

[129] Nieuwenhuijzen, H., de Jager, C., 1995, A&A, 302, 811

[130] Nieuwenhuijzen, H., de Jager, C., Cuntz, M., 1994, A&A, 285, 595

[131] Oudmaijer R.D., Groenewegen M.A.T., Matthews H.E., Blommaert J.A.D.L., Sahu K.C., 1996, MNRAS, 280, 1062